

---

This item was submitted to [Loughborough's Research Repository](#) by the author.  
Items in Figshare are protected by copyright, with all rights reserved, unless otherwise indicated.

## Surface modification of and adhesion to polystyrene

PLEASE CITE THE PUBLISHED VERSION

PUBLISHER

© Ng, Ting Ting

PUBLISHER STATEMENT

This work is made available according to the conditions of the Creative Commons Attribution-NonCommercial-NoDerivatives 4.0 International (CC BY-NC-ND 4.0) licence. Full details of this licence are available at:  
<https://creativecommons.org/licenses/by-nc-nd/4.0/>

LICENCE

CC BY-NC-ND 4.0

REPOSITORY RECORD

Ng, Ting-Ting. 2018. "Surface Modification of and Adhesion to Polystyrene". figshare.  
<https://hdl.handle.net/2134/34260>.

**University Library**

Author/Filing Title NG. T.T.

Class Mark I

Please note that fines are charged on ALL  
overdue items.

**FOR REFERENCE ONLY**

0403481570





---

# **SURFACE MODIFICATION OF AND ADHESION TO POLYSTYRENE**

**By**

**Ng, Ting Ting**  
**B. Sc., M. Sc.**

**A doctoral thesis submitted in partial fulfilment of the requirements for the award  
of the Degree of Doctor of Philosophy**

**of**

**Loughborough University**

**July 2006**


**Department:**

**Institute of Polymer Technology & Materials Engineering (IPTME)**

**Supervisor: Dr Richard J. Heath**

**Co-supervisor: Dr Ian Sutherland**

**© Ng, Ting Ting 2006**

	<b>Loughborough University</b> Pilkington Library
Date	6/2008
Class	T
Acc No.	0403481570

**Dedicated To The Ones I Love,**

**My Dad, Mr Ng Chee Guan**

**My Mom, Mdm Goh Ah Tee**

**My Sisters, Wenru, Xinhui, Chuyun,**

**Our Dog, Nancy**

---

## **ACKNOWLEDGEMENTS**

I would like to thank my department, IPTME, for the research studentship.

I am indebted to both my research supervisors, Dr Richard J Heath and Dr Ian Sutherland, for their advice, suggestion, support, understanding and guidance throughout this research. I could not adequately express my sincere gratitude to Dr Ian Sutherland, especially, for his constant criticisms and encouragement in my project.

I am appreciative to the following staffs in IPTME for generating the analysis of my samples. They are Dr I Mathieson and Mr D Hall for the XPS data, Dr D Grandy for the AFM data.

I would also like to express my thanks to all the technicians. They are Mr R Owens, Mr A Stevens, Mr T Atkinson and Mr A J Woolley of IPTME and Mr D Wilson of Chemistry Department for their assistance during this project.

My thanks would also like to go out to my colleagues and friends in both IPTME and Chemistry Department. They are Dr J Palenzuela, Dr J Paget, Emma, Phil and Susan, Ajufa, Luke, Ben and Mark for their friendship and encouragement extended during my research time.

I thank all my friends in Loughborough for their friendship, especially to my dining hall work colleagues, Mrs M Mckenzie, Mrs J Kinsella and Mr M Connor. My thanks also go out to my ex-ICI colleagues, ex-Lubrians and friends for showing their constant support from Singapore.

Last but not least, my indebt gratitude to my family for their continuous support, both financially and emotionally, and for believing in me from the time I embarked on my study journey in United Kingdom nearly a decade ago.

---

## ABSTRACT

Polystyrene (PS) is a non-polar polymer that has limited surface properties since it lacks polar functional groups. In this project, different polar functional groups were incorporated onto PS by various methods such as surface treatments (flame treated and chromic acid treated), non-reactive and reactive compounding (at different loadings of copolymers) and grafting of copolymer chains induced by UV irradiation. These functional groups, namely carboxylic acid, hydroxyl, styrene maleic anhydride (compounded and grafted) and poly(vinyl methyl ether) (PVME), introduced during treatment and modification of PS, may diffuse away from the surface into the bulk and vice versa.

The treated and modified surfaces were investigated and compared using a range of surface analysis techniques, which include X-ray photoelectron spectroscopy (XPS), attenuated total reflection infrared spectroscopy (ATR-IR), atomic force microscopy (AFM) and contact angle measurement in conjunction with chemical derivatisation. In addition, adhesion lap shear tests were performed to evaluate joint strengths of the various functional surfaces with a standard epoxy adhesive. The temperature dependence of the work of adhesion ( $W_{ad}$ ) was measured and the enthalpy ( $H_{ad}$ ) and entropy ( $S_{ad}$ ) estimated.

Contact angle hysteresis had been observed on the various PS systems and can be attributed to the surface reorganisation and/or incorporation of water. Carboxylic acid groups were found to be largely accounted for on the strong adhesion joint strength with epoxy adhesive on the surface treated samples. Acid anhydride copolymers and PVME were found to be adhesion promoters when incorporated onto PS, by both non-reactive and reactive processes. Adhesion strength was further improved after extraction in methanol, which was attributed to the removal



---

of weak boundary layer. In addition, a low level of copolymer was found to be sufficient in achieving about the same adhesion strength as a high loading. Acid anhydride groups present at concentration below the detection limit of XPS were still effective in enhancing adhesion. Styrene maleic anhydride copolymers chains grafted onto untreated PS had proven to be excellent in enhancing adhesion strength when compared to the compounded samples. In comparison, surface treatment has been more effective in promoting high adhesive joint strength than the other modifications.

Entropies and enthalpies of adhesion between water and the treated surfaces were measured and there seems to be some correlation with adhesive joint strength. Changes in enthalpy of adhesion as a result of surface treatment can be readily understand to be due to the polar-polar interactions at the interface. The changes in entropy of adhesion are more complicated but it is suggested that they may be due impart to changes in mobility of water molecules at the interface.

## TABLE OF CONTENTS

	PAGE NO
ACKNOWLEDGEMENTS	i
ABSTRACT	ii
TABLE OF CONTENTS	iv
LIST OF FIGURES	xii
LIST OF TABLES	xvi
LIST OF ABBREVIATIONS AND ACRONYMS	xix
CHAPTER 1      INTRODUCTION	1
CHAPTER 2      LITERATURE SURVEY	3
2.1      Adhesion Theories (Mechanisms)	3
2.1.1      General Adhesion	4
a) Electrical Theory	4
b) Mechanical Theory	4
c) Diffusion Theory	5
d) Adsorption Theory	6
e) Acid-Base Theory	6
f) Weak Boundary Layer (WBL) Theory	6
g) Combination of Theories	7
2.1.2      Adhesion Test Methods	7
2.2      Surface Free Energy	9
2.2.1      Introduction	9
2.2.2      Surface Free Energy and Surface Tension	10

## Table of Contents

<b>2.3</b>	<b>Surface Free Energy Based On Different Approaches</b>	<b>12</b>
2.3.1	Introduction	12
2.3.2	Young's Equation	12
	a) Equilibrium Spreading Pressure	14
2.3.3	Good and Girifalco's Approach	16
2.3.4	Fowkes' Approach	16
2.3.5	Owens and Wendt's Approach	17
2.3.6	Wu's Approach	18
2.3.7	Equation of State Approach	19
2.3.8	Acid-Base Interactions	19
2.3.9	Thermodynamic Work of Adhesion	21
<b>2.4</b>	<b>Hydrophobicity</b>	<b>22</b>
<b>2.5</b>	<b>Temperature Dependence of Surface Free Energy</b>	<b>23</b>
<b>2.6</b>	<b>Temperature Dependence of Contact Angle</b>	<b>25</b>
<b>2.7</b>	<b>Contact Angle Hysteresis</b>	<b>27</b>
2.7.1	Introduction	27
2.7.2	Surface Roughness	28
2.7.3	Surface Chemical Heterogeneity	28
<b>2.8</b>	<b>Compounding</b>	<b>29</b>
2.8.1	Introduction	29
2.8.2	Polystyrene (PS)	29
2.8.3	Styrene Maleic Anhydride (SMA) Copolymers	31
2.8.4	Non-Reactive Compounding	33

## Table of Contents

---

	a) Study of miscibility	33
	b) Non-Compatible Blends	34
	c) Compatible (or Partially Compatible) Blends	34
2.8.5	Reactive Compounding	35
<b>2.9</b>	<b>Surface Modification Methods</b>	<b>37</b>
2.9.1	Introduction	37
2.9.2	Plasma Treatment	38
2.9.3	Corona-discharge Treatment	41
2.9.4	Flame Treatment	44
2.9.5	Chemical Etching	46
2.9.6	Polymer Grafting	47
<b>2.10</b>	<b>Surface Characterisation</b>	<b>49</b>
2.10.1	Introduction	49
2.10.2	Contact Angle Measurement	50
2.10.3	X-ray Photoelectron Spectroscopy (XPS)	51
2.10.4	Chemical Derivatisation	54
2.10.5	Atomic Force Microscopy (AFM)	55
	a) Contact Mode AFM (C-AFM)	58
	b) Non-Contact Mode AFM (NC-AFM)	59
	c) Intermittent Contact Mode AFM (IC-AFM)	59
2.10.6	Attenuated Total Reflection Infrared Spectroscopy (ATR-IR)	60

---

---

<b>CHAPTER 3</b>	<b>EXPERIMENTAL</b>	<b>63</b>
<b>3.1</b>	<b>Materials and Chemicals</b>	<b>64</b>
3.1.1	Standard Polymer	64
3.1.2	Styrene Maleic Anhydride (SMA) Copolymers	64
3.1.3	Solvents and Other Chemicals	64
<b>3.2</b>	<b>Experimental Work</b>	<b>65</b>
3.2.1	Sample Preparation	65
3.2.2	Surface Cleaning of Samples	67
3.2.3	Sample Pretreatments	67
	a) Flame Treatment	67
	b) Chromic Acid Etching	69
3.2.4	Compounding	70
3.2.5	Photo-induced Vapour Grafting	71
3.2.6	Chemical Derivatisation	73
3.2.7	Spin-coating	75
3.2.8	Lap shear Joint Preparation	75
<b>3.3</b>	<b>Methods of Analysis</b>	<b>75</b>
3.3.1	X-ray Photoelectron Spectroscopy	75
3.3.2	Attenuated Total Reflection Infrared Spectroscopy	76
3.3.3	Atomic Force Microscopy	76
3.3.4	Contact Angle	76
	a) Surface Tension of Test Liquid	76
	b) Contact Angle Measurement	77
3.3.5	Adhesion Lap shear Joint Test	79

---

---

<b>CHAPTER 4</b>	<b>RESULTS AND DISCUSSION</b>	<b>81</b>
<b>4.1</b>	<b>Design of the Contact Angle Instrument</b>	<b>81</b>
4.1.1	Introduction	81
4.1.2	Description and Features	82
4.1.3	Software for Contact Angle Measurement	85
4.1.4	Summary	87
<b>4.2</b>	<b>Characterisation of Polystyrene Polymers</b>	<b>88</b>
4.2.1	Introduction	88
4.2.2	X-ray Photoelectron Spectroscopy	88
4.2.3	Attenuated Total Reflection Infrared Spectroscopy	89
4.2.4	Atomic Force Microscopy	91
4.2.5	Contact Angle Measurement	92
4.2.6	Summary	93
<b>4.3</b>	<b>Characterisation of Styrene Maleic Anhydride Copolymers</b>	<b>94</b>
4.3.1	Introduction	94
4.3.2	X-ray Photoelectron Spectroscopy	94
4.3.3	Attenuated Total Reflection Infrared Spectroscopy	97
4.3.4	Atomic Force Microscopy	102
4.3.5	Contact Angle Measurement	102
4.3.6	Summary	104
<b>4.4</b>	<b>Surface Treatment</b>	<b>106</b>
4.4.1	Introduction	106
4.4.2	X-ray Photoelectron Spectroscopy	106
4.4.3	Atomic Force Microscopy	109

---

## Table of Contents

---

4.4.4	Contact Angle Measurement	111
4.4.5	Adhesion	114
4.4.6	Summary	115
<b>4.5</b>	<b>Non-Reactive Compounding</b>	<b>116</b>
4.5.1	Introduction	116
4.5.2	X-ray Photoelectron Spectroscopy	116
4.5.3	Attenuated Total Reflection Infrared Spectroscopy	120
4.5.4	Atomic Force Microscopy	121
4.5.5	Contact Angle Measurement	124
4.5.6	Adhesion	126
4.5.7	Summary	129
<b>4.6</b>	<b>Reactive Compounding</b>	<b>130</b>
4.6.1	Introduction	130
4.6.2	X-ray Photoelectron Spectroscopy	130
4.6.3	Attenuated Total Reflection Infrared Spectroscopy	134
4.6.4	Atomic Force Microscopy	135
4.6.5	Contact Angle Measurement	137
4.6.6	Adhesion	139
4.6.7	Summary	141
<b>4.7</b>	<b>Grafting</b>	<b>143</b>
4.7.1	Introduction	143
4.7.2	X-ray Photoelectron Spectroscopy	143
4.7.3	Contact Angle Measurement	144
4.7.4	Adhesion	146
4.7.5	Summary	147

---

## Table of Contents

<b>4.8</b>	<b>Temperature Dependence Contact Angle Measurement</b>	<b>149</b>
4.8.1	Introduction	149
4.8.2	Evaluation of Equilibrium Spreading Pressure	149
4.8.3	Effect of Temperature on the Work of Adhesion	151
	a) Untreated Polystyrene	151
	b) Styrene Maleic Anhydride Copolymers	153
	c) Surface Treated Polystyrene	155
	d) Non-reactively Compounded Polystyrene	158
	e) Reactively Compounded Polystyrene	163
	f) Grafted Polystyrene	168
4.8.4	Enthalpy and Entropy of Adhesion	170
4.8.5	Summary	173
<b>CHAPTER 5</b>	<b>CONCLUSIONS</b>	<b>174</b>
<b>5.1</b>	<b>Surface Treatment</b>	<b>174</b>
<b>5.2</b>	<b>Non-Reactive Compounding</b>	<b>175</b>
<b>5.3</b>	<b>Reactive Compounding</b>	<b>175</b>
<b>5.4</b>	<b>Grafting</b>	<b>176</b>
<b>5.5</b>	<b>Cross Comparison of Systems</b>	<b>176</b>
<b>5.6</b>	<b>Enthalpy and Entropy of Adhesion</b>	<b>176</b>



## Table of Contents

---

<b>CHAPTER 6</b>	<b>REFERENCES</b>	<b>178</b>
 <b>APPENDICES</b>		 <b>196</b>
Appendix A		196
Appendix B		198
Appendix C		200

---

**LIST OF FIGURES**

- 2.1** Some commonly used adhesion test methods.
- 2.2** A liquid drop on a substrate.
- 2.3** The work of separation defined by two states.
- 2.4** Surface free energy of liquid water as a function of temperature.
- 2.5** Mechanism of styrene monomer production.
- 2.6** PS chemical structure.
- 2.7** SMA chemical structure.
- 2.8** Basic steps in free radical initiation mechanism.
- 2.9** Schematic of plasma treatment unit.
- 2.10** Mechanism of oxygen-plasma treatment.
- 2.11** Schematic of corona-discharge treatment.
- 2.12** Mechanism of corona-discharge treatment in an oxygen containing gas.
- 2.13** Schematic of flame treatment.
- 2.14** Mechanism of grafting polymerisation.
- 2.15** Schematic representation of the photoemission process.
- 2.16** Schematic diagram of a typical atomic force microscope.
- 2.17** Force/distance curve of AFM tip/sample interactions.
- 2.18** Schematic diagram of a multiple reflection ATR system.
  
- 3.1** Assemblies of the moulding of PS plaques.
- 3.2** Schematic diagram of flame treatment rig (used in laboratory).
- 3.3** Flow chart illustrating the compounding procedures.
- 3.4** Schematic diagram of UV-induced apparatus set up.
- 3.5** Schematic of vacuum frame.
- 3.6** Schematic diagram of lap shear assembled test piece.
  
- 4.1** In house contact angle apparatus.
- 4.2** Schematic diagram of optical setup.

---

<b>4.3</b>	An enlarged diagram in plan view.
<b>4.4</b>	A left-hand side of the contact angle liquid drop.
<b>4.5</b>	XPS broad scan of untreated PS.
<b>4.6</b>	ATR-IR spectrum of untreated PS.
<b>4.7</b>	AFM scan of untreated PS.
<b>4.8</b>	Reaction of SMA copolymers with derivatising agent TFE in full conversion.
<b>4.9</b>	Reaction of SMA copolymers with derivatising agent TFE in partial conversion.
<b>4.10</b>	ATR-IR spectrum of SMA 50:50 copolymer.
<b>4.11</b>	ATR-IR spectrum of SMA 66:34 copolymer.
<b>4.12</b>	ATR-IR spectrum of SMA 75:25 copolymer.
<b>4.13</b>	Correlation of peak ratio and molar ratio of SMA copolymers.
<b>4.14</b>	Correlation of contact angle hysteresis and number of maleic anhydride groups.
<b>4.15</b>	XPS broad scan of flame treated PS.
<b>4.16</b>	XPS broad scan of chromic acid treated PS.
<b>4.17</b>	AFM scan of flame treated PS.
<b>4.18</b>	AFM scan of chromic acid treated PS.
<b>4.19</b>	Effect of contact angles of surface treated PS subjected to thermal treatment.
<b>4.20</b>	XPS broad scan of PS-SMA 66:34 of 0.1% loading.
<b>4.21</b>	XPS broad scan of PS-SMA 66:34 of 1% loading.
<b>4.22</b>	XPS broad scan of PS-SMA 66:34 of 10% loading.
<b>4.23</b>	AFM scan of non-reactively compounded PS-SMA 66:34 10% loading before extraction.
<b>4.24</b>	AFM scan of non-reactively compounded PS-SMA 66:34 10% loading after extraction.
<b>4.25</b>	Effect of adhesive joint strength on non-reactively compounded PS-SMA compositions.
<b>4.26</b>	XPS broad scan of PS-SMA 66:34 of 0.1% loading.

---

---

<b>4.27</b>	XPS broad scan of PS-SMA 66:34 of 1% loading.
<b>4.28</b>	XPS broad scan of PS-SMA 66:34 of 10% loading.
<b>4.29</b>	AFM scan of reactively compounded PS-SMA 66:34 10% loading before extraction.
<b>4.30</b>	AFM scan of reactively compounded PS-SMA 66:34 10% loading after extraction.
<b>4.31</b>	Effect of adhesive joint strength on reactively compounded PS-SMA compositions.
<b>4.32</b>	Effect of temperature on contact angles of untreated PS.
<b>4.33</b>	Effect of temperature on work of adhesion of untreated PS.
<b>4.34</b>	Effect of temperature on contact angles of SMA 66:34 copolymer.
<b>4.35</b>	Effect of temperature on work of adhesion of SMA 66:34 copolymer.
<b>4.36</b>	Effect of temperature on contact angles of flame treated PS.
<b>4.37</b>	Effect of temperature on work of adhesion of flame treated PS.
<b>4.38</b>	Effect of temperature on contact angles of chromic acid treated PS.
<b>4.39</b>	Effect of temperature on work of adhesion of chromic acid treated PS.
<b>4.40</b>	Effect of temperature on contact angles of non-reactively compounded PS-SMA 66:34 1% loading.
<b>4.41</b>	Effect of temperature on work of adhesion of non-reactively compounded PS-SMA 66:34 1% loading.
<b>4.42</b>	Effect of temperature on contact angles of non-reactively compounded PS-SMA 66:34 10% loading.
<b>4.43</b>	Effect of temperature on work of adhesion of non-reactively compounded PS-SMA 66:34 10% loading.
<b>4.44</b>	Effect of temperature on contact angles of non-reactively compounded PS-PVME 1% loading.
<b>4.45</b>	Effect of temperature on work of adhesion of non-reactively compounded PS-PVME 1% loading.
<b>4.46</b>	Effect of temperature on contact angles of non-reactively compounded PS-PVME 10% loading.

---

- 4.47** Effect of temperature on work of adhesion of non-reactively compounded PS-PVME 10% loading.
- 4.48** Effect of temperature on contact angles of reactively compounded PS-SMA 66:34 1% loading.
- 4.49** Effect of temperature on work of adhesion of reactively compounded PS-SMA 66:34 1% loading.
- 4.50** Effect of temperature on contact angles of reactively compounded PS-SMA 66:34 10% loading.
- 4.51** Effect of temperature on work of adhesion of reactively compounded PS-SMA 66:34 10% loading.
- 4.52** Effect of temperature on contact angles of reactively compounded PS-PVME 1% loading.
- 4.53** Effect of temperature on work of adhesion of reactively compounded PS-PVME 1% loading.
- 4.54** Effect of temperature on contact angles of reactively compounded PS-PVME 10% loading.
- 4.55** Effect of temperature on work of adhesion of reactively compounded PS-PVME 10% loading.
- 4.56** Effect of temperature on contact angles of grafted PS.
- 4.57** Effect of temperature on work of adhesion of grafted PS.

---

**LIST OF TABLES**

---

- 2.1** Calculated spreading pressure of *n*-alkanes on PTFE.
- 2.2** Surface energy parameters of solid surfaces at ~ 20°C.
- 2.3** Temperature dependence of advancing contact angle of the tested liquids on butyl rubber.
  
- 3.1** Measured surface tension of water testing liquid.
- 3.2** Literature values of surface free energy of contact angle liquid.
  
- 4.1** IR wavenumber peak assignments of untreated PS.
- 4.2** Contact angles of untreated PS at ~ 25°C.
- 4.3** Elemental compositions of SMA copolymers at different take-off angles.
- 4.4** Calculated bulk and measured surface ratio of elemental compositions of SMA copolymers.
- 4.5** Calculated and measured ratio of elemental compositions of SMA copolymers after derivatisation.
- 4.6** IR peak assignments of SMA copolymers.
- 4.7** Measured peak ratio of SMA copolymers by ATR-IR.
- 4.8** Contact angles of SMA copolymers at ~25°C.
- 4.9** Elemental compositions of surface treated PS.
- 4.10** Elemental compositions of surface treated PS after chemical derivatisation.
- 4.11** Surface roughness of untreated and surface treated PS.
- 4.12** Contact angles of untreated and surface treated PS at ~ 25°C.
- 4.13** Contact angles of untreated and surface treated PS after derivatisation at ~ 25°C.
- 4.14** Adhesive joint strength of untreated and surface treated PS.
- 4.15** Adhesive joint strength of untreated and surface treated PS after chemical derivatisation.

---

<b>4.16</b>	Elemental compositions of non-reactively compounded PS-SMA 66:34 at different loadings.
<b>4.17</b>	Elemental compositions of non-reactively compounded PS-SMA 66:34 at different loadings after extraction in methanol.
<b>4.18</b>	Effect of derivatisation on non-reactively compounded PS-SMA 66:34 after extraction in methanol.
<b>4.19</b>	Molar ratio at bulk and surface of non-reactively compounded PS-SMA.
<b>4.20</b>	Surface roughness of non-reactively compounded PS-SMA 66:34 before and after extraction in methanol.
<b>4.21</b>	Contact angles of non-reactively compounded PS at ~ 25°C.
<b>4.22</b>	Effect of derivatisation on contact angles of non-reactively compounded PS after extraction at ~ 25°C in methanol.
<b>4.23</b>	Effect of derivatisation on adhesive joint strength of non-reactively compounded PS after extraction in methanol.
<b>4.24</b>	Elemental compositions of reactively compounded PS-SMA 66:34 at different loadings.
<b>4.25</b>	Elemental compositions of reactively compounded PS-SMA 66:34 at different loadings after extraction in methanol.
<b>4.26</b>	Effect of chemical derivatisation on reactively compounded PS-SMA 66:34 after extraction in methanol.
<b>4.27</b>	Molar ratio at bulk and surface of reactively compounded PS-SMA.
<b>4.28</b>	Surface roughness of reactively compounded PS-SMA 66:34 before and after extraction in methanol.
<b>4.29</b>	Contact angles of reactively compounded PS at ~ 25°C.
<b>4.30</b>	Effect of derivatisation on contact angles of reactively compounded PS after extraction at ~ 25°C in methanol.
<b>4.31</b>	Effect of derivatisation on adhesive joint strength of reactively compounded PS after extraction in methanol.
<b>4.32</b>	Elemental compositions of blank and grafted PS.
<b>4.33</b>	Contact angles of blank and grafted PS at ~ 25°C.

---

- 4.34** Effect of derivatisation on contact angles of blank and grafted PS after extraction at  $\sim 25^{\circ}\text{C}$  in methanol.
- 4.35** Adhesive joint strength of blank and grafted PS before and after extraction in methanol.
- 4.36** Effect of derivatisation on adhesive joint strength of blank and grafted PS after extraction in methanol.
- 4.37** Effect of  $\pi_*$  on contact angles of untreated PS.
- 4.38** Effect of  $\pi_*$  on contact angles of chromic acid treated PS.
- 4.39** Work of adhesion ( $W_{ad}$ ), enthalpy ( $H_{ad}$ ) and entropy ( $S_{ad}$ ) of various PS systems at temperature  $30^{\circ}\text{C}$ .



---

**LIST OF ABBREVIATIONS AND ACRONYMS**

---

<b>ABS</b>	<b>acrylonitrile butadiene styrene</b>
<b>AFM</b>	<b>atomic force microscopy</b>
<b>ATR-IR</b>	<b>attenuated total reflection infrared spectroscopy</b>
<b>DIM</b>	<b>diiodomethane</b>
<b>DSC</b>	<b>differential scanning calorimetry</b>
<b>HIPS</b>	<b>high impact polystyrene</b>
<b>LLDPE</b>	<b>linear low density polyethylene</b>
<b>PA</b>	<b>polyamide</b>
<b>PE</b>	<b>polyethylene</b>
<b>PET</b>	<b>poly(ethylene terephthalate)</b>
<b>PMMA</b>	<b>poly(methyl methacrylate)</b>
<b>PP</b>	<b>polypropylene</b>
<b>PS</b>	<b>polystyrene</b>
<b>PTFE</b>	<b>polytetrafluoroethylene</b>
<b>PVC</b>	<b>poly(vinyl chloride)</b>
<b>PVME</b>	<b>poly(vinyl methyl ether)</b>
<b>SAN</b>	<b>styrene acrylonitrile</b>
<b>SBR</b>	<b>styrene butadiene rubber</b>
<b>SPM</b>	<b>scanning probe microscopy</b>
<b>SMA</b>	<b>styrene maleic anhydride</b>
<b>SEM</b>	<b>scanning electron microscopy</b>
<b>SSIMS</b>	<b>static secondary ion mass spectrometry</b>
<b>TFE</b>	<b>trifluoroethanol</b>
<b>THF</b>	<b>tetrahydrofuran</b>
<b>XPS</b>	<b>X-ray photoelectron spectroscopy</b>
<b>WBL</b>	<b>weak boundary layer</b>

## CHAPTER 1 INTRODUCTION

Polymers have excellent bulk properties for a relatively wide range of technological applications. However, adhesion problems often limit their suitability, especially in areas such as printing in the packaging industry, paint adhesion, etc. . This is mainly due to their inherent low surface energy, associated with a relatively low chemical reactivity. For good adhesion, therefore, some form of surface treatment for a polymer is required, e.g. flame, corona, plasma, chemical treatments, etc. .

PS, like polyolefins, has limited adhesion capability without the addition of functional groups. It is thought that the presence of the aromatic ring as a side group bonded to every other carbon atom along the PS chain; a linear hydrocarbon polymer, as the polyolefins, would provide some significant differences to surface treatment and adhesion compared to the polyolefins. This type of repeat group functionality is expected to have an influence on the type of modification produced by surface treatment. Oxidative surface treatment of PS is known to introduce polar functional groups onto its surface, thereby increasing its free surface energy [1 - 3]. The incorporation of functional groups onto PS to increase its adhesion to various substances has enabled polyfunctionalised PS being used for a variety of applications [4, 5].

The start of this research involved constructing a temperature dependent contact angle equipment and a rigorous way of interpreting contact angle results in terms of thermodynamic parameters has been used. This approach has not been extensively used in the past, as one needs to measure a contact angle (i.e. subtended between test liquid droplet on a solid surface), to within  $1^\circ$  for accurate results, since the temperature coefficient of angle is small. With improved illumination, optics, recently introduced methods of digital photography, and software written for digital analysis of images (run by a high speed personal

computer), accurate droplet profiles and angles can be measured reliably and repeatedly. With careful work on well defined surfaces, it is anticipated that the relative enthalpic and entropic contributions due to different functional groups on a polymer's surface could be identified. The results of this work are given in Section 4.8.4

In the rest of the research programme, a number of surface treatments and modifications for PS and analysis techniques were used. PS samples have been subjected to flame and chromic acid treatments and the work of adhesion measured by the temperature dependence contact angle equipment was analysed. Having understood the relationship of the thermodynamic properties of normal PS and surface treated functionalised PS by quantitative means, the technique was further utilised to examine the action of other functional groups introduced by other methods onto PS. These involved the incorporation of low molecular weight copolymer, styrene maleic anhydride (SMA) and poly(vinyl methyl ether) (PVME) into and onto PS, by non-reactive and reactive compounding in vary concentrations. It has been thought that the low molecular weight functional groups would have the mobility to migrate or segregate to the PS's surface. Grafting of copolymer chains onto PS was also carried out in the vapour phase.

In addition, adhesion tests using a standard epoxy resin, (anticipated to be able to react across the interface with the acid groups [6]), was performed using the single lap shear test method and the strengths recorded. Chemical derivatisation blocks the acid functional groups at the surface, so making them inactive, preventing certain chemical reactions at the interface and the resulting reduction of adhesion strengths were measured thereafter. In this way, the contributions of specific functional groups to adhesion can be identified.

The aims of this research were to examine and compare the surface, adhesion effects and work of adhesion of functionalised PS produced by surface treatments, non-reactive compounding, reactive compounding and grafting.

## **CHAPTER 2 LITERATURE SURVEY**

In this chapter, the literature survey, will cover the issues of polymer surface free energy, in terms of thermodynamic theory, and provide a background to compounding, surface modification and characterisation.

### **2.1 ADHESION THEORIES (MECHANISMS)**

Adhesion may be defined as the state in which interfacial forces, which may consist of valence forces or interlocking action or both, hold two surfaces together. An adhesive is defined as a material, which when applied to the surface of another material, will join them together so that they resist separation. Many authors have reviewed adhesion mechanisms [7 - 9]. Usually more than one theory is employed to explain all observed interactions between an adhesive and substrate (i.e. also known as an adherend). The theories commonly employed to explain adhesion could be divided into five mechanisms, namely:

- electrical theory;
- mechanical theory;
- diffusion theory;
- adsorption theory;
- acid-base theory;
- weak boundary layer theory.

### **2.1.1 General Adhesion**

#### **a) *Electrical Theory***

Deryaguin et. al. [10 - 12] have suggested that if an adhesive and substrate have different electronic band structures then there will be some electron transfer on contact, in order to balance the Fermi levels. This will result in the formation of a double layer of electrical charge at the interface. It has been demonstrated in a peel test experiment, that some of the joints were found to be charged upon separation [11].

It has been suggested that the electrostatic forces between the charged surfaces might contribute significantly to adhesion. This statement has led to a debate and criticisms from many authors [13 - 16]. Wake [17] has reviewed the electrical double layer theory and concluded that, when films of adhesive substances adhere to substrates, the electrical phenomena observed when they are peeled or otherwise separated, does not contribute appreciably to the force required to complete the separation.

#### **b) *Mechanical Theory***

This theory proposes that an adhesive fills the irregularities or interstices (e.g. pores, cracks, holes, etc.) in an adherend's surface, hence providing mechanical interlocking once the adhesive is solidified. This effect can be enhanced by some surface pretreatments, such as mechanical abrasion or chemical etching, which increase the roughness of a substrate's surface, enabling the adhesive to come into close contact with a greater surface area. It should be noted that due to the high viscosity of the adhesive or low surface free energy of the adherend, an adhesive might not be able to penetrate completely into the irregularities. This is likely to lead to the formation of voids and weaken the joint.

---

There has been a suggestion that increasing the surface roughness will improve the bond strength in certain systems. Jennings [18] has reported that Packham et. al. have shown that improved adhesion between PE and metal is achieved if the metal surface is roughened. On the other hand, Tabor [19, 20] has demonstrated that good adhesion can be achieved between two smooth mica surfaces. The mechanical factors cannot therefore be the only ones contributing to adhesion.

### **c) Diffusion Theory**

This theory proposed by Voyutskii [15, 21, 22], states that the adhesion between two polymers is due to mutual migration or interdiffusion across the developed interface. This happens only when the molecules have sufficient mobility to migrate i.e. above their glass transition temperature,  $T_g$  and in a plasticised state and the polymers must be mutually soluble, i.e. their solubility parameters must be similar. The solubility parameter is an index of compatibility of two components. The basis of using solubility parameters is that substances with similar values are compatible. These requirements are mostly found in the auto-adhesion of elastomers, and in the solvent or thermal welding of similar plastics.

Voyutskii has supported these views with evidence based upon contact time, temperature and pressure. Vasenin has developed a mathematical model for the diffusion theory of adhesion based upon Fick's laws [23 - 25]. He predicted that with a diffusion coefficient of  $10^{-18} \text{ m}^2 \text{ s}^{-1}$ , it takes approximately 100 hours for polymer chain segments of polybutylene sheets to penetrate each other to the depth of 10  $\mu\text{m}$ . This happened in cases where the same materials are studied. On the other hand, where the solubility parameters differ, no interdiffusion has been detected. This theory has been extend to polymer/metal systems but has not been successful [17], hence is thought to be an unlikely phenomenon.

---

**d)     *Adsorption Theory***

According to this theory many types of forces may act across the interface. This theory proposed that, when there is intimate molecular contact across the interface, adhesion would occur due to intermolecular forces. These forces include Van der Waals' forces and hydrogen bonding. Van der Waals' forces include London (dispersion), Keesom (dipole-dipole) and Debye (dipole-induced dipole) forces. These forces differ in strength and give rise to energies of interaction in the range from about 2 to 50 kJ mol<sup>-1</sup> [26]. It is from this theory that the surface and interfacial thermodynamic models have developed, permitting calculation of surface free energy. In some cases, a substrate may react chemically with an adhesive. The chemical bond is stronger than Van der Waals' interactions having typical values of 200 to 500 kJ mol<sup>-1</sup>. Chemical bonding at an interface can lead to high adhesive bond strength [27].

**e)     *Acid-Base Theory***

The adhesion mechanisms also involve the formation of acid-base interactions across the interface [28]. The acid-base term arises as a result of interactions between Lewis-acids (electrophiles) and Lewis bases (nucleophiles). This theory will be further explained in Section 2.3.8.

**f)     *Weak Boundary Layer (WBL) Theory***

Bikerman [29] was the first to propose the WBL theory. He suggested that if a region of low cohesive strength occurred between an adhesive and an adherend, then low bond strength would result. This region is the 'weak boundary layer' and could arise from the adhesive, adherend or from the surrounding environment. These environmentally induced WBL may include the presence of contaminants,

---

e.g. dust, silicones, grease, etc. . These also include low molecular weight materials, e.g. stabilisers, plasticisers, etc., which may migrate from the bulk of a material (especially polymers) to the surface of the substrate. Published work on polyolefins and fluoropolymers in this area has been reviewed by Brewis [30].

### **g) Combination of Theories**

There has been a suggestion that the overall measured adhesion can be due to a combination of all the theories [31]. That is,

$$\psi = a\psi_E + b\psi_M + c\psi_D + d\psi_A + \dots \quad \{2.1\}$$

where  $\psi$  is the overall adhesion. Subscripts  $E$ ,  $M$ ,  $D$  and  $A$  represent electrical, mechanical, diffusion and adsorption contribution to the adhesion, respectively. Coefficients  $a$ ,  $b$ ,  $c$  and  $d$  are their respective constants. Other theories also include the effect of substrate [32] and the plastic deformation where there is viscoelastic energy loss resulting in more bulk energy dissipation, thus leading to higher overall measured adhesion [33, 34].

### **2.1.2 Adhesion Test Methods**

During the process of adhesion, an adhesive is usually applied in the form of a fluid, which is then allowed to solidify to form a strong coherent material. The adhesives used are commonly thermosetting polymers, e.g. epoxides, polyurethanes, acrylics, etc. [35]. A joint is cured at room or elevated temperature and pressure may often be applied to the joint to maximise bonding, e.g. aiding spreading. Other adhesives also include pressure sensitive systems and hot melts, which harden by cooling [35]. The strength of the joint will, in general, depend on the testing rate, temperature and joint geometry.



Different types of test are employed to evaluate the adhesion levels, depending on the nature of the sample [36]. Figure 2.1 shows some of the commonly used test methods.

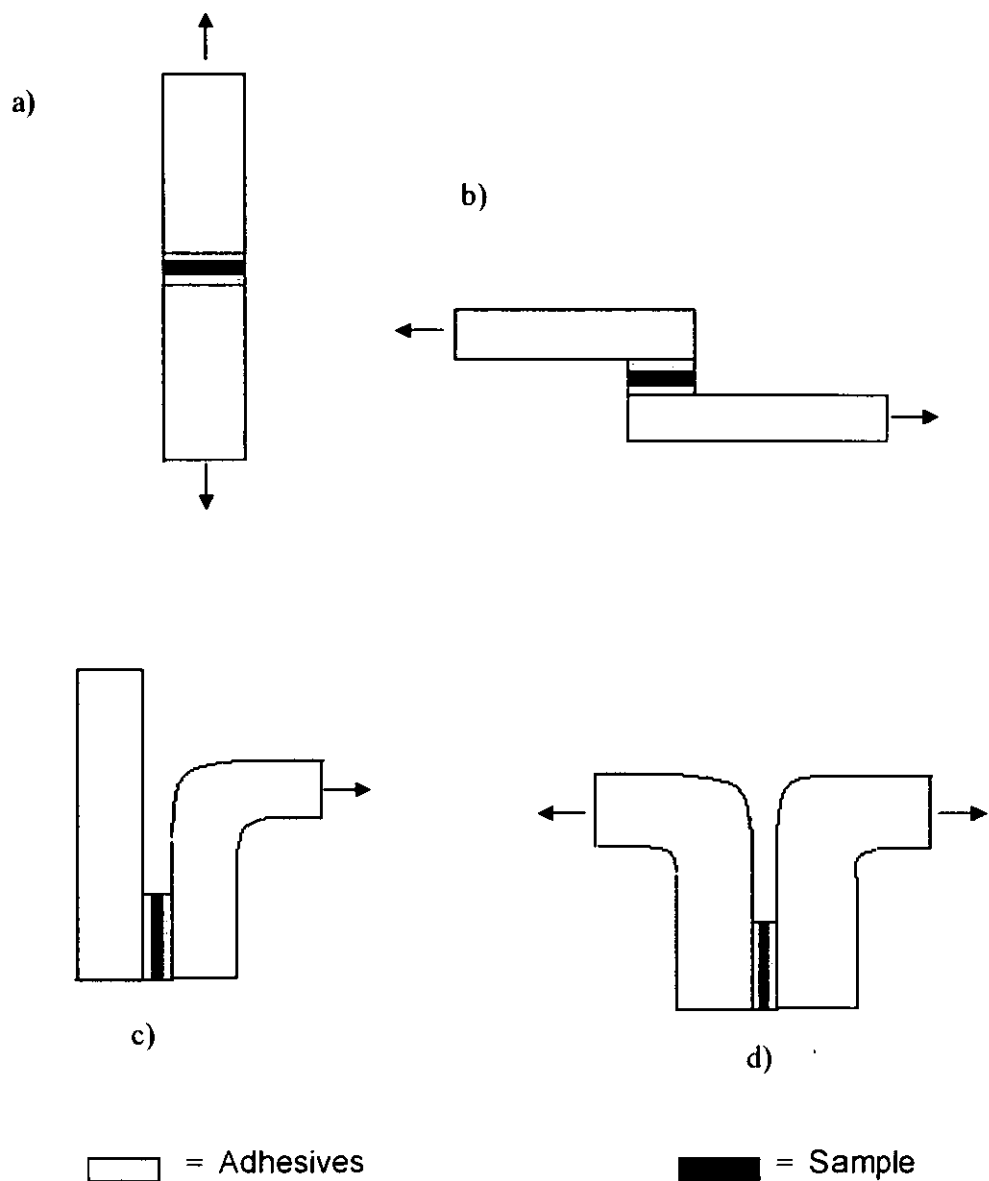


**Figure 2.1** Some commonly used adhesion test methods. a) tensile, b) single lap shear, c) 90° peel and d) T-peel.

## 2.2 SURFACE FREE ENERGY

### 2.2.1 Introduction

A review [37] of molecular interactions occurring at interfaces, shows that wetting can be described in terms of thermodynamic parameters, such as surface and interfacial free energies, which characterise the interacting materials. Surfaces which have a surface free energy  $>100 \text{ mJ m}^{-2}$ , are classified as high energy surfaces and include inorganic solids, glasses and metals. Low energy surfaces will have surface free energy  $<100 \text{ mJ m}^{-2}$  and include all organic liquids, waxes and organic polymeric solids.

When a drop of liquid is placed on a solid surface, it will make a contact angle,  $\theta$ , with the surface, see Figure 2.2. Contact angles may be used to study surface energy, wettability and adhesion on low surface energy materials like polymers. This measurement has been used extensively to indirectly monitor changes in the surface composition, because it is sensitive to the chemical composition of the surface monolayers. Contact angles are often measured in conjunction with spectroscopic techniques such as X-ray photoelectron spectroscopy (XPS). This will be discussed in more detail in Section 2.10.2. Figure 2.2 shows the contact angle ( $\theta$ ) made by a liquid drop on a substrate.

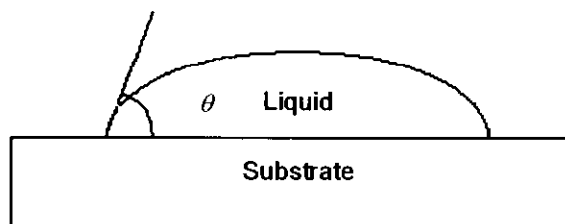


**Figure 2.2** A liquid drop on a substrate.

---

### 2.2.2 Surface Free Energy and Surface Tension

Atoms and molecules at the surface of an adherend or adhesive are in an environment markedly different from the environment of their bulk counterparts [38, 39]. In the bulk phase of a material, molecules are attracted in all directions, by their neighbouring molecules and atoms and thus, in a symmetrical force field. In contrast, molecules at the very surface are surrounded by fewer like neighbours and so subjected to less intermolecular attraction from their neighbours, as there are no like atoms or molecules above them. This anisotropic distribution of these neighbours is a characteristic only of a surface [39]. The surface molecules are thus in a state of higher free energy than those in the bulk phase.

There is, then, a free energy change associated with the isothermal, reversible formation of a liquid surface and which is termed the surface free energy or excess surface free energy ( $G^S$ ). The terms are often used to mean specific (i.e. per unit area) surface free energy, the unit of which is  $\text{mJ m}^{-2}$ . It is noted that this surface free energy is not the total free energy of the surface molecules, but rather the excess free energy, which the molecules possess by the virtue of their being in the surface. The atoms and molecules tend to leave the surface region due to a Boltzman distribution between two states of different energy. At equilibrium the lower density at the surface means that the intermolecular distance is greater and hence puts the surface under tension. This is equivalent to saying that the surface itself is in a state of lateral tension and leads to the concept of surface tension ( $\gamma$ ), which is a direct result of the intermolecular forces at the surface. The unit of surface tension is  $\text{mN m}^{-1}$ .

Therefore, the specific surface excess free energy ( $G^S$ ), is defined as the reversible work done in creating unit area of fresh, flat, free surface ( $A$ ) by a process of division [40] and surface tension ( $\gamma$ ) is the tangential stress in the surface layer.

Though these two are often used interchangeable, they are not necessarily the same. The relationship between  $\gamma$  and  $G^s$  is shown below [37, 41 - 43],

$$\gamma = G^s + A \left( \frac{\partial G^s}{\partial A} \right)_{T,P} \quad \{2.2\}$$

The difference between the two terms can be explained by considering the production of a new surface of a solid or liquid. In the first step, the solid or liquid is divided to produce two surfaces but the atoms and molecules are kept in exactly the same positions that they occupied when they were in the bulk phase. In the second step, the atoms and molecules in the newly formed surfaces are allowed to rearrange to achieve their most stable equilibrium configuration.

The liquid surface is always at equilibrium, therefore the last term in Equation {2.2} must, by definition, be zero. This means the surface tension is equal to the specific surface free energy, that is  $\gamma = G^s$ . On the other hand, in a solid system, the second step of molecule rearrangement will occur much more slowly, due to the immobility of the surface molecules [44]. Therefore, the solid surface may be stretched or compressed with no change in the number of atoms or molecules, and in this case, the last term in Equation {2.2} is not equal to zero, hence  $\gamma \neq G^s$  and the relationship between  $\gamma$  and  $G^s$  is governed by Equation {2.2}. Solid surfaces are rarely at thermodynamic equilibrium.

## 2.3 SURFACE FREE ENERGY BASED ON DIFFERENT APPROACHES

### 2.3.1 Introduction

When a liquid is brought into contact with a solid, a solid/liquid ( $SL$ ) interface is created, the energy of which depends on the natures of the two dissimilar materials. The degree of wettability is indicated by the value of the contact angle ( $\theta$ ). If  $\theta = 0^\circ$ , then the liquid is said to have maximum interfacial contact with the solid, which is hence said to be completely wetted.

Several methods have been devised that allow the measurement of contact angles on a solid, which are included in the list below [45],

- equilibrium sessile drop method
- advancing & receding drop method (used in this research)
- advancing and receding bubble
- drop on a tilted plate

### 2.3.2 Young's Equation

A drop of pure liquid resting on a smooth, homogeneous, rigid and isotropic solid surface, gives the following relationship when the drop is at equilibrium,

$$G_{SV}^s = G_{SL}^s + G_{LV}^s \cos \theta \quad \{2.3\}$$

where  $G_{SV}^s$  is the surface free energy of the solid in equilibrium with vapour of the contact angle liquid,  $G_{SL}^s$  is the surface free energy of the solid/liquid interface,  $G_{LV}^s$

is the surface free energy of the liquid in equilibrium with its vapour and  $\theta$  is the contact angle of the liquid drop on the surface. This equation is known as Young's equation [46].

As the wetting ability of a liquid on the solid surface is important in practical problems of adhesion or lubrication, much work has been carried out to determine the interfacial energies. In Figure 2.3, two states are presented for an interface, before and after separation. The thermodynamic work of adhesion ( $W_{ad}$ ) is the reversible work done in separation of unit area of solid/liquid interface. This is given by,

$$W_{ad} = G_{SV}^S + G_{LV}^S - G_{SL}^S \quad \{2.4\}$$

Equation {2.4} is known as Dupré's equation.

By combining Equations {2.3} and {2.4}, an expression for contact angle is obtained; this is the Young-Dupré equation,

$$W_{ad} = G_{LV}^S (1 + \cos \theta) \quad \{2.5\}$$

This implies that if a liquid of known surface free energy,  $G_{LV}^S$  is used, and the contact angle ( $\theta$ ) measured, then the value of  $W_{ad}$  can be obtained. The equation is true for all low energy surfaces that exhibit a single unique contact angle.

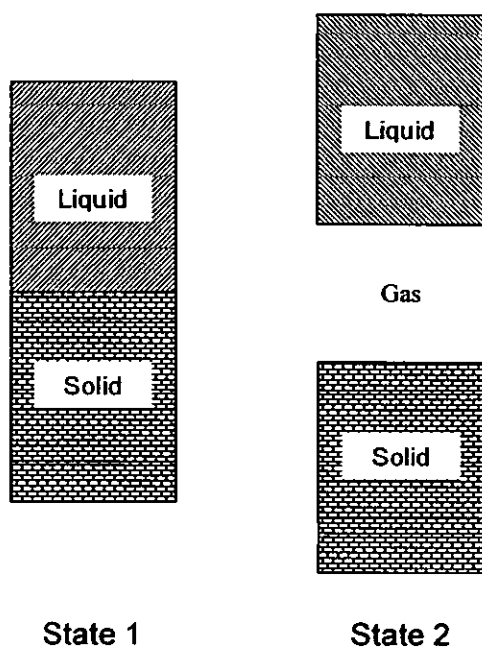


**Figure 2.3** The work of separation defined by two states.

**a) Equilibrium Spreading Pressure**

When a liquid makes contact with a solid surface, the surface is said to be wetted. If the solid adsorbs the liquid's vapour, then the solid surface free energy,  $G_s^s$ , is reduced to  $G_{sv}^s$ . The adsorption of vapour on a solid surface will change the surface free energy of the solid. The change will be greatest when there is high affinity for the solid. The lowering of surface free energy is known as the equilibrium spreading pressure,  $\pi_e$ , and is given by,

$$\pi_e = G_s^s - G_{sv}^s \quad \{2.6\}$$

where  $G_s^s$  is the surface free energy of the solid in a vacuum and  $G_{sv}^s$  is the surface free energy when in equilibrium with the saturated vapour. Spreading pressure can be measured from vapour adsorption using Equation {2.7},

$$\pi_s = \int_{p_o}^p \Gamma_s d\mu = RT \int_{p_o}^p \Gamma_s d(\ln p) \quad \{2.7\}$$

where  $p$  is the vapour pressure,  $p_o$  is the saturated vapour pressure,  $\Gamma$  is the number of moles adsorbed per unit area and  $\mu$  is the chemical potential of the adsorbate (i.e. the adherend).

There is a general belief that,  $\pi_s$  is usually negligible when  $\theta > 10^\circ$ , such that  $G_s^s = G_{sv}^s$  [48]. Values of  $\pi_s$  have been found and reported to be negligible for liquids that have a non-zero contact angle on low surface energy substrates such as polymers [43]. Likewise, Good [49] has shown that there is reason to believe that  $\pi_s$  is probably negligible on homogeneous, low energy solids for pure liquids that form non-zero contact angles. In his paper [49], he has reported data with values of  $\pi_s$  calculated for  $n$ -alkanes tested on polytetrafluoroethylene (PTFE), see Table 2.1.

**Table 2.1** Calculated spreading pressure of  $n$ -alkanes on PTFE.

	$\theta / ^\circ$	$\pi_s / \text{mJ m}^{-2}$
Hexadecane	72	$1.5 \times 10^{-4}$
Octane	56	$2.3 \times 10^{-2}$
Pentane	0	0.23
Butane	0	0.48

He concluded that the calculated  $\pi_s$  is negligible for alkanes  $C_7$  or higher on PTFE, i.e. when  $\theta > 0$ .



### 2.3.3 Good and Girifalco's Approach

Girifalco and Good [50] introduced an interaction parameter,  $\phi$ , by which work of adhesion between two phases could be evaluated, i.e.,

$$W_{ad} = 2 \phi (G_s^s G_L^s)^{0.5} \quad \{2.8\}$$

This interaction parameter may be estimated from the molecular properties of both phases. Therefore, if  $\phi$  and  $G_L^s$  are known, then  $G_s^s$  may be determined from Equations {2.5} and {2.8}. For common systems, the  $\phi$  lies between 0.5 and 1.2. However, this method of calculating  $W_{ad}$  is seldom used since it requires a precise knowledge of the exact compositions of the interacting surfaces. The reader is referred to other papers for further details [50 - 54].

### 2.3.4 Fowkes' Approach

Fowkes was the first to propose the theory of fractional polarity [55 - 59]. He suggested that the surface free energy of a solid could be given by the sum of several independent contributions arising from dispersion interactions, polar interactions and hydrogen bonding interaction, i.e.,

$$G_s^s = G_s^d + G_s^p + G_s^h \quad \{2.9\}$$

where  $G_s^s$  is the surface free energy of the solid,  $G_s^d$  is the dispersion component of the surface free energy,  $G_s^p$  is the polar component of the surface energy and  $G_s^h$  is the hydrogen bonding component of surface free energy. Often the hydrogen bonding and polar components are encompassed in the single term  $G_s^p$ .

Fowkes suggested that a non-polar solid could not interact with a polar liquid through a permanent dipole. He proposed that the thermodynamic work of adhesion might be given by the following relationship using the geometric mean approximation for dispersion force interactions,

$$W_{ad} = 2 (G_S^d G_L^d)^{0.5} \quad \{2.10\}$$

The above equation allows the calculation of dispersion component of free energy of solid when the dispersion component of free energy of liquid and  $W_{ad}$  are known.

### 2.3.5 Owens and Wendt's Approach

Owens and Wendt [60, 61] extended Fowkes' equation by employing a theory of fractional polarity to approximate the surface free energy of solids. This was done by resolving the surface energy into contributions from dispersion and polar forces and considering the hydrogen bonding forces and the polar contribution as a single component. This then leads to a more comprehensive relationship of the interfacial free energy and its components,

$$W_{ad} = 2 (G_S^d G_L^d)^{0.5} + 2 (G_S^p G_L^p)^{0.5} \quad \{2.11\}$$

Hence, by measuring the contact angles of two or more liquids of known  $G_L^d$  and  $G_L^p$ , it is possible to evaluate the  $G_S^p$  and  $G_S^d$  of solids, using Equation {2.12}, obtained by combining Equations {2.5} and {2.11},

$$W_{ad} = G_L^s (1 + \cos\theta) = 2 (G_S^d G_L^d)^{0.5} + 2 (G_S^p G_L^p)^{0.5} \quad \{2.12\}$$

Owens and Wendt [60] demonstrated that, with their method, they were able to achieve reasonable agreement with data generated by Zisman's ( $\gamma_c$ ) and Fowkes' ( $\gamma^d$ ) methods. They suggested that their method is also useful for semi-quantitative measure of surface composition, since  $G_s^d$  and  $G_s^h$  are both sensitive to surface composition.

There is some debate as to whether this geometric mean approach is the best way of approximating the polar interactions at an interface. It has been suggested that the geometric mean could be replaced by the arithmetic, anharmonic or harmonic mean approaches in certain circumstances [62 - 64].

Nevertheless, the geometric mean approximation has remained popular and widely used, as the measurements involved are simple and require no prior knowledge of the surface concerned. Table 2.2 gives surface energies for some polymers (see List of Abbreviations and Acronyms) determined by this method.

**Table 2.2** Surface energy parameters of solid surfaces at  $\sim 20^\circ\text{C}$  [35].

Polymers	$G_s^d / \text{mJ m}^{-2}$	$G_s^p / \text{mJ m}^{-2}$	$G_s^s / \text{mJ m}^{-2}$
PTFE	18.6	0.5	19.1
PP	30.2	0.0	30.2
PMMA	35.9	4.3	40.2
PA 66	35.9	4.3	40.2
PVC	40.0	1.5	41.5
PS	41.4	0.6	42.0

### 2.3.6 Wu's Approach

Wu [62] has used a harmonic mean method to calculate the forces acting across the interface, and proposed the following equation,

---


$$G_{SL} = G_S + G_L - \frac{4 G_S^d G_L^d}{G_S^d + G_L^d} - \frac{4 G_S^p G_L^p}{G_S^p + G_L^p} \quad \{2.13\}$$

He claimed that this equation give more consistent results for the interfacial free energy between low energy systems, such as liquids on polymers and adhesives on polymers, while geometric means are more appropriate for high energy systems, such as adhesives on metals [42]. Good [49] has shown that part of the equation is invalid. It had been found that this method gave higher  $G_s^d$  values and significantly higher  $G_s^p$  for untreated PP [6].

### 2.3.7 Equation of State Approach

Ward and Neumann [65] have suggested an approach by considering an equation of state and thermodynamic theory,

$$G_{SL} = G_S (G_{SV} , G_{LV}) \quad \{2.14\}$$

which means that the interfacial free energy is only a function of the total solid and liquid surface free energies. Spelt et. al. [66] reported the contact angles of two liquids with different polarities on the same solid were identical, if their total surface tensions were equal. Their finding is consistent with the equation of state approach.

### 2.3.8 Acid-Base Interactions

As stated earlier, all polar interactions are often combined into a single term,  $G^p$ . However, it has been suggested that the primary polar interactions across an interface are due to electron donor-acceptor interactions (i.e. maybe interpreted by

a Lewis acid-base approach). These interactions are principally hydrogen bonding and therefore may be considered separately [67, 68]. As a consequence, the work of adhesion,  $W_{ad}$  is written in terms of the work of adhesion due to London-dispersion interactions,  $W^d$  and the work of adhesion due to acid-base interactions,  $W^{AB}$ :

$$W_{ad} = W^d + W^{AB} \quad \{2.15\}$$

A solid surface can be probed using a variety of liquids having different acid/base characteristics. These acid/base characteristics are obtained by measurement of the interaction energies of the various molecules concerned, in a neutral solvent.

A theory was developed centring on the enthalpy of neutralisation the acid and basic sites,

$$W_{AB} = - f n_{AB} \Delta H_{AB} \quad \{2.16\}$$

where  $n$  is the number of acid/base pairs per unit area,  $f$  is a factor that converts the enthalpy per unit area to surface free energy and is assumed to have a value equal or near unity and  $\Delta H_{AB}$  is the enthalpy of neutralisation [69, 70].

Drago and colleagues [69, 70] suggested that summing dispersion and acid/base interactions could approximate intermolecular interactions in solution. That is, the characterisation of different Lewis acids,  $A$  and bases,  $B$ , by two constants  $C$  and  $E$  was possible by measurement of the enthalpy of neutralisation for those acids and bases in a neutral solvent,  $\Delta H_{AB}$ ,

$$-\Delta H_{AB} = C_A C_B + E_A E_B \quad \{2.17\}$$

However, the usefulness of this method for the practical evaluation of surface free energies/acid-base characteristics is somewhat limited through the lack of Drago coefficient  $C$  and  $E$ , which can be difficult to find.

A study undertaken by Hutterer and co-workers [71] showed that different values of  $W_{ad}$  could be obtained, when the pH value of a test liquid is varied from 1 to 14. Their work shows the importance of analysing the type of acid or base used, as the nature of the counter ion will strongly influence the interactions with the surface of the solids and thus the work of adhesion.

### 2.3.9 Thermodynamic Work of Adhesion

As mentioned earlier, the thermodynamic work of adhesion,  $W_{ad}$ , is defined as the reversible work done in separation of unit area of solid/liquid interface. The thermodynamic work of adhesion will have entropic ( $S_{ad}$ ) and enthalpic ( $H_{ad}$ ) contributions. The work of adhesion is [72 - 75],

$$W_{ad} = H_{ad} - TS_{ad} \quad \{2.18\}$$

$W_{ad}$  is measured by contact angle at a range of temperatures and  $S_{ad}$  is given by

$$S_{ad} = - \left( \frac{\partial W_{ad}}{\partial T} \right), \quad \{2.19\}$$

Combining Equation {2.5} and Equation {2.18} gives

$$W_{ad} = G_L^s (1 + \cos\theta) = H_{ad} - TS_{ad} \quad \{2.20\}$$

---

where

$$H_{ad} = H_s + H_L - H_{SL} \quad \{2.21\}$$

and

$$S_{ad} = S_s + S_L - S_{SL} \quad \{2.22\}$$

$S_s$  is the entropy of the solid (e.g. a polymer),  $S_L$  is the entropy of liquid (e.g. water) and  $S_{SL}$  is the entropy of interfacial between polymer and water. From the temperature dependence of  $W_{ad}$ , it is possible to evaluate the behaviour of  $S_{ad}$  and  $H_{ad}$ . Surface treatment of a non-polar polymer to introduce polar groups onto its surface, would be expected to affect both enthalpy and entropy of adhesion.

## 2.4 HYDROPHOBICITY

Hydrophobic surfaces are characterised by a high contact angle of a water droplet. Theories of interaction across the interface indicate that water and a hydrophobic substance interact only through dispersion forces. Water is a liquid with unusual properties, which have been reviewed extensively in literature [76 - 78]. Relative to other liquids, water has certain anomalous thermodynamic properties, that is, a temperature of maximum density in the liquid phase over a wide range of pressures, an unusually high surface free energy, a minimum in the isothermal compressibility as a function of temperature and a large heat capacity throughout its liquid range. These properties are thought to arise from the ability of water to form tetrahedrally coordinated hydrogen bonds. The hydrogen bond is a strong dipole-dipole interaction. The hydrogen atom is positively polarised and as a result of its small size, the hydrogen atom can interact strongly with nearby

electronegative atoms. Water molecules form *H*-bonds with each other, and this influences their interactions with non-polar molecules that are incapable of forming the *H*-bonds. When non-polar molecules are introduced into water, they disrupt the hydrogen bonding network.

There are ways to salvaging lost *H*-bonds. If the non-polar solute molecule is not too large, it is possible for water molecules to pack around it without giving up any of their hydrogen bonding sites. Example of such arrangements is known as clathrate 'cages', which are formed by water molecules around a dissolved non-polar solute molecule. Such structures are not rigid but labile and their *H*-bonds are not stronger than in pure water, but the water molecules forming these cages are more ordered than in the bulk liquid [79]. Formation of the cage is associated with an increase in order and therefore a decrease in entropy. The entropy change dominates the free energy of mixing between water and non-polar molecules. Ordering of water has also been observed at non-polar surfaces [79]

## 2.5 TEMPERATURE DEPENDENCE OF SURFACE FREE ENERGY

The specific surface excess free energy (maximum available energy per unit area),  $G^s$ , is defined by Equation {2.23},

$$G^s = H^s - TS^s \quad \{2.23\}$$

where  $H^s$  is the specific surface enthalpy, i.e., the heat absorbed by the system per unit surface area created,  $T$  is the temperature and  $S^s$  is the specific surface entropy,  $S^s$  is given by



---


$$\left( \frac{\partial G^s}{\partial T} \right)_P = -S^s \quad \{2.24\}$$

where  $P$  is the pressure. The specific surface entropy can be obtained from temperature dependence of the surface free energy [39]. Surface free energy of polymers varies approximately linearly with temperature [64].

Figure 2.4 presents a typical plot of surface free energy of water decreasing with increasing temperature [80]. Figure 2.4 shows that the surface entropy of water must be positive. This is true for all liquids and it has been suggested that it is due to the greater mobility of surface molecules compared to those in the bulk [72]. Therefore determination of surface free energy as a function of temperature is believed to be a means of providing information about surface structure and entropy.

The specific surface entropy of liquids can be easily measure accurately in this way but measurement of the specific surface entropy values of solid polymers, is more difficult. For a polymer, the values are obtained from extrapolation from melt data or by calculation using the cell model. Van Ness et. al. [81, 82] described a cell model for the calculation of specific surface excess free energy and entropy of polymer liquids. Three contributions are identified as contributing to the surface entropy. They are combinational terms due to the mixing of molecules and vacant cells or holes in the surface monolayer, terms due to the potential energy when all molecules are at their cell centres and terms containing the average energy of interaction between segments as they move about the cell.

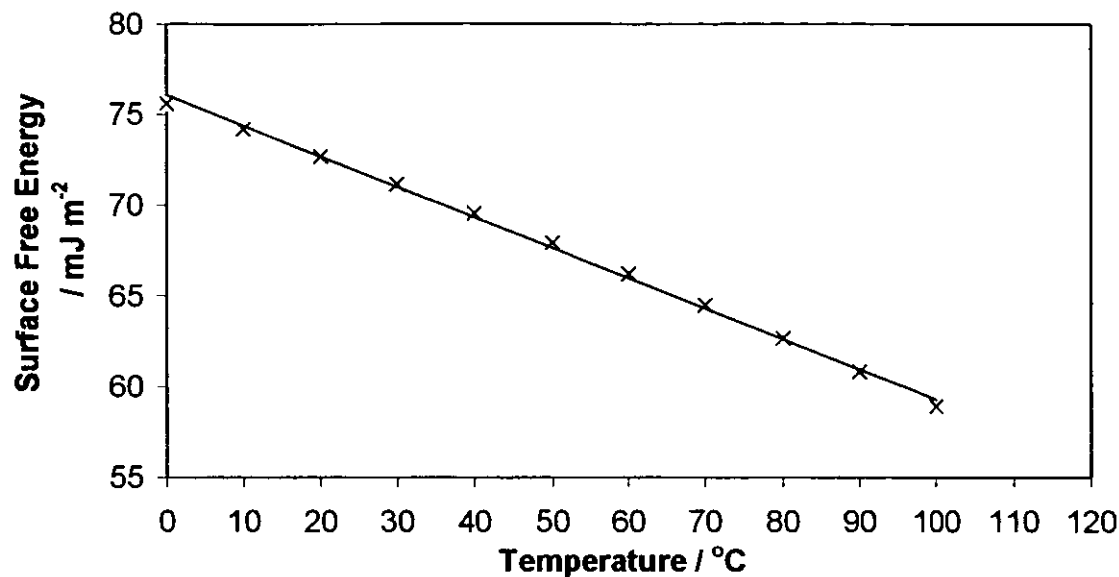


Figure 2.4 Surface free energy of liquid water as a function of temperature.

2.6 TEMPERATURE DEPENDENCE OF CONTACT ANGLE

Budziak et. al. [83] have measured contact angles for three liquids, namely glycerol, ethylene glycol and diethylene glycol, on butyl rubber over the temperature range 23°C to 120°C. Their results showed that contact angle values did not change dramatically with temperature, as seen in Table 2.3.

Table 2.3 Temperature dependence of advancing contact angle of the tested liquids on butyl rubber [83].

Temperature / °C	Contact angle ( $\theta$ ) / °		
	Glycerol	Ethylene glycol	Diethylene glycol
23	99.7	84.4	81.7
30	99.2	83.2	81.8
40	99.2	85.4	80.7
60	101.9	86.3	81.0
80	100.9	88.8	81.8
100	105.5	86.9	82.3

Padday [84] examined the temperature dependence contact angle of pure water wetting on a paraffin wax surface, over the temperature range 20°C to 45°C. His results showed that the work of adhesion increased with increasing temperature for advancing conditions, but in contrast, decreased with receding conditions (details of advancing and receding contact angle technique are given in Section 2.7.1). For advancing conditions, he suggested that the structure of water at the liquid-air interface is different from that at the solid-liquid interface. For the receding conditions, he postulated that it is possible that the surface inhomogeneities become important because of hydration effects.

The effect of temperature on the contact angle between a liquid and a solid has also been measured by Johnson and Dettre [85], who reported that the advancing contact angle for their system, hexadecane on a fluoropolymer, did not change significantly with temperature variation. In contrast, research by Phillips and Riddiford [86] showed diminishing contact angle when the temperature is raised, in their different systems of water, sodium chloride solution and *n*-butyric acid on a siliconed glass surface.

In another experiment [87] of temperature dependence of the contact angles of water and diiodomethane (DIM) on a side-chain liquid, crystalline polyacrylate, showed that the value of contact angle changed significantly at a temperature slightly below the polymer's  $T_g$  (~47°C) when the polymer was tested between 24°C and 73°C. In general, changes in contact angle with temperature are very small and accurate measurement is needed to determine the entropy of adhesion.

---

## 2.7 CONTACT ANGLE HYSTERESIS

### 2.7.1 Introduction

For an ideal, flat and homogeneous solid surface, there is only one contact angle for a given liquid and this is known as the Young or equilibrium contact angle. The Young equation is only valid if the system exhibits a single equilibrium contact angle. However, in most situations, real surfaces normally give a range of contact angles, with a strong dependence on how the measurement is made [41].

A test liquid droplet is placed on a solid surface and then advanced across the surface by addition of further liquid (e.g. from a hypodermic syringe), and allowed to reach equilibrium before an advancing contact angle ( $\theta_{adv}$ ) is measured. The receding contact angle ( $\theta_{rec}$ ) is measured after some liquid has been withdrawn from a drop. If the three phase point of contact is moving while the contact angle is measured then the angle is said to be dynamic. On the other hand, if the three phase point of contact is not moving then the angle is said to be static.

The advancing contact angle is the maximum angle made by the liquid drop, whereas the receding contact angle is the minimum angle. The difference between the advancing angle and receding angle is known as contact angle hysteresis. Zisman [88] proposed that both advancing and receding contact angles have to be measured carefully for thermodynamic purposes, to ensure the experimental conditions remain as close as possible to equilibrium. He went on to report that no contact angle hysteresis could be found if the surface contained no pores or valleys into which the liquid could penetrate. Hysteresis is observed in almost all practical contact angle experiments. It is common to find hysteresis, on practical surfaces, in range of  $10^\circ$  or more and as much as  $50^\circ$ , in some cases [48]. There are a number of causes of hysteresis, which may occur under certain conditions: surface roughness, surface heterogeneity, diffusion, swelling, and reorientation.

The first two causes, surface roughness [89] and surface heterogeneity [90, 91] are the most common and have been studied in great detail. Contact angle measurement may be used to give an indication of these properties.

### **2.7.2 Surface Roughness**

Contact angle hysteresis on rough surfaces can be quantitatively explained by assuming that the advancing and receding contact angle is determined by a balance between the macroscopic vibrational energy of drop and the heights of the energy barriers. The energy barriers which are caused by the ridges and troughs on the surface must be overcome for a liquid to spread across the surface [45]. Roughness needs to be in excess of  $0.1\ \mu\text{m}$  to begin to affect hysteresis [92].

### **2.7.3 Surface Chemical Heterogeneity**

Sometimes, even on smooth surfaces, contact angle hysteresis may still be present. This is sometimes attributed to the chemical heterogeneity. This will occur when different regions of the surface have different values of surface free energy, which is especially true for block copolymers [37], where chemical/molecular compositions vary. The surface of a block copolymer may consist of domains, which have a surface free energy characteristic of the polymers comprising the different blocks. This is also true with migratory polymer additives, moving and concentrating on a surface to different levels, as well as the selective contaminant of a solid surface by an external agent.

---

## 2.8 COMPOUNDING

### 2.8.1 Introduction

One significant development in the use of polymers is the rapid developments in the use of polymer blends or compounds. Polymer blends can be used to fill gaps in performance of existing polymers. Their properties can be tailored by a combination of composition and processing. Under favourable experimental conditions, it is possible to achieve a significant improvement in a property or a group of properties without the need for the development of new polymers [93]. The action of polymer compounding covers many areas of science, from the surface chemistry, thermodynamics and interface science to rheology and processing. The following briefly introduce the main polymer used in this research, PS, and the SMA copolymer, together with discussion on non-reactive compounding and reactive compounding.

### 2.8.2 Polystyrene (PS)

The name “polystyrene” designates a family of plastics derived from styrene monomer. Styrene is a colourless mobile liquid at  $\sim 20^{\circ}\text{C}$  with a “fruity” smell when in pure state but exhibit an unpleasant odour due to trace of aldehydes and ketones if allowed to oxidise by exposure to air. The commercial preparation of styrene involves three stages. The first stage involves the reaction of benzene and ethylene to produce ethylbenzene, in the presence of a Friedel-Crafts catalyst such as aluminium chloride at  $\sim 95^{\circ}\text{C}$ , see Figure 2.5a. In the second stage, the styrene is produced, in a crude form, from ethylbenzene by a process of dehydrogenation, an endothermic reaction, at  $\sim 630^{\circ}\text{C}$ , see Figure 2.5b. The final stage is the styrene purification where the ‘crude styrene’ goes through distillation to remove any by products and impurities [94].

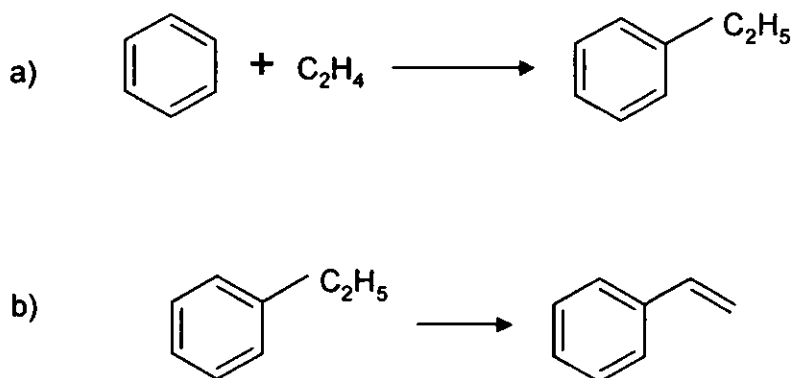
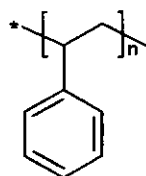


**Figure 2.5** Mechanism of styrene monomer production.

PS was said to be first made by E. Simon in 1839, which he believed to be an oxidation produce and called it styrol oxide [94]. Since then, the polymerisation of styrene has been extensively studied. There are four polymerisation methods, namely, mass, suspension, solution and emulsion, with the first two being the most important. Mass polymerisation produces polymer of high clarity and very good electrical insulation, however, due to exothermic reaction, these posses severe practical problems and the product has a broad molecular weight distribution. Solution polymerisation reduces the exotherm but may lead to problems of solvent recovery and solvent hazards. While suspension polymerisation avoids most of these problems, there is some contamination of the polymer by water and the suspension agent, as the polymer must be dried and aggregated before being sold as pellets suitable for injection moulding and extrusion. Emulsion polymerisation, which affects clarity and electrical insulation characteristics, is used only for the production of PS latex [95].

PS is amorphous and has a  $T_g$  of 100°C [96] and is widely used as an injection moulding and vacuum forming materials due to its several excellent properties

such as its low cost, good mouldability, good dimensional stability, reasonable chemical resistance, low moisture adsorption, etc. . The primary limitations of PS are its brittleness, inability to withstand boiling water temperatures and its poor oil resistance. There is a wide range of grades of PS to meet the needs of a large variety of applications of PS. These include PS modified with rubber copolymers, e.g. styrene butadiene rubber (SBR), high impact polystyrene (HIPS), acrylonitrile butadiene styrene (ABS), etc. [95]. Applications include refrigerators, batteries, lighting, food containers, toys, etc. [97]. Figure 2.6 showed the chemical structure of PS.



where n = repeating unit

**Figure 2.6 PS chemical structure.**

Good adhesion is needed in this number of applications such as surface painting, printing, adhesive bonding, etc. However, with their non-polar surface properties, they are not easily wetted by most liquids. Therefore, in order to achieve good adhesion, some other kind of modifications, other than surface treatment, is necessary. These include compounding/blending with reactive compatilisers e.g. styrene maleic anhydride, to increase its polarity [98].

### **2.8.3 Styrene Maleic Anhydride (SMA) Copolymers**

These are random copolymers of styrene with a small amount of maleic anhydride (see Figure 2.7), which can be manufactured with a range of molecular weights.



Low molecular weight copolymers with 25 to 50% maleic anhydride content have been made available by Elf Atochem with emphasis on the reactivity of such materials [97].

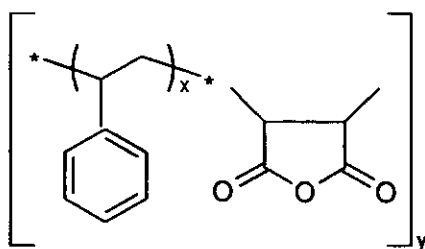


**Figure 2.7** SMA chemical structure.

These unmodified and transparent copolymers have a  $T_g$  and deflection temperature under load in excess of 125°C. The copolymers can be toughened by incorporating a graftable rubber during polymerisation or reinforcement with glass fibre, which can be obtained by melt blending of polymers. The SMA copolymers flow easily though they have higher setting temperature than PS [95].

SMA copolymers exhibit good properties such as low shrinkage, good heat resistance, good rigidity, good dimensional stability, etc. . They have been used in many applications, e.g. as a car roof lining, car heating, ventilating systems and transparent microwave packing materials. These copolymers are mostly incorporated/blended with non-polar polymers to improve the base polymer's functionality [95].

---

## 2.8.4 Non-Reactive Compounding

### a) *Study of Miscibility*

Polymer pairs are usually immiscible due to their low entropy of mixing,  $\Delta S$ , in comparison to small molecules. Any small, unfavourable heat of mixing, positive  $\Delta H$ , would prevent miscibility. Blends that are homogeneous at the molecular level are known as miscible. A miscible (i.e. compatible) polymer blend has to be a mechanically processable blend that resists phase segregation. Most blends are immiscible, (i.e. non-compatible), to a certain degree, with complex phase morphologies that depend on the chemical character of the components and their individual rheological properties.

Polymer blends can be investigated for miscibility in several ways [99 – 101]. One such method is the analysis of  $T_g$ , by far the most popular and convenient way to study the miscibility. When the blend is immiscible, the  $T_g$  values of both constituent polymers will be observed, whereas if the blend is miscible, then only one  $T_g$  is observed. However, this method may have its limitations if the  $T_g$  values of both polymers are close or if there is a small quantity of one polymer in the blend, then the resolution of the  $T_g$  values may be difficult. The crystalline melting point of a polymer,  $T_m$ , can also be used to indicate miscibility by measuring the depression in the melting points of crystalline polymers in blends. This can be used to calculate the interaction parameter. Optical clarity is usually an indication that two polymers are miscible. This, however, can be deceptive if the refractive indices of both components of the blend are similar. The miscibility of polymer blends can also be followed by the analysis of AFM [102] and IR spectroscopy [103]. All these analyses give different indications of the extent of miscibility because they examine different physical properties.

---

**b) Non-Compatible Blends**

Block and random copolymers, as reactive compatibilisers, have successfully turned several otherwise incompatible blends into useful polymer blends. The choice of a copolymer is based on the miscibility of its segments with the blend components. Cho et. al. [104] have investigated the effects of SMA random copolymer, a reactive compatibiliser, on the morphology and rheological behaviour of immiscible amorphous polyamide/styrene acrylonitrile (PA/SAN) blends. Their results showed that finer dispersions of SAN domains with a rather narrow distribution, were obtained when SMA was added to the blend. Similarly, the effect of SMA copolymers on interfacial adhesion between amorphous polyamide and PS, was reported by Lee and co-workers [105]. They have reported that when SMA layer was formed between the amorphous polyamide and polystyrene, it significantly improved the interfacial fracture toughness in comparison with the low fracture toughness of a polyamide/PS interface.

**c) Compatible (or Partially Compatible) Blends**

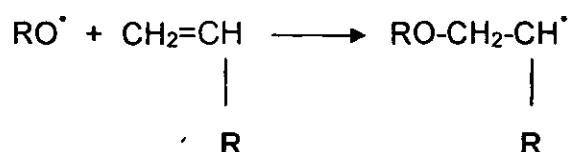
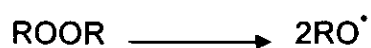
Among polymers that are chemically dissimilar, there are only a few pairs in which compatibility has been demonstrated over the whole range of compositions. One such example is the blend of PS with poly(vinyl methyl ether) (PVME). It was reported that both compatible and partially compatible PS-PVME could be obtained by choosing suitable solvents for a film casting process [106]. Mixtures cast from solvents such as trichloroethylene or chloroform at 25°C, form two phase systems, which retain properties characteristic of the homopolymer components and remained two phase systems when heated. In contrast, mixtures cast at 25°C from solvents, such as toluene or xylene, form visually homogeneous or compatible systems, but upon heating above 125°C, visual phase separation occurs.

There is a question as to whether the compatible or the incompatible mixture represents the thermodynamically preferred state. Kwei et. al. [107] investigated this thermally induced phase separation process in order to determine the interaction parameter of these two polymers, PS and PVME. There have been other studies on the molecular weight effects [108], entanglement effects [109] and shear induced effects [110, 111] on this phase separation mixture and the reader is referred to the references listed for more details.

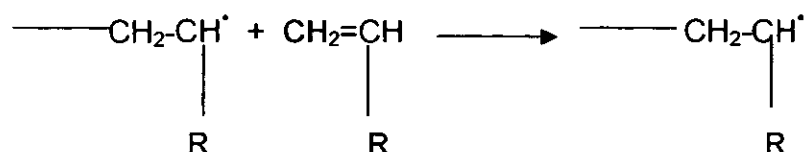
### **2.8.5 Reactive Compounding**

Reactive compounding typically involves the use of free radical grafting in the mixing process. The initiation mechanism involves the production of a free radical via the initiator peroxide, allowing a site for grafting of functional groups onto the polymers [112], see Figure 2.8. There are several options for functionalising common non-polar polymers, such as PP [112, 113] using maleic anhydride and acrylic acid in the presence of dicumyl peroxide as free radical initiator, and PE [114], using styrene and maleic anhydride in the presence of 2,5-dimethyl-2,5-di-(*t*-butyl peroxy), an organic peroxide, as the initiator.

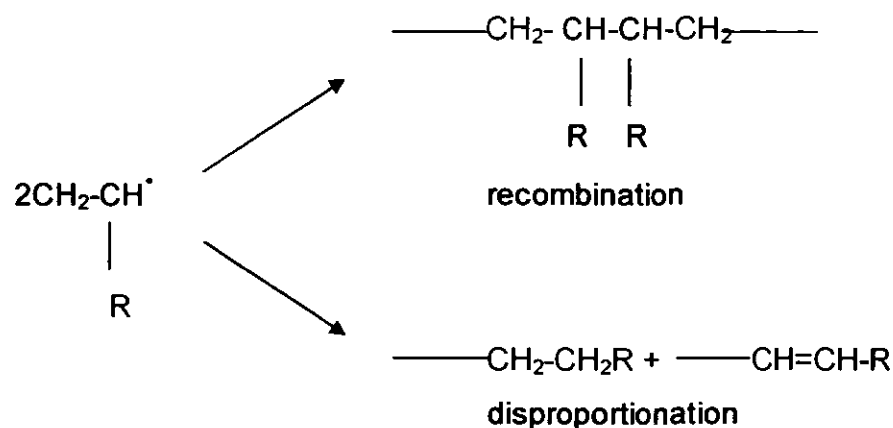
Initiation:



Propagation:



Termination:

**Figure 2.8** Basic steps in free radical initiation mechanism.

PS homopolymer has limited capability without the incorporation functional groups. Desirable physical and mechanical properties of PS, such as thermal stability and

mechanical strength, have been obtained by anchoring specific functional groups [115 - 117]. The free radical reactivity of PS is less than that of polyolefins, which may suggest why chemical modification of PS homopolymer, such as cross-linking, through reactive processing using a free radical initiator, is not a very common practice. Despite that, PS does have a certain degree of free radical reactivity which was confirmed in the work of Hajian et. al. [118].

Functionalised PS having groups such as epichlorohydrin, epoxy, acetyl, C=C double bond and carboxyl, located on the aromatic ring, where grafting took place in the presence of various Lewis acid catalysts have been attempted and where adhesion and corrosion resistance capabilities have been studied [119]. The researchers observed that the polymer's adhesion strength and corrosion resistance increased with the quantity of bonded functional groups to polystyrene. It was also observed that the quantity of the functional group bonded to the aromatic ring of polystyrene depends on both the nature of the functional groups used and the activity of the cationic catalysts.

## **2.9 SURFACE MODIFICATION METHODS**

### **2.9.1 Introduction**

Surface modification of polymers has become an important research area in the plastics industry and subsequently used in mass manufacture. Commercial commodity polymers usually have good bulk properties and are inexpensive. Many industrial applications such as adhesives, biomaterials, protective coatings, etc., require these polymers to have special surface properties. However, many polymers are relatively inert and have low surface energy values, see Table 2.2, which means their surfaces are difficult to wet and bond. In addition, other problems, such as the presence of contaminants and other weak boundary layer

materials, may also interfere and weaken the bonding strength of the polymer and adhesives.

Surface treatments of polymers may be used to change surface chemical composition, increase the surface energy, modify the crystalline morphology, change surface topography or remove contaminants and other weak boundary layers. Such treatments have been designed to alter chemical and physical properties of polymer surfaces without affecting bulk properties. Frequently employed surface modification treatments include plasma treatment, corona treatment or electrical discharge treatment, flame treatment, abrasion treatment, chemical treatment, compounding, surface grafting, etc. some of which will be discussed in the following sections.

### **2.9.2 Plasma Treatment**

Plasma treatment is a technique where a plasma is produced by ionising a gas with a high electric field, see Figure 2.9. Plasmas can be generally described as gases that contain charged and neutral species, including electrons, positive and negative ions, radicals, atoms and molecules [120, 121].

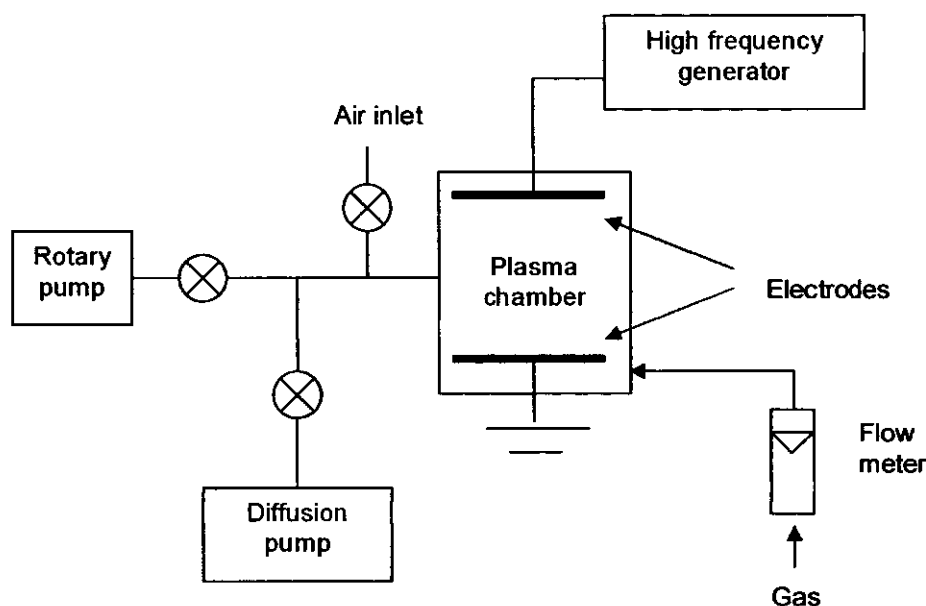
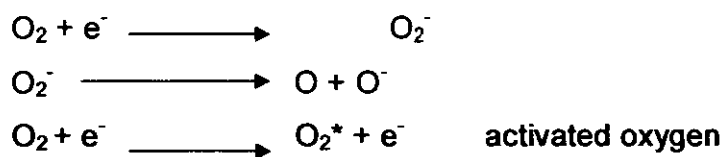
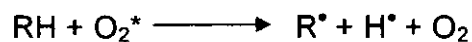


**Figure 2.9** Schematic of plasma treatment unit.

The ions and radicals are formed by collisions of electrons and ions. Therefore the charges in plasma will gain energy in the presence of an appropriate electric field, see Figure 2.10 for the mechanism of plasma treatment [6].

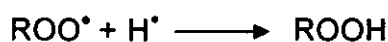
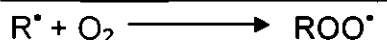


Free radicals produced during plasma treatment of polyolefins.



Further reactions of alkyl radical R may be written as,





A variety of functional groups may be generated from hydroperoxides

**Figure 2.10** Mechanism of oxygen-plasma treatment.

Advantages of plasma treatment include:

- Modifications are confined to the surface layer without modifying the bulk properties.
- Excited species in gas plasma can modify the surface of all polymers.
- Choice of gas used can allow introduction of particular functionality to a treated surface.
- There is no residual solvent on the surface, or swelling of the substance, otherwise associated with wet techniques.
- Treatment is fairly uniform and can be used for three-dimensional objects.

However, disadvantages include:

- Treatment must be carried out in vacuum and this increase the cost and duration of the operation.
- The optimal parameters developed for one system usually cannot be adopted for another system.
- It is difficult to control the precise number of functional groups formed on a surface.

Various plasma gases include air, oxygen, nitrogen, methane, argon and halogenated vapours like  $CF_4$  [122 - 126] have been employed to increase the hydrophilicity of surfaces usually through free radical surface oxidation. Marchant et. al. [123] have reported that oxygen incorporation after nitrogen or argon plasma treatment could occur through the post-treatment with atmospheric oxygen or

water. Lhoest et. al. [127] had developed a plasma-based method to promote cell adhesion via a microelectronic photosensitive resin that was spin coated onto PS substrates. Characterisation by surface analysis techniques indicated that hydrophilic paths were created on the otherwise more hydrophobic PS substrate.

The characterisation of plasma treated surfaces usually requires the use of surface-specific techniques, such as XPS, SSIMS and contact angle measurement [128]. Yuen and Marchant [129] studied the plasma polymerisation on a plasma polymer-modified PE surface, which was analysed showing a significant water contact angle hysteresis and a much lower advancing contact angle than that of unmodified polyethylene. Foerch and co-workers [130] have studied the effect of remote nitrogen plasma on PS and PE, in addition to other treatments of corona and ozone post plasma processing. They observed that when the plasma reached a steady state composition of oxygen and nitrogen, the functional groups continued to change, as monitored by XPS. Dupont-Gillain et. al. [131] were able to determine the presence of various oxygen-containing groups, including carboxyl functionals on the surface of oxygen plasma treated PS using surface analysis methods.

### **2.9.3 Corona-discharge Treatment**

Corona discharge is a relatively simple and inexpensive process, and as a result, a popular industrial technique especially for the high speed surface treatment of continuous polyolefin films. In a corona discharge system, plasma is produced when air is ionised by a high electric field. This treatment causes various chemical and physical changes on a polymer surface, so by improving bondability and printability. The general set-up involves an electrode connected to high voltage and a roller that carries a film, as shown in Figure 2.11.

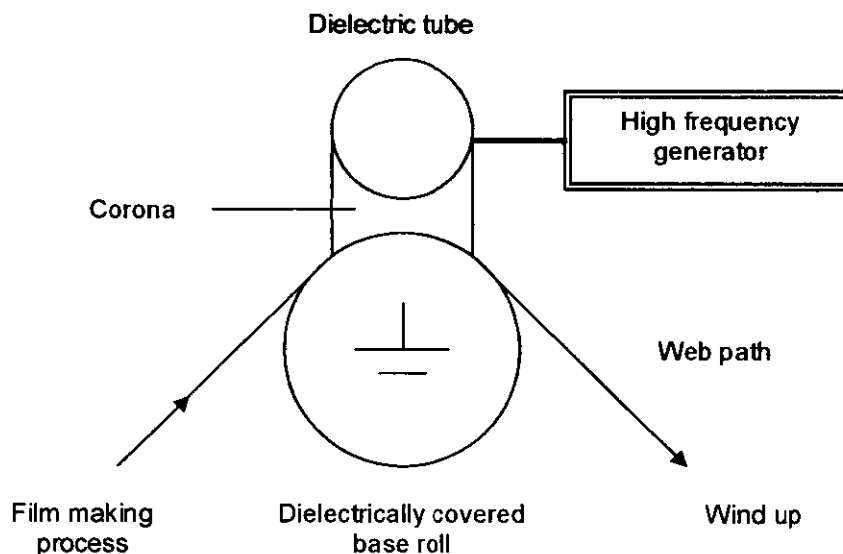


**Figure 2.11** Schematic of corona-discharge treatment.

An electrical discharge is struck to the sample from an electrode at high voltage several millimetres above the surface. The reactions between the polymer film and corona discharge then involve the generation of free radicals, formed by the high energy particles such as electrons, ions excited neutrals and photons [89]. These radicals react rapidly with atmospheric oxygen to form hydroperoxides from which different functionalities are produced, including  $\text{-OH}$ ,  $\text{>C=O}$ ,  $\text{-COOH}$ , etc. . The likely mechanism is shown below,

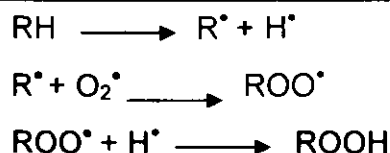


**Figure 2.12** Mechanism of corona-discharge treatment in an oxygen containing gas.

The most important process parameters that control the surface properties of a treated film include the power consumption, air-gap thickness, film speed, chemical nature of the gas and treatment temperature. The nature of the polymer also plays an important part in determining the optimal setting for each parameter. For example, corona treatment has been found to become less effective in enhancing self-adhesion of PE films when the density of the polymer is increased [132]. Additives, such as slip agents and antioxidants, can adversely affect corona treatment over a period of time [133]. As treatment is on the exposed surface only, if additives migrate to the polymer's surface before treatment is carried out, then inferior adhesion may result. This is because there will be a tendency to chemically modify the additives rather than the underlying polymer chains.

Corona treatment has also been used to modify the surface of PS film to improve its molecular interaction with lacquers, paints and adhesives [134]. Bousmina et. al. have investigated the effect of corona treatment and block copolymer addition on the rheological properties of PS/PE blends [135]. The reader is referred to these papers for more details.

### 2.9.4 Flame Treatment

Another commonly used surface modification method is flame treatment, which is more economical, in comparison with plasma and corona discharge treatments. Flame treatment is usually used for thicker sectioned articles, particularly, blow moulded plastics bottles and car bumpers (i.e. use more on irregular shapes). A schematic representation of flame treatment is shown in Figure 2.13.

The process uses a ribbon burner. Single or double row ribbon burners can be used. A mixture of compressed air and fuel gas is supplied to the burner. Natural gas (predominantly methane), propane, butane, coal gas or any mixture of these can be used as a fuel gas. The object is rotated slowly around a central axis so that every point of its surface is passes through the flame. For car bumpers, a moving burner is passed over the bumper surface.

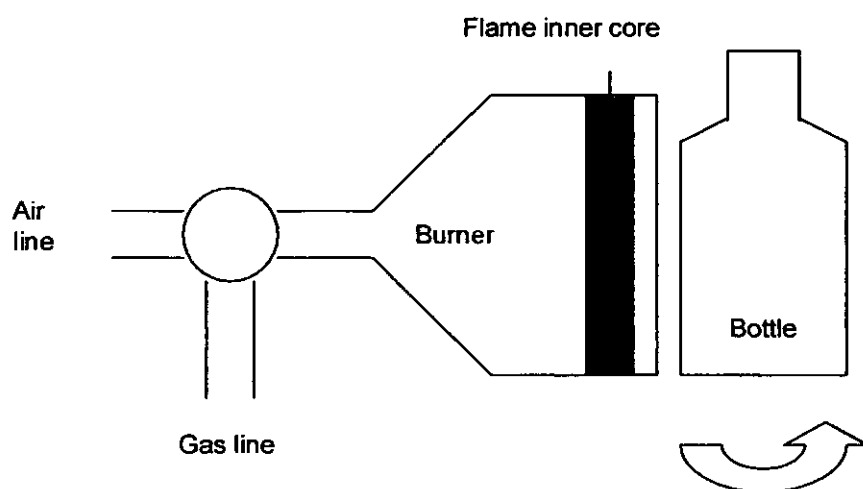


**Figure 2.13** Schematic of flame treatment.

Flame treatment is employed to promote surface oxidation, thereby increasing the polarity of the treated surfaces by the development of oxygen-rich functionals and so improving the wetting/adhesion characteristics. Important variables for flame treatment are air-to-gas ratio, the total flame rate (i.e. flame intensity), the distance from the flame inner cone tip to the surface to be treated, contact time, i.e., the time required for a single point on the surface to pass through. The effect of these variables for flame treatment of PP was studied by Sutherland et. al. [136]. They found that optimum surface oxidation and water wettability was achieved at an air-to-gas ratio of ~11:1. In addition the increase in flame intensity increased the level of surface oxidation, however, the degree of water wettability did not continue to improve.

Garbassi and co-workers [137] found that the flame treatment of PP resulted in large increase of adhesion of two pack urethane or acrylic paints to the polymer. A study of flame treatment on rubber-modified PP showed that an initial rapid decrease in water advancing contact angle with surface oxygen concentration, the water advancing contact angle was found to level off. It was attributed to the reorientation of functional groups, incorporated during flame treatment, away from the surface.

The flame treatment introduces functional groups such as hydroxyl, carbonyl, carboxylic acid, etc. onto the polymer surface, in a similar manner to corona discharge treatment [35]. The mechanism of the flame process is quite complex and many species are present in a flame. It is probable that the flame treatment follows a free radical process and this resembles plasma and corona treatment. The process could involve the attack of flame radicals on surfaces. A detailed possible mechanism of the flame chemistry has been attempted by Popat [138].

---

### 2.9.5 Chemical Etching

Chemical treatment has been used in industry to treat large objects that would be difficult to treat by other commonly used industrial techniques, such as flame and corona discharge treatments. Chemical etchants are used to convert smooth hydrophobic polymer surfaces to rougher hydrophilic surfaces, by dissolution of amorphous regions and by surface oxidation. The choice of etchant is polymer dependent, as very different morphologies can be produced from using the same chemical. Various strong oxidising reagents have been used for surface pretreatments such as chromic acid, concentrated sulphuric acid fuming and nitric acid, of which chromic acid is of interest and will be reviewed here [139, 140].

Chromic acid has been the most widely used etchant for polyolefins and other polymers. Several chromic acid formulations have been used [6], e.g.,

- 1)  $\text{K}_2\text{Cr}_2\text{O}_7 / \text{H}_2\text{O} / \text{H}_2\text{SO}_4$  (conc. specific gravity = 1.84), 5:8:100 by weight
- 2)  $\text{CrO}_3 / \text{H}_2\text{O} / \text{H}_2\text{SO}_4$  (conc. specific gravity = 1.84), 100:145:100 by weight

of which formulation 1 is most extensively and commercially used. The treatment can be carried out at room temperature or at an elevated temperature. Chromic acid has been used to selectively attack the rubber particles in ABS polymer [141]. It is also found that chromic acid etches both the amorphous and crystalline regions of PP at similar rates [142]. The etching rate is faster with PP, intermediate with branched PE and slowest with linear PE [139]. The surface topography of etched polymers can be observed by SEM and wettability angle measurement. XPS analysis has been used to detect hydroxyl, carbonyl, carboxylic acid and sulphuric acid groups on chromic acid etched polyolefins [143].

---

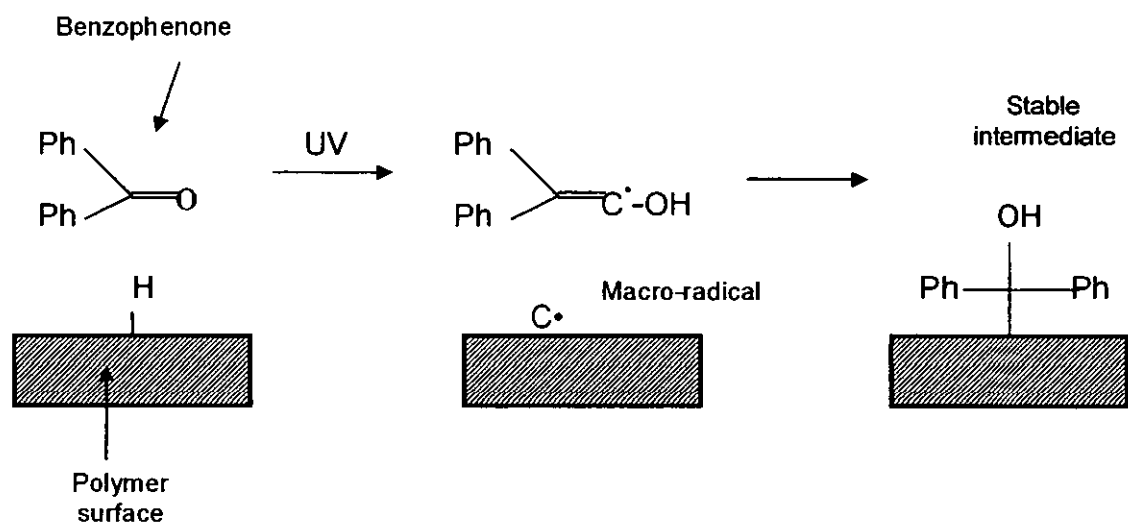
### 2.9.6 Polymer Grafting

The grafting of monomers containing functional groups, to “backbone” polymers is a useful procedure to modify the polymer’s surface. Two main methods are used. The first involves using pre-irradiation to introduce functionality, e.g. ozone or plasma, producing  $\text{OO}^\bullet$  and  $\text{OOH}$  groups on the surface. The polymer is then heated in the presence of the monomer. Garnett and co-workers [144] have reported grafting a trypsin enzyme onto a polymer surface using photo-grafting, to produce a biocompatible material. Studies were also carried out on improving metal-polymer adhesion, using photo-grafting of monomers, like acrylamide and acrylonitrile that contain functional groups that interact with metals [145]. There has been research on photo-grafting used to improve the electrostatic properties of PS and PE films, as well as fabrics with water-soluble ionic polymers to dissipate static charge more quickly [146].

The second method is by the exposure of a polymer to a radiation source such as high energy electrons, plasmas, UV light or  $\gamma$ -radiation, in the presence of a modifying monomer usually in a solvent. The radiation initiates a polymerisation reaction between the polymer and the solvated monomer [147]. Benzophenone and its derivatives are commonly used as photo-initiators. The grafting process involves two stages, see Figure 2.14. In the first stage, under UV radiation, the photo-initiator is excited to its first singlet state and then rapidly relaxes to a more stable triplet state through intersystem crossing [148]. Once in its triplet state, it can abstract a hydrogen from a donor, which is the polymer surface, and produce a macro-radical. Recombination leaves a stable intermediate. In the second stage, the macro-radical is regenerated by UV radiation in the presence of the monomers. The macro-radical then initiates polymerisation. The benzylhydryl radicals produced are too bulky to undergo polymerisation and so instead take part in termination reactions [149]. Figure 2.14 illustrates the grafting polymerisation.



First stage:



Second stage:

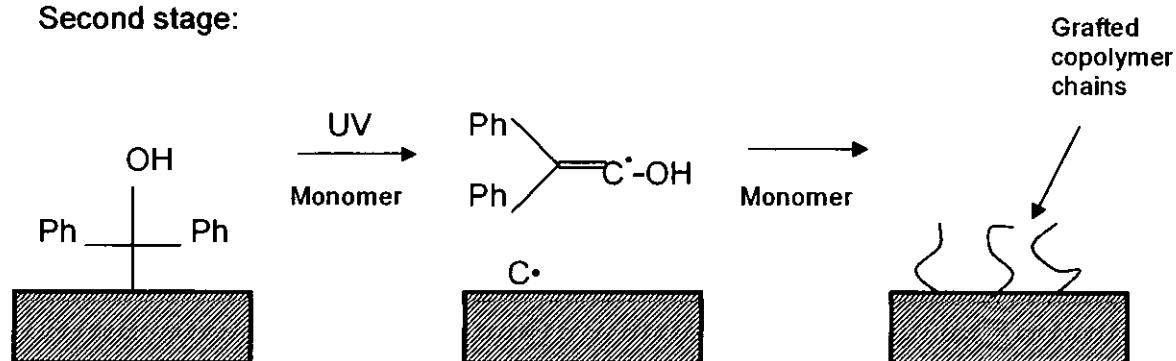


**Figure 2.14** Mechanism of grafting polymerisation.

Photo-grafting can be conducted in either the vapour phase or liquid phase. Vapour phase grafting is typically carried out in a heated nitrogen atmosphere with the monomers in the vapour phase and in the presence of a polymer [150]. Liquid

phase or solution grafting, is performed in solution, where the solution contains the monomer, polymer and initiator dissolved in a solvent or mixture of solvents [151].

Factors affecting grafting include polymer crystallinity, which can slow the rate of grafting [152]. This is because crystallinity prevents penetration of the reaction mixture into part of the polymer. The stability of the grafted layer is also dependent on the mobility of the polymer chains. An important component in this method is the choice of solvent. It should be inert towards initiators and should wet the polymer surface.

Characterisation techniques are performed as a mean of identification and quantification of the functionalisation of the grafted polymer surfaces, as in the case of Lopez-Gejo et. al. [153]. They have used ATR-IR (see Section 2.10.6), and contact angle measurements to analyse the functionalisation of PS surfaces undergone vacuum ultra-violet-photochemically initiated oxidation. They observed an increase of the concentrations of OH and C=O groups on the polymer's surface, both reaching limiting values. In another piece of work, AFM and XPS have been used to investigate the surface and sub-surface properties of PS substrates, having undergone irradiation treatment in oxygen (UV-ozone), in nitrogen (UV-only) and in the absence of UV (ozone-only) atmospheres [154].

## **2.10 SURFACE CHARACTERISATION**

### **2.10.1 Introduction**

Improvements in surface modification techniques cannot be made without an in-depth understanding of the chemical and physical properties of polymer surfaces. Techniques commonly used for characterisation of bulk properties are not suitable

because only the chemical and physical properties within the first few nm of the surface are normally relevant for understanding surface and adhesion properties.

In the study of adhesion science, a wide range of surface characterisation techniques are available, including X-ray photoelectron spectroscopy (XPS), static secondary ion mass spectrometry (SSIMS), scanning electron microscopy (SEM), atomic force microscopy (AFM), attenuated total reflection infrared spectroscopy (ATR-IR), contact angle measurement, etc., for determining both physical and chemical properties. To better understand surface treatment, a multi-technique approach should be used. Complementary information is provided by each analysis method, which can be built up to form more complete picture, than by using information from any one technique alone. In this review, contact angle measurement, XPS, AFM and ATR-IR are briefly described.

#### **2.10.2 Contact Angle Measurement**

The thermodynamic principles have been reviewed in Section 2.3.9. Contact angle measurement has been used extensively in studying changes in polymer surface composition, caused by various surface treatment techniques, ageing characteristics of surfaces, migration of hydrophobic and hydrophilic functional groups in aqueous and non-aqueous environments, etc. [155, 156].

The contact angle of a liquid on a solid surface is sensitive to the chemical composition of the top molecular layer of the solid. For example, time-dependent contact angle measurements have been employed to follow the dynamics of the surface modification of various polymeric surfaces of different hydrophilicities by Lee and Ruckenstein [157]. Similar research by Yasuda and Sharma used contact angle studies to monitor the effect of orientation and mobility of polymer molecules at surfaces [158].

Flame treatment of polymers generally introduces polar functional groups to the surface. The increase in concentration of these polar groups tends to decrease the water contact angle, which it is thought to show the change in concentration of polar groups at the polymer surface [159, 160]. Wang et. al. were able to conclude that the results of surface contact angle of glycerol and water on PS films were dependent on the extent of uniaxial draw of atactic PS [161]. The wettability of smooth surfaces of polyamide, poly(ethylene terephthalate) (PET) and PS using a variety of test liquids was studied by measuring the contact angle on the solids [162]. These researchers have concluded that the wettability by polar hydrogen bonding liquids is increased by the presence of both the amide group and the ester group in the solid's surface. Their findings also showed that the wettability by halogenated liquids, is less affected by the amide and ester groups, due to these organic liquids' inability to form hydrogen bonds [162].

### 2.10.3 X-ray Photoelectron Spectroscopy (XPS)

XPS is generally considered a non-destructive and surface specific technique, which permits reliable detection of surface compounds and offers accurate semi-quantitative measurements. In XPS, a sample is bombarded with a beam of soft X-rays (usually Mg K $\alpha$  or Al K $\alpha$  with energies of 1253.6 and 1486.6 eV, respectively), in ultra high vacuum (UHV) [163] and the area analysed is anything from 1 cm<sup>2</sup> down to 10  $\mu$ m<sup>2</sup> depending on the spatial resolution of the spectrometer used. X-ray absorption causes an electron to be ejected from one of the core electronic levels. This photoelectron escapes with a certain kinetic energy ( $KE$ ), which is governed by the binding energy ( $BE$ ) of the core-electron in the atom and the work function of the spectrometer ( $\phi$ ) according to,

$$KE = h\nu - BE - \phi \quad \{2.25\}$$

where  $h\nu$  is the X-ray energy [164]. The photoemission process is shown schematically in Figure 2.15. For each and every orbital (e.g. C, N, O), there will be a characteristic binding energy [164]. In addition, the intensity of each peak is related to the concentration of the atom within the sampled region via the sensitivity factors based upon predicted collision cross-sections and instrument dependent factors.

The X-rays penetrate the sample and reach to a depth of  $\mu\text{m}$ , however, the ejected photoelectrons will collide with other electrons and lose energy. Only photoelectrons that have come from atoms in the top atom layers (i.e. the first few nm), escape the sample with a characteristic energy. These are collected and energy analysed by the instrument.

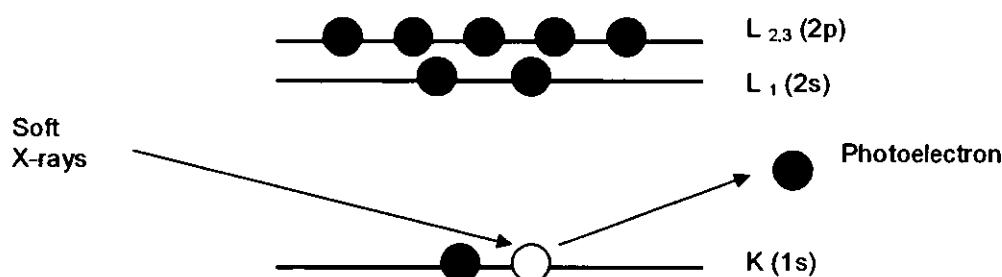


**Figure 2.15** Schematic representation of the photoemission process.

After a photoelectron has been ejected from a core state, the vacancy it leaves may be filled by another electron from another orbital. This process yields energy that can be transferred to another electron that, if sufficient, will eject it and this is referred to as Auger emission.

With XPS, one can change the angle with respect to the surface that the electrons are collected, known as take-off angle,  $\theta$ . The vertical sampling depth,  $d$ , is given by:

$$d = 3\lambda \sin \theta \quad \{2.26\}$$

Therefore, at low  $\theta$ ,  $d$  is reduced.  $\lambda$  is the attenuation length (inelastic mean free path), i.e. the distance that an electron will travel before they undergo collision and lose energy. Comparison of the relative peak intensities at high and low take-off angles can reveal the presence of thin surface layers [164].

It has been recognised that XPS is unable to resolve similar multiple functional groups. This is because the dynamic range of these chemical shifts is not sufficient to resolve similar functional groups such as C-O-O and C-O-H, which have very similar binding energies.

Because of the ability of this equipment to distinguish different elements and different chemical configurations, XPS has been one of the main surface analysis techniques used to provide information on surface elemental compositions and functional groups, through chemical shift data for numerous polymeric systems. Thomas and co-workers have utilised XPS to investigate the influence of chemical composition and film casting solvent on the surface structure of polystyrene-poly(ethylene oxide) diblock copolymers. Their XPS results indicated that the compositions of the surfaces are significantly different from the overall bulk compositions [165]. XPS technique was used in the research work of PS's surfaces and has been reported elsewhere [130, 131].

---

#### 2.10.4 Chemical Derivatisation

Even though XPS is an invaluable device for elucidating surface elemental composition, functional groups cannot always conclusively be identified from their chemical shift alone. In the chemical derivatisation technique, a specific derivatising reagent is made to react with a specific functional group, and in doing so labels it with a distinctive element, which was not previously present on the surface. This will increase the detection sensitivity when the elemental 'tag' has a higher photoelectron cross-section than C 1s, O 1s or N 1s. Modified polymer surfaces contain a variety of functional groups and thus a variety of reagents have been employed. These include trifluoroacetic anhydride for hydroxyl groups; hydrazine and pentafluorophenylhydrazine for carbonyl groups; sodium hydroxide, triethylamine and trifluoroethanol for carboxylic groups [166].

Subsequent XPS analysis then provides an estimate of the relative concentration of the functional group of interest. In principle, these reagents should react selectively and analytically with only the intended functional group. In addition, the reagents should react full with those functional surface groups, however, this is not always the case. Trifluoroacetic anhydride had been used to determine the concentration of hydroxyl groups on chromic acid treated PP surfaces, where no hydroxyl groups were detected as researched by Sheng [6]. His work also showed that the removal of hydroxyl groups on flame treated homopropylene surfaces by the reaction with trifluoroacetic groups reduced the surface wettability but had little effect on the adhesion with epoxy adhesive.

Vapour phase derivatisation is more frequently used than solution derivatisation as the latter can pose some problems. The use of solutions may increase the polymer chain mobility at the surface (i.e. by solvation/plasticisation) and hence result in the movement of some functional groups into the bulk and away from the surface (e.g. by segmental rotation). In addition, the solvent can also dissolve low molecular weight materials from the surface. Reorientation of functional groups could also

arise if the surface is exposed to high temperatures, long reaction times and prolonged washing after reaction. Solution derivatisation has been studied by Everhart and Reilley [167], where a number of reactions were used to analyse various functional groups on PE surfaces modified by plasma. These researchers used NaOH to derivatise acid groups but found that sodium incorporation was not reproducible and was dependent on washing conditions.

The vapour phase method poses fewer problems than seen with the solution phase method. Dickie and co-workers [168] have used trifluoroacetic anhydride in the vapour phase to derivatise a hydroxyl containing polymer. Their findings have suggested that the hydroxyl groups existed in an orientation away from the surface and that this had not been disturbed by the derivatisation. Gerenser [169] identified and quantified hydroperoxy, hydroxyl, carbonyl, epoxy and acid groups on corona discharged treated PE surfaces. Briggs [170] has summarised a variety of gas phase derivatisation reactions for different functional groups. As contamination is much less likely to be introduced in the gas phase, vapour is preferred over liquid derivatisation. Several investigations on vapour phase derivatisation and selectivity functional groups can be found elsewhere [147, 171 - 173].

#### **2.10.5 Atomic Force Microscopy (AFM)**

AFM is part of the family generally known as scanning probe microscopy (SPM). This technique can produce three-dimensional images of solid surface at very high resolution, and is suitable for imaging non-conducting samples, such as polymers and ceramics. In recent years, AFM has shown great promise for producing surface polymer morphological information [174 - 176].

In one study, the surface structure of PS and poly(2,6-dimethyl-1,4phenylene oxide) films were studied with AFM before and after the application of a tensile load [177]. Before the application of strain, the surfaces of the films were smooth.



Immediately after the application of strain, the surfaces of the stretched polymer film remained smooth. However, topographic bumps were detected by AFM on the stretched polymer films as ageing time increased. The technique has also been applied to study the surface structure of copolymers [178], morphology of electrochemically induced polymerised poly(phenyl oxide) film [179]. AFM has also been used to study the wettability of PS microspheres, of various radii, with water [180].

The AFM probe consists of a silicon or silicon nitride tip, that is  $>10$  nm in diameter, located at the free end of a cantilever onto which a laser beam is focussed, see Figure 2.16. The beam is reflected from the back of the cantilever while the tip is scanned across a surface, to the photo-sensitive detector where the deflections are detected. The deflections allow a computer to generate a map based on the feedback information. The main purpose of this instrument is to quantitatively measure surface roughness with a nominal 5 nm lateral and 0.01 nm vertical resolution on all types of samples.

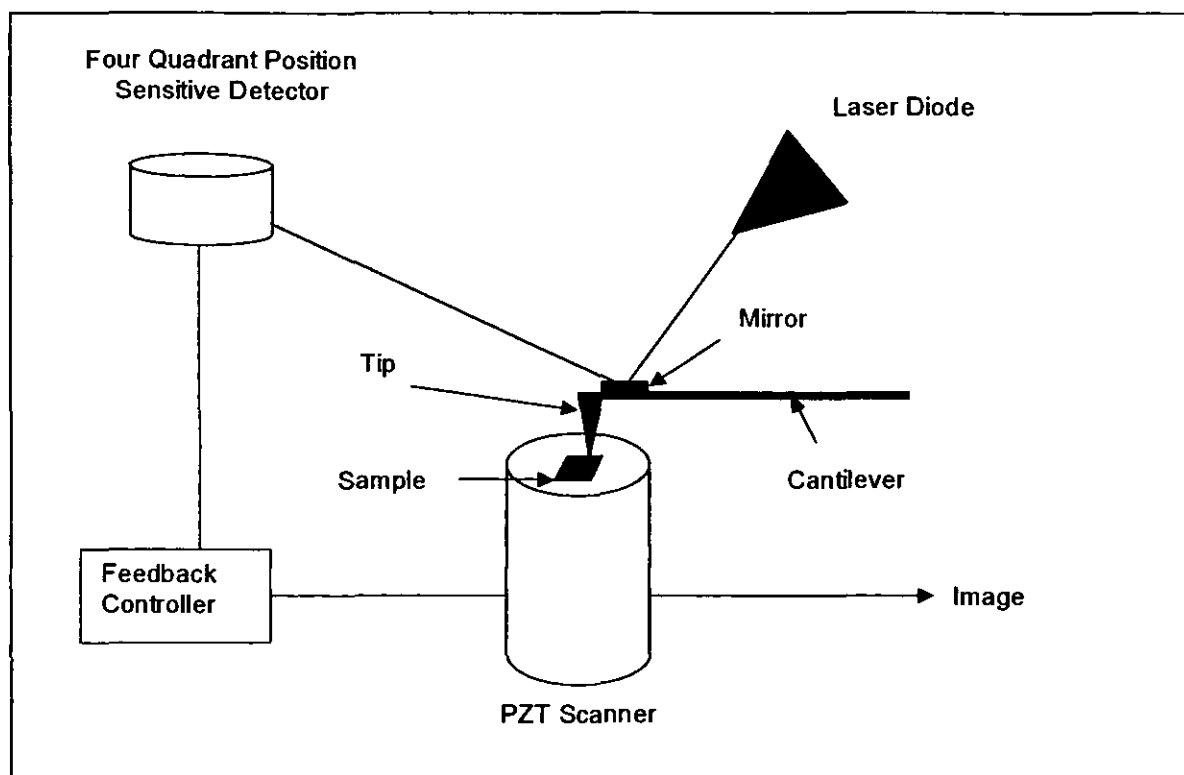


**Figure 2.16** Schematic diagram of a typical atomic force microscope.

Several types of forces contribute to the tip deflection of the cantilever. The forces most commonly influencing the tip are Van der Waals. AFM is becoming the companion technique to XPS in polymer surface analysis, due to its high resolution and visual image [181]. Functionalisation of the tip itself has led to interesting developments that enable different force and functional groups to be imaged [181]. The interaction of the tip and the sample surface can be classified as contact mode (repulsive), non-contact mode (attractive) and tapping mode. A brief description of these various imaging modes used in analysis is given in Figure 2.17.

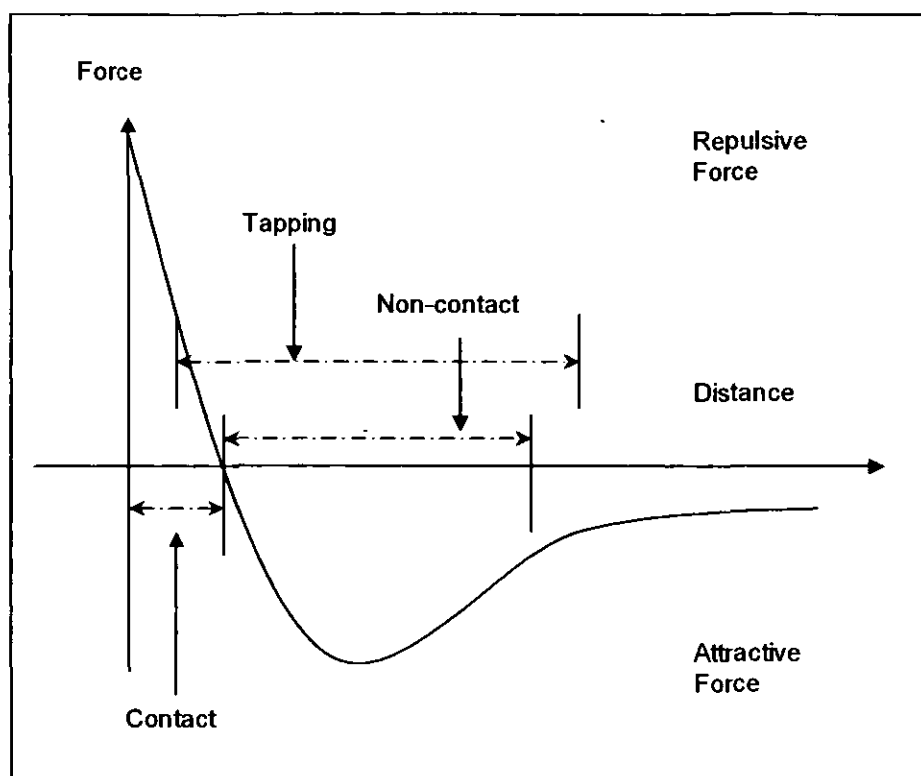


**Figure 2.17** Force/distance curve of AFM tip/sample interactions.

**a) Contact Mode AFM (C-AFM)**

In this mode, the tip makes soft 'physical contact' with the sample. The tip is attached to a cantilever spring. As the sample is scanned, the contact force allows the cantilever to bend and follow the changes in topography. In this mode, the sample may be damaged by contact with the tip. Other forces may also be present during contact mode scanning. Under ambient conditions, a layer of adsorbed gases, consisting mainly water, covers the sample surface. When the probe touches this contaminant layer, there is a formation of meniscus. Operation can be done with the sample and cantilever immersed in aqueous solution.

---

**b)     *Non-Contact Mode AFM (NC-AFM)***

In NC-AFM, the tip oscillates at resonance frequency above the surface. This provides a method for measuring topography with no contact from tip and is useful for soft samples. However, the Van der Waals forces sensed at this distance are much smaller than the C-AFM and consequently are much harder to monitor. However, these attractive forces can alter the amplitude, phase and frequency. This mode is usually performed in ultra high vacuum (UHV) in order to avoid the formation of meniscus with adsorbed water.

**c)     *Intermittent Contact Mode AFM (IC-AFM)***

This is also known as tapping mode that allows high resolution topographic imaging of sample surfaces that are easily damaged or difficult to image by other AFM techniques. Intermittent contact imaging combines, to a certain extent, the advantages of contact and non-contact modes. There is a larger oscillation of probe so that it strikes the surface at high frequency of 50 to 500 kHz. During tapping mode operation, the cantilever oscillation amplitude is maintained constant by a feedback loop. Unlike contact and non-contact modes, when the tip contacts the surface, it has sufficient oscillation amplitude to overcome the tip-sample adhesion (lateral) forces. Contact and tapping modes were used to study the surface morphology of solvent cast PS film, where wavy features are observed to form with a predominantly perpendicular orientation with respect to the scan direction [182].

The disadvantage of AFM is that the area of analysis is small, about 0.1 by 0.1 mm, as opposed to conventional profilometry that can analyse area much smaller than 0.1 mm, hence may be looking in on representative areas. Nonetheless, AFM is a quantitative technique, in particular, the use of  $R_a$  parameter of roughness in

this study.  $R_a$  is the arithmetic roughness average of the absolute values of the measured profile height deviations [183], given by:

$$R_a = \frac{1}{n} \sum_{i=1}^n \left| z_i - \bar{z} \right| \quad \{2.27\}$$

where  $n$  is the number of height positions along the line profile,  $z_i$  is the height at position  $i$  and  $\bar{z}$  is the average height. In addition, there are other parameters that are available to fully describe the surface factor such as the spacing parameter,  $R_{sm}$ , and other peak roughness values such as  $R_{tm}$ ,  $R_q$  and  $R_{max}$  [183]. It is important to note that the  $R_a$  value does not fully describe the surface feature but it does give a widely used indication of roughness. However this necessarily does not indicate the maximum roughness of a surface.

#### 2.10.6 Attenuated Total Reflection Infrared Spectroscopy (ATR-IR)

Infrared (IR) spectroscopy is one of the oldest spectroscopic techniques. It is the most widely used analytical technique for routine analysis of organic compounds and as an important research tool. There are many different forms of IR spectroscopy such as transmission, emission, photoacoustic and diffuse reflectance (DRIFT), to name but a few [184, 185]. The many forms of IR also include ATR, which will be the only one discussed here.

ATR uses the internal reflection of radiation in a medium. It requires an infrared transparent material with a refractive index ( $n$ ) higher than 2.5. Single or multiple reflections can be used. Typical materials include Ge, ZnSe, Si, KRS-5 and sapphire all of which are used because of their transparency in the wide range of the mid-infrared region [186].

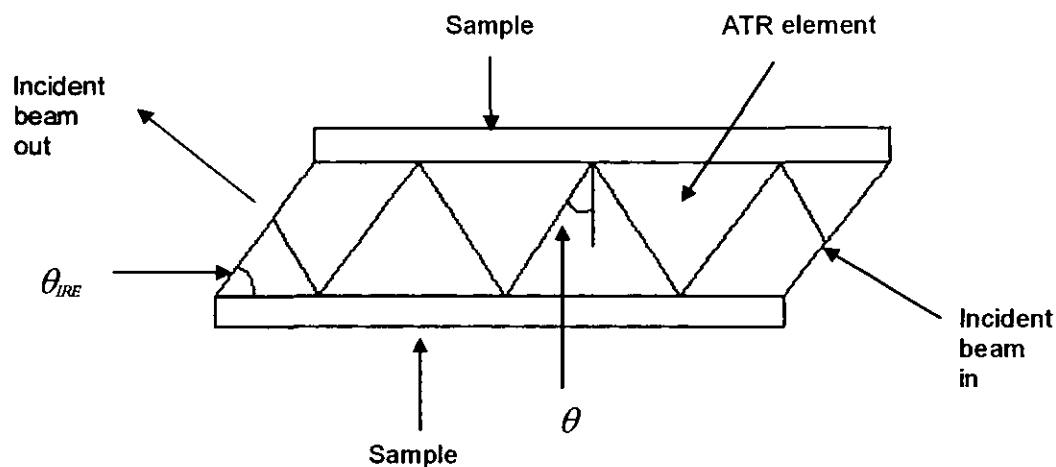


**Figure 2.18** Schematic diagram of a multiple reflection ATR system.

As illustrated in Figure 2.18, a sample is placed in contact with the optical dense prism and the radiation is totally internally reflected in the prism. The reflected radiation continues to reflect until it exits from the prism. At the point of reflection, the radiation leaving the prism forms an evanescent wave, which is an interference wave of the incident and reflected waves. The amplitude of the evanescent wave in the rare medium (sample) decays exponentially with the distance from the boundary with the denser medium (prism). When the IR absorbing sample is in contact with the prism, this evanescent wave interacts with the sample and causes the attenuation of the propagating IR beam inside the ATR prism. In this case, an infrared spectrum is obtained by detecting the absorbed radiation at the exit of the prism.

The penetration depth is a function of the refractive index ratio between the prism and the sample, angle of incidence and frequency. It is possible to change the penetration depth by changing these parameters and this feature is used to provide

a depth profile. The penetration depth,  $d_p$ , can be calculated using Equation 2.28 [186],

$$d_p = \frac{\lambda}{2 \left\{ \sin^2 \theta - \left( \frac{n_s}{n_p} \right)^2 \right\}^{0.5}} \quad \{2.28\}$$

The angle of incidence,  $\theta$ , is

$$\theta = \theta_{IRA} - \sin^{-1} \left\{ \frac{\sin (\theta_{IRA} - \theta_{IRE})}{n_p} \right\} \quad \{2.29\}$$

- where  $\lambda$  = wavelength  
 $n_s$  = refractive index of sample  
 $n_p$  = refractive index of prism  
 $\theta_{IRA}$  = angle designated on the scale  
 $\theta_{IRE}$  = angle of the prism face

IR has been used to confirm the existence of maleic anhydride at the terminated anhydride functionalised PS chain in the range of 1700 to 1900  $\text{cm}^{-1}$  [187]. Bulk syndiotactic PS undergoes crystallisation, which leads to the formation of  $\alpha$  or  $\beta$ -form crystals or the mixed ( $\alpha + \beta$ ) form crystals, which may not be, identify clearly from differential scanning calorimetry (DSC) thermograms [188 - 191]. IR spectroscopy had been used as a simple and direct method for detecting the complicated bulk syndiotactic polystyrene crystallisation behaviour. Most importantly, using this technique, researchers were able to analyse the phase-transformation between the  $\alpha$  and  $\beta$ -form crystal during the cold crystallisation heating treatment process [192].

## **CHAPTER 3 EXPERIMENTAL**

The experimental chapter is divided into three sections. The first section comprises the description of the manufacture and grade of the materials and chemicals used in this work. These include the polystyrene (PS), used as the main and only standard polymer here. Low molecular weight copolymer, styrene maleic anhydride (SMA) and poly(vinyl methyl ether) (PVME) were used. Solvents and other chemicals, like peroxide initiator, used in the sample preparation for the analyses are listed as well.

The second section gives details of the experimental work and procedures. These include flame and chromic acid treatments, non-reactive and reactive compounding and photo-induced vapour grafting. Other experimental details, like spin coating, chemical derivatisation and lapshear joint preparation had been described as part of the complete analysis.

The final section describes the methods of analysis, i.e. the experimental equipment and conditions used. Many different techniques were used to analyse the samples. XPS was used to examine the surface elemental composition on the samples, before and after treatments and modifications, aided by the analysis of contact angle measurement. Adhesion joint strength was performed to evaluate adhesion between the various surface treated and modified samples. Other techniques, such as ATR-IR and AFM were used to try and give a complete and coherent picture of what was happening



---

## 3.1 MATERIALS AND CHEMICALS

### 3.1.1 Standard Polymer

Polystyrene (PS) homopolymer (ex Nova Chemicals) was obtained in the form of "crystal" pellets, although the polymer is approximately 100% amorphous. The polymer is high heat extrusion and injection grade 202.

### 3.1.2 Styrene Maleic Anhydride (SMA) Copolymers

Low molar mass styrene maleic anhydride copolymers (SMA) (ex Elf Atochem-Atofina) were obtained in the solid-flakes form. The copolymers were supplied with molar ratio of 50:50, 66:34 and 75:25 styrene to maleic anhydride.

### 3.1.3 Solvents and Other Chemicals

Heptane, 2-propanol and methanol (ex Fischer Chemicals, general laboratory reagent grade) were distilled and stored in chromic acid cleaned glass storage bottles.

Tetrahydrofuran (THF) and toluene (ex Fisher Chemicals, general laboratory reagent grade) were used as purchased. Sodium hydroxide and sodium sulphate (ex Fisher Chemicals, specified reagent for laboratory work) were used as purchased. Sulphuric acid (ex Fisher Chemicals, specific gravity = 1.84, 98% purity) was used as purchased.

Styrene (ex Aldrich, 99% purity), di-*tert*-butylcarbodiimide (Di-*t*BuC) (ex Aldrich, 99% purity), pyridine (ex Aldrich, 99% purity), maleic anhydride (ex Aldrich,

powder, 95% purity), benzophenone (ex Aldrich, 99% purity) were used as purchased, unless stated otherwise. Trichloroethylene (Aldrich, 98% purity) and potassium dichromate (ex Aldrich, 99%) were used as purchased. 2,2,2-trifluoroethanol (TFE) (ex Fluorochem Limited) was used as purchased.

Epoxy adhesive used in the adhesion tests was Araldite 2011 A/B Vantico (AW106 and HV953U) supplied by Europia Limited. Poly(ethylene terephthalate) (PET) film (Melinex) was used as supplied in laboratory.

Organic peroxide, 1,3-bis(*tert*-butyl peroxy isopropyl)benzene, Tradename: Varox<sup>®</sup> 802-40C (ex R.T. Company, Inc) in powder form, was used as purchased as an initiator for reactive compounding. Poly(vinyl methyl ether) (PVME), Lutonal M 40 (ex BASF, 50% in water) was used as purchased.

The liquid used for contact angle measurement was doubly distilled water produced in laboratory.

## 3.2 EXPERIMENTAL WORK

### 3.2.1 Sample Preparation

A melt pressing method was found to be the most suitable for preparing a flat, contaminant free surface. After much experimentation the following method was found to be optimum. A plaque of polymer 15 mm x 15 mm x 2 mm thickness was made by compression press in a mild steel mould, sandwiched between sheets of PET films as a release aid. Prior to use, the PET was first cleaned with distilled heptane in an ultrasonic bath for 15 minutes and then dried, followed by cleaning with distilled 2-propanol, using the same procedure as for distilled heptane. The purpose of cleaning PET film was to remove any silicone molecules with the non-

polar heptane, and elimination of any polar molecules and cyclic trimers on the surface with 2-propanol solvent. PET film has been shown to be free of transferable contamination after washing in an ultrasonic cleaner with fresh organic solvent such as methanol, acetone or *n*-heptane for 15 minutes [164].

Glass microscope slides were also used to sandwich PET film (see Figure 3.1), in order to provide an evenly flat surface for the plaque, which is very important for contact angle measurement. The pressing was done at 145°C, a temperature above the PS  $T_g$  of which is 100°C and below the melting point of PET, ~ 220°C. This was to decrease the chance of transfer of low molecular weight materials from the PET to PS surfaces, hence avoiding changes in surface chemistry. The polymer pellets were left to pre-heat for 30 minutes, after which the molten PS was pressed at 2.5 MPa for a further 30 minutes, thereby ensuring the elimination of air voids or bubbles.

In cases where an extraction process was carried out, the samples were refluxed by soxhlet extraction in methanol solvent for at least 6 hours.

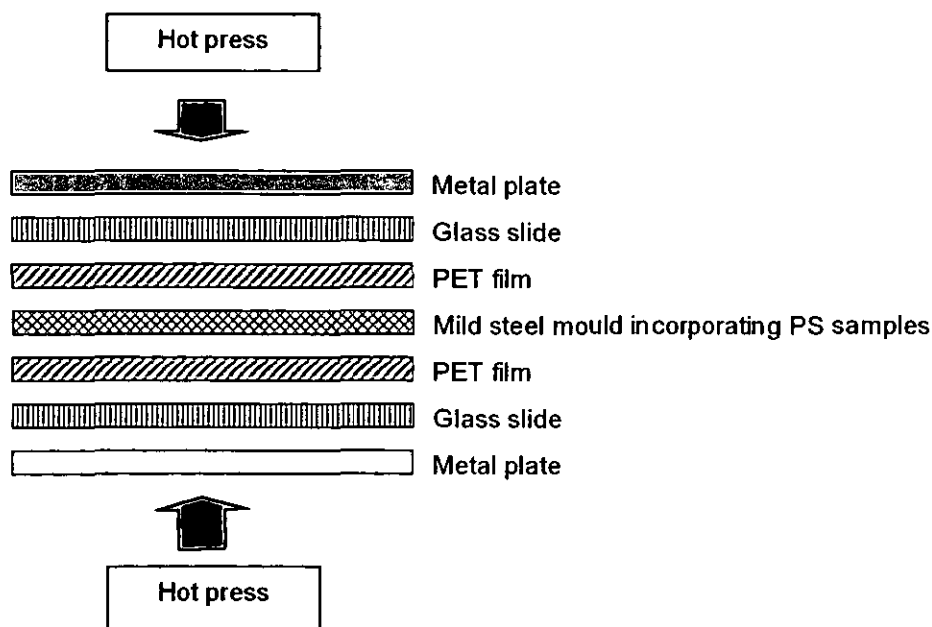


**Figure 3.1** Assemblies of the moulding of PS plaques.

---

### 3.2.2 Surface Cleaning of Samples

Each of the resulting PS plaques with smooth surfaces was then cleaned with distilled heptane in an ultrasonic bath for 15 minutes and dried. The sample was then washed with distilled 2-propanol in an ultrasonic bath again for 15 minutes, dried and stored in chromic acid cleaned sample tubes. All glassware used for cleaning the PS plaque was chromic acid washed and dried thoroughly. PS samples were handled with solvent-cleaned tools and the use of a glove was avoided, to prevent contamination.

### 3.2.3 Sample Pretreatments

#### *a) Flame Treatment*

PS samples were flame treated as shown in Figure 3.2. The treatment employs a double row ribbon burner (ex WSA Components), a conveyor chain system and an air/methane mixture supplying system. In order to produce an evenly treated surface, the burner which consists of two rows of closely spaced jets, was inclined at an angle of  $\sim 12^\circ$ .

The burner is fixed to a base with a toothed pinion, which engages with a non-movable rack. The base with the burner can be moved forward or backward to facilitate the variation of the distance from burner to the polymer film surface. Flame contact time, i.e. the time required for a single point on the polymer surface to pass through the flame, can be varied by changing the speed of the conveyor chain via a control box.

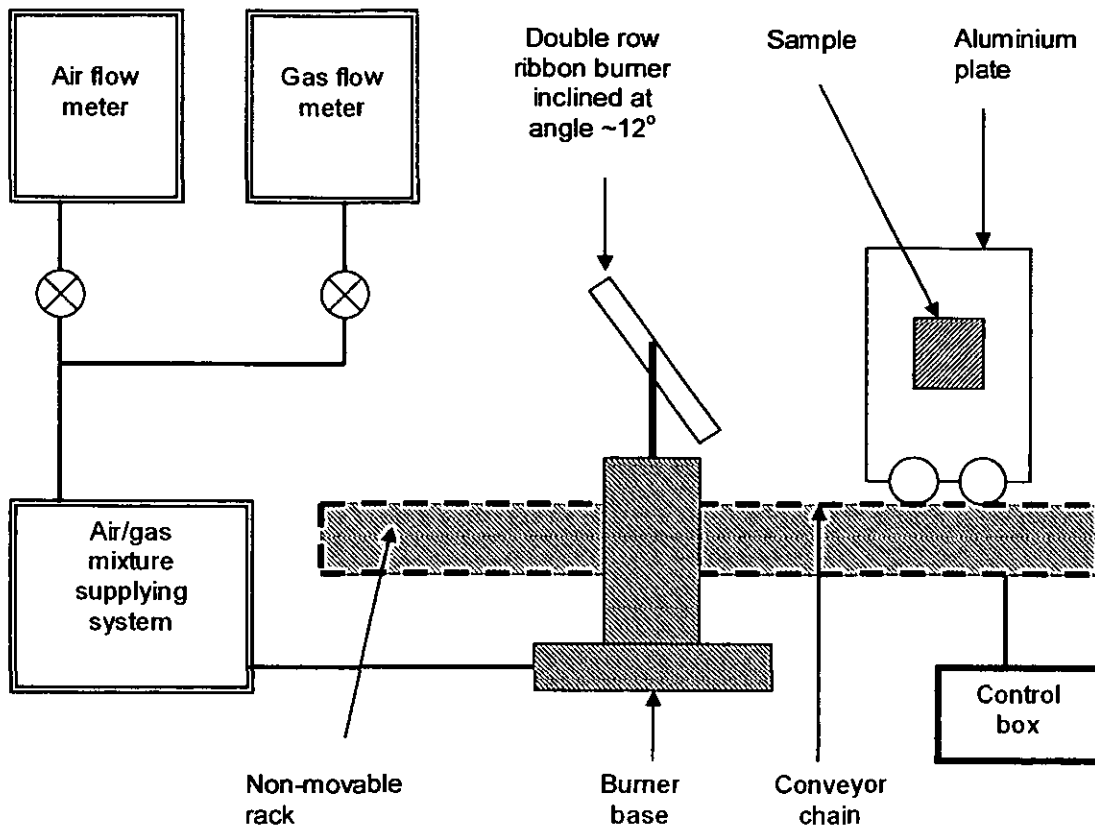


**Figure 3.2** Schematic diagram of flame treatment rig (used in laboratory).

A mixture of air (supplied at  $\sim 0.3$  MPa) and methane gas (supplied at  $\sim 2 \times 10^{-2}$  MPa) was fed into the burner. Flow rates of air and methane were monitored by two flow meters that were calibrated for air at standard temperature and pressure (S.T.P) by the manufacturers. Further calibration of the flow meters was carried out [6]. The air to methane ratio or flame intensity can be varied by altering the flow rates of air and methane.

In this research, the flame treatment conditions employed were based on the total flow rate of  $40 \text{ l min}^{-1}$ , following from Sheng's earlier work in flame treatment [6], to generate relative high oxygen concentration. The air:methane ratio was set at 11:1

and hence the air and methane flow rates (after flow meter calibration [6]) are 22.4 l min<sup>-1</sup> and 2.6 l min<sup>-1</sup>.

The distance between the inner cone tip of the flame and the sample's surface was set at 0.01m and the flame contact time was controlled at 0.04 seconds, which was employed as a safe maximum to avoid overheating the polymer, and causing distortion and even melting [6]. A PS plaque was mounted onto aluminium plate by double-sided adhesive tape. The plaque sample was passed through the flame. The plaque was flame treated in 8 rotation positions in order to achieve a uniformly treated surface. The treated sample was then removed using cleaned metal tweezers and kept in a sealed sample tube.

### ***b) Chromic Acid Etching***

Chromic acid solution was prepared as follows. It consisted of 5 parts (w/v) of potassium dichromate in 8 parts (w/v) of distilled water. While stirring, 100 parts of concentrated sulphuric acid (w/v) was slowly added to the mixture. The clear, purple red solution was then cooled down to room temperature and stored in a clean glass bottle.

Each PS plaque was dipped in a solution of chromic acid in a sample tube for 15 minutes at room temperature. The etching time was determined, based on earlier research [6] which had shown that an etching time of 15 minutes is adequate for PP. Thereafter, the treated plaque was removed and washed once with doubly distilled water before rinsing thoroughly in doubly distilled water in a beaker in an ultrasonic bath for 15 minutes. Fresh chromic acid solution was used for each sample etching. The treated plaque was then transferred to sample tube and left to dry in fumehood overnight, before storing in sealed sample tube.

---

### 3.2.4 Compounding

The compounding was carried out on a Haake Rheocord 90, a mini mixer that is a computer controlled torque rheometer. Using the rheometer it is possible to set and control the temperature and rotor speed. PS extracted pellets and SMA copolymers were individually ground into powder form, using a clean coffee grinder. The purpose was to encourage even mixing and distribution of the copolymers in the PS during compounding. Prior to PS-SMA mixing, the rheometer's chamber was flushed with powder form PS at 150°C, in order to remove any contaminate left behind in the mixing chamber due to previous mixing.

The rheometer was set at 200°C for non-reactive compounding. SMA copolymers of 0.1%, 1% and 10% of the total weight (50 g) were each measured out and pre-mixed with PS before adding into the pre-heated chamber. The mixing was carried out for 5 minutes at 50 rpm rotation speed. The mixture was removed and allowed to cool, then re-ground into powder and pressed into plaques for analysis.

For reactive compounding, the peroxide initiator concentration used was 0.1% by weight, that was thought to be an adequate amount needed for the process [113]. The initiator was pre-mixed together with the required copolymer and PS before adding to the mixing chamber. The temperature was set at 180°C (initiator peroxide may degrade above 200°C) and the mixing was carried out for the same duration and rotation speed.

PVME of 1% and 10% of the total weight (50 g) were prepared and dissolved in toluene in the ratio of 1:2. The mixture was mixed and stirred with the powder form PS, to ensure as even distribution as possible. The final mixture was held in vacuum for an hour at 80°C, i.e. below the  $T_g$  of PS, in order to remove the solvent. The resulting dried lumpy mixture was then left exposed overnight in a fumehood, before grinding into powder. The PS-PVME mixing was then carried out at under the same conditions as the PS-SMA non-reactive and reactive compounding.

---

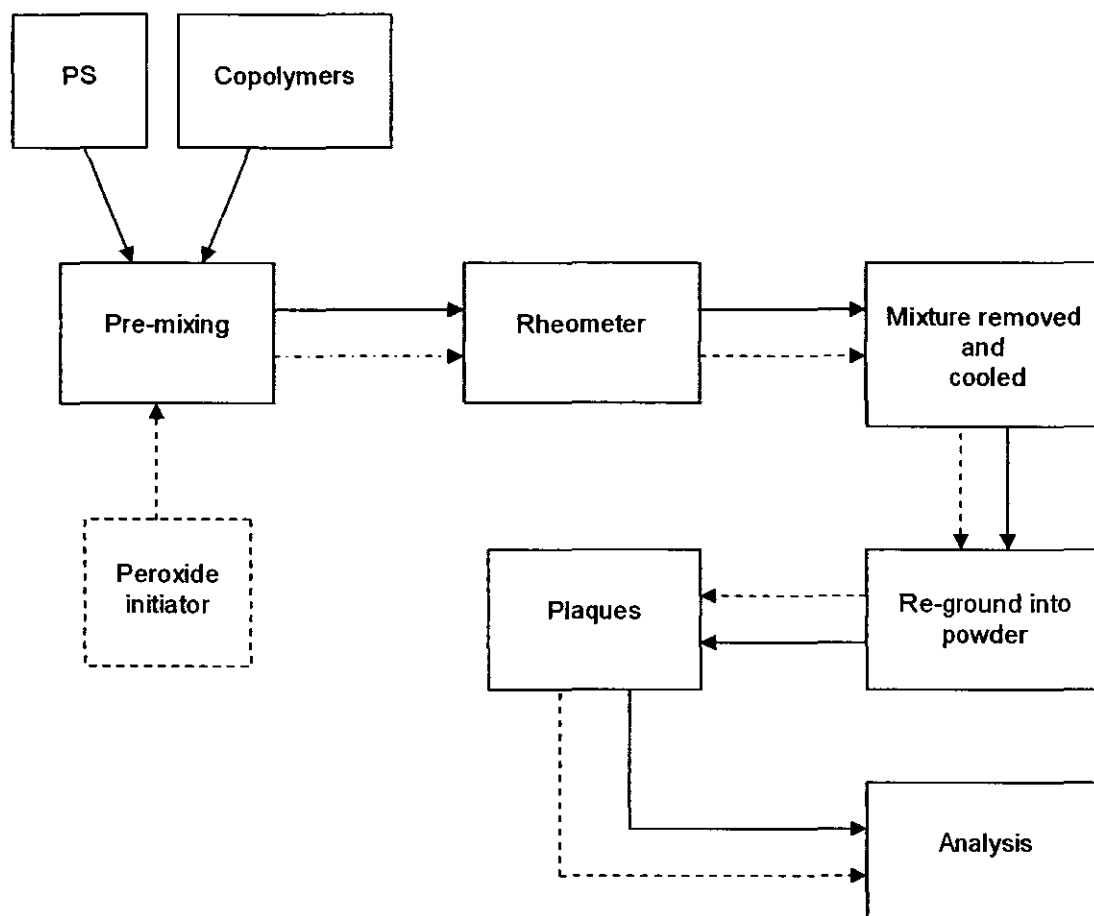


Figure 3.3 Flow chart illustrating the compounding procedures.

### 3.2.5 Photo-induced Vapour Grafting

Stabiliser was removed from the styrene monomer by washing with sodium hydroxide, and the styrene was dried with sodium sulphate. These processes were all carried out in the fumehood. The de-stabilised styrene monomer was then stored in a sealed container and kept in a refrigerator at  $\sim -20^{\circ}\text{C}$  until further use. A solution of benzophenone in methanol (0.2 M) was prepared [148, 193]. Each PS plaque was immersed in the solution for 2 hrs, so as to allow the benzophenone



photo-initiators to diffuse into. The samples were then dried overnight exposed in a fumehood. The UV-induced apparatus and the grafting experiment were carried out inside a wooden box, which is sealed with black paper and aluminium foil to prevent direct eye contact with the UV light and with the operator wearing an anti-UV safety goggles.

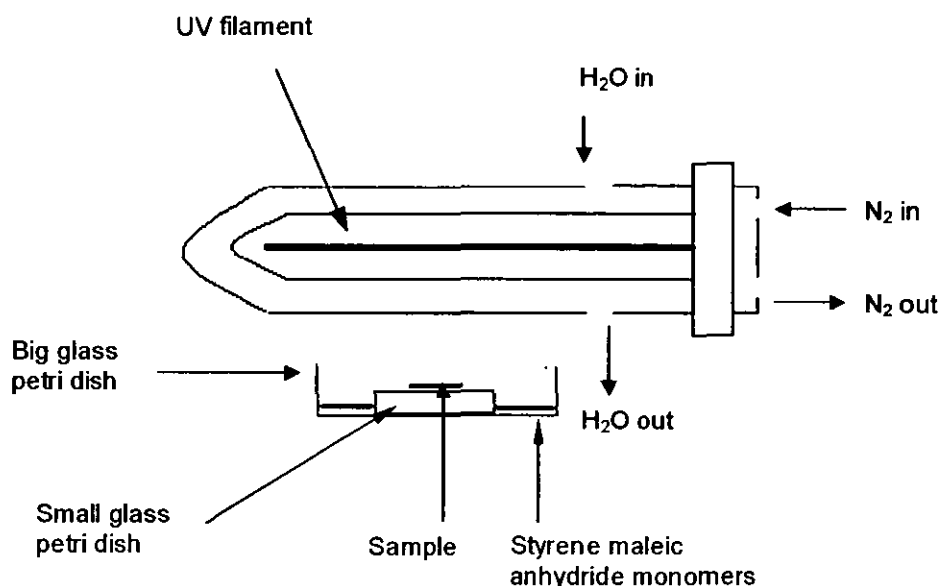


**Figure 3.4** Schematic diagram of UV-induced apparatus set up.

The sample was irradiated for 15 minutes on both sides under nitrogen to produce the intermediate (see Figure 2.14). A maleic anhydride, styrene and toluene (2:1:2 ratio) monomer solution was prepared. The solution was heated to about 50°C and immediately transferred to a big glass petri dish. The sample to be treated was placed on a small glass petri dish, which has been placed upside down in the big glass petri dish, as shown in Figure 3.4. The UV reactor was purged with nitrogen for 5 minutes and water was circulated to cool the UV filament during irradiation. The sample was irradiated with UV radiation for 15 minutes on one side. It was then turned over and irradiated for another 15 minutes on the other side. The

irradiation was carried out in the box, inside the fumehood. The sample was then cooled down for 30 minutes before washing with methanol, dried and exposing overnight in fumehood and then kept sealed in tube ready for characterisation.

As stated in Section 2.9.6, the benzophenone initiates chain growth of a styrene maleic anhydride copolymers from the vapour phase monomers [147 – 150]. This copolymer chain is attached to the PS backbone and as such is a grafted copolymer, see Figure 2.14.

### 3.2.6 Chemical Derivatisation

A mixture of TFE, pyridine and di-*tert*-butylcarbodiimide, in the ratio of 9:4:3 by volume [194], was prepared and used to derivatise carboxylic acid groups [6, 166, 173]. The derivatising reagent was kept in a clean, air-free flask (purged with nitrogen), wrapped in aluminium foil to minimise exposure to light when not in use. Prior to exposing the samples to the derivatising agent, a freeze/thaw regime using liquid nitrogen was implemented to expel the impurities in the derivatising reagent flask. Vapour phase derivatisation was carried out under a vacuum of about  $10^{-5}$  Torr on a vacuum frame, see Figure 3.5. The sub-frames, under the main frame, provided a contamination free system. The samples in the tube were pumped down before exposing to the derivatising reagent. The derivatisation reaction was then allowed to start and was left overnight ( $\geq 16$  hours). After that, the vacuum frame was pumped down again overnight, before removing the samples. The samples produced were kept in sealed tubes, but analysed on the same day.

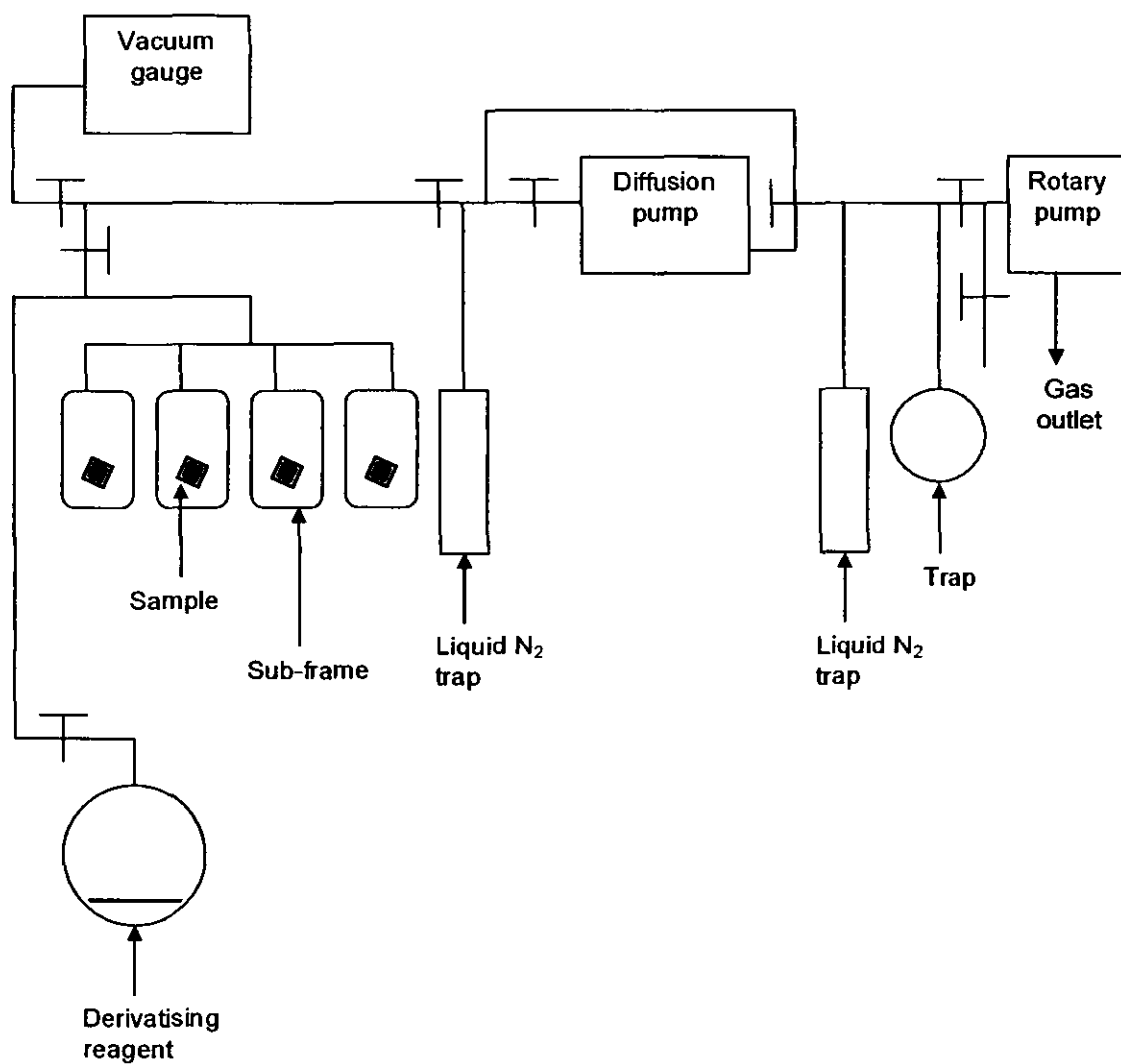


**Figure 3.5** Schematic of vacuum frame.

---

### 3.2.7 Spin-coating

A 2% SMA copolymer solution in THF was prepared and spun onto a clean microscopic glass slide, held by vacuum in the spin coater (Spincoater Model P6700 series), at a speed of 4000 rpm spinning speed for 60 seconds under a nitrogen atmosphere. The samples were then dried, exposing in a fumehood overnight.

### 3.2.8 Lap Shear Joint Preparation

Metal strips (15 mm x 70 mm x 3 mm thickness) were sandblasted and degreased in trichloroethylene in ultrasonic bath for 30 seconds and air dried before use in bonding. A two-part epoxy (see Section 3.1.3) was mixed in equal quantities by weight as per the manufacturer's instruction. 1% of Ballotini by weight (maximum sphere diameter approx 250  $\mu\text{m}$ ) were added to the adhesive mixture to give a consistent bondline thickness. The lap shear joints were made by sandwiching the PS plaque between two metal strips as shown in Figure 2.1b. The joint was held by paperclips and was allowed to cure at room temperature for at least 24 hours before testing.

## 3.3 METHODS OF ANALYSIS

### 3.3.1 X-ray Photoelectron Spectroscopy

XPS experiments were performed on a VG ESCALAB MKI spectrometer using an Al-K $\alpha$  X-ray source (1486.6 eV), at a take-off angle of 90°, with respect to the surface. Low resolution spectra were obtained at a pass energy of 100 eV with 5 scans. For low resolution scans, 5 mm diameter inlet and 10 by 4 mm exit slits

were used. Binding energy was measured relative to adventitious carbon at 285.0 eV. Quantification was made using relative sensitivity factors that take into account photoelectron cross-section angular asymmetry parameters and attenuation length [136].

### **3.3.2 Attenuated Total Reflection Infrared Spectroscopy**

A Shimadzu Fourier Transform Infrared Spectrophotometer (FTIR) 8300 was used in conjunction with an ATR attachment to acquire ATR-IR spectra. The apparatus had a diamond crystal. The system is MKII Golden Gate Single Reflection ATR system. 150 scans were collected over the range of 625 to 4000 wavenumbers. Two measurements were carried out and averaged. The spectrum of water vapour was subtracted from the spectra.

### **3.3.3 Atomic Force Microscopy**

AFM was employed to measure the topographical features of a sample's surface. Two measurements were carried out across the specimen's surface using a TM Microscopes Explorer AFM, operated in intermittent contact (Tapping<sup>TM</sup>) mode. The probe used is TM Microscopes Non-Contact Low Resonant Frequency (LRF) Silicon Probe (PIN 1660-00).

### **3.3.4 Contact Angle**

#### **a) *Surface Tension of Test Liquid***

The surface tension of doubly distilled water was measured by the Du Noüy ring method in detachment mode on a Krüss K10T Tensiometer. The measuring vessel

was cleaned with chromic acid solution and dried thoroughly. Before each measurement, the platinum ring was flamed, by holding in a hot Bunsen burner flame until the metal was bright glowing red, in order to remove any contaminant organic species. The torsion balance had been calibrated with weights range from 0.2 to 1g. Measured surface tensions (scale readings), were subject to correction by the Harkins and Jordan method [195]. The correction factor was required in order to account for the inner and outer ring radii not being equal and for the weight of liquid that remains on the ring after the rupture of the meniscus [138]; this has been justified theoretically by Freud and Freud [196]. An average of 3 measurements was carried out, at three temperatures and fresh test liquid was used every time. Table 3.1 shows the results before and after correction. The results were in good agreement with literature values. A detailed calculation of the correction factor can be found in Appendix A.

**Table 3.1** Measured surface tension of water testing liquid.

Temperature / °C	Experimental $\gamma_{sl} / \text{mN m}^{-1}$	Correction Factor	Corrected $\gamma_{sl} / \text{mN m}^{-1}$	Literature $\gamma_{sl} / \text{mN m}^{-1}$ [75]
19.9	77.4	0.9390	72.7	72.8
30.1	75.8	0.9380	71.1	71.2
40.0	74.2	0.9365	69.5	69.6

### **b) Contact Angle Measurement**

The syringe barrel and plunger were cleaned with chromic acid, followed by thorough washing with doubly distilled water and they were then dried overnight. The syringe needle was washed with doubly distilled water and dried overnight. The syringe was rinsed and purged several times with the water test liquid before measurement was carried out. Table 3.2 shows the literature values of surface free

energy for the contact angle liquid. In this work, the corrected value of the water test liquid was used in the calculation of work of adhesion, see Table 3.1.

**Table 3.2** Literature values of surface free energy of contact angle liquid [45].

Liquid	$G_L^s$ (mJ m <sup>-2</sup> )	$G_L^p$ (mJ m <sup>-2</sup> )	$G_L^d$ (mJ m <sup>-2</sup> )
Water	72.8	51.0	21.8

The sample was placed on a microscope glass slide, which was then placed on the sample platform (see Section 4.1.2). A droplet of liquid diameter between 2 to 4 mm was placed onto the PS surface via the syringe.

The droplet was allowed to equilibrate for about 2 seconds, before measurements were taken. The advancing angle was measured after further liquid was introduced into the water droplet on the sample surface, with the needle being maintained in the droplet throughout measurement, in order not to perturb it. The receding angle was measured by the same procedure, except that the liquid was slowly withdrawn into the syringe. At least 8 drops were placed across the specimen and their contact angle values averaged from. All contact angle measurements were initially carried out at room temperature between 20°C to 25°C.

For the temperature dependence measurement, measurements were carried out over the temperature range 10°C to 45°C. The temperature was adjusted via the water bath. A small beaker containing doubly distilled water was placed in the metal box (see Section 4.1.2) to create a saturated atmosphere of water vapour. The purpose was to keep the spreading pressure the same for all measurements. The water in the beaker was cooled down to 10°C and placed in the metal box. This allowed the temperature of water to gradually build up with the test temperature, increasing from 10°C to 45°C during measurement. When cooling down the system, the water was removed to avoid condensation.

### **3.3.5 Adhesion Lap shear Joint Test**

Lap shear joint testing was carried out at room temperature, on a Lloyd tensiometer with a 10 kN load cell, at a crosshead speed of  $12.7 \text{ mm min}^{-1}$ . The initial jaw separation was 40 mm. Six readings were taken for each sample type and the average taken. Two extra pieces of metal (30 mm x 15 mm x 5 mm thickness) were gripped at the jig jaw's end in order to distribute evenly the stress around the joint during pulling, see Figure 3.6.



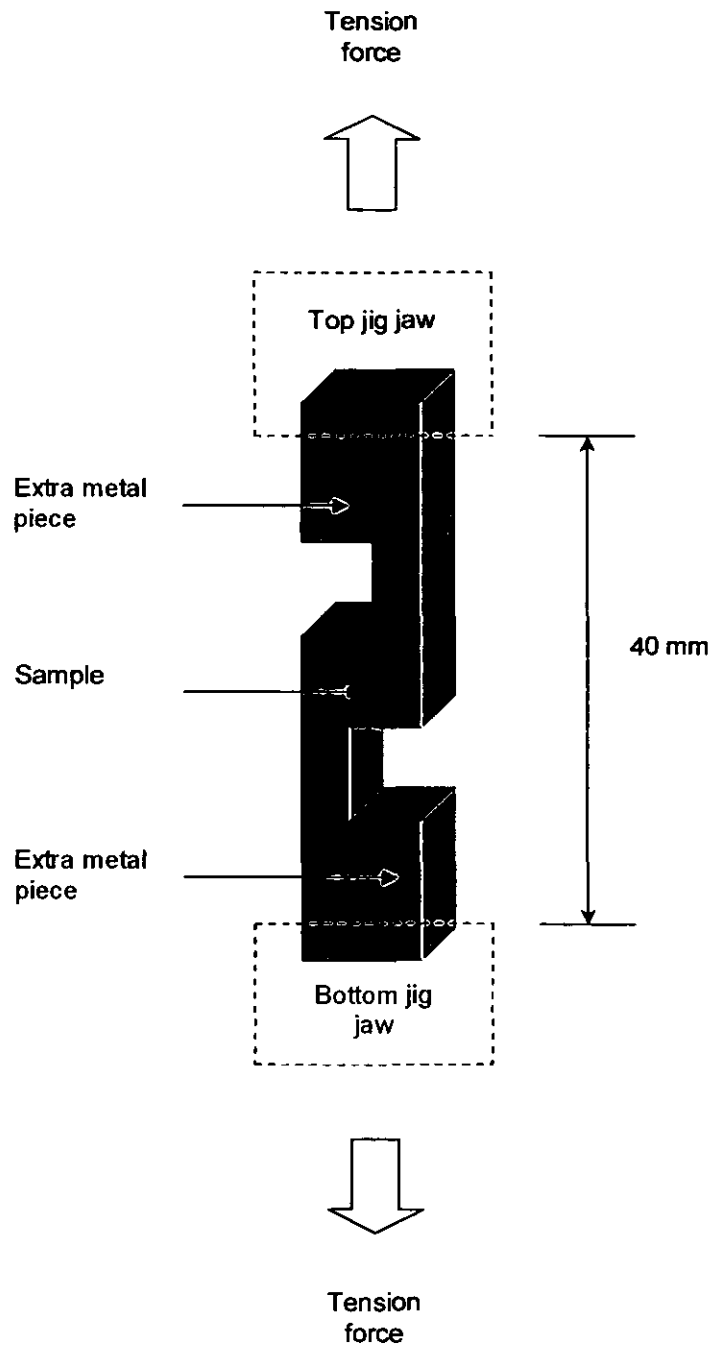


**Figure 3.6** Schematic diagram of lap shear assembled test piece.

## **CHAPTER 4 RESULTS AND DISCUSSION**

This chapter consists of eight sections. Section 4.1 gives a brief description of the built contact angle instrument, its optic features and software used. Sections 4.2 and 4.3 describe the results from the characterisation of the base polymer, PS and the SMA copolymers. Sections 4.4 to 4.7 outline the results of surface treatment, non-reactive, reactive compounding and photo-induced grafting, respectively. The discussion aimed to provide an explanation as well as a comparison between the different treatments and modifications. Lastly, Section 4.8 focuses on the temperature dependence contact angle measurement and thermodynamic work of adhesion, in terms of enthalpy and entropy, of the various PS systems.

### **4.1 DESIGN OF THE CONTACT ANGLE INSTRUMENT**

#### **4.1.1 Introduction**

As reported by several authors [83 – 87, 197], contact angles may either decrease or increase with temperature. However, the change in the contact angle measurement is quite small. The contact angle apparatus used in this study has been built in-house (see Figure 4.1). The optics and software have been designed to give the accurate measurement of angle needed to study small changes in contact angle with temperature.

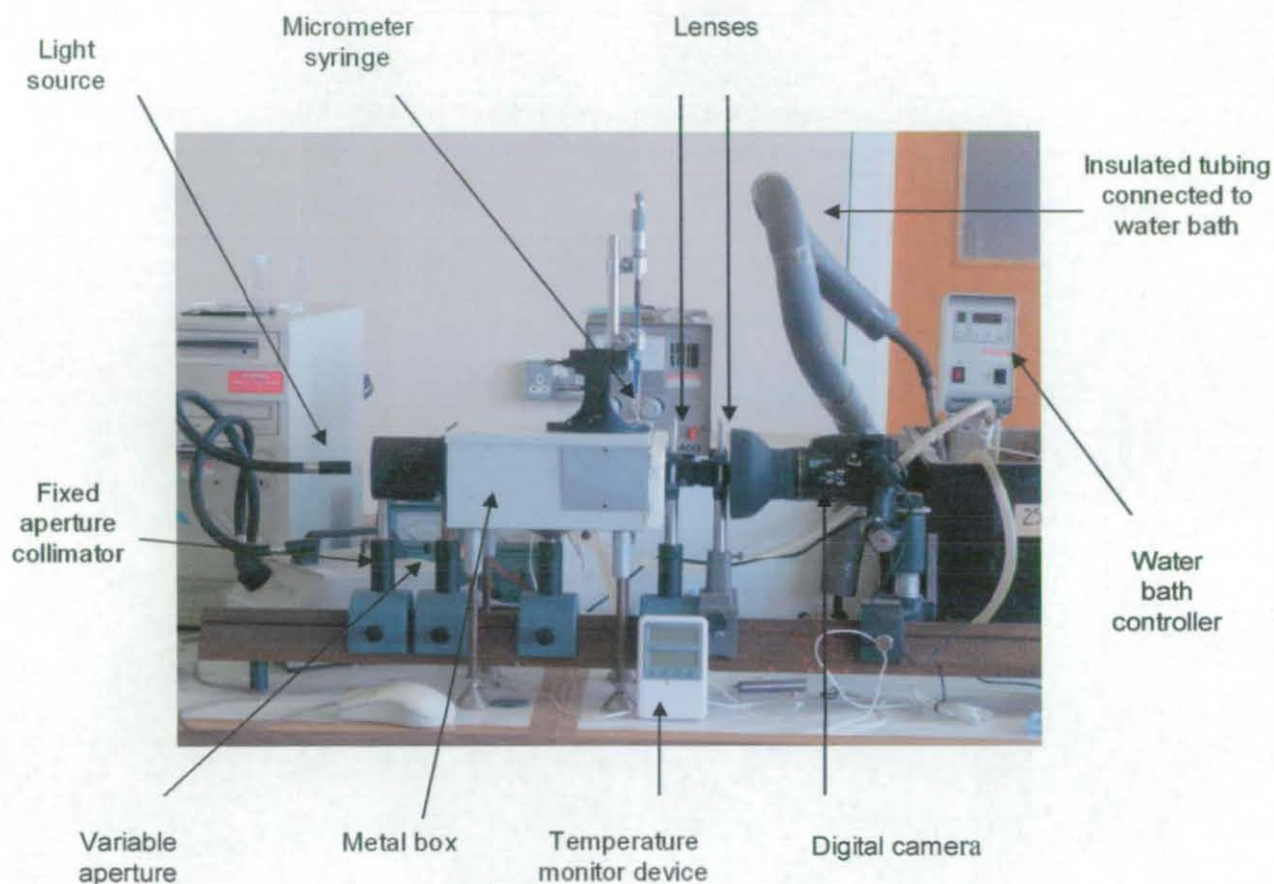
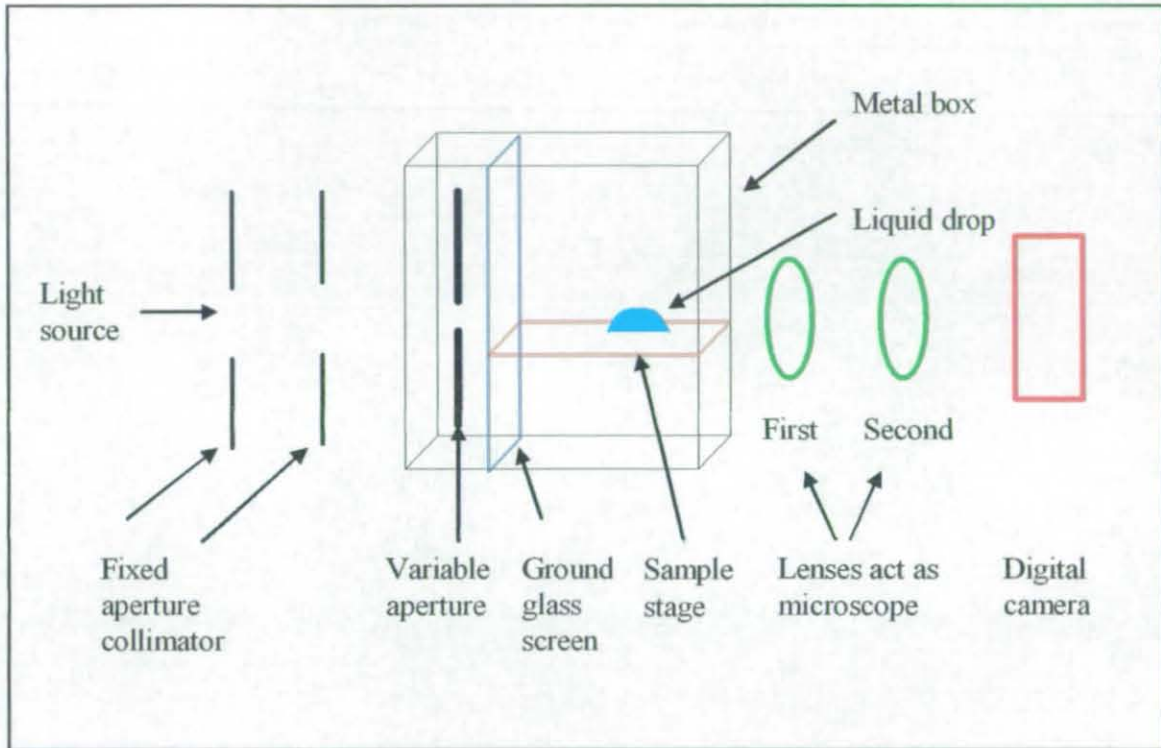


Figure 4.1 In house contact angle apparatus.

4.1.2 Description and Features

Figure 4.2 presents a schematic diagram of the optics of the contact angle apparatus. This comprises a light source that is aligned to pass through an aperture; the size of the aperture can be varied. This is important in terms of reducing systematic error in contact angle measurement. The size of the variable aperture is smaller than the fixed aperture size and adjusted to produce a sharp silhouette of the liquid drop. The first lens produces an enlarged virtual image and

the second lens produces a real inverted image, which is captured by the digital camera.



**Figure 4.2** Schematic diagram of optical setup.

Figure 4.3 shows an enlarged diagram where the size of variable aperture is adjusted according to the size of the drop.  $a$  is the size of the liquid drop,  $b$  is the distance from the first lens to the liquid drop and  $c$  is the total distance from the first lens to the ground glass screen.  $x$  is calculated, according to Equation {4.1} and represents the diameter of the variable aperture, which is then adjusted,

$$\frac{a}{b} = \frac{x}{c} \quad \{4.1\}$$

The aperture size must be equal to or less than  $x$ . If greater than  $x$ , then the front side of the drop is illuminated and this results in an inaccurate drop profile [198].

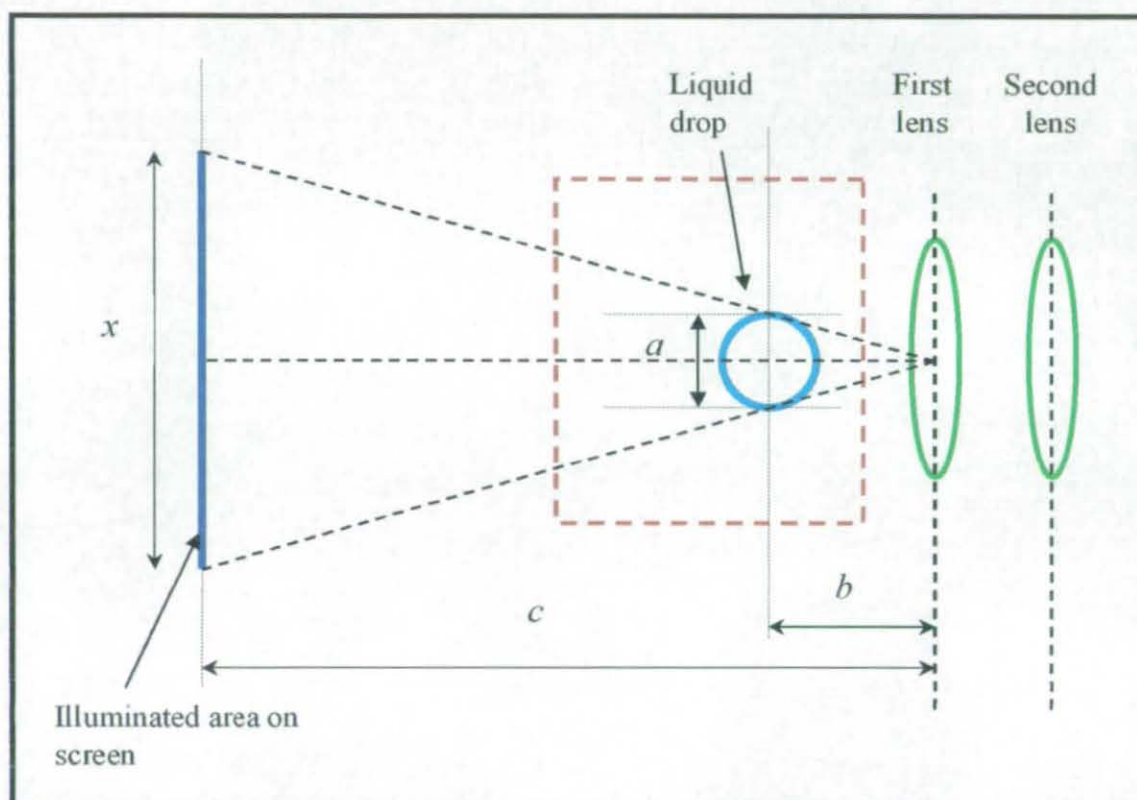


**Figure 4.3** An enlarged diagram in plan view.

A micrometer syringe is securely fastened above the metal box, which has been layered with black-painted foil inside. The purpose here is to eliminate reflected light from all directions. This means the only source of light is from the illuminated ground glass screen. The box houses a sample stage where the sample under



study is placed. The sample stage could be adjusted in height and tilt (both along the direction of the optics and perpendicular to them).

A copper heating coil painted black was fixed inside the box and connected with tubing at both ends, to a water bath. The temperature was set and adjusted via the water bath and water pumped and run through the tubing and coil. A fan is installed next to the coil to circulate air in the box and ensure a uniform temperature. The box is heavily insulated with polystyrene foam. The apparatus is able to measure contact angles over a range of 0°C to 40°C. The temperature is monitored by a device.

### 4.1.3 Software for Contact Angle Measurement

The image is processed using software specially written for the equipment. The accurate position of the liquid/air interface is measured by scanning across the digital image and monitoring the change in brightness. Differentiation using Savitsky-Golay [199] convolutional techniques followed by interpolation between pixels gives a precise position of the interface. The interface is assumed to be at the point where the maximum rate of change of brightness is detected between the light background and the dark silhouette of the drop.

The accurate profile of the drop obtained was then iteratively fitted to a quadratic in the region of the polymer surface, using a non-linear least squares method and Mac Lauren's expansion [200]. This provides a superior method of evaluating contact angle at the polymer surface compared to fitting a straight line to a limited number of data points very close to the surface, see Figure 4.4.

Figure 4.4 presents a left-hand contact angle drop profile. The last fifty points of the contact angle picture were used to fit to a quadratic curve rather than a straight line. The dots represent the data points as interpreted by the software. It can be

seen that the quadratic fit is a much better representation of the contact angle drop than represented by the linear fit. Angles obtained by the quadratic fit are typically 2 to 3° greater than the linear fit and from Figure 4.4 they are seen to be more accurate. The straight line clearly underestimates the true angle. The quadratic fit will, if anything, lead to a small but reasonably consistent overestimation.

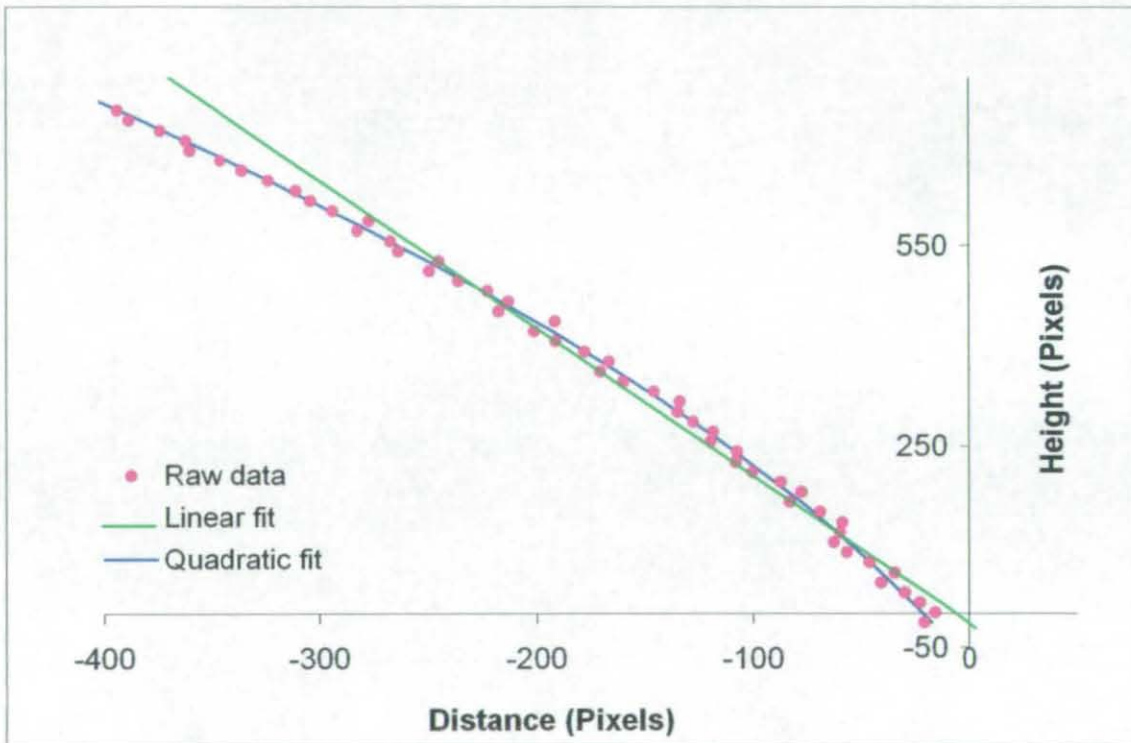


**Figure 4.4** A left-hand side of the contact angle liquid drop.

Magnification by the apparatus was measured using a calibrated scale. Magnification is typically  $\times 28$  and will vary slightly depending on the precise position of the drop. This means that pixels (Figure 4.4) are equivalent to about 7 microns. It has been found that the apparatus can measure the contact angle of

water on PS with a reproducibility of  $\pm 1.4^\circ$ . The main source of random error is probably the positioning of the baseline.

### 4.1.4 Summary

The contact angle apparatus and developed software can be used to obtain a clear profile of the contact angle and with a quadratic fit will give accurate contact angle measurements. This is important as the change in contact angle with temperature is very small. The apparatus was used in all the contact angle measurements for all the experiments discussed in the following sections.



---

## **4.2 CHARACTERISATION OF POLYSTYRENE POLYMERS**

### **4.2.1 Introduction**

This section reports the initial characterisation of the base polystyrene (PS) material used. The surface of untreated PS was characterised by XPS, ATR-IR, AFM and contact angle measurement. The results have been compared to literature values.

### **4.2.2 X-ray Photoelectron Spectroscopy**

XPS was used to determine the surface elemental composition of the untreated PS. An analysis was carried out on the untreated PS before solvent extraction (see Section 3.2.1). The analysis revealed 2.4 atom % of oxygen on the untreated PS before extraction, which suggested the presence of additives in the PS as received. The initial contact angle before extraction was 70°.

After the removal of additives by solvent extraction, the XPS broad scan in Figure 4.5 showed the presence of carbon, referenced to 285.0 eV (99.0 atom %) on the untreated PS surface. The amount of oxygen had been greatly reduced, but was still detectable at a low level (1.0 atom %). The contact angle was also higher at 90°. This is consistent with the removal of polar molecules from the surface. It was not thought that these oxygen groups could have come from the cross-contamination from PET film used to press the sample, given that the PET film was cleaned and washed with suitable solvent to remove species including cyclic trimers (see Section 3.2.1) [164].

One explanation could be that some surface oxidation may have occurred on the untreated PS during pressing. Another possible source of oxygen could be end groups of the PS chains.

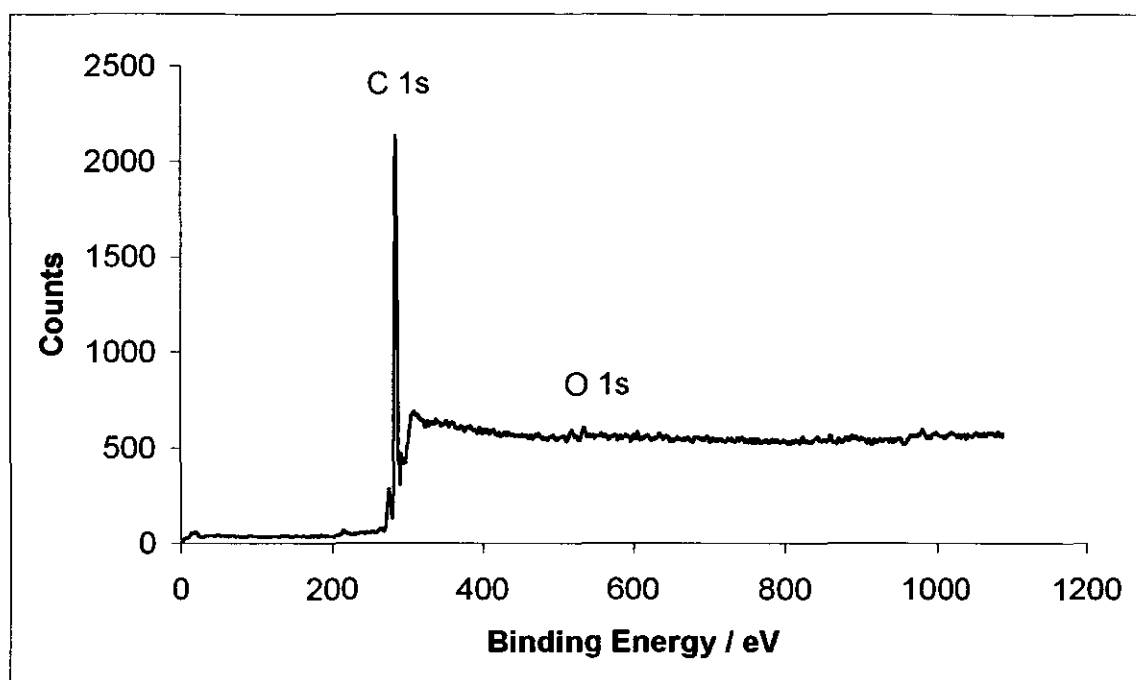
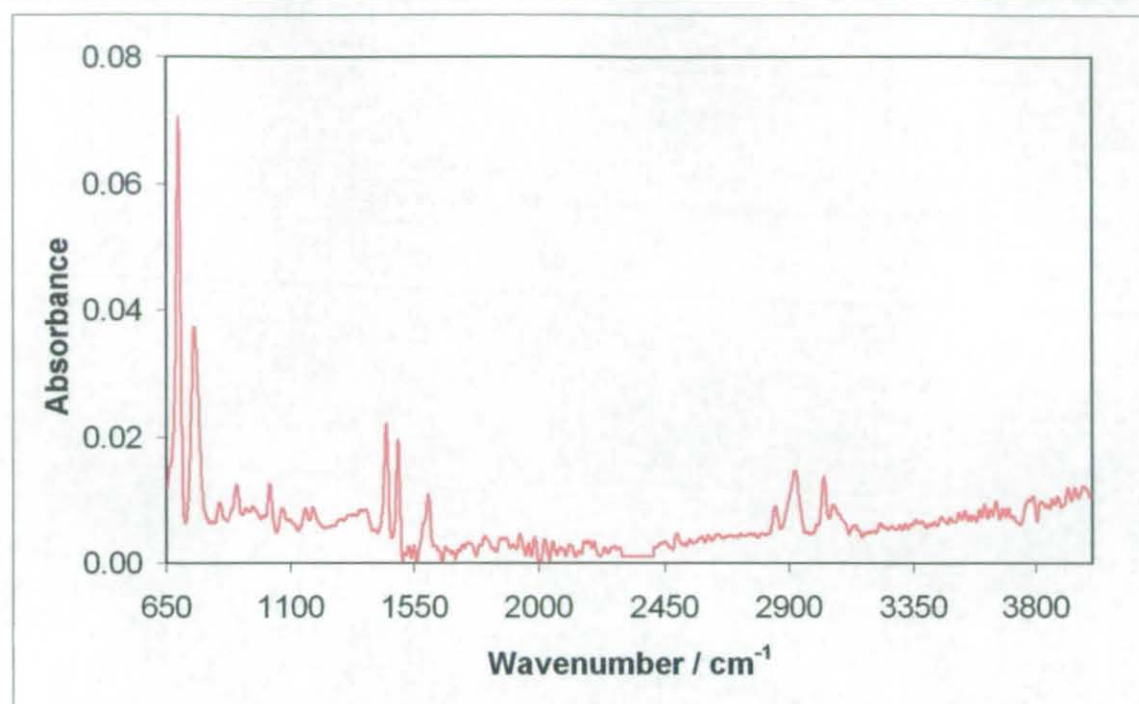


Figure 4.5 XPS broad scan of untreated PS.

#### 4.2.3 Attenuated Total Reflection Infrared Spectroscopy

An infrared analysis for untreated PS was carried out and the spectrum is displayed in Figure 4.6. The peak assignments were compared to the literature values and are tabulated in Table 4.1. As can be seen, the measured peak values were close to the literature values. The out-of-plane C-H bending vibrations produced a group of bands below  $900\text{ cm}^{-1}$ . The frequency of this C-H out-of-plane vibration was determined by the number of adjacent hydrogen atoms on the ring, hence the frequency is a means of determining the substitution pattern [201]. The two strong absorptions occurred between  $770\text{ to }730\text{ cm}^{-1}$  and  $720\text{ to }680\text{ cm}^{-1}$  indicated a mono-substituted benzene ring [202].



**Figure 4.6** ATR-IR spectrum of untreated PS.

The bands in the  $1600$  to  $1450\text{ cm}^{-1}$  regions have been shown to be mostly due to six-membered  $\text{C}=\text{C}$  aromatic ring systems and are also due to stretching vibration modes. The backbone  $\text{CH}/\text{CH}_2$  portions of PS will give rise to two characteristic saturated stretching vibrations at  $2850\text{ cm}^{-1}$  and  $2930\text{ cm}^{-1}$ . No peaks other than those attributable to PS were detected.

**Table 4.1** IR wavenumber peak assignments of untreated PS [201 – 203].

Peak / $\text{cm}^{-1}$ (Measured)	Peak / $\text{cm}^{-1}$ (Literature)	Assignments
696	695	Aromatic C-H out-of-plane vibrations
751	750	
841	840	Alkyl C-H deformations
915	915	
1018	1020	Aromatic =C-H in-plane deformation vibrations
1449	1450	Aromatic –C=C- stretching vibrations
1491	1490	Alkyl $\text{CH}_2$ scissor vibrations
1599	1600	Aromatic –C=C- stretching vibrations
2852	2850	Aromatic and alkyl C-H stretching vibrations
2920	2920	
3021	3020	Aromatic =C-H stretching vibrations
3055	3055	

#### 4.2.4 Atomic Force Microscopy

The surface roughness of pressed, untreated PS was determined by AFM, see Figure 4.7. The data was collected from two different regions on the sample's surface. The surface roughness,  $R_a$ , was measured at 61 nm with estimated error of between 1 to 2 nm. The compression pressing of PS produced a reasonably smooth surface, which was thought suitable for contact angle measurements.

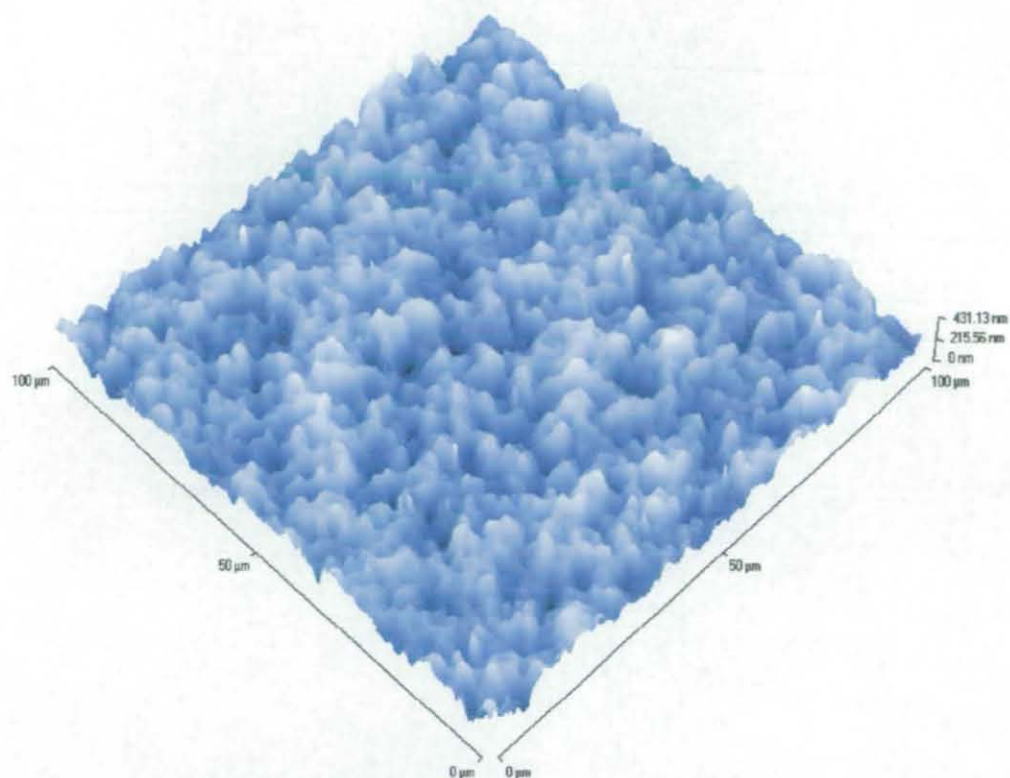


Figure 4.7 AFM scan of untreated PS.

#### 4.2.5 Contact Angle Measurement

Advancing ( $\theta_{adv}$ ) and receding ( $\theta_{rec}$ ) water contact angles were measured and data are presented in Table 4.2.

Table 4.2 Contact angles of untreated PS at  $\sim 25^\circ\text{C}$ .

Polystyrene	$\theta_{adv} / ^\circ$	$\theta_{rec} / ^\circ$	$\Delta\theta / ^\circ$
Untreated	90.9 (1.4)	80.3 (1.2)	10.6

Note: Standard deviations are given in brackets

The advancing angle was  $90.9^\circ$ , which is in good agreement with the literature values of  $91.3^\circ$  [204, 205] and  $91^\circ$  [162]. A measurable water contact angle hysteresis value, ( $\Delta\theta = \theta_{adv} - \theta_{rec}$ ), is shown in Table 4.2. As discussed in Section 2.7, there are several causes of hysteresis. The analysis by AFM showed a surface roughness of 61 nm. Kwok et. al. [204] have concluded that roughness smaller than approximately  $0.1\ \mu\text{m}$  will have no influence on contact angles, as reported by Sedev and co-workers [206] and this was also in agreement with other workers [92, 162, 207]. Therefore the hysteresis value  $10.6^\circ$  seen here is not attributed to the surface roughness of the PS.

It is possible that some surface reorganisation may have occurred. That is, there might be a different orientation of phenyl rings in the PS surface in contact with water, compared to that when in contact with air. This has been postulated by Good [208], where he reported an average reading of  $26^\circ$  for contact angle hysteresis on PS. Incorporation of some water molecules in the surface leaving the receding surface different from the advancing one, would also be a possibility.

### 4.2.6 Summary

It is observed that surface oxidation or chain end groups may contribute to the small amount of oxygen detected on the PS surface. IR spectroscopy has identified the bands similar to those indicated in literature. Accurate water contact angles were measured and found to be in good agreement with literature values. AFM analysis has shown that pressing of the sample does not produce a rough surface. The contact angle hysteresis may have been caused by the surface reorganisation and/or incorporation of water.

## 4.3 CHARACTERISATION OF STYRENE MALEIC ANHYDRIDE COPOLYMERS

### 4.3.1 Introduction

In this section, the copolymers having various compositions were characterised by XPS, ATR-IR, AFM and contact angle measurement. The purpose is to provide an understanding of the characteristics of the copolymers. The results were compared with the literature values wherever possible. Derivatisation with 2,2,2-trifluoroethanol (TFE) was used to identify the oxygen containing groups on the copolymers. The derivatised samples were also surface characterised by the various analysis techniques.

### 4.3.2 X-ray Photoelectron Spectroscopy

XPS analyses were carried out on the copolymers before and after derivatisation. Low take-off angle can show the presence of a thin surface layer, here two different take-off angles were used on 50:50 and 75:25 copolymers. The purpose was to quantify the number of available maleic anhydride groups on the surface compared to the subsurface. The results are presented in Table 4.3.

**Table 4.3** Elemental compositions of SMA copolymers at different take-off angles.

S:MA	Angle of photoelectron collection / °	Elemental Compositions / Atom %	
		[C]	[O]
50:50	30	83.7	16.3
	90	83.6	16.4
75:25	30	90.3	9.7
	90	90.2	9.8

At both take-off angles, the 50:50 copolymer showed no significant difference in the amount of maleic anhydride groups in the surface and subsurface. In the same manner, the 75:25 copolymer also showed no significant difference in the amount of maleic anhydride groups. Therefore this indicated that the surface and subsurface have similar compositions over the range of about 10 nm. The concentrations of carbon and oxygen at the bulk were calculated for all copolymers and compared to the measured compositions at the surfaces, as summarised in Table 4.4.

**Table 4.4** Calculated bulk and measured surface ratio of elemental compositions of SMA copolymers.

S:MA	Elemental Compositions / Atom %			
	Calculated bulk composition		Measured surface composition	
	[C]	[O]	[C]	[O]
<b>50:50</b>	80.0	20.0	83.6	16.4
<b>66:34</b>	87.0	13.0	85.4	14.6
<b>75:25</b>	90.3	9.7	90.2	9.8

The measured surface composition of oxygen observed in the 50:50 copolymer was slightly lower than the amount determined in the bulk, given that the percentage error in XPS measurement is between 5 to 10%. On the other hand, the 66:34 copolymer exhibited similar amounts of oxygen at the surface in comparison to the bulk, as did the 75:25 copolymer. To conclude, the measured concentration of oxygen observed at the surface of the copolymers, in all cases, is in approximate agreement with the amount expected from the bulk composition. There are no large scale differences in surface as compared to bulk composition.

The copolymers underwent derivatisation with TFE derivatising reagent. Figure 4.8 shows its reaction with full conversion, that is assuming two CF<sub>3</sub> group per anhydride molecule. Table 4.5 shows the carbon, oxygen and fluorine



concentrations calculated, assuming full conversion. These values are compared to those obtained by XPS.

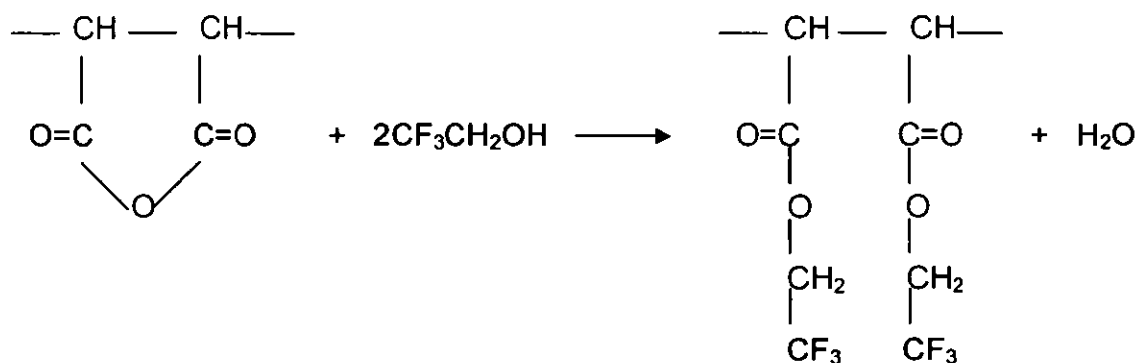


**Figure 4.8** Reaction of SMA copolymers with derivatising agent TFE in full conversion.

**Table 4.5** Calculated and measured ratio of elemental compositions of SMA copolymers after derivatisation.

S:MA	Elemental Compositions / Atom %					
	Composition calculated assuming full conversion			Composition measured by XPS		
	[C]	[O]	[F]	[C]	[O]	[F]
<b>50:50</b>	61.5	15.4	23.1	66.6	25	8.4
<b>66:34</b>	70.8	11.5	17.7	79.4	13	7.7
<b>75:25</b>	76.2	9.5	14.3	77.8	15.6	6.6

The results in the table revealed that fewer  $\text{CF}_3$  groups than expected were detected. The bulk composition was calculated assuming full conversion, that is, two  $\text{CF}_3$  group per anhydride molecule. It is likely that there was only partial

conversion of the maleic anhydride group into  $\text{CF}_3$  during derivatisation, with possibly only one  $\text{CF}_3$  group per anhydride molecule. Figure 4.9 shows the partial conversion reaction structure. Assuming partial conversion in the reaction, then the new expected fluorine concentration will be 14.3 atom %, 10.4 atom % and 8.1 atom % for SMA copolymers of 50:50, 66:34 and 75:25, respectively. These are closer to the observed values. Despite that, the measured fluorine concentration was still slightly lower than that predicted.

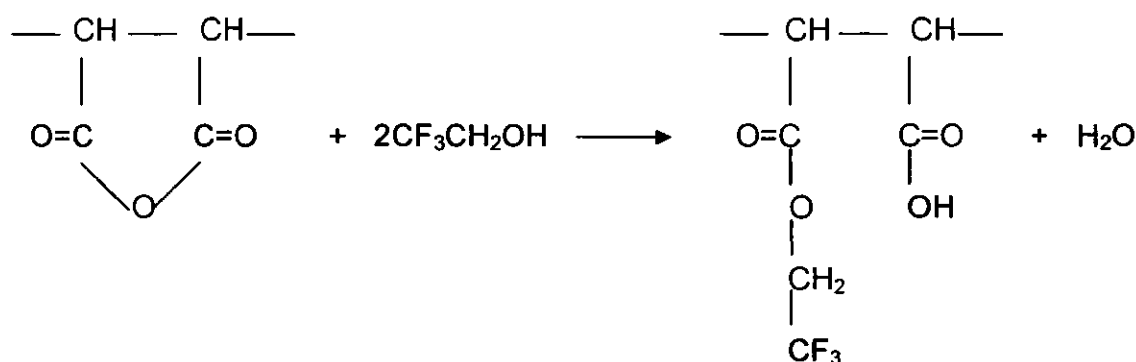


**Figure 4.9** Reaction of SMA copolymers with derivatising agent TFE in partial conversion.

#### 4.3.3 Attenuated Total Reflection Infrared Spectroscopy

Infrared spectra were recorded for SMA 50:50, 66:34 and 75:25 copolymers and are shown in Figures 4.10 to 4.12. The peak assignments are presented in Table 4.6.

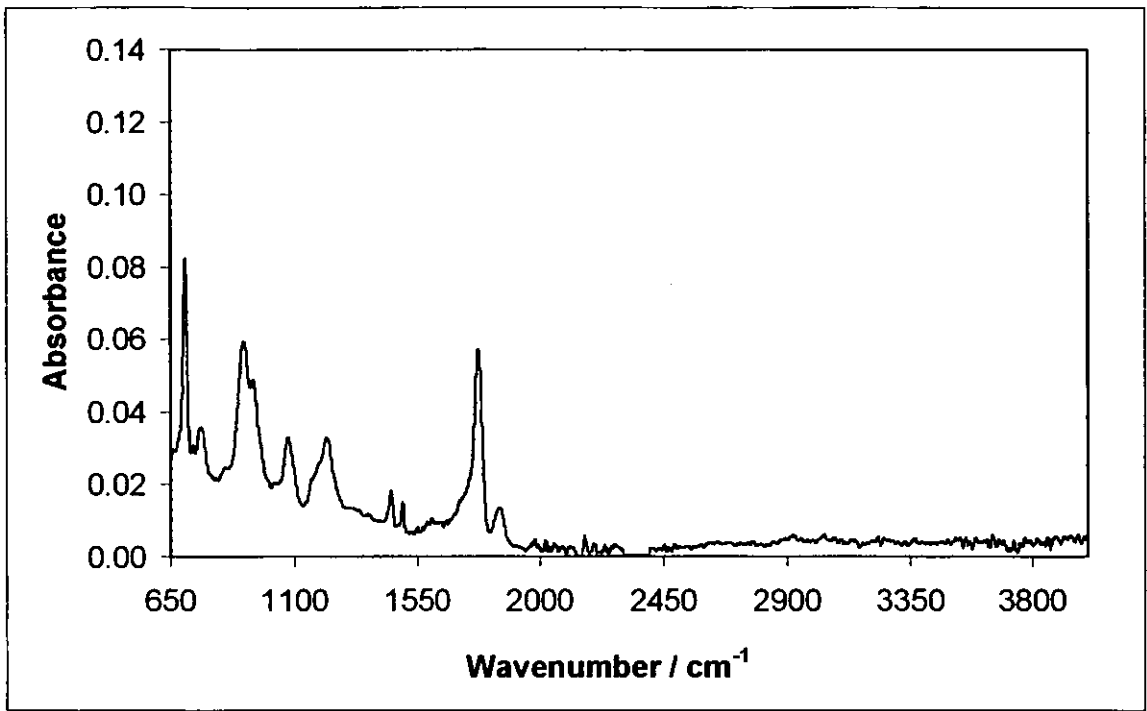


Figure 4.10 ATR-IR spectrum of SMA 50:50 copolymer.

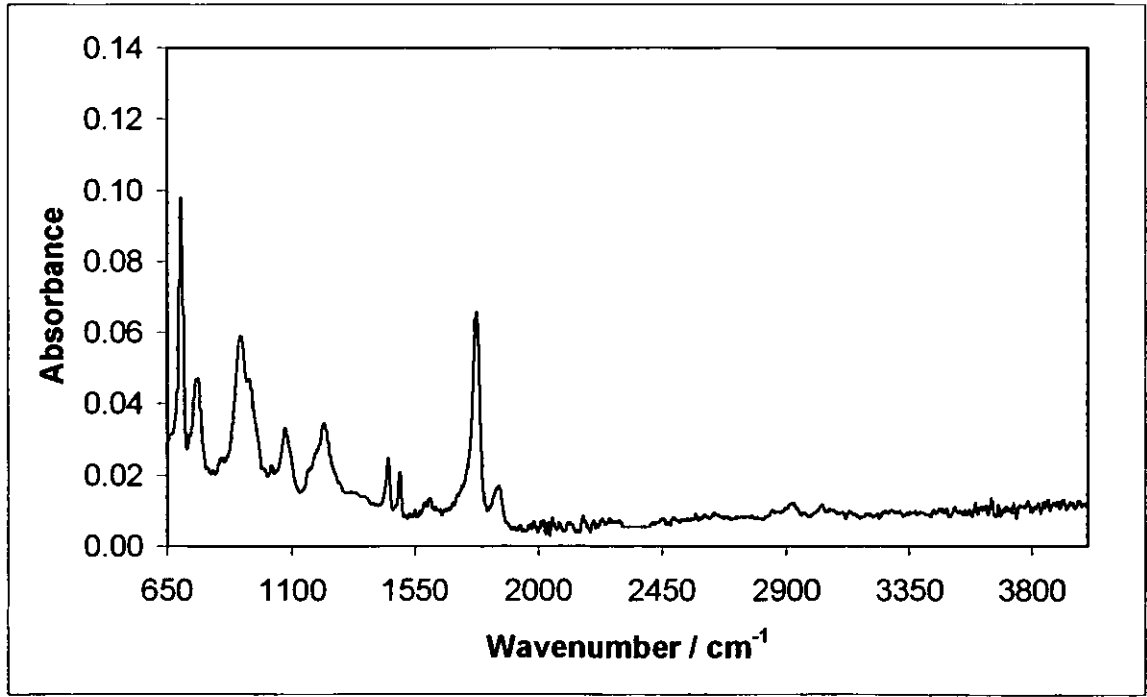
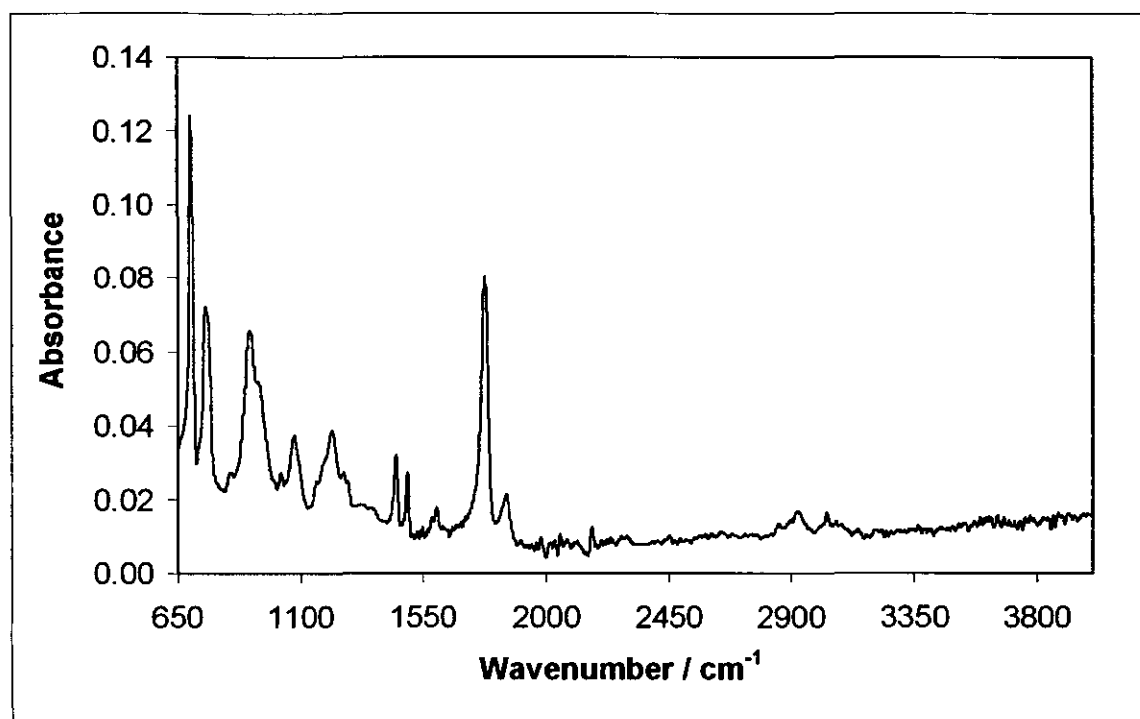


Figure 4.11 ATR-IR spectrum of SMA 66:34 copolymer.



**Figure 4.12** ATR-IR spectrum of SMA 75:25 copolymer.

**Table 4.6** IR peak assignments of SMA copolymers [201 – 203].

Peak / $\text{cm}^{-1}$ (Measured)	Peak / $\text{cm}^{-1}$ (Literature)	Assignments
697	695	Aromatic C-H out-of-plane vibrations
752	750	
921	920	C-H out-of-plane deformation
1062	1060	C-O stretching
1211	1210	
1449	1450	Aromatic $\text{C}=\text{C}$ - stretching vibration
1490	1490	Alkyl $\text{CH}_2$ scissor vibration
1599	1600	Aromatic $\text{C}=\text{C}$ - stretching vibration
1771	1770	Acid anhydrides
1846	1845	
2935	2850-3055	Aromatic and alkyl C-H stretching vibrations

The band at  $920\text{ cm}^{-1}$  arises due to C-H out-of-plane deformation. When the double bond is conjugated with, for example, a  $\text{C}=\text{O}$  group, this band is shifted towards  $990\text{ cm}^{-1}$  [201]. Two strong bands due to C-O stretching, occur between  $1300$  to  $1060\text{ cm}^{-1}$ . These absorptions were not observed with PS (see Table 4.1).

Acid anhydride groups were identified by two bands between  $1850$  to  $1800\text{ cm}^{-1}$  and  $1790$  to  $1740\text{ cm}^{-1}$  [206]. In comparison, these bands were not present for PS (see table 4.1). The two bands are usually separated by about  $60\text{ cm}^{-1}$  [201]. The higher frequency band is more intense in the acyclic anhydride and the lower frequency band is more intense in cyclic anhydrides.

As expected it was observed that the aromatic absorption bands at  $1600$  to  $1450\text{ cm}^{-1}$  become more intense as the styrene to maleic anhydride ratio increased. This same trend was also seen in the  $3055$  to  $2850\text{ cm}^{-1}$  region [206]. The areas under the aromatic and anhydride peaks were measured (Appendix B), see Table 4.7.

The estimated error of the peak ratio was between 0.2 to 0.4. The frequencies of the peaks representative of ring and anhydride were 1449 and 1779  $\text{cm}^{-1}$ , respectively. The results in the table showed that the peak ratio decreased as the styrene to maleic anhydride compositions increased.

**Table 4.7** Measured peak ratio of SMA copolymers by ATR-IR.

<b>S:MA</b>	<b>Peak ratio (MA:S)</b>
50:50	11.5
66:34	7.6
75:25	5.4

When the data was plotted graphically, it was observed that the relationship was not quite linear, see Figure 4.13. A possible interpretation is that the transition moment for the vibration changes. That is, the transition probability increases as more functional groups like C=O are present.

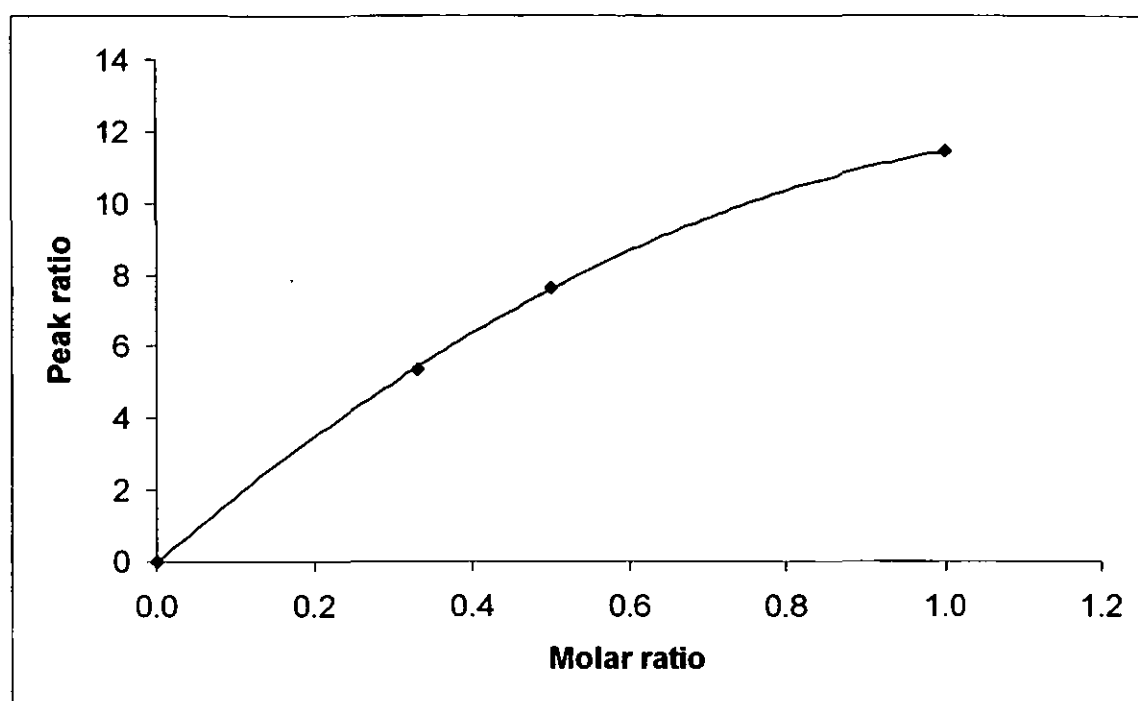


**Figure 4.13** Correlation of peak ratio and molar ratio of SMA copolymers.

#### **4.3.4 Atomic Force Microscopy**

Surface roughness of the spin-coated SMA copolymers was measured by AFM. The results showed that the SMA 50:50 composition had a degree roughness of 10 nm, which is about the same as SMA 66:34 and SMA 75:25 with a degree roughness of 7 and 8 nm, respectively. The estimated error of surface roughness was between 1 to 2 nm.

#### **4.3.5 Contact Angle Measurement**

Contact angle measurements were performed on the spin-coated SMA copolymers and presented in Table 4.8.

**Table 4.8** Contact angles of SMA copolymers at ~25°C.

<b>S:MA</b>	$\theta_{adv} / ^\circ$	$\theta_{rec} / ^\circ$	$\Delta\theta / ^\circ$
<b>50:50</b>	81.5 (2.4)	51.9 (1.4)	29.6
<b>66:34</b>	84.4 (3.1)	66.6 (2.9)	17.8
<b>75:25</b>	90.3 (1.7)	75.0 (3.3)	15.3

Note: Standard deviations are given in brackets

It can be seen that the advancing contact angles increased as the maleic anhydride content decreased. The receding contact angles also increased as the maleic anhydride content decreased. It can also be seen that the receding angles were more affected than the advancing angles.

The 50:50 SMA compositions showed the higher contact angle hysteresis of all the copolymers. Hysteresis may be due to many factors such as roughness, reorientation, heterogeneity, etc. (see Section 2.7). The surface roughness reported in Section 4.3.4 was not high enough to give rise to appreciable hysteresis (205, 162). Also it does not seem likely that the copolymers, being a single component system, would be able to give rise to surface heterogeneity on the scale needed to affect hysteresis. It seems that the most probable explanation would be surface reorientation and/or incorporation of water into the surface. The surface left as the drop recedes is probably different from that before wetting.

The contact angle hysteresis of SMA copolymers is substantially greater than that for the untreated PS (see Section 4.2.5) despite the copolymers having a much smaller surface roughness. This also suggests surface reorientation and/or incorporation of water.



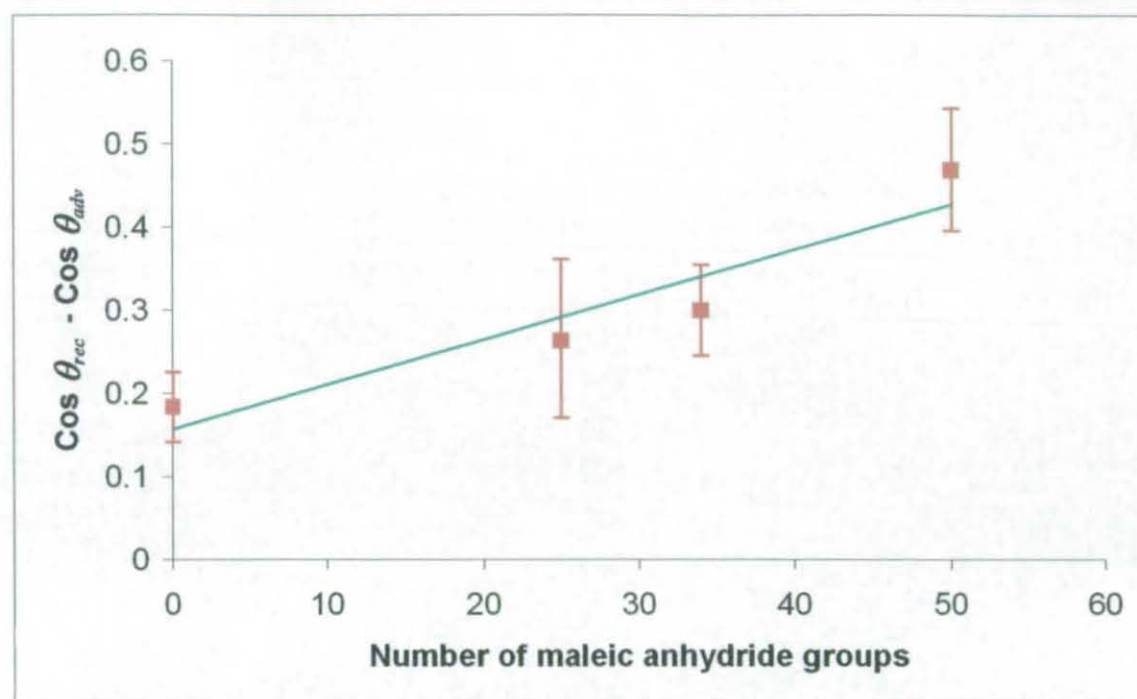


**Figure 4.14** Correlation of contact angle hysteresis and number of maleic anhydride groups.

Figure 4.14 shows graphically that the contact angle hysteresis increases as the maleic anhydride content increases. This is consistent with the explanation for hysteresis given earlier, which was due to reorganisation and/or incorporation of water. Both of these factors would vary with the amount of maleic anhydride groups present.

#### 4.3.6 Summary

IR spectroscopy had identified approximately the same absorptions as those tabulated in the literature. Unlike PS spectra, bands were identified for carbonyl stretching and acid anhydride groups. As expected the anhydride to aromatic peak ratio value was found to decrease as the styrene to maleic anhydride ratio increased. The increases however, were not linear. This could be due to the

change in the transition moment. There was no significant surface roughness observed on the SMA copolymers. Both advancing and receding contact angles increased as the maleic anhydride content decreased. The 50:50 copolymers have greater contact angle hysteresis than the rest and it is not believed to be caused by surface roughness. It is more likely that there is surface reorganisation and/or incorporation of water. The derivatisation process showed only partial conversion. There is lower level of fluorine for all copolymers than expected.

---

## 4.4 SURFACE TREATMENT

### 4.4.1 Introduction

Having characterised the untreated PS as detailed in the previous section, in this part of the work, untreated PS samples are surface treated to increase their surface free energy and wettability. Polar functional groups such as carboxylic acid (COOH) and hydroxyl (OH) groups, were introduced onto the untreated PS surface by two treatments, namely flame treatment and chromic acid treatment; see Sections 3.2.3.a and 3.2.3.b. The treated surfaces were then characterised by XPS, ATR-IR, AFM and contact angle measurement. Lapshear tests were also carried out to measure the adhesive joint strengths. The purpose was to evaluate the effect of functional groups on the joint strength for the two types of treatments. Derivatisation was performed on the treated surfaces to identify the functional groups and the derivatised samples were also surface characterised. The adhesive joint strength for the derivatised sample was also measured in order to determine the contribution of carboxylic acid groups to the joint strength.

### 4.4.2 X-ray Photoelectron Spectroscopy

The broad scan spectrum of the flame treated and chromic acid treated PS samples revealed the presence of oxygen as shown in Figures 4.15 and 4.16. Table 4.9 shows the elemental compositions of the surface treated PS samples.

A small amount of sulphur was detected on the chromic acid treated PS and this was attributed to the sulphuric acid used to make the chromic acid solution. In addition, a trace of nitrogen was detected at 0.3 atom %. Both flame treatment and chromic acid treatment have been shown to introduce oxygen containing functionalities onto the PS surface, as demonstrated by the XPS analysis.

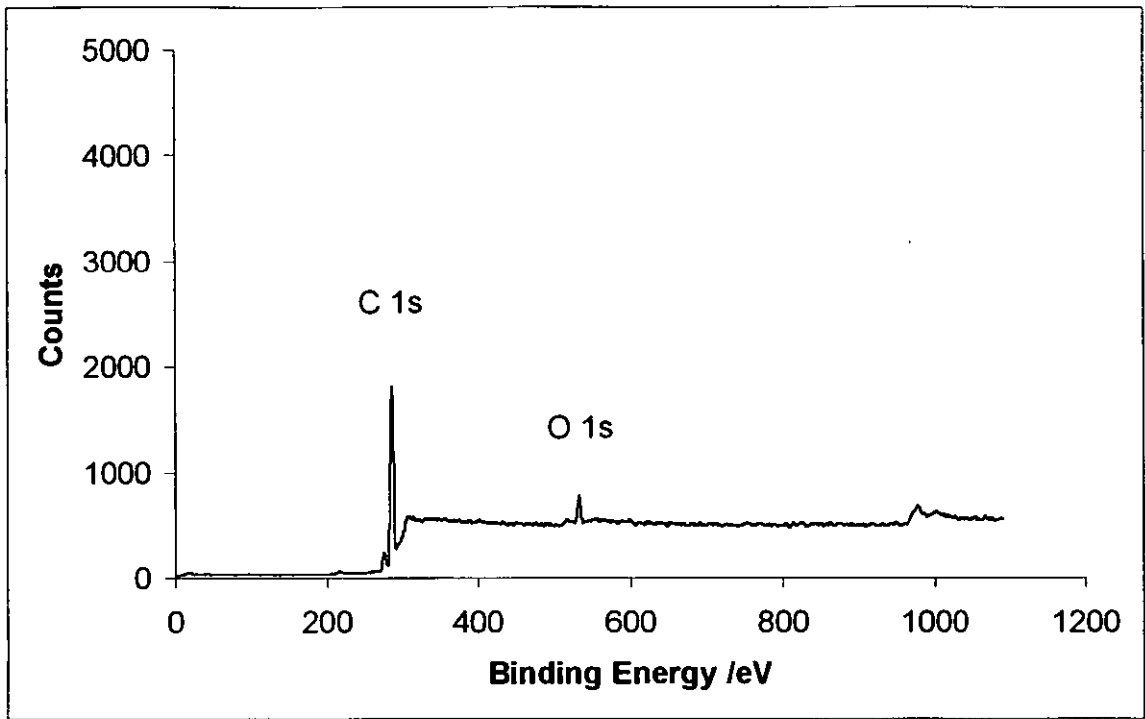


Figure 4.15 XPS broad scan of flame treated PS.

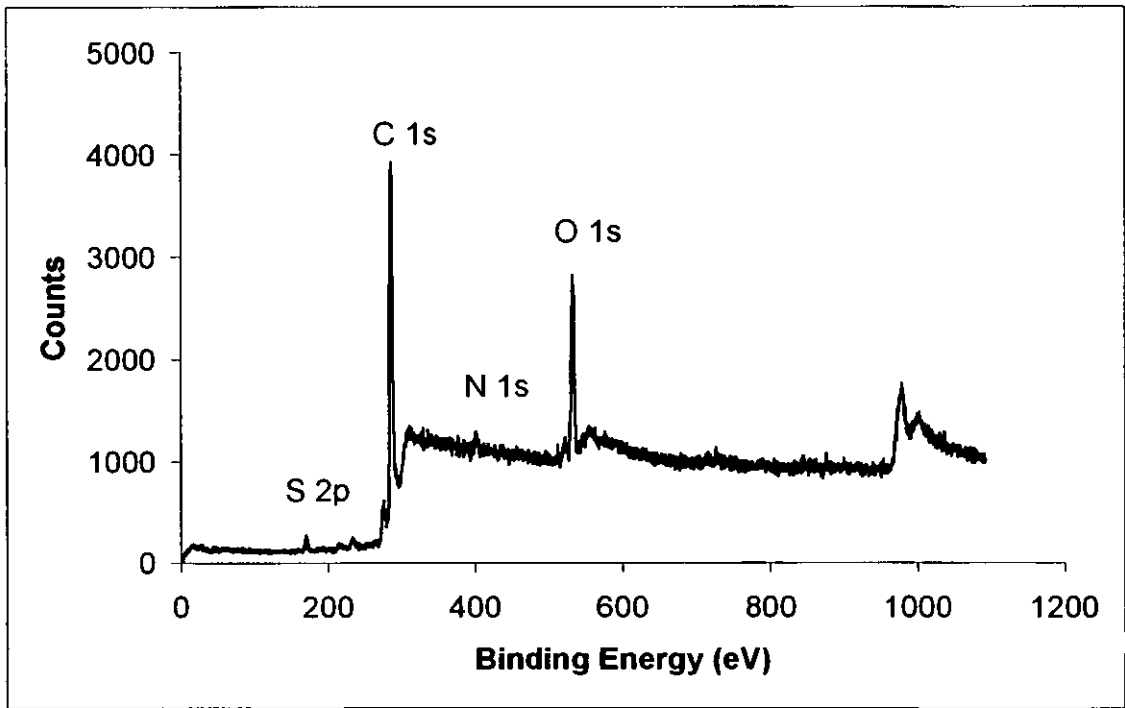


Figure 4.16 XPS broad scan of chromic acid treated PS.

**Table 4.9** Elemental compositions of surface treated PS.

Sample systems	Elemental Composition / Atom %			
	[C]	[O]	[S]	[N]
Flame treated	90.0	10.0	-	-
Chromic acid treated	83.1	14.6	2.0	0.3

The amount of oxygen detected on both the surface treated PS samples, was similar to those seen for PE after the same treatments [209, 210]. Though there was more oxygen on the chromic acid treated surfaces, most of it come from sulphate and perhaps some from nitrate as well. If these amounts are taken into consideration, then there are generally fewer oxygen containing functional groups on the chromic acid treated surfaces than the flame treated surfaces.

The surface treated samples underwent chemical derivatisation to react with the carboxylic acid functional groups. The results are tabulated in Table 4.10. The chromic acid treated surfaces showed more fluorine than the flame treated surfaces. Since there are fewer oxygen containing functional groups present on the chromic acid treated samples, it must be true that a much higher proportion of them are carboxylic acid groups. Chromic acid is a strong oxidising agent and this is to be expected. The results are consistent with studies on other polymers using chromic acid [139, 140].

**Table 4.10** Elemental compositions of surface treated PS after chemical derivatisation.

Sample systems	Elemental Composition / Atom %			
	[C]	[O]	[F]	[S]
Flame treated	89.4	8.2	2.4	-
Chromic acid treated	84.6	11.9	3.1	0.4

4.4.3 Atomic Force Microscopy

The AFM images, see Figures 4.17 and 4.18, did not show much topographical variation on the surface treated PS, compared to untreated PS. The surface roughness,  $R_a$ , is shown in Table 4.11. The error in  $R_a$  is estimated at about 1 to 2 nm.

Table 4.11 Surface roughness of untreated and surface treated PS.

Sample systems	Area $R_a$ (nm)	Area RMS (nm)
Untreated	61	79
Flame treated	55	72
Chromic acid treated	61	78

From these results, flame treated PS possibly shows a slightly smoother surface than the untreated and chromic acid treated PS. This may be due to the heat deposited in the surface during flame treatment. The surface treatments oxidise the surface but do not cause any substantial roughening to the surface. The roughness is too low to influence the contact angle hysteresis. This is because the effect of roughness below 0.1  $\mu\text{m}$  level is negligible [211], as already discussed in Section 4.2.5.

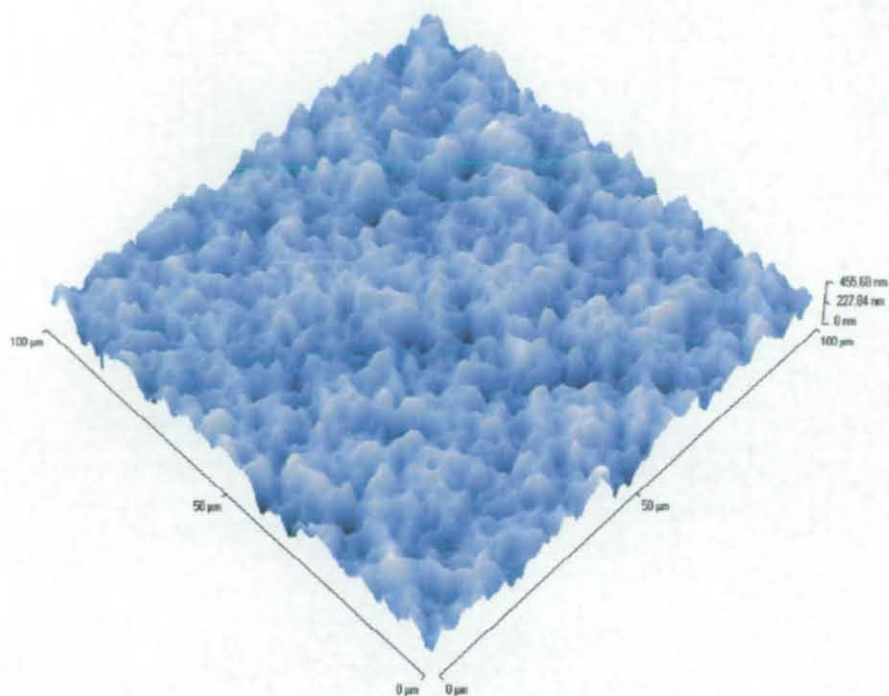


**Figure 4.17** AFM scan of flame treated PS.

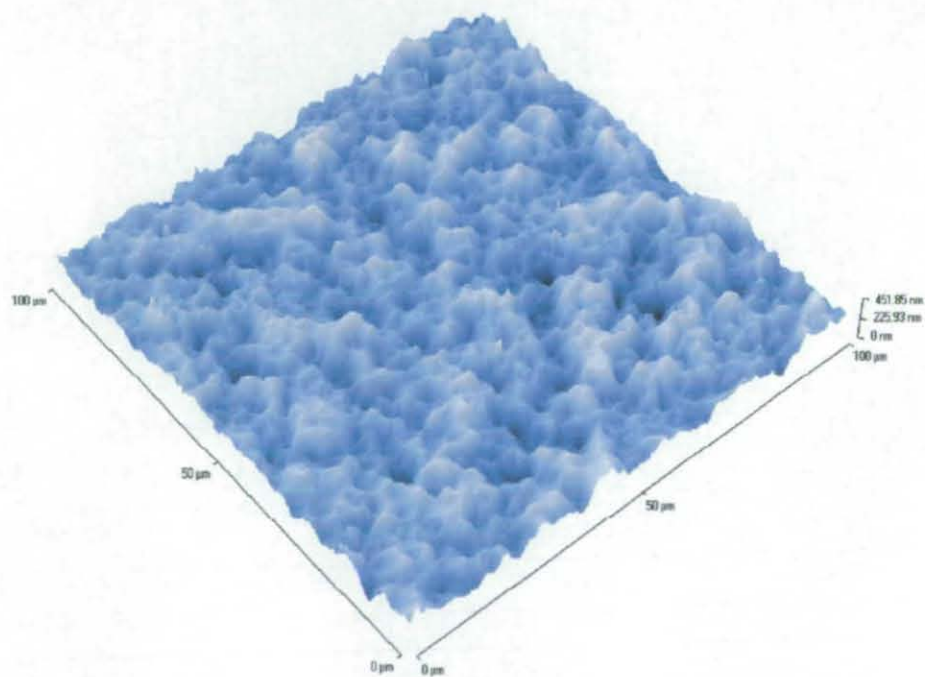


**Figure 4.18** AFM scan of chromic acid treated PS.

#### 4.4.4 Contact Angle Measurement

After surface treatment, lower water advancing angles were obtained, compared to untreated PS (see Table 4.12). This was attributed to the polar functional groups introduced onto the PS surfaces, hence increasing the surface free energy and making the surface more wettable.

**Table 4.12** Contact angles of untreated and surface treated PS at ~ 25°C.

Sample systems	$\theta_{adv} / ^\circ$	$\theta_{rec} / ^\circ$	$\Delta\theta / ^\circ$
Untreated	90.9 (1.4)	80.3 (1.2)	10.6
Flame treated	71.6 (3.2)	30.7 (2.7)	40.9
Chromic acid treated	64.1 (2.5)	24.3 (3.5)	39.8

Note: Standard deviations are in brackets

Contact angle hysteresis for both surface treated PS samples, was higher than that obtained for untreated PS. The large hysteresis cannot be attributed to any surface roughness, since AFM (see Section 4.4.3) showed no increase in roughness as a result of surface treatment. The reason may be surface reorganisation and/or incorporation of water.

The potential for reorganisation and/or incorporation of water is clearly much greater for surface treated surfaces than for untreated PS and explains the greater hysteresis in the contact angle. Heterogeneous surfaces also give rise to contact angle hysteresis and some contribution due to heterogeneity cannot be discounted. However, it is not clear how the temperature dependence of contact angle hysteresis (discussed in Section 4.8) can be accounted solely by heterogeneity.

After chemical derivatisation, both the advancing and receding contact angles increased slightly for both surface treated samples, see Table 4.13. This was



expected because the absence of carboxylic acid groups has made the surface less wettable. It was noted that the contact angle hysteresis, however, remained approximately the same, compared to before derivatisation.

**Table 4.13** Contact angles of untreated and surface treated PS after derivatisation at  $\sim 25^{\circ}\text{C}$ .

Sample systems	$\theta_{adv} / ^{\circ}$	$\theta_{rec} / ^{\circ}$	$\Delta\theta / ^{\circ}$
Untreated	89.7 (2.0)	81.7 (1.8)	8.0
Flame treated	77.1 (2.8)	35.2 (3.2)	41.9
Chromic acid treated	73.5 (1.9)	35.0 (2.1)	38.5

Note: Standard deviations are given in brackets

Results in Table 4.13 are consistent with the slightly lower level of fluorine detected by XPS for derivatised flame treated materials. The contact angle on flamed treated material does not change very much as a result of derivatisation. The contact angle results seem to be in accordance with the proposition that there are fewer carboxylic acid groups introduced onto the flame treated surface.

In this work it was proposed to study the temperature dependence of contact angle measurement. Before starting this work (which is described in Section 4.1.2), it was necessary to show that the surfaces were stable over the temperature range to be used. PS has a  $T_g$  of  $100^{\circ}\text{C}$  [96] and functional groups would be expected to be relatively immobile below this temperature, e.g. not capable of segmental rotation, lacking the necessary free volume. However, surface functional groups are known to be more mobile than those in the bulk and the treated surfaces may also contain some stresses and strains that may be relieved at temperature below the  $T_g$ .

In order to identify the temperature at which those molecules at the polymer's surface will undergoes molecular orientation or segmental rotation, samples of

surface treated PS were heated in an oven at 40, 60, 80 and 100°C. The samples were removed from the oven after 2 hours and allowed to cool down to room temperature ( $\sim 20^{\circ}\text{C}$ ). Contact angles were measured and the estimated error was approximately  $\pm 3^{\circ}$ . Contact angles of the samples did not change significantly until the temperatures exceeded  $50^{\circ}\text{C}$ , see Figure 4.19. After this point, the advancing contact angles rose steadily reaching about  $80^{\circ}$  after heating to a temperature of  $95^{\circ}\text{C}$ . This represents a substantial increase on the advancing contact angles at room temperature of 60 to  $65^{\circ}$ . It is assumed that this must be due to reorientation of functional groups away from the surface with consequent reduction in surface energy. The variable temperature contact angle measurements described in Section 4.1.2 were therefore carried out up to a maximum temperature of  $40^{\circ}\text{C}$ . The reversion of PS in bulk phase is at  $T_g$  or slightly above  $T_g$ , therefore the surface molecules of PS had showed greater freedom than those in the bulk.

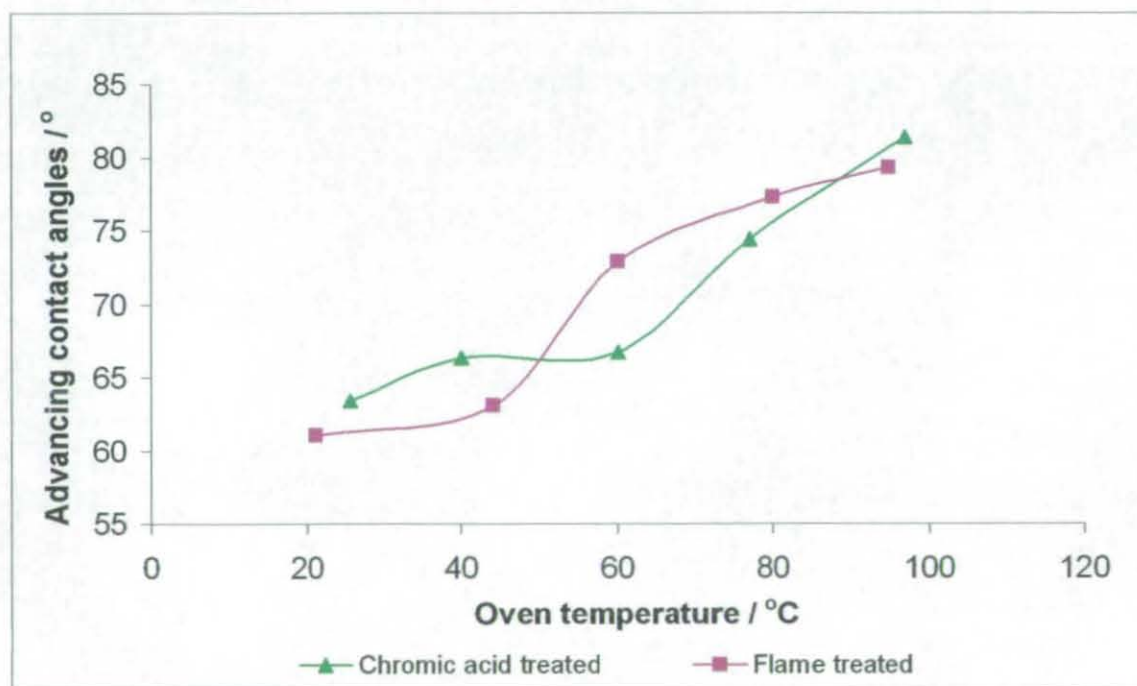


**Figure 4.19** Effect of contact angles of surface treated PS subjected to thermal treatment.

#### 4.4.5 Adhesion

Adhesive joint strengths were determined for the surface treated samples and compared to those of the untreated samples, reported in Table 4.14. After surface treatment, it can be seen that the lap shear adhesive joint strength showed a large increase compared to that of the untreated PS. This is attributed to the strong interaction between the epoxide groups of the adhesives and the polar functional groups, i.e. hydroxyl and carboxylic acid, that had been introduced onto the polymer surface. There is no difference in adhesive joint strength, (allowing for errors), between the flame treated and chromic acid treated samples.

**Table 4.14** Adhesive joint strength of untreated and surface treated PS.

Sample systems	Joint Strength (N)	Standard Deviation (N)
Untreated	260	5
Flame treated	1710	69
Chromic acid treated	1990	268

It has been suggested that derivatisation could “shut down” or block the acid functional groups at the surface, making them inactive [147, 171 - 173]. The derivatised samples were tested for lap shear strength and the results are presented in Table 4.15.

**Table 4.15** Adhesive joint strength of untreated and surface treated PS after chemical derivatisation.

Sample systems	Joint Strength (N)	Standard Deviation (N)
Untreated	268	25
Flame treated	1139	176
Chromic acid treated	1253	44

There is no difference in the adhesive joint strength of untreated PS before and after derivatisation, which was to be expected. Both surface treated samples showed about the same adhesive joint strength, (allowing for errors), after derivatisation. It can be seen that the adhesive joint strength of the surface treated samples reduced substantially by about one-third of that before derivatisation. It is concluded that a maximum of one-third of the joint strength can be attributed to carboxylic acid groups. Selective derivatisation may be a useful technique for assessing the importance of other functional groups in adhesion. Here it is probable that there have been chemical bonds formed between the acid groups and the epoxy resin [26, 27, 35, 212].

### 4.4.6 Summary

Chromic acid treated surfaces revealed a higher oxygen concentration than flame treated PS. AFM analyses demonstrated that both types of surface treatment do not cause significant surface roughness and that the flame treated samples showed the smoother surfaces. The large contact angle hysteresis may be explained by reorientation and/or incorporation of water. Chromic acid treated surfaces have fewer oxygen-containing functional group than the flame treated surfaces but a higher proportion of them were carboxylic acid groups. This leads to both surface treated samples having similar joint strengths. A high lapshear joint strength was seen on both flame treated and chromic acid treated samples. The adhesive joint strength on the surface treated samples was reduced due to chemical modification by derivatisation. This shows the importance of carboxylic acid groups for the adhesive between polymers and epoxy resins. There was no evidence of substantial reorientation of functional groups up to 50°C in both the surface treated samples as a result of heat treatment.

---

## 4.5 NON-REACTIVE COMPOUNDING

### 4.5.1 Introduction

As reported in previous section, the PS was surface treated by two different treatments, to incorporate oxygen functionalities and the resulting effect on the adhesion strength were evaluated. Compounding is another common way of introducing functional groups. In this section, PS was compounded with three compositions of SMA copolymers (50:50, 66:34 and 75:25). The aim of the work was to determine whether the copolymers would migrate to the surface and act as adhesion promoters. The compounding was done in different loadings of 0.1%, 1% and 10% by weight, in order to quantify the amount needed to improve adhesion to PS. PVME was also compounded into PS, as a comparison to the SMA copolymers, using loadings of 1% and 10%. There is some evidence [106, 107] that PVME is miscible with PS. The surfaces of the non-reactively compounded samples were characterised by XPS, ATR-IR, AFM and contact angle measurement. Lapshear tests were made on the non-reactively compounded samples and after derivatisation. Extraction of the non-reactively compounded samples was carried out (see Section 3.2.1). The effect of extraction and of derivatisation, were analysed by the surface characterisation techniques and lapshear tests. In addition, an untreated PS sample was processed using the same compounding conditions, but without SMA or PVME, to act as a control.

### 4.5.2 X-ray Photoelectron Spectroscopy

All PS-SMA copolymers were analysed. All spectra showed the presence of carbon and oxygen, irrespective of loading level. The results from samples compounded with 66:34 SMA are presented in Figures 4.20 to 4.22 and the elemental compositions discussed in Table 4.17.

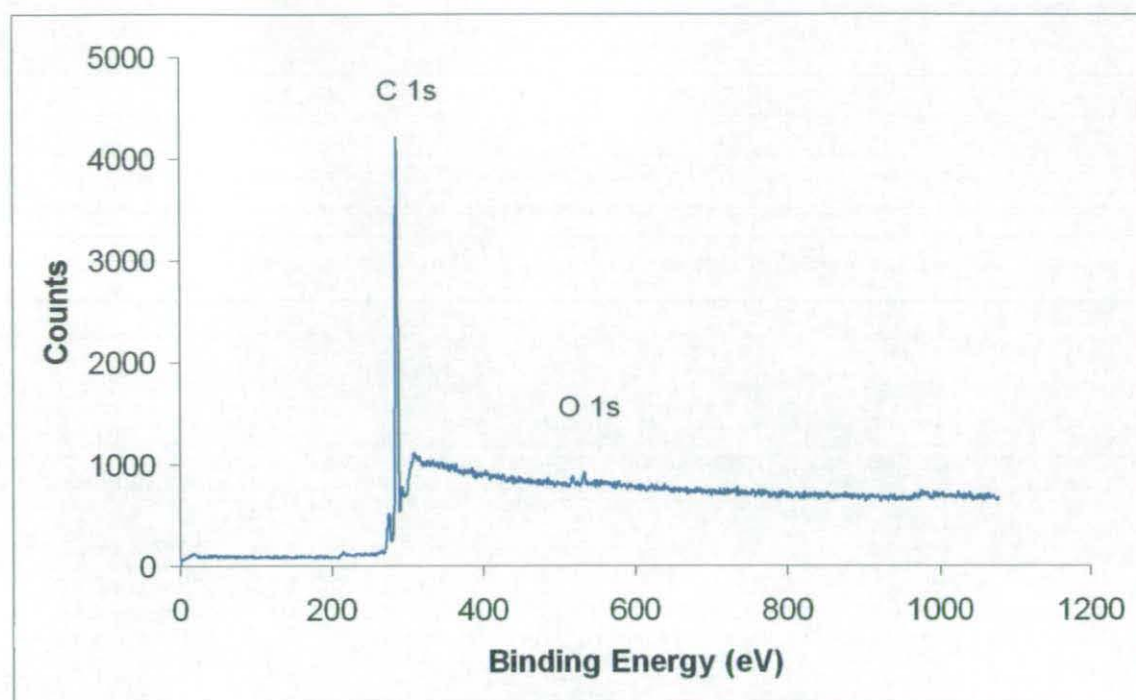


**Figure 4.20** XPS broad scan of PS-SMA 66:34 of 0.1% loading.

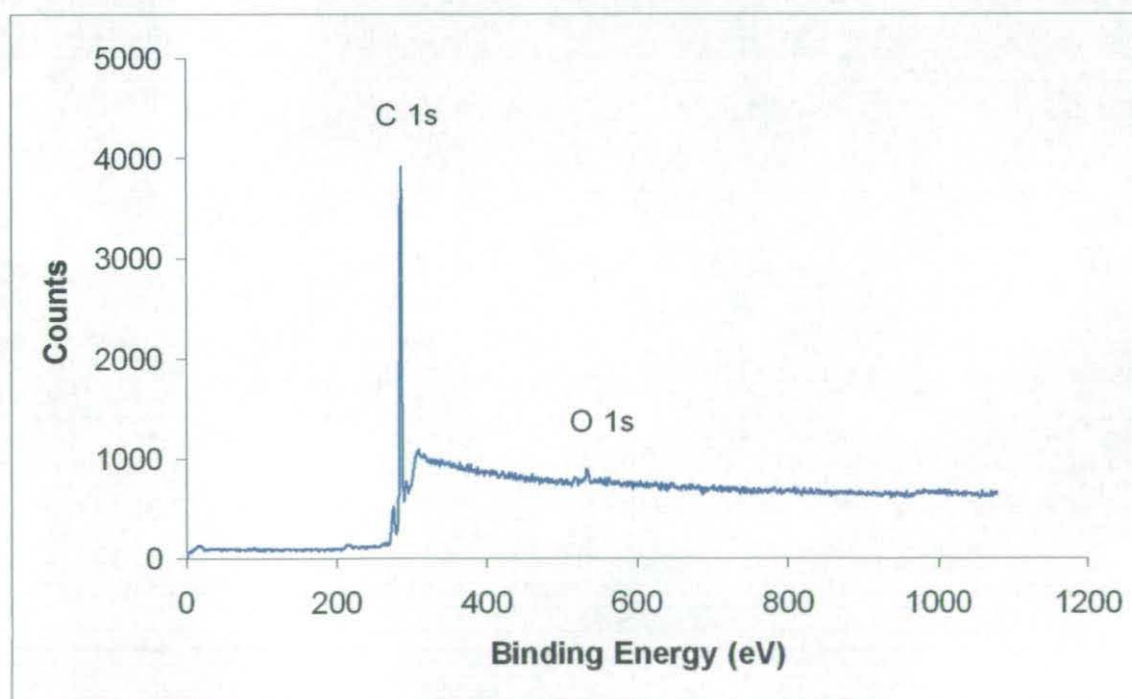


**Figure 4.21** XPS broad scan of PS-SMA 66:34 of 1% loading.



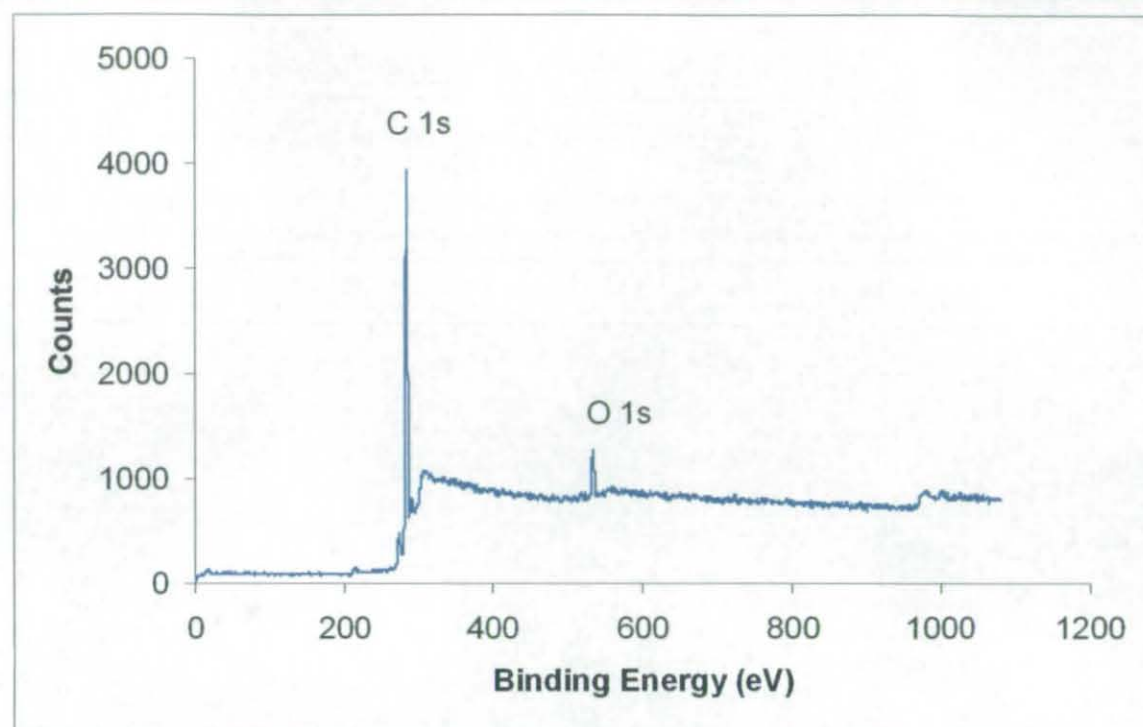


**Figure 4.22** XPS broad scan of PS-SMA 66:34 of 10% loading.

Table 4.16 shows that there was a small amount of oxygen in the PS control, and possible sources for this were discussed in Section 4.2.2. Taking into account the initial oxygen concentration in the PS control, the oxygen concentration detected at the surface of the 0.1% loading was below the detection limit of XPS, (i.e. 0.2 atom %). The oxygen concentration of 0.2 atom % in the 1% loaded sample was at the limit of detection for XPS. The 10% loading showed 3.6 atom % of oxygen and was about that expected from the bulk composition, considering the XPS errors of about 5 to 10%. Therefore given that there was oxygen initially present on the PS surface, it seems that the amount of SMA in the surface was broadly the same as that in the bulk, after allowing for surface oxidation.

**Table 4.16** Elemental compositions of non-reactively compounded PS-SMA 66:34 at different loadings.

Sample systems	Elemental Composition / Atom %			
	Calculated bulk composition		Measured surface composition	
	[C]	[O]	[C]	[O]
PS control	100	0	98.8	1.2
0.1%	99.96	0.04	98.8	1.2 (0)
1%	99.6	0.4	98.6	1.4 (0.2)
10%	96.0	4.0	95.2	4.8 (3.6)

Note: The number reported in brackets is the actual oxygen atom % concentration after subtraction of the amount detected in the control.

The samples were subjected to extraction in methanol and the results are presented in Table 4.17. However, as can be seen extraction with methanol had no significant effect, that is, there was no difference in oxygen concentration in PS control, 0.1% and 1% loading levels before and after extraction. The 10% loading may have shown a slightly increase in oxygen concentration due to extraction but the effect (if any) was small.

**Table 4.17** Elemental compositions of non-reactively compounded PS-SMA 66:34 at different loadings after extraction in methanol.

Sample systems	Elemental composition / Atom %	
	[C]	[O]
PS control	98.8	1.2
0.1%	98.0	1.2 (0)
1%	98.2	1.5 (0.3)
10%	91.4	5.5 (4.3)

Note: The number reported in brackets is the actual oxygen atom % concentration after subtraction of the amount detected in the control.



PS-SMA of 66:34 compositions in 1% and 10% loadings were chemically derivatised and the results were tabulated in Table 4.18. The number of fluorine tagged groups detected was very low for both loadings. This again suggests that there is a low number of functional groups available for reaction at the surface of all the compounded samples.

**Table 4.18** Effect of derivatisation on non-reactively compounded PS-SMA 66:34 after extraction in methanol.

Sample systems	Elemental Composition / Atom %		
	[C]	[O]	[F]
PS control	98.8	1.2	0
1%	98.6	1.3	0.1
10%	94.7	4.5	0.8

In comparison with the surface treated PS samples, non-reactively compounded samples greatly showed lower oxygen concentration for all loadings, both before and after derivatisation.

#### 4.5.3 Attenuated Total Reflection Infrared Spectroscopy

In order to know whether there was an adequate number of an oxygen group at the surface, ATR-IR analyses of the surface were performed. The XPS can be used to sample several nanometres into a polymer surface whereas the ATR probes more deeply to a depth of several  $\mu\text{m}$ . Non-reactively compounded samples of 1% and 10% loadings of all copolymer compositions were analysed and the peak areas measured from the spectra. The analysis was done on extracted samples. The molar ratio (anhydride/PS), was calculated from the peak area for the surface (measured) and compared to that for the bulk (calculated), see Appendix B, as

shown in Table 4.19. The estimated error was 0.0003 for the 1% loaded samples and 0.001 for the 10% loaded samples, respectively.

**Table 4.19** Molar ratio at bulk and surface of non-reactively compounded PS-SMA.

<b>S:MA</b>	<b>1%</b>		<b>10%</b>	
	<b>Bulk (Calculated)</b>	<b>Surface (Measured)</b>	<b>Bulk (Calculated)</b>	<b>Surface (Measured)</b>
<b>50:50</b>	0.0052	0.0062	0.0573	0.0707
<b>66:34</b>	0.0034	0.0041	0.0378	0.0420
<b>75:25</b>	0.0026	0.0037	0.0282	0.0300

The measured surface compositions are consistently higher than those anticipated from the bulk concentration, but the difference is not large. This suggests that there may be some slight enrichment of the copolymer in the outer few  $\mu\text{m}$ . XPS probes a much smaller distance into the sample and so would not necessarily show the same trend. Due to the small area under anhydride peak for the 1% loaded samples, the percentage error in the molar ratio was higher for these samples than that for the 10% loading.

**4.5.4 Atomic Force Microscopy**

AFM was carried out to determine whether the presence of copolymers would roughen the surface of sample. The 66:34 SMA was analysed. The degree of roughness,  $R_a$ , is shown in Table 4.20. The error in  $R_a$  is estimated at about 2 to 4 nm. These values are not large enough as to cause any significant surface roughness of the non-reactively compounded sample surfaces (see Section 4.2.5).

**Table 4.20** Surface roughness of non-reactively compounded PS-SMA 66:34 before and after extraction in methanol.

Sample systems	Area $R_a$ (nm)		Area RMS (nm)	
	Non-extracted	Extracted	Non-extracted	Extracted
PS control	90	90	114	115
1%	88	108	112	143
10%	128	198	175	281

Roughness values for both the PS control before and after extraction, were very similar, though slightly higher than untreated PS of 61 nm. The roughness of samples containing 1% by weight of PS-SMA was the same as the PS control. The samples with 10% PS-SMA had a significantly greater roughness than the PS control. However, for both 1% and 10% loadings, the surface roughness increased on extraction. This could be due to removal of SMA copolymers from the surface or perhaps some reorganisation of groups in the surface. The 10% loading showed the greatest increase in surface roughness after extraction, (see Figures 4.23 and 4.24). In comparison, the non-reactively compounded samples at two loadings, exhibited higher surface roughness values than the surface treated samples. The reason may have been due to compounding, as the PS control also showed higher surface roughness value than the untreated PS.

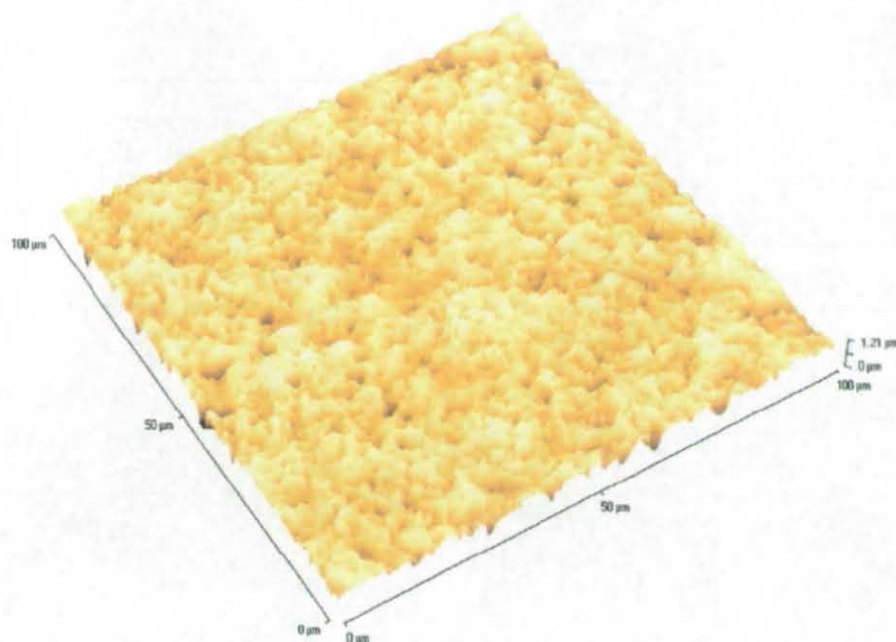


**Figure 4.23** AFM scan of non-reactively compounded PS-SMA 66:34 10% loading before extraction.

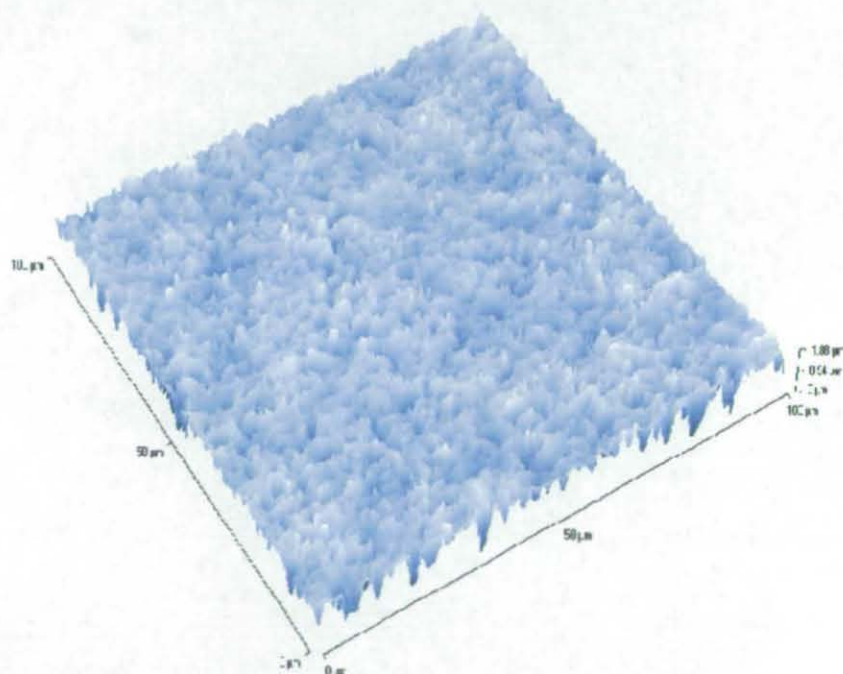


**Figure 4.24** AFM scan of non-reactively compounded PS-SMA 66:34 10% loading after extraction.

#### 4.5.5 Contact Angle Measurement

Contact angle measurement was carried out on samples with 1% and 10% loading of PS-SMA 66:34 and for the PS-PVME samples, before and after extraction in methanol. The results are presented in Table 4.21.

**Table 4.21** Contact angles of non-reactively compounded PS at ~ 25°C.

Sample systems	$\theta_{adv} / ^\circ$		$\theta_{rec} / ^\circ$		$\Delta\theta / ^\circ$	
	Non-extracted	Extracted	Non-extracted	Extracted	Non-extracted	Extracted
<b>PS control</b>	89.8 (1.1)	90.2 (2.1)	74.1 (1.4)	73.3 (1.8)	15.7	16.9
<b>SMA 1%</b>	84.7 (1.9)	87.4 (2.2)	70.2 (2.6)	65.7 (3.2)	14.5	21.7
<b>SMA 10%</b>	83.2 (2.5)	85.4 (2.1)	63.5 (3.1)	57.6 (2.8)	19.7	27.8
<b>PVME 1%</b>	85.1 (1.3)	86.9 (2.7)	69.6 (2.9)	66.1 (1.7)	15.5	20.8
<b>PVME 10%</b>	85.8 (2.3)	83.3 (2.5)	68.7 (3.1)	62.7 (1.8)	17.1	20.6

Note: Standard deviations are given in brackets

In general, for the PS-SMA samples, the advancing angles may have increased slightly with extraction, approaching more closely those of untreated PS. The receding angles decreased, again slightly. Hysteresis therefore increased. This would be consistent with the reorganisation of functional groups in the surface creating regions of different surface energy. The increase in surface roughness (see Table 4.20), was generally thought to be too small to make an appreciable contribution to hysteresis in this case [207].

For the non-reactively compounded samples containing PVME, there is no measurable change in advancing angle, following extraction but there may have been a slight decrease in receding angle, producing a larger hysteresis on the extracted samples.

After chemical derivatisation, the advancing angles increased slightly for both the non-reactively compounded sample systems, regardless of loading levels; see Table 4.22. This was expected since the derivatised groups will have interacted to a lesser extent with the water than anhydride groups.

**Table 4.22** Effect of derivatisation on contact angles of non-reactively compounded PS after extraction at  $\sim 25^{\circ}\text{C}$  in methanol.

Sample systems	$\theta_{adv} / ^{\circ}$	$\theta_{rec} / ^{\circ}$	$\Delta\theta / ^{\circ}$
PS Control	89.1 (2.3)	74.8 (3.1)	12.3
SMA 1%	89.3 (1.9)	71.1 (2.9)	18.6
SMA 10%	86.9 (2.8)	63.1 (1.3)	23.8
PVME 1%	88.1 (3.2)	70.3 (1.4)	17.8
PVME 10%	87.9 (2.5)	65.8 (1.2)	22.1

Note: Standard deviations are given in brackets

In the same way, the receding angle values also increased for all systems, as there were fewer oxygen containing groups available to interact strongly with water. However, it seemed that the receding angle was generally slightly more affected by derivatisation than the advancing angle.

The surface treated samples showed significantly lower advancing contact angles than the non-reactively compounded samples, both before and after derivatisation. This suggests the surface treated samples have more oxygen functional groups than the non-reactively compounded samples. The receding contact angle values of non-reactively compounded samples were also much higher than those for the

surface treated samples. Non-reactively compounded samples demonstrated smaller contact angle hysteresis than that of surface treated samples, however, non-reactively compounded samples had a greater roughness. The differences in hysteresis cannot be explained by surface roughness. It is possible that the surface treated samples retain more water when the drop is receded, leaving a surface substantially different to that before wetting.

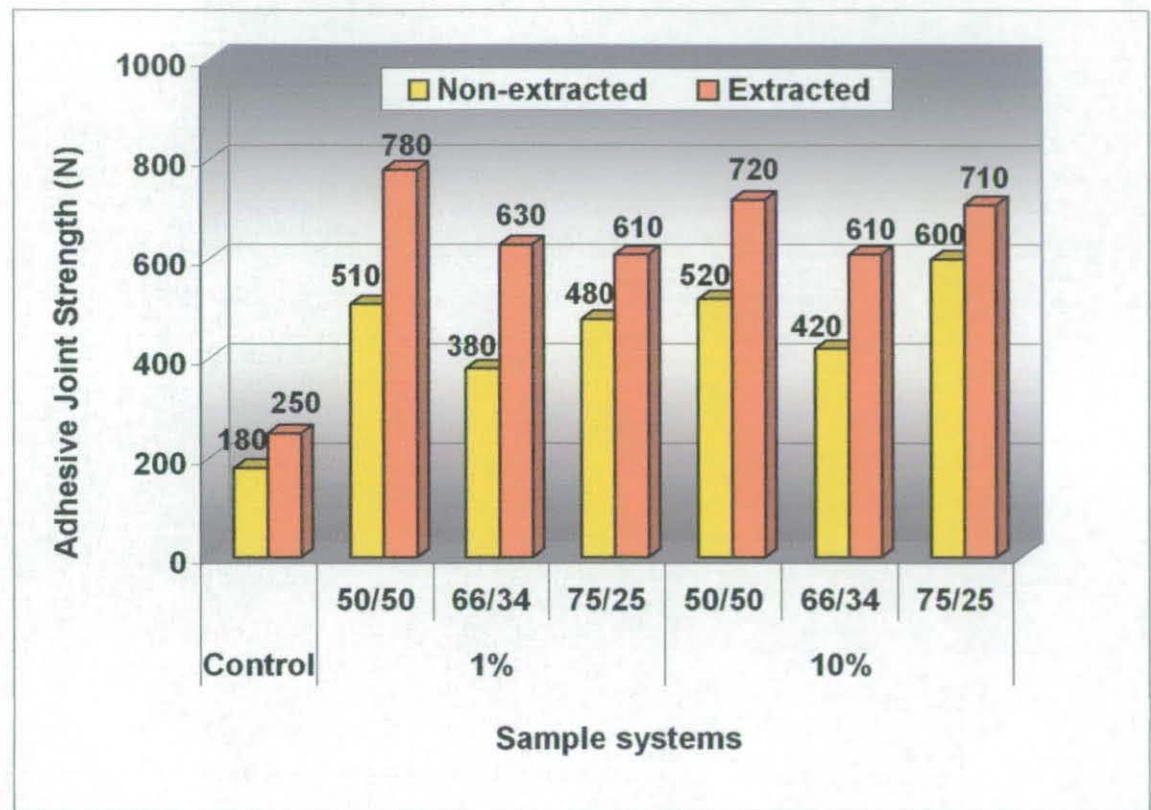
### 4.5.6 Adhesion

The lap shear joint strength properties were measured for all PS-SMA compositions at 1% and 10% loadings and on a PS control; this is shown in Figure 4.25. As seen, all non-reactively compounded samples showed an increase in adhesion when compared to the PS control. This indicates that compounding with copolymers has improved adhesion, with the copolymers acting as adhesion promoters.

It is also noted that extraction further improved adhesion strength, across all systems. There are several factors that can affect adhesion. One factor is surface roughness. AFM has revealed an increase in surface roughness of up to about 50% after extraction and this may have given rise to a substantial increase in area of contact, to enhance adhesion. Another factor is the weak boundary layer. It is possible that extraction has also caused the removal of the weak boundary layer, which also increases the adhesion strength. Since the increase in roughness is more pronounced for the 10% loading and this is not reflected in the adhesive joint strength, the weak boundary layer explanation seems the more plausible explanation in this case.

In general, there was not much difference in joint strength between the various copolymer compositions. There was also not much difference in joint strength between the 1% and 10% loaded samples. This was despite the fact that the 10%

loaded sample showed more oxygen at the surface as measured by XPS and ATR. This shows that a low loading was sufficient to achieve improved adhesion. This is very important if this compound is to be used as an adhesion promoter, since low levels of additive will have less affect on the desired bulk properties of the PS.



Note: Standard deviations were between 29 and 41 N

**Figure 4.25** Effect of adhesive joint strength on non-reactively compounded PS-SMA compositions.

The joint strength was also measured for 1% and 10% loaded PS-PVME before and after extraction. The adhesive joint strength before extraction for 1% and 10% loadings were 240 N and 270 N, respectively. After extraction, the adhesive joint strength increased to 320 N for 1% loading and 360 N for 10% loading. The



increase was probably due to the removal of a weak boundary layer. The standard deviations, before and after extraction, for both loadings were between 33 and 56 N. However, as compared to the PS-SMA non-reactively compounded samples, the adhesive joint strength was lower for the PS-PVME non-reactively compounded samples, both before and after extraction. A possible reason could be that acid anhydride groups interacted more strongly with epoxy adhesive than PVME. Nevertheless small amounts of PVME were effective as adhesion promoters.

Chemical derivatisation was carried out on the 66:34 compositions, non-reactively compounded samples and the PS-PVME non-reactively compounded samples after extraction, see Table 4.23. No difference was seen for the PS control, which was as expected. There was perhaps only a small effect in the case of PVME. Large changes were not expected since the derivatising agent should not have reacted with PVME. Substantial differences were seen for the PS-SMA systems of both loadings. Adhesive joint strengths were reduced to the same level observed for the PS control and PVME samples. The presence of acid anhydride clearly accounts for the majority of the increased joint strength in these cases. Since substantial improvements in adhesion were obtained from a small number of functional groups, it is possible that a chemical reaction is occurring between the anhydride groups and the adhesive.

**Table 4.23** Effect of derivatisation on adhesive joint strength of non-reactively compounded PS after extraction in methanol.

Sample systems	Adhesive Joint Strength (N)	
	Before derivatisation	After derivatisation
PS control	250 (16)	252 (12)
SMA 1%	630 (9)	193 (21)
SMA 10%	610 (30)	277 (11)
PVME 1%	320 (28)	280 (31)
PVME 10%	260 (18)	199 (26)

Standard deviations are given in brackets

#### 4.5.7 Summary

The amount of oxygen detected at the surface of the non-reactively compounded samples was lower than that seen for surface treated materials. The adhesive joint strength was improved by the presence of compounded SMA copolymers but still less than that seen for surface treated materials. Low levels of SMA were as effective as higher ones in promoting adhesion. The 1% PS-SMA samples showed significant improvements in adhesion despite the fact that the number of anhydride groups in the surface was below the detection limit of the XPS technique. Derivatisation confirmed that these acid anhydride groups were indeed present and contributed to adhesion. This may in part be due to the ability of these groups to chemically react with the adhesive. There may also be a smaller contribution from surface roughening.

---

## 4.6 REACTIVE COMPOUNDING

### 4.6.1 Introduction

In the previous section, it was reported that SMA copolymers had been compounded in PS without the aid of an initiator, which may catalysed the grafting of SMA to the PS. It was of interest to see how the results compared when the PS was reactively compounded with the copolymers. In this part of work, SMA copolymers of various compositions (50:50, 66:34, 75:25) were each compounded with PS at three loadings of 0.1%, 1% and 10% by weight. The initiator used was a 0.1% organic peroxide, which had been suggested as the optimum amount needed to graft additives onto a polymer [113]. The objective of these experiments was to compare the effect of reactive and non-reactive compounding in these systems. PVME was also compounded with PS with the same initiator. The untreated PS sample was compounded using the same compounding conditions with 0.1% initiator, and acted as a control. As before, the reactively compounded samples were characterised by XPS, ATR-IR, AFM and contact angle measurement. Lapshear tests were also performed. The effect of extraction and of derivatisation, were analysed by the same surface characterisation techniques and lapshear tests.

### 4.6.2 X-ray Photoelectron Spectroscopy

Reactively compounded PS-SMA 66:34 samples of loadings 0.1%, 1% and 10% were selected for analysis and the spectra are presented in Figures 4.26 to 4.28, respectively. The measured elemental compositions are tabulated in Table 4.24.

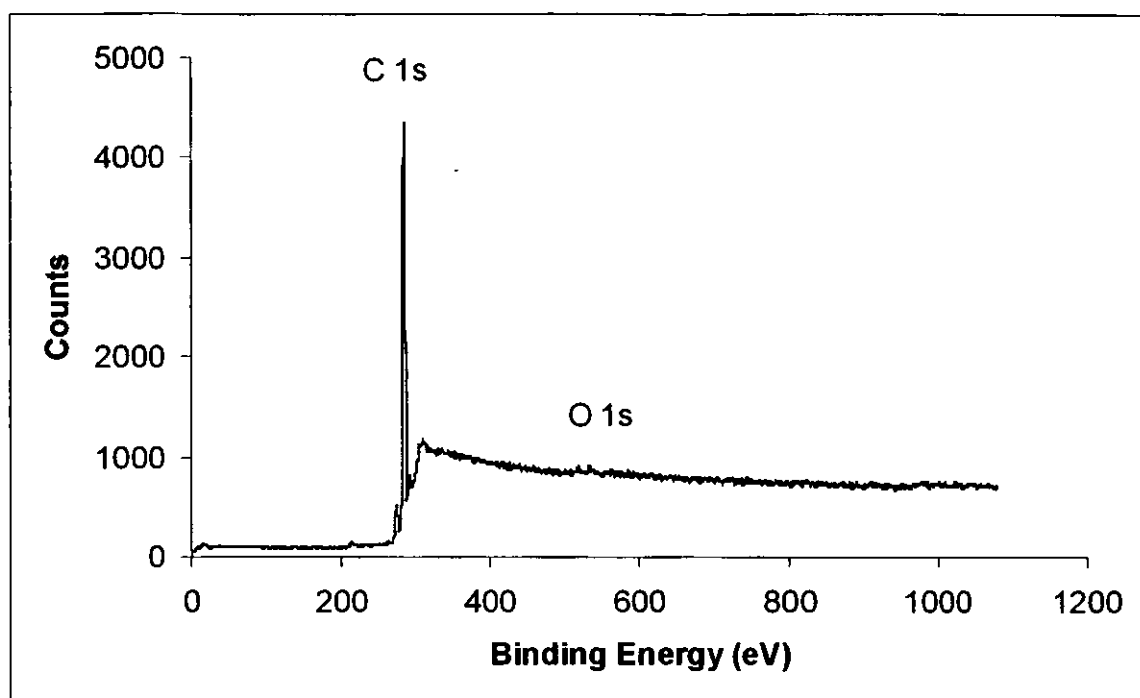


Figure 4.26 XPS broad scan of PS-SMA 66:34 of 0.1% loading.

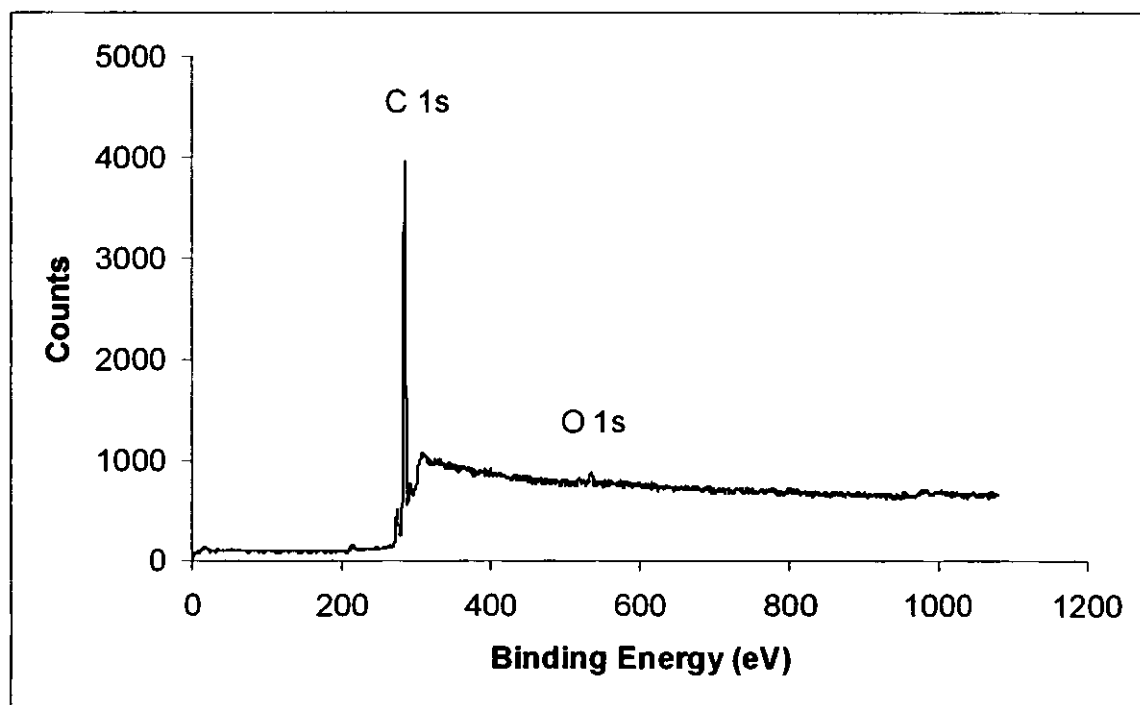
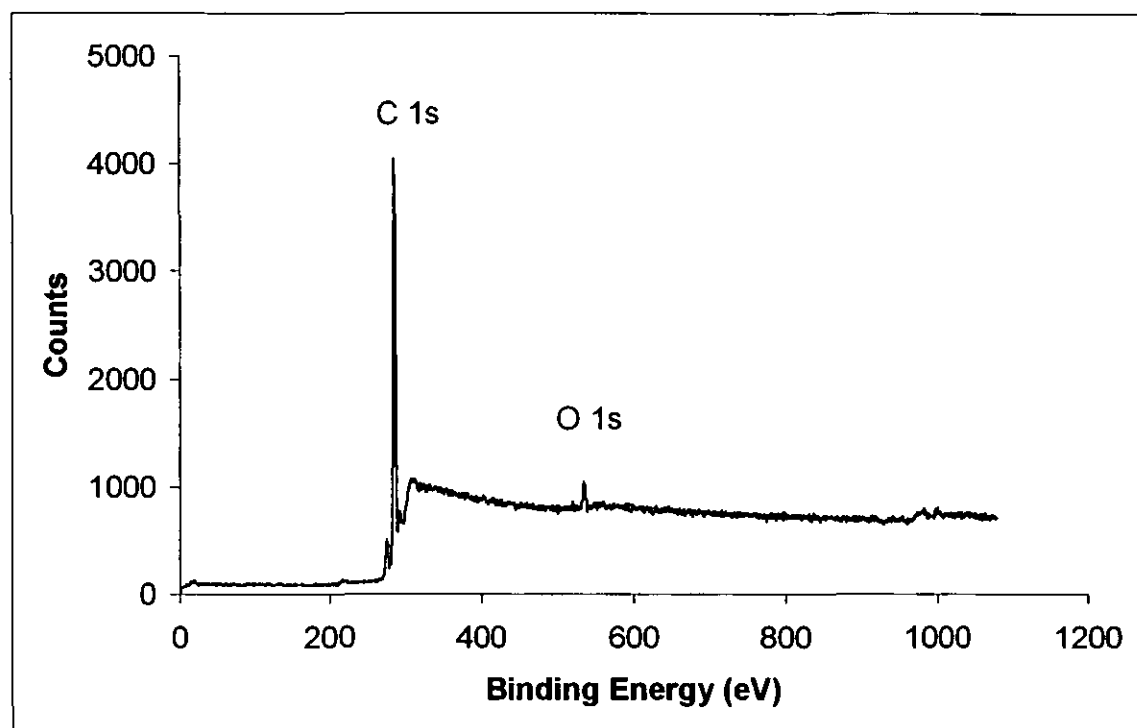


Figure 4.27 XPS broad scan of PS-SMA 66:34 of 1% loading.



**Figure 4.28** XPS broad scan of PS-SMA 66:34 of 10% loading.

As seen in Table 4.24, the PS control showed an oxygen concentration of 1.2 atom % as discussed in Section 4.2.2. Allowing for this, the 0.1% loading sample showed no clear evidence of SMA groups on the surface, which was as expected. In the case of both 1% and 10% loaded samples, the oxygen concentrations were lower than those expected for bulk composition.

**Table 4.24** Elemental compositions of reactively compounded PS-SMA 66:34 at different loadings.

Sample systems	Elemental Composition / Atom %			
	Calculated bulk composition		Measured surface composition	
	[C]	[O]	[C]	[O]
PS control	100	0	98.8	1.2
0.1%	99.96	0.04	98.8	1.2 (0)
1%	99.6	0.4	98.7	1.3 (0.1)
10%	96.0	4.0	97.6	3.3 (2.1)

Note: The number reported in brackets is the actual oxygen atom % concentration after subtraction of the amount detected in the control.

Table 4.25 shows the results after solvent extraction. The PS control, again, showed an amount of 1.2 atom % oxygen, possible reasons for this have been discussed in Section 4.2.2. Considering the XPS errors, there was no significant difference in the oxygen concentration on the surface before and after extraction.

**Table 4.25** Elemental compositions of reactively compounded PS-SMA 66:34 at different loadings after extraction in methanol.

Sample systems	Elemental composition / Atom %	
	[C]	[O]
PS control	98.8	1.2
0.1%	98.8	1.2 (0)
1%	98.5	1.5 (0.3)
10%	95.0	3.7 (2.5)

In general the concentrations of oxygen detected at the surface of the reactively compounded samples were not significantly affected by extraction. The amount of oxygen detected was perhaps slightly less than that seen for the corresponding non-reactively compounded samples. However, the difference is small. The oxygen

concentrations measured were also perhaps slightly less than those anticipated for the bulk composition. The near-surface was not enriched in anhydride groups.

The extracted reactively compounded samples also underwent chemical derivatisation. The results are tabulated in Table 4.26. As seen, the fluorine conversion was very low and not much different from the non-reactively compounded samples.

**Table 4.26** Effect of chemical derivatisation on reactively compounded PS-SMA 66:34 after extraction in methanol.

Sample systems	Elemental Composition / Atom %		
	[C]	[O]	[F]
PS control	98.8	1.2	0
1%	96.5	1.4	0.1
10%	96.2	3.3	0.5

In comparison, the oxygen concentrations detected for both the non-reactively compounded and reactively compounded samples, were much less than those seen for the surface treated samples, whether before or after extraction and derivatisation.

#### 4.6.3 Attenuated Total Reflection Infrared Spectroscopy

PS-SMA samples of 1% and 10% loadings of all compositions were analysed and the peak area measured from the spectra. The analysis was done on extracted samples. The molar ratio was calculated for the surface (measured) and compared to the bulk (calculated), see Appendix B, as shown in Table 4.27. The estimated error was 0.0004 for 1% loading samples and 0.001 for 10% loading samples, respectively.

**Table 4.27** Molar ratio at bulk and surface of reactively compounded PS-SMA.

<b>S:MA</b>	<b>1%</b>		<b>10%</b>	
	<b>Bulk (Calculated)</b>	<b>Surface (Measured)</b>	<b>Bulk (Calculated)</b>	<b>Surface (Measured)</b>
<b>50:50</b>	0.0052	0.0062	0.0573	0.0551
<b>66:34</b>	0.0034	0.0049	0.0378	0.0328
<b>75:25</b>	0.0026	0.0023	0.0282	0.0297

The surface and bulk compositions were similar. This is different from the non-reactively compounded samples where the measured compositions were consistently slightly higher than the bulk composition. In the same manner to the non-reactively compounded samples, the 1% loading samples had higher percentage errors in the ratio.

#### 4.6.4 Atomic Force Microscopy

The degree of surface roughness,  $R_a$ , was measured on the reactively compounded samples and shown in Table 4.28. The error in  $R_a$  was estimated at about 2 to 4 nm. The degree of roughness for all samples was sub- $\mu\text{m}$ . There was no difference in the degree of roughness on extraction for both loadings. This was different from the non-reactively compounded samples. This may be that some copolymers were more strongly and reactively bonded to the PS chain and did not rearrange under extraction. The 10% loading showed higher roughness than the 1% loading. Figures 4.29 and 4.30 show the AFM scan images of the 10% samples before and extraction. In comparison, reactively compounded samples have lower surface roughness than non-reactively compounded samples, but higher roughness than surface treated samples.



**Table 4.28** Surface roughness of reactively compounded PS-SMA 66:34 before and after extraction in methanol.

Sample systems	Area $R_a$ (nm)		Area RMS (nm)	
	Non-extracted	Extracted	Non-extracted	Extracted
PS Control	90	90	114	115
1%	85	89	114	116
10%	106	104	142	132

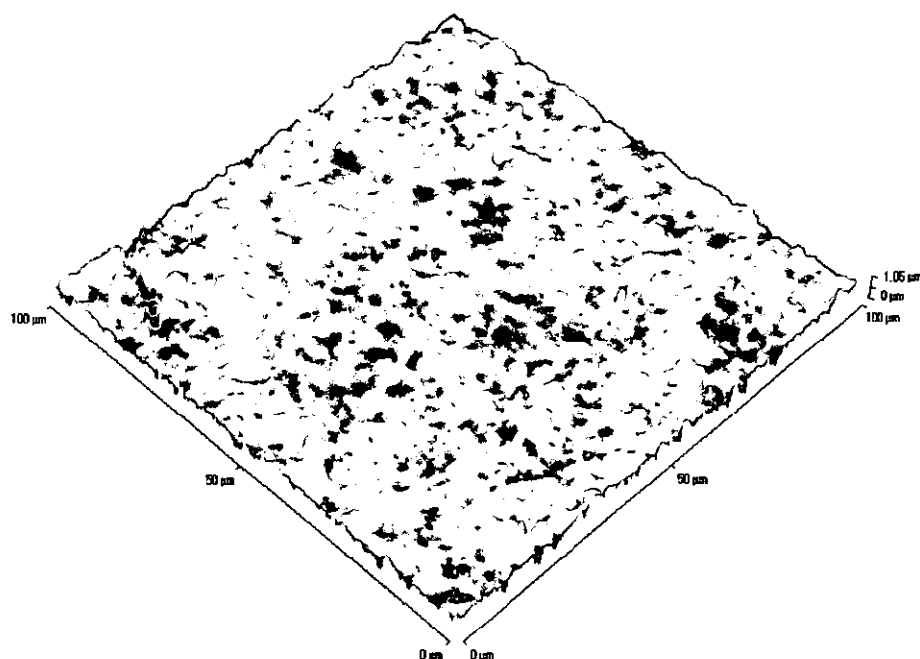


**Figure 4.29** AFM scan of reactively compounded PS-SMA 66:34 10% loading before extraction.

**Table 4.28** Surface roughness of reactively compounded PS-SMA 66:34 before and after extraction in methanol.

Sample systems	Area $R_a$ (nm)		Area RMS (nm)	
	Non-extracted	Extracted	Non-extracted	Extracted
PS Control	90	90	114	115
1%	85	89	114	116
10%	106	104	142	132

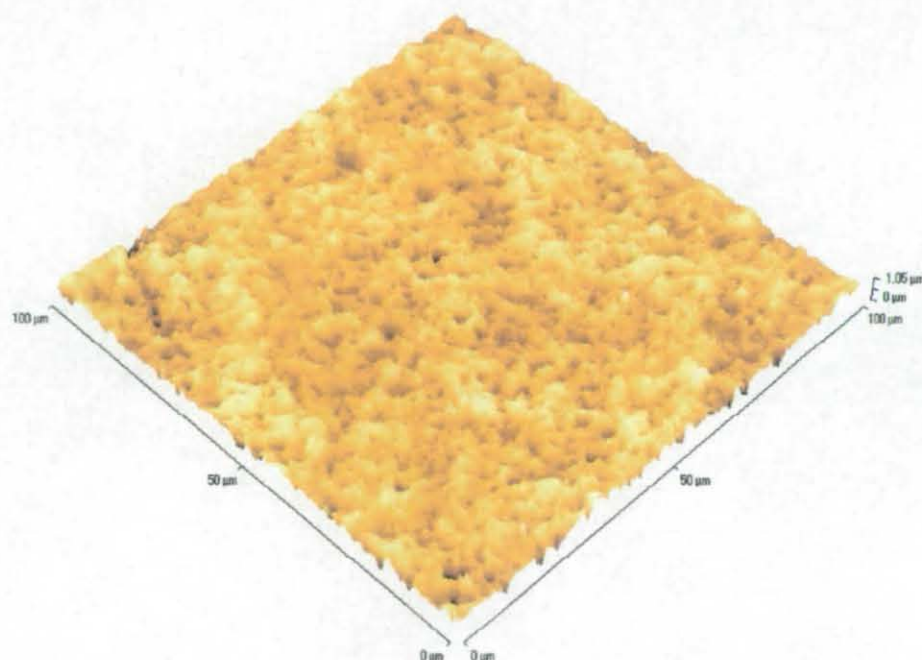


**Figure 4.29** AFM scan of reactively compounded PS-SMA 66:34 10% loading before extraction.

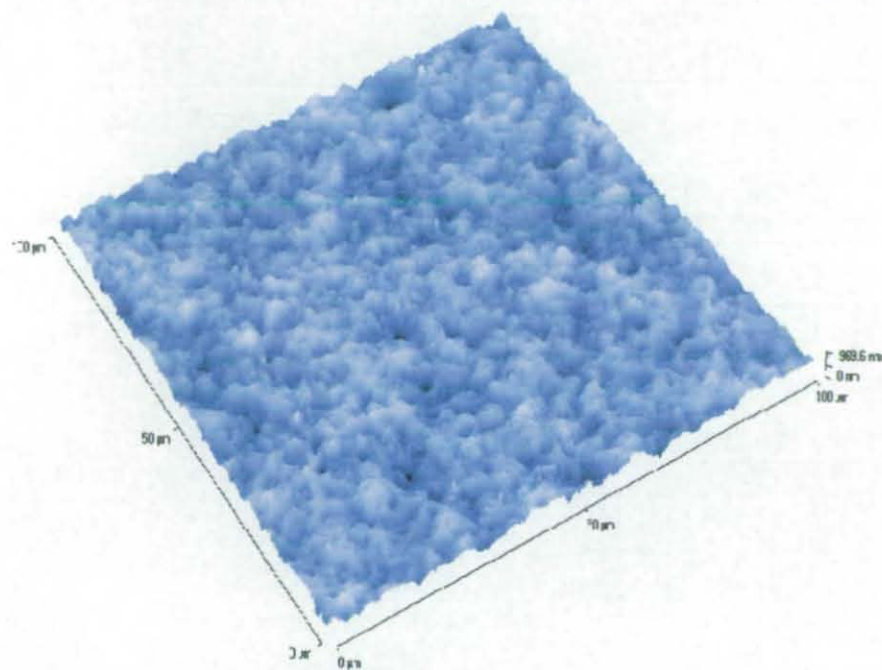


**Figure 4.30** AFM scan of reactively compounded PS-SMA 66:34 10% loading after extraction.

#### 4.6.5 Contact Angle Measurement

Contact angle measurements were performed on samples having PS-SMA 66:34 at 1% and 10% loading, before and after extraction. Samples compounded with PVME were also studied. All results are presented in Table 4.29.

The contact angles were generally lower than those observed for the non-reactively compounded samples (see Table 4.21). This was particularly the case for receding angles. Again contact angles did not seem to depend on the amount of copolymer or PVME added. Extraction does seem to lead to lower receding angles. This could not have been due to surface roughness since AFM (see Table 4.28) showed that extraction did not affect surface roughness.

**Table 4.29** Contact angles of reactively compounded PS at ~ 25°C.

Sample systems	$\theta_{adv} / ^\circ$		$\theta_{rec} / ^\circ$		$\Delta\theta / ^\circ$	
	Non-extracted	Extracted	Non-extracted	Extracted	Non-extracted	Extracted
<b>PS Control</b>	89.8 (2.4)	90.2 (1.4)	74.1 (1.5)	73.3 (1.9)	15.7	16.9
<b>SMA 1%</b>	82.4 (2.1)	84.3 (2.4)	58.9 (1.8)	46.9 (1.1)	23.5	37.4
<b>SMA 10%</b>	84.1 (2.9)	80.8 (1.4)	61.3 (2.3)	58.4 (1.6)	22.8	22.4
<b>PVME 1%</b>	83.5 (1.1)	81.3 (2.8)	58.1 (2.3)	54.8 (1.4)	25.4	26.5
<b>PVME 10%</b>	80.5 (1.3)	78.1 (2.1)	54.9 (2.4)	51.7 (1.9)	25.6	26.4

Note: Standard deviations are given in brackets

The samples underwent chemical derivatisation and the results are reported in Table 4.30. Both advancing and receding angles increased slightly as a result of derivatisation.

**Table 4.30** Effect of derivatisation on contact angles of reactively compounded PS after extraction at ~ 25°C in methanol.

Sample systems	$\theta_{adv} / ^\circ$	$\theta_{rec} / ^\circ$	$\Delta\theta / ^\circ$
<b>PS control</b>	89.1 (2.3)	76.8 (1.9)	12.3
<b>SMA 1%</b>	86.2 (1.8)	52.6 (2.1)	33.6
<b>SMA 10%</b>	82.4 (1.3)	63.5 (1.8)	18.9
<b>PVME 1%</b>	82.5 (2.5)	60.3 (2.1)	22.2
<b>PVME 10%</b>	80.7 (2.2)	63.8 (1.7)	16.9

Note: Standard deviations are given in brackets.

It is noted that the 1% loading has the largest contact angle hysteresis, quite near to that of surface treated samples, in particular, that of the chromic acid treated sample. This was not seen for the non-reactively compounded samples. This may be due to the surface reorientation of the functional groups upon receding measurement. The 10% loading has the lowest contact angle hysteresis among the rest.

### 4.6.6 Adhesion

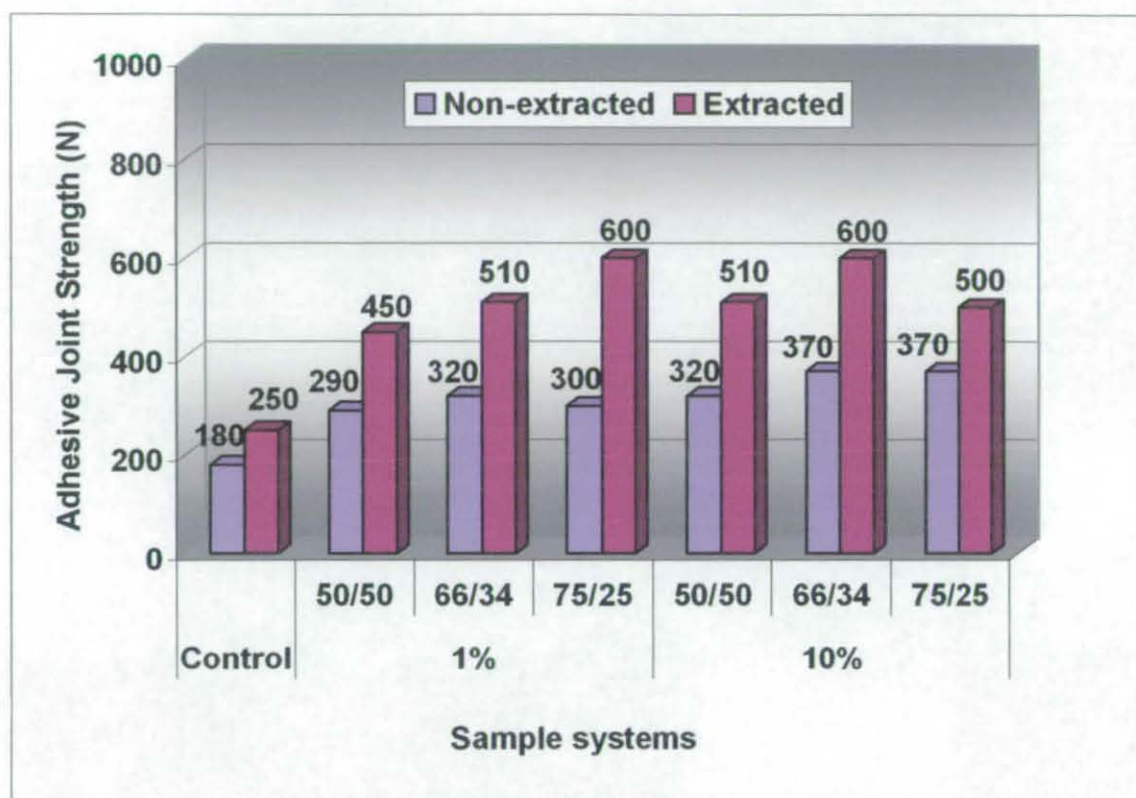
Lap shear joint strength values measured for all samples at 1% and 10% loadings, before and after extraction. The results are shown in Figure 4.31. The adhesive joint strength increased for the reactively compounded samples, compared to PS control. The adhesive joint strength increased after extraction for all systems and this could have been affected by several factors. As reported in Section 4.6.4, there was no difference in the degree of roughness on extraction for all systems; hence the increase in joint strength was not due to roughness. The increase may have been due to the removal of weak boundary layer during extraction.

It was observed that, on average, there was no difference in adhesive joint strength between the various copolymer compositions with the same loading, before and after extraction. For the reactive system, there was no difference in adhesive joint strength between 1% and 10% loading.

The adhesive joint strength was also performed on PS-PVME of both loadings, after and before extraction. Before extraction, the adhesive joint strength values were 240 N and 210 N respectively for 1% and 10% loadings. The adhesive joint strength increased to 310 N for 1% loading and to 300 N for 10% loading upon extraction. The increase could be due to the removal of the weak boundary layer. The standard deviations, before and after extraction, for both loadings were between 32 and 51 N. However, as compared to the PS-SMA samples, the



adhesive joint strength was lower for the PS-PVME samples, both before and after extraction.



Note: Standard deviation between 19 and 45 N

**Figure 4.31** Effect of adhesive joint strength on reactively compounded PS-SMA compositions.

Chemical derivatisation was carried out on the PS-SMA 66:34 copolymer samples and the PS-PVME samples after extraction, see Table 4.31. There was no difference in adhesive joint strength for the PS control, which was as expected. Adhesive joint strength values decreased on derivatisation for all SMA copolymer systems. The decreases in adhesive joint strength were as expected. This was thought to be due to some oxygen containing groups being “shut down” and hence

there were fewer acid anhydride groups available to react with the adhesive. As expected, derivatisation had little or no effect on the samples containing PVME.

**Table 4.31** Effect of derivatisation on adhesive joint strength of reactively compounded PS after extraction in methanol.

Sample systems	Adhesive Joint Strength (N)	
	Before derivatisation	After derivatisation
PS control	249 (10)	248 (12)
SMA 1%	510 (10)	213 (15)
SMA 10%	600 (30)	330 (11)
PVME 1%	310 (25)	260 (31)
PVME 10%	300 (18)	260 (29)

Standard deviations are given in brackets.

It was noted that the adhesive joint strength of the non-reactively compounded samples, was higher than that of reactively compounded samples for all compositions.

**4.6.7 Summary**

The adhesive joint strength increased after reactive compounding. After extraction, adhesion was further improved due to the removal of weak boundary layer. There was no difference in adhesive joint strength between 1% and 10% loaded samples. After derivatisation, the adhesive joint strength decreased as expected, as there would have been fewer oxygen groups on the surface available for reaction. As compared to non-reactively compounded samples, the reactively compounded samples showed lower adhesive joint strength. The reason why the reactively compounded SMA samples have a lower joint strength was unclear. At first sight the evidence is contradictory. There may be slightly fewer acid anhydride groups

present at the surface of the reactively compounded samples, according to XPS and FTIR measurements, compared to non-reactive compounding. However, the contact angle data showed that the reactively compounded samples were slightly more wettable. This difference is particularly evident in the receding angle. The reactively compounded samples were not as rough as their non-reactively compounded counterparts and this may have contributed to the lower adhesion. It was also possible that the presence of the organic peroxide initiator leads to a different surface chemistry with fewer available acid anhydride groups. Reactive compounding is a widely used technique but for these systems it clearly has no advantages over non-reactive compounding in improving adhesion.



---

## **4.7 GRAFTING**

### **4.7.1 Introduction**

In this part of work, another way of increasing the functionality of untreated PS was attempted. SMA copolymer chains were grown in situ on the PS surface from vapour phase monomers. The process was initiated by UV irradiation. The copolymer chains grown on the surface of the polymer will be chemically attached to the substrate and the anhydride groups will be available to react with suitable adhesives. The grafted chains will be located only at the surface of the polystyrene. The grafted samples were characterised by selected analyses, which included XPS, contact angle measurement and lapshear testing, before and after extraction and chemical derivatisation. The results were compared to those obtained in previous experiments.

### **4.7.2 X-ray Photoelectron Spectroscopy**

The grafted samples were analysed by XPS before and after extraction. The UV irradiated blank untreated PS samples were also analysed as a comparison. The results are tabulated in Table 4.32. There was a small amount of oxygen detected in the UV blank and its occurrence has been discussed in Section 4.2.2. It can be seen that there is no significant difference in the oxygen concentration before and after extraction. In comparison, the grafted samples showed higher oxygen concentration than the non-reactively compounded and reactively compounded sample, of 1% loading level. The concentrations are slightly below those of the 10% reactively compounded samples.

**Table 4.32** Elemental compositions of blank and grafted PS.

Sample systems	Elemental compositions / Atom %	
	[C]	[O]
Blank	98.9	1.1
Non-extracted	97.7	2.3
Extracted	97.3	2.7

After chemical derivatisation, 0.8 atom % of fluorine was detected. However, this is still much less than that found for pure copolymers. This concentration was higher than all the non-reactively compounded and reactively compounded samples, irrespective of loading level. In comparison with the surface treated samples, the grafted samples showed lower fluorine concentration.

#### 4.7.3 Contact Angle Measurement

Contact angle measurements were carried out on the blank and grafted samples before and after extraction and the results are presented in Table 4.33. As expected there was no difference in both advancing and receding contact angles for the blank sample before and after extraction. The contact angles reduced slightly after grafting. This indicated that there was a presence of anhydride groups, grafted onto the surface. There was little, if any, change in the advancing and receding angles for grafted samples before and after extraction. Some hysteresis was observed and this may have been due to reorganisation of the functional groups on the surface and/or incorporation of water. This behaviour was also observed for non-reactively compounded and reactively compounded samples, but the hysteresis for grafted samples was much less than that observed for flame and chromic acid treated samples.

Table 4.33 Contact angles of blank and grafted PS at ~ 25°C.

Sample systems	$\theta_{adv} / ^\circ$		$\theta_{rec} / ^\circ$		$\Delta\theta / ^\circ$	
	Non-extracted	Extracted	Non-extracted	Extracted	Non-extracted	Extracted
Blank	90.4 (2.1)	89.1 (1.4)	81.8 (1.3)	79.5 (1.9)	8.6	9.6
Grafted	82.8 (1.2)	83.2 (1.9)	70.1 (2.1)	68.9 (2.2)	12.7	14.3

Note: Standard deviations are given in brackets

The grafted samples were subjected to chemical derivatisation, and then contact angle measurement was carried out; results are reported in Table 4.34. As expected, no difference was observed for the blank sample. Derivatised samples showed increased values for both advancing and receding angle values. This increase was consistent with the result of derivatisation, where there were fewer polar functional groups available to enhance wetting. The increase was more prominent in receding angle than in advancing angles.

Table 4.34 Effect of derivatisation on contact angles of blank and grafted PS after extraction at ~ 25°C in methanol.

Sample systems	$\theta_{adv} / ^\circ$	$\theta_{rec} / ^\circ$	$\Delta\theta / ^\circ$
Blank	88.9 (1.9)	78.1 (1.3)	10.8
Grafted	85.6 (2.2)	74.7 (1.5)	10.9

Note: Standard deviations are given in brackets

#### 4.7.4 Adhesion

An adhesive lap shear joint strength test was also performed on the grafted samples, for comparison with the other systems studied. The lap shear tests were carried out for blank and grafted samples before and after extraction. The results are found in Table 4.35. There was no significant change in adhesive joint strength for the blank sample, as a result of extraction.

Adhesive joint strength increased after the grafting process where the grafted sample displayed a value of 787 N, about twice that of the blank sample. This value is also higher than those of the non-reactively compounded and reactively compounded samples of all systems

The adhesive joint strength of grafted samples was further increased by extraction in methanol and was also much higher than those of the non-reactively compounded and reactively compounded samples. It was thought that the increase of joint strength was probably due to the removal of small molecules by extraction, e.g. the weak boundary layer.

**Table 4.35** Adhesive joint strength of blank and grafted PS before and after extraction in methanol.

Sample systems	Joint Strength (N)	
	Non-extracted	Extracted
Blank	381 (15)	401 (10)
Grafted	787 (20)	1070 (23)

Note: Standard deviations are given in brackets

The grafted samples were also subjected to chemical derivatisation, followed by adhesive joint strength testing; results are tabulated in Table 4.36. Not much

difference in the strength of adhesion between the blank sample before and after derivatisation was observed.

Grafted samples showed lower readings after derivatisation, as expected, as there were fewer functional groups available for bonding. Overall the grafted samples demonstrated higher adhesive joint strength than those of the non-reactively compounded and reactively compounded samples, and only slightly below that of surface treated samples.

**Table 4.36** Effect of derivatisation on adhesive joint strength of blank and grafted PS after extraction in methanol.

Sample systems	Joint Strength (N)	Standard Deviation
Blank	395	35
Grafted	895	61

4.7.5 Summary

The oxygen concentration remained about the same for grafted samples before and after extraction. After derivatisation, there was a low concentration of fluorine groups present. Contact angle hysteresis was lower on the grafted samples than for the others studied. It was possible that grafted samples showed less reorganisation and/or incorporation of water than the other surfaces studied. The presence of covalently bonded copolymer groups on the PS surface was found to have increased the adhesive joint strength, compared to the blank sample. This increase was not caused by the oxidation due to the UV irradiation of the blank sample, but due to the presence of functional groups in the copolymer chain. Adhesive joint strength was further improved by extraction, and this could have been due to the removal of the weak boundary layers, perhaps due to the presence of non-grafted copolymer on the surface. After derivatisation, the

adhesive strength was found to have been reduced slightly, which was expected. In general, the grafted samples showed improved adhesive joint strengths that were comparable to the surface treated samples. Adhesive joint strength was significantly higher than for the compounded samples, which had similar amounts of surface oxygen (determined by XPS). This was expected, since the anhydride groups would probably have been concentrated nearer the surface for the grafted samples and therefore a higher proportion would be available for interaction with the epoxy resin adhesive used.

---

## **4.8 TEMPERATURE DEPENDENCE CONTACT ANGLE MEASUREMENT**

### **4.8.1 Introduction**

As demonstrated in Section 2.6, the effect of environmental temperature on the work of adhesion will be able to give a greater insight into the problem of wetting than measurement of the free energy at only one temperature. This will allow the enthalpy and entropy of adhesion for each system to be calculated. This approach requires accurate measurement of contact angle and also precise control of experimental conditions.

### **4.8.2 Evaluation of Equilibrium Spreading Pressure**

As described in Section 2.3.2.a, the presence of adsorbed vapour will cause a reduction of the surface free energy of the solid. The reduction is known as the equilibrium spreading pressure,  $\pi_e$ , and is often assumed to be negligible for those liquids which have a non-zero contact angle on polymers. Good [49] explained that the presence of  $\pi_e$  could affect the contact angle on a solid and that the variation of  $\pi_e$  could be controlled by creating a saturated vapour atmosphere surrounding the test area before measuring contact angle. This will keep the spreading pressure constant throughout the measurement.

An experiment, therefore, was undertaken to establish whether the contact angle measurements would be affected by spreading pressure, see Section 3.3.4.b. The temperature dependence of water contact angles on untreated PS, (see Table 4.37) and chromic acid treated PS, (see Table 4.38), was measured with and without the presence of a saturated vapour of water.

Table 4.37 Effect of  $\pi_c$  on contact angles of untreated PS.

Temperature / °C (approx.)	Contact angle measurement			
	Absence of saturated vapour		Presence of saturated vapour	
	$\theta_{adv}$ / °	$\theta_{rec}$ / °	$\theta_{adv}$ / °	$\theta_{rec}$ / °
15.7	88.6 (1.1)	80.2 (1.4)	90.3 (2.1)	81.3 (2.1)
20.5	87.1 (1.2)	82.3 (1.4)	88.9 (1.9)	81.1 (1.9)
25.7	84.8 (1.1)	79.6 (1.2)	85.9 (1.5)	80.0 (1.9)
30.8	84.7 (1.1)	76.5 (1.4)	83.8 (1.2)	75.4 (1.3)
35.0	82.3 (1.5)	73.8 (2.1)	83.1 (1.3)	74.7 (1.1)
40.9	86.5 (1.2)	81.9 (1.9)	88.6 (1.1)	82.3 (1.2)
45.0	82.4 (1.7)	77.6 (1.8)	81.9 (1.2)	78.7 (1.8)

Note: Standard deviations are given in brackets.

Table 4.38 Effect of  $\pi_c$  on contact angles of chromic acid treated PS.

Temperature / °C (approx.)	Contact angle measurement			
	Absence of saturated vapour		Presence of saturated vapour	
	$\theta_{adv}$ / °	$\theta_{rec}$ / °	$\theta_{adv}$ / °	$\theta_{rec}$ / °
16.0	61.2 (1.5)	23.2 (1.4)	59.4 (1.3)	22.1 (1.3)
20.2	61.1 (1.2)	23.9 (2.0))	62.3 (2.1)	24.8 (2.1)
24.9	63.5 (1.9)	23.6 (1.1)	62.4 (1.9)	24.9 (1.4)
31.3	65.4 (2.1)	25.9 (1.1)	64.4 (1.4)	24.3 (1.1)
36.0	62.7 (2.2)	26.1 (1.5)	63.1 (1.4)	25.8 (1.1)
41.6	63.0 (1.5)	24.4 (1.8)	62.4 (1.1)	25.9 (1.2)
45.9	64.0 (1.9)	25.7 (1.9)	63.0 (1.5)	26.6 (1.6)

Note: Standard deviations are given in brackets.



The results for untreated PS show that the contact angles in a non-saturated vapour environment were not much different from those made in the saturated environment. The difference was found to be only 1 or 2°, which was considered not to be significant. This is also true for the chromic acid treated PS. These results indicate that the contact angle measurement was not affected by vapour pressure. It is of course likely that the region in close proximity to the drop is always exposed to same vapour.

### **4.8.3 Effect of Temperature on the Work of Adhesion**

#### **a) *Untreated Polystyrene***

The work of adhesion is calculated according to Equation {2.5} (see Section 2.3.2). The calculation takes into account the temperature dependence of the surface free energy of the water testing liquid, with reference to Figure 2.4. An example of the calculation of work of adhesion is presented in Appendix C. Data presented in Figure 4.33 indicates that the receding value of work of adhesion, decreased with rising temperature while that of the advancing value did not. The results are in good agreement with Padday [84] for both advancing and receding angles, see Section 2.6. The observed changes in the work of adhesion were reproducible.

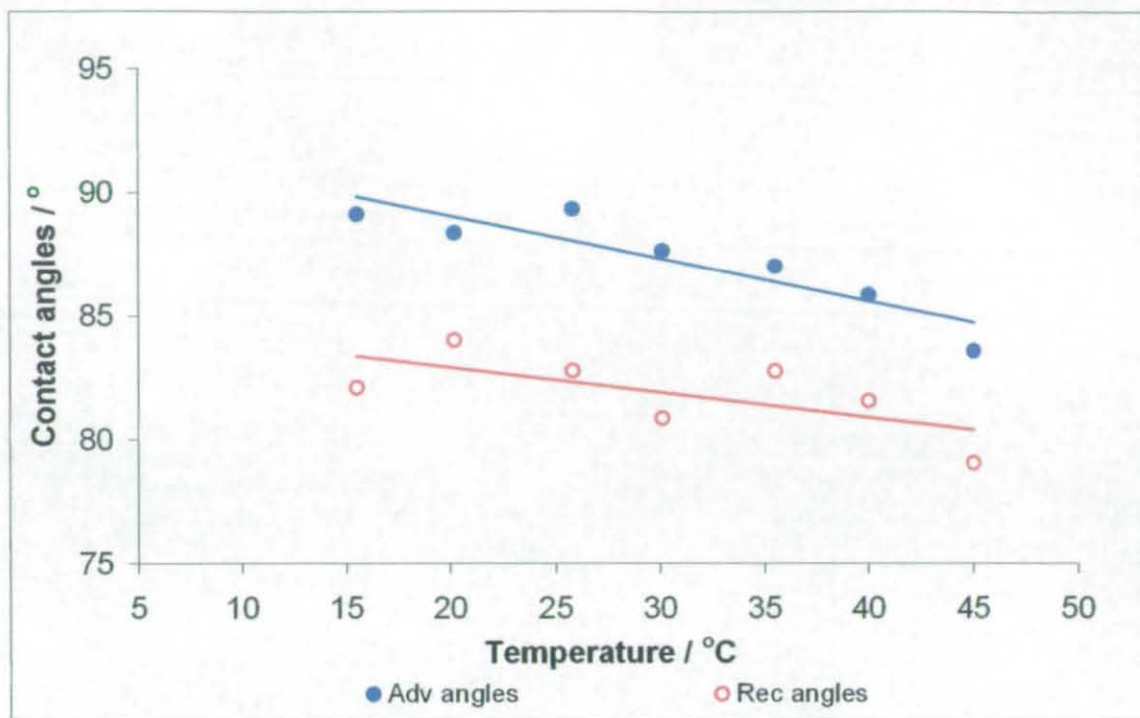


Figure 4.32 Effect of temperature on contact angles of untreated PS.

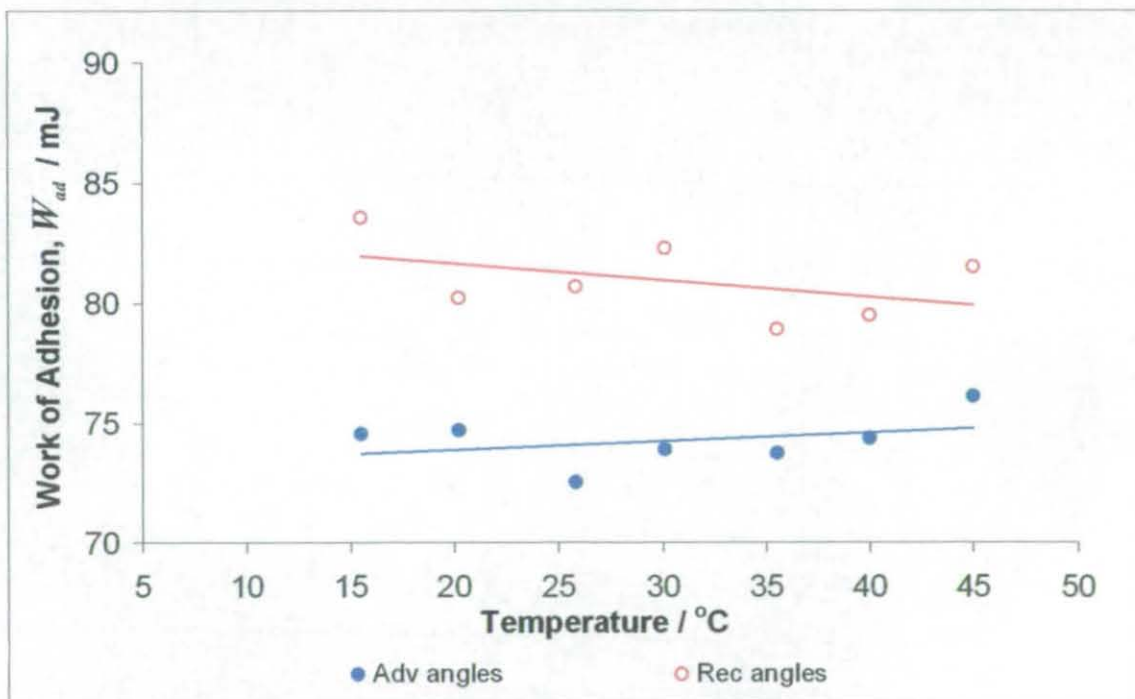


Figure 4.33 Effect of temperature on work of adhesion of untreated PS.

---

**b) Styrene Maleic Anhydride Copolymers**

The contact angle temperature dependence was studied on the various SMA copolymers. All the SMA copolymers compositions showed the same trend, that is, both advancing and receding angles decreased with increasing temperature. The results from the 66:34 copolymer are presented here. The work of adhesion is shown in Figure 4.35. The work of adhesion for both advancing and receding conditions decreased with temperature. The behaviour was different from that observed on the untreated PS.

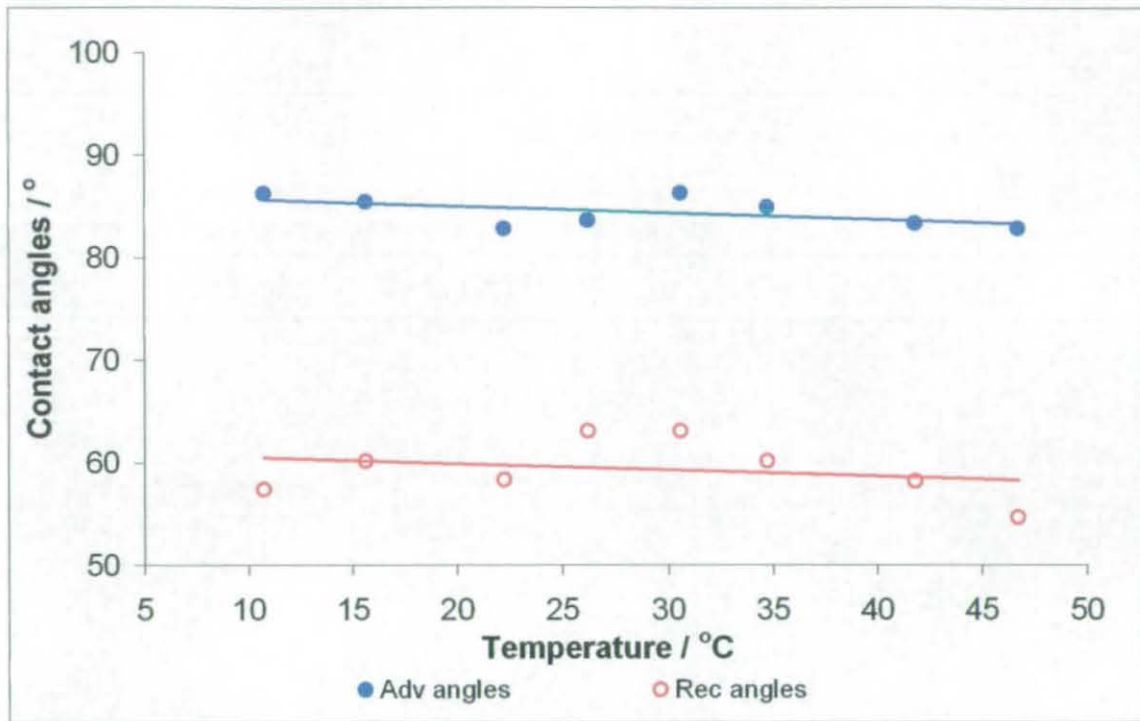


Figure 4.34 Effect of temperature on contact angles of SMA 66:34 copolymer.

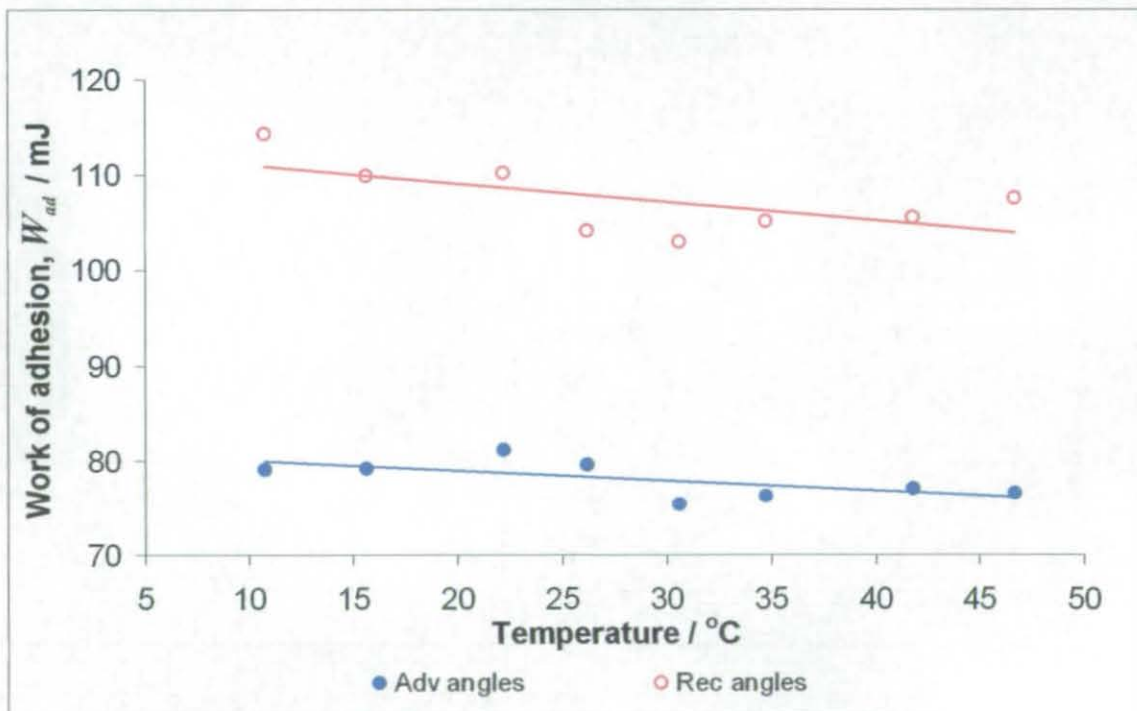


Figure 4.35 Effect of temperature on work of adhesion of SMA 66:34 copolymer.

---

**c) *Surface Treated Polystyrene***

For surface treated PS samples, contact angles increased with temperature; see Figures 4.36 and 4.38. Changes in contact angles of up to  $30^\circ$  were observed over the range studied. Both surface treated samples, therefore, showed a decrease in work of adhesion with temperature, see Figures 4.37 and 4.39. For flame treated samples, the receding angle was more affected by temperature than the advancing angle. It is not possible to explain this behaviour in terms of surface roughness or surface heterogeneity. Therefore it is proposed that this must have been due to the surface left by the receding drop being different to that before contact with water. For this to happen suggests some reorganisation of the polymers' surface and/or incorporation of water, and is consistent with the interpretation of hysteresis made in previous sections. The chromic acid treated surfaces showed less difference between advancing and receding conditions. Overall, the changes in work of adhesion with temperature were much greater for surface treated PS than untreated PS.



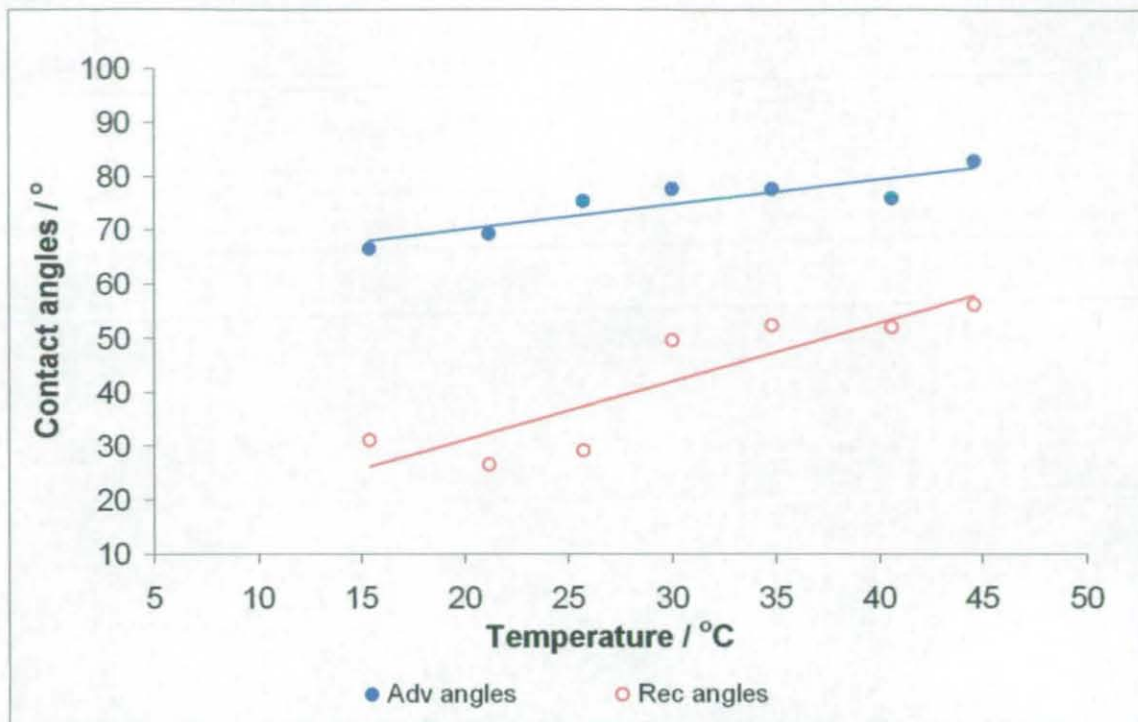


Figure 4.36 Effect of temperature on contact angles of flame treated PS.

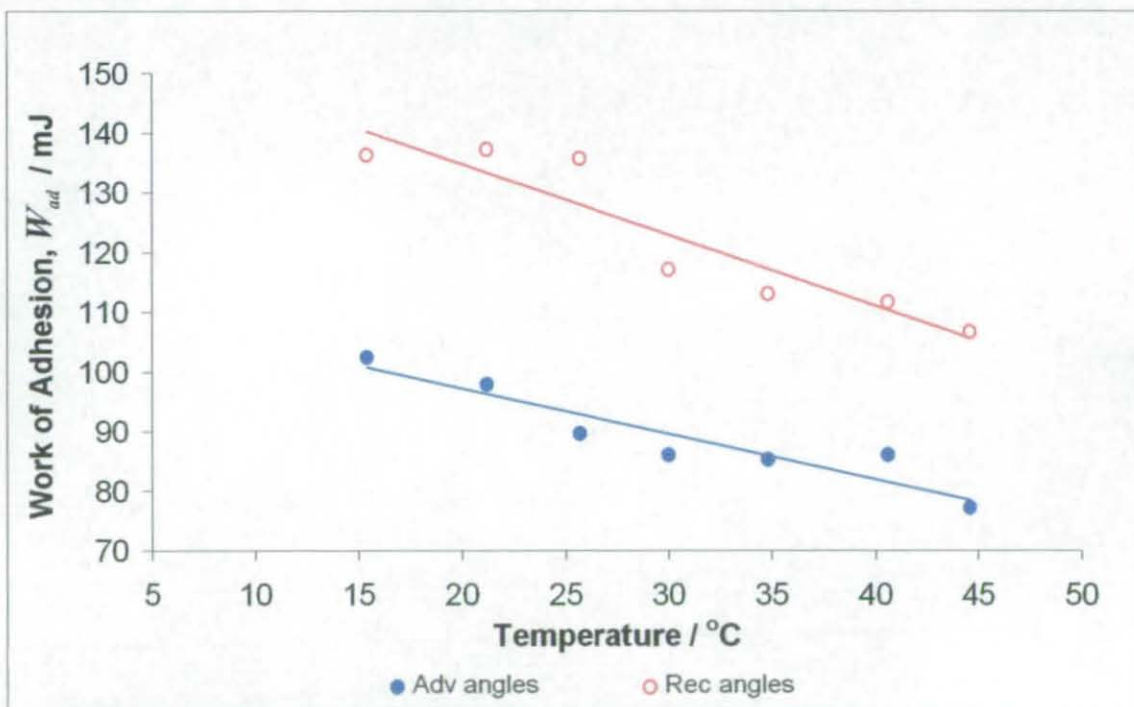


Figure 4.37 Effect of temperature on work of adhesion of flame treated PS.

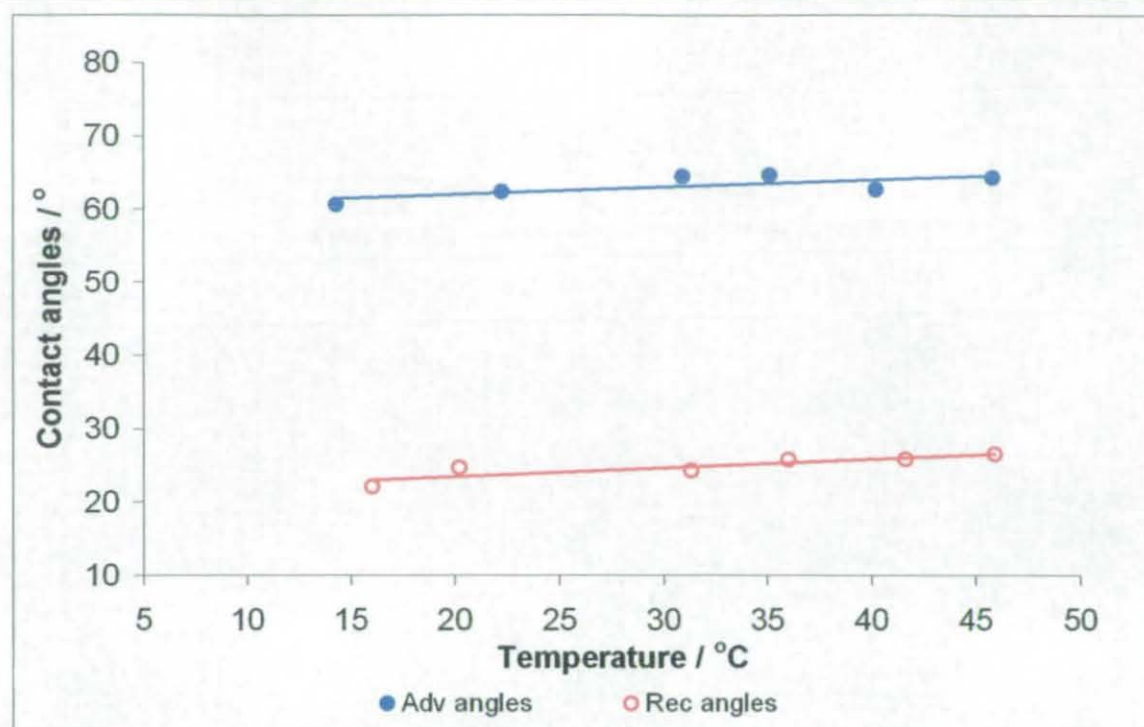


Figure 4.38 Effect of temperature on contact angles of chromic acid treated PS.

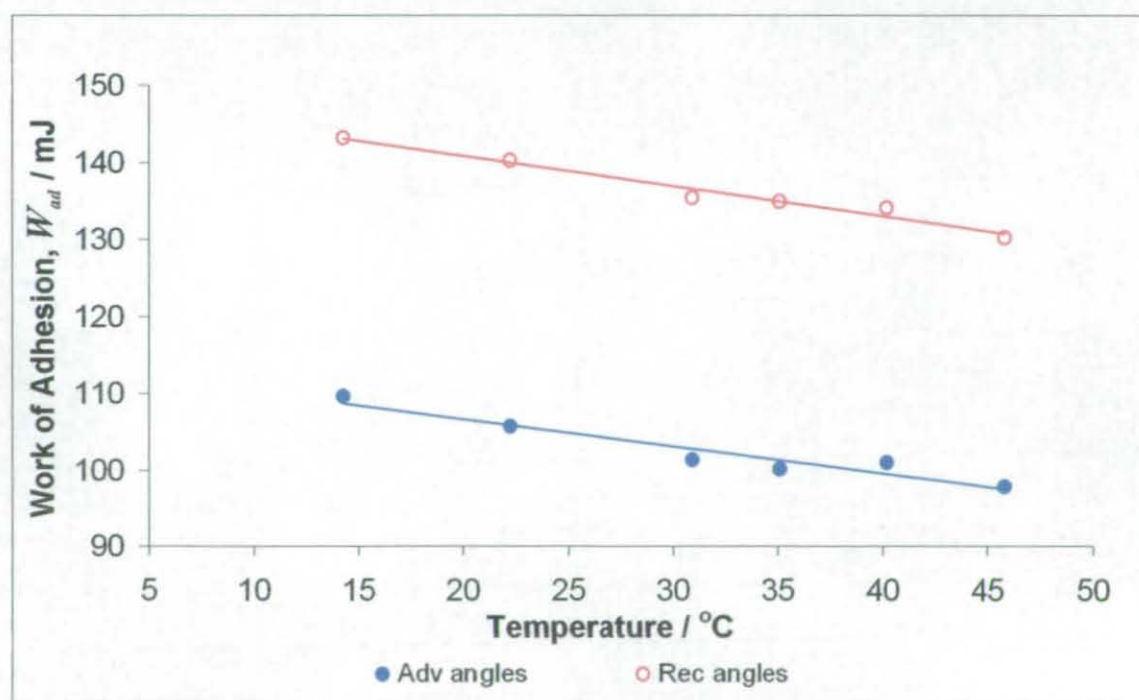


Figure 4.39 Effect of temperature on work of adhesion of chromic acid treated PS.

---

**d) *Non-reactively Compounded Polystyrene***

The temperature dependence of the contact angle on 1% and 10% loadings of PS-SMA 66:34 after extraction are evaluated and presented in Figures 4.40 to 4.43. For 1% loaded samples, the contact angle decreased with increasing temperature for both advancing and receding conditions. The receding angles though decreasing with temperature did not vary much. The 1% of PS-PVME loaded samples displayed only increasing advancing angles with temperature, which was the same as the 10% loaded PS-SMA samples. The 10% loaded PVME samples both showed decreasing advancing and receding angles with temperature, the same as the 1% loaded PS-SMA samples. These behaviours are all different from the surface treated samples where both advancing and receding angles increased with temperature.

It was observed that contact angle hysteresis increased with temperature for all samples, in contrast to the flame treated surfaces. The changes in work of adhesion with temperature are also generally less pronounced than for the surface treated samples.



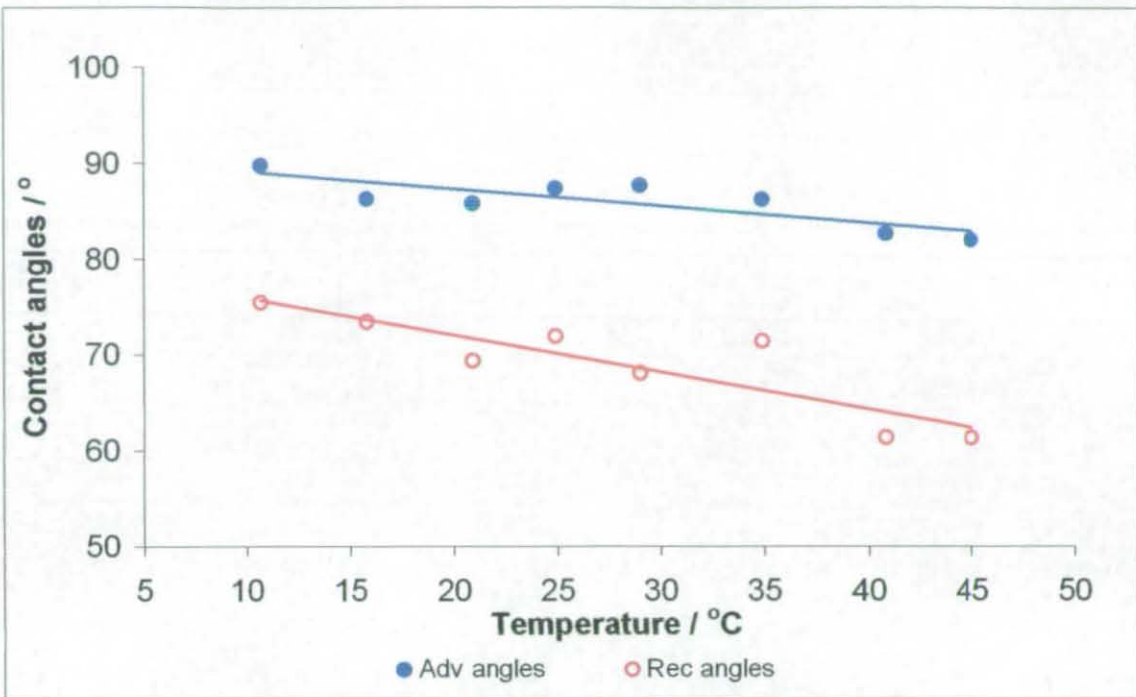


**Figure 4.40** Effect of temperature on contact angles of non-reactively compounded PS-SMA 66:34 1% loading.

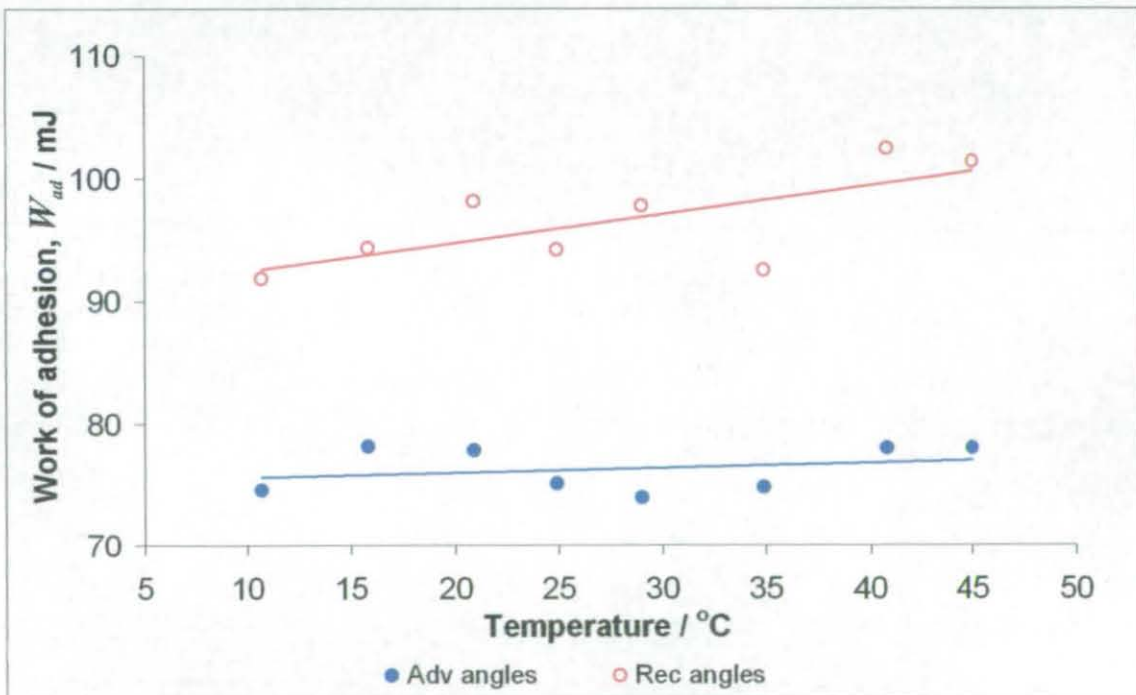


**Figure 4.41** Effect of temperature on work of adhesion of non-reactively compounded PS-SMA 66:34 1% loading.

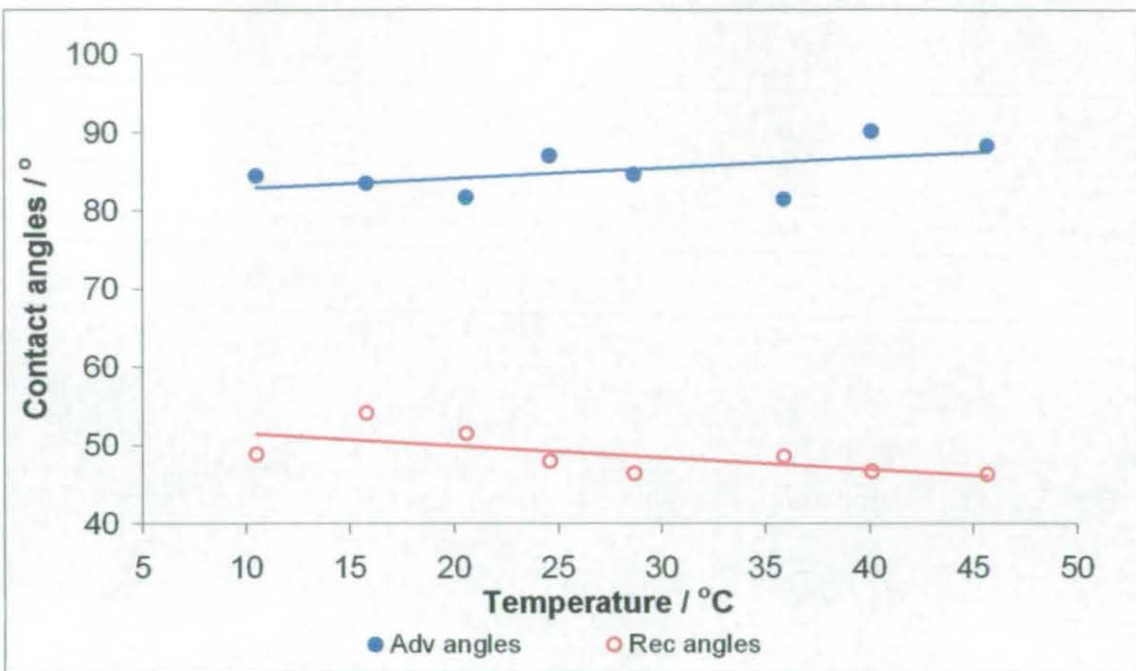


**Figure 4.42** Effect of temperature on contact angles of non-reactively compounded PS-SMA 66:34 10% loading.

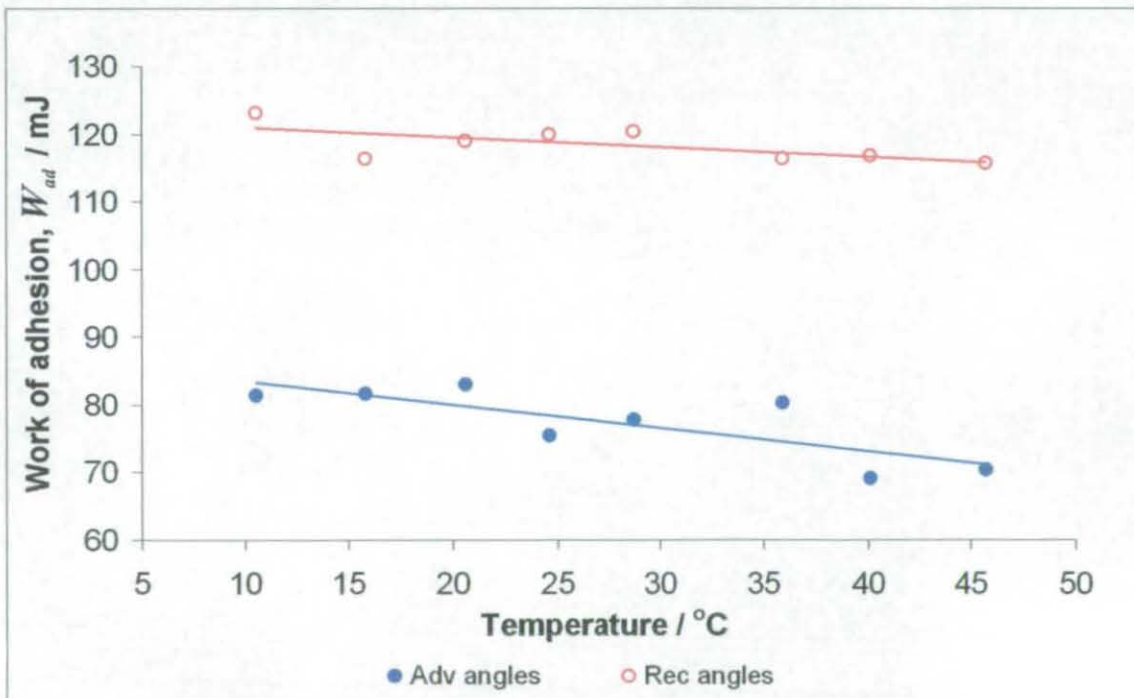


**Figure 4.43** Effect of temperature on work adhesion of non-reactively compounded PS-SMA 66:34 10% loading.

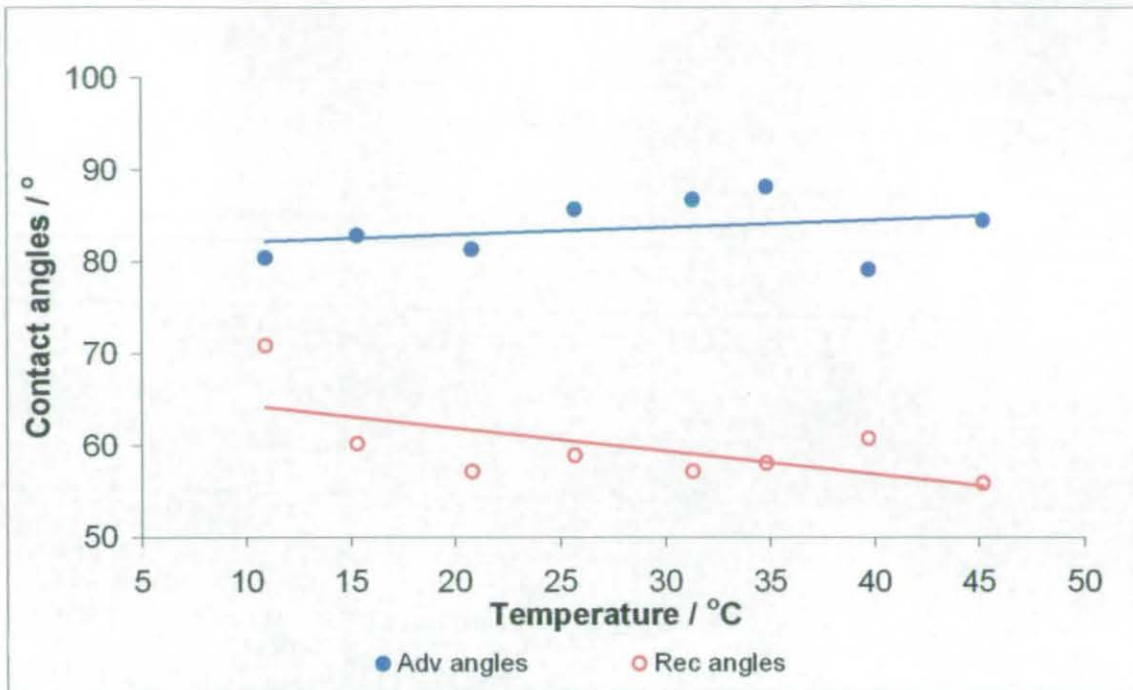


**Figure 4.44** Effect of temperature on contact angles of non-reactively compounded PS-PVME 1% loading.

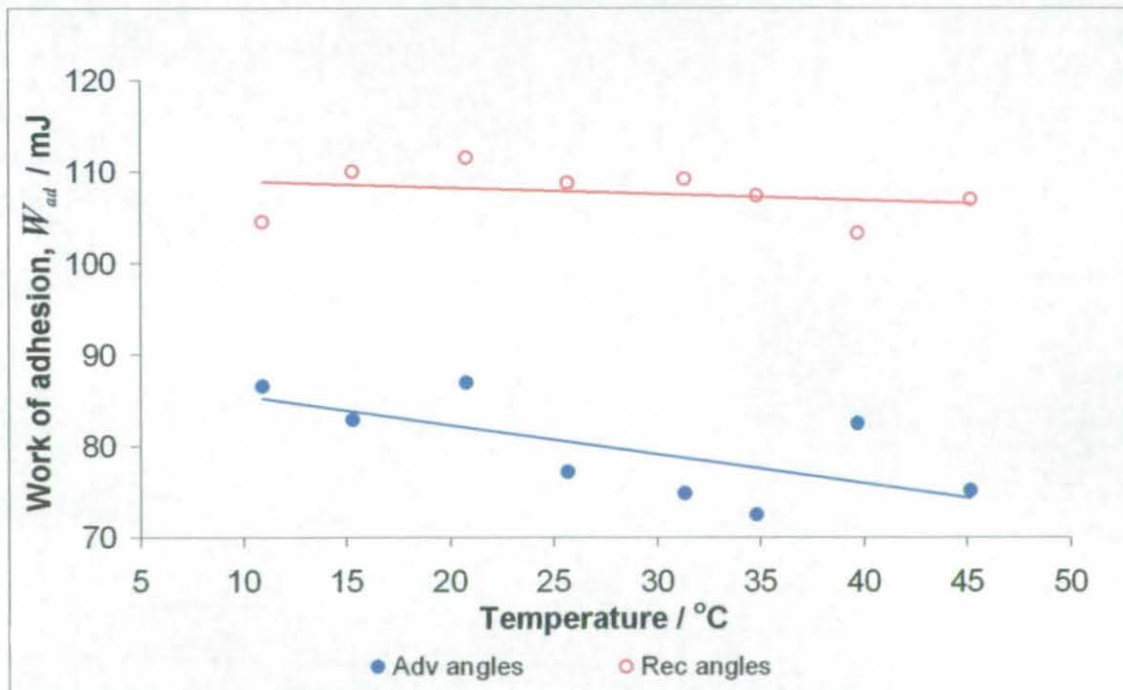


**Figure 4.45** Effect of temperature on work of adhesion of non-reactively compounded PS-PVME 1% loading.

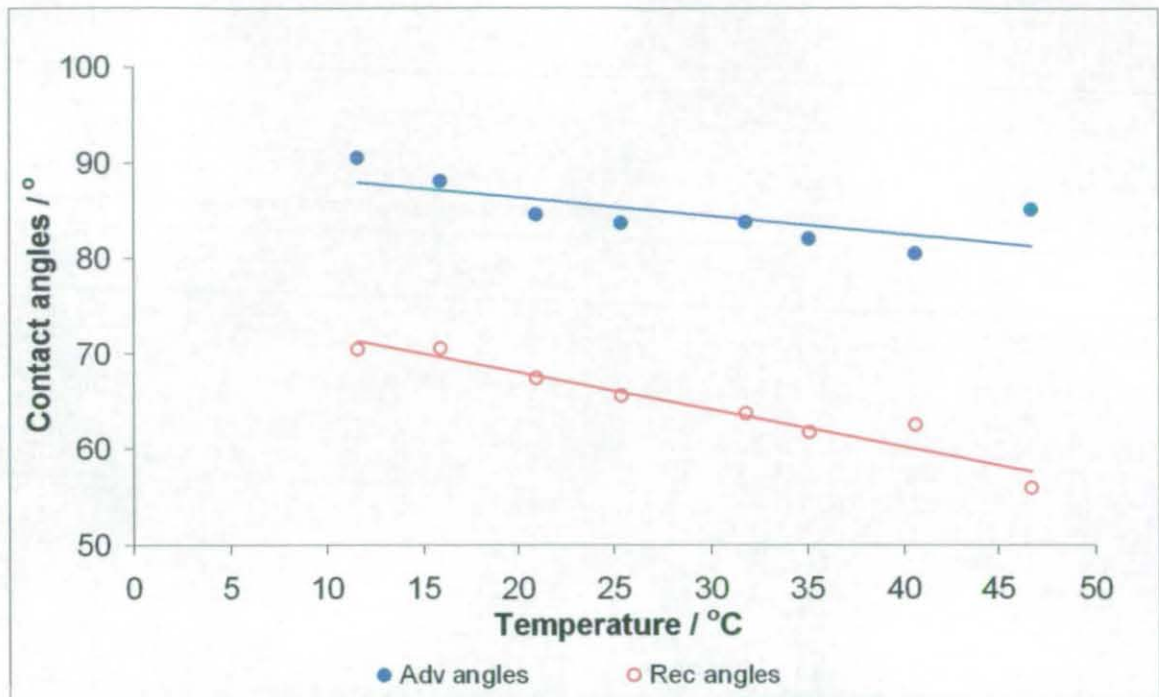


**Figure 4.46** Effect of temperature on contact angles of non-reactively compounded PS-PVME 10% loading.

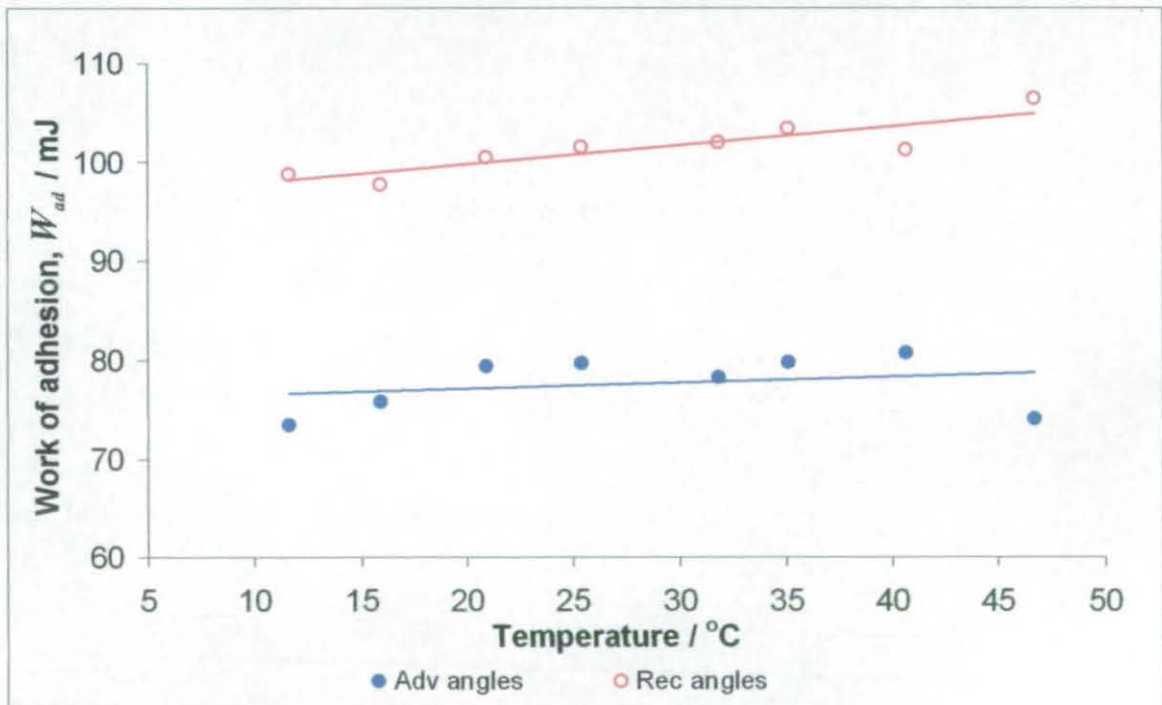


**Figure 4.47** Effect of temperature on work of adhesion of non-reactively compounded PS-PVME 10% loading.



---

**e) *Reactively Compounded Polystyrene***

The temperature dependence of water contact angles for reactively compounded PS-SMA 66:34 both after extraction and with 1% and 10% loading, were measured and are presented in Figures 4.48 to 4.51. It was observed that only the advancing angles of 1% and 10% PS-SMA loaded samples increased with temperature. This behaviour was also seen in the 1% loaded PS-PVME samples, see Figure 4.52. The 10% loaded PS-PVME samples, however, exhibited decreasing advancing and receding angles with increasing temperature, see Figure 4.54.

In many respects, the results are similar to those of non-reactively compounded samples. Contact angle hysteresis always increased with temperature and the dependence of the work of adhesion on temperature was weaker than that observed for the surface treated samples.

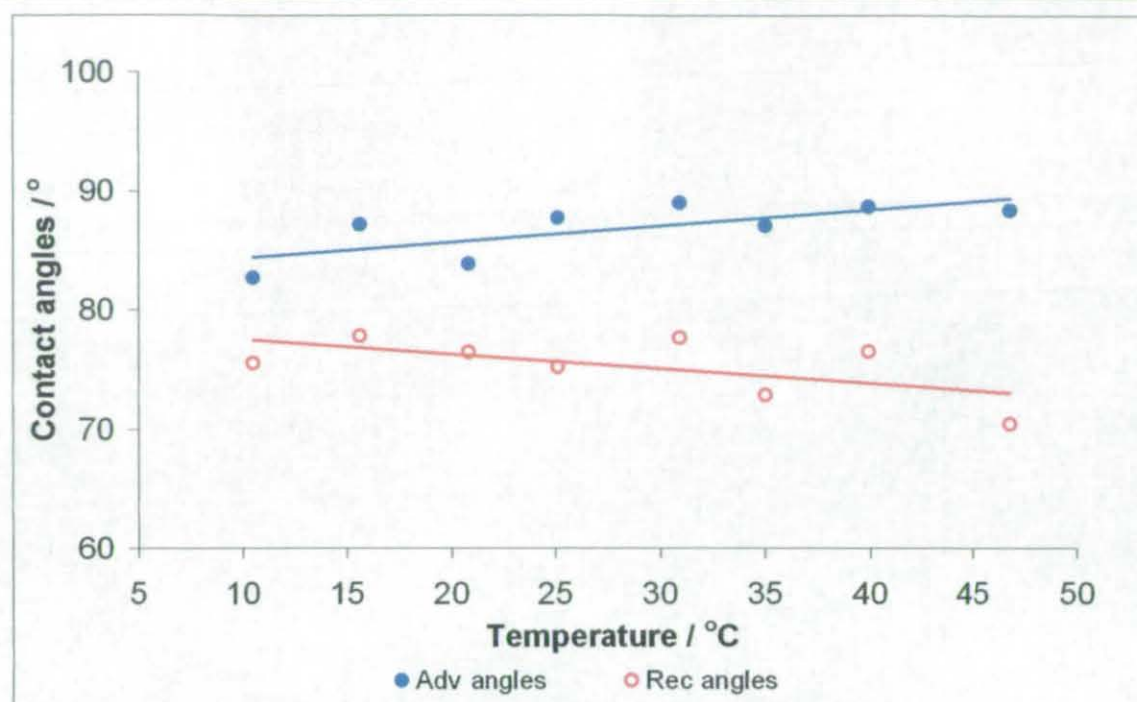


**Figure 4.48** Effect of temperature on contact angles of reactively compounded PS-SMA 66:34 1% loading.

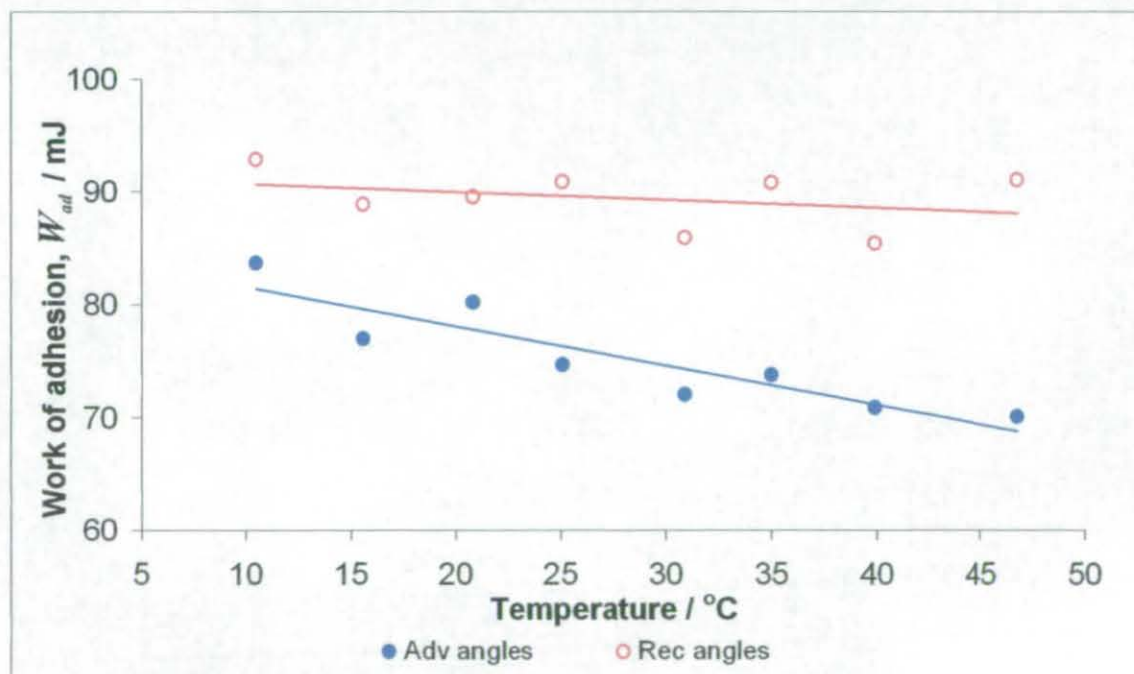


**Figure 4.49** Effect of temperature on work of adhesion of reactively compounded PS-SMA 66:34 1% loading.

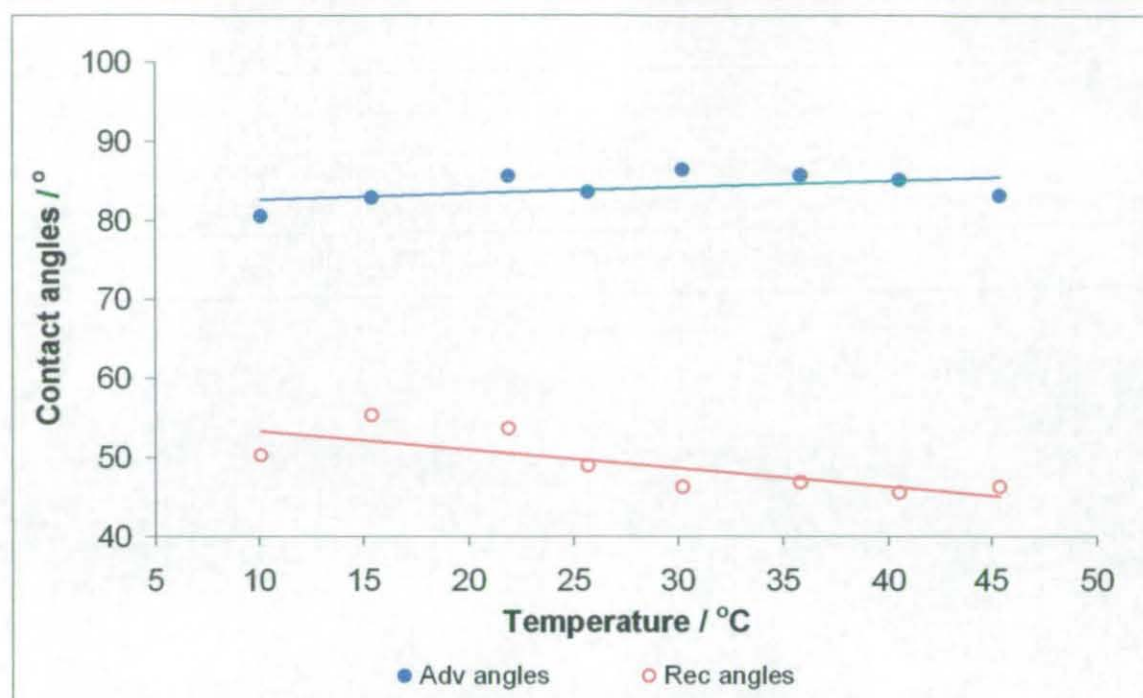


**Figure 4.50** Effect of temperature on contact angles of reactively compounded PS-SMA 66:34 10% loading.

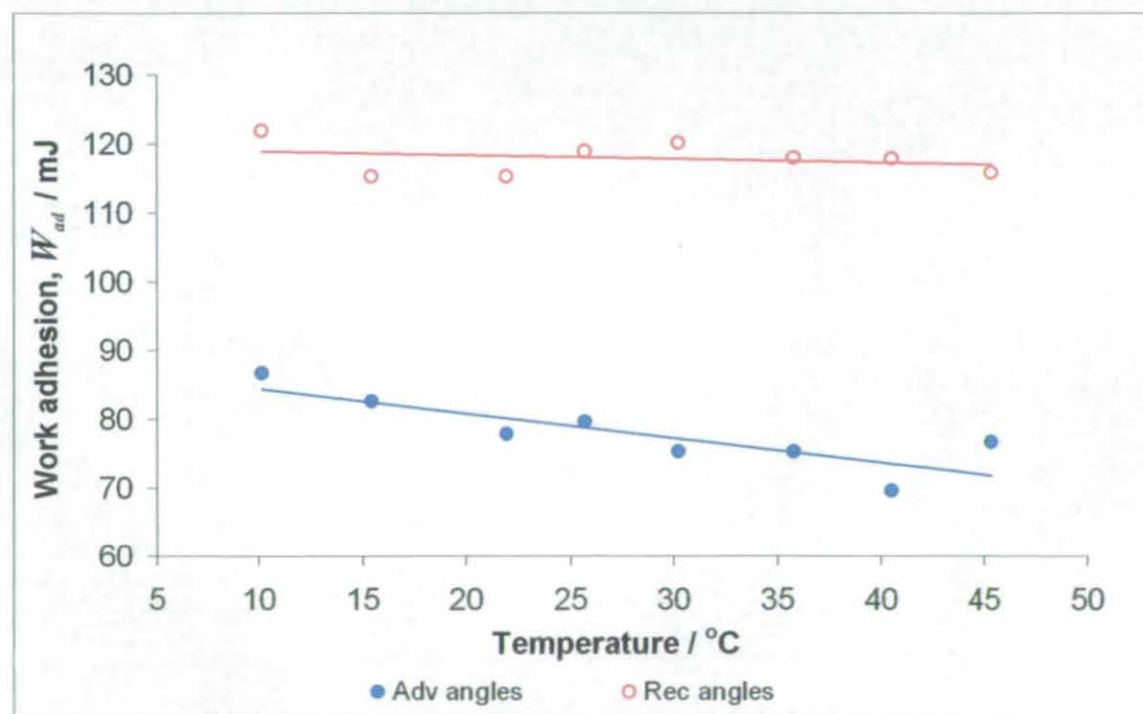


**Figure 4.51** Effect of temperature on work of adhesion of reactively compounded PS-SMA 66:34 10% loading.

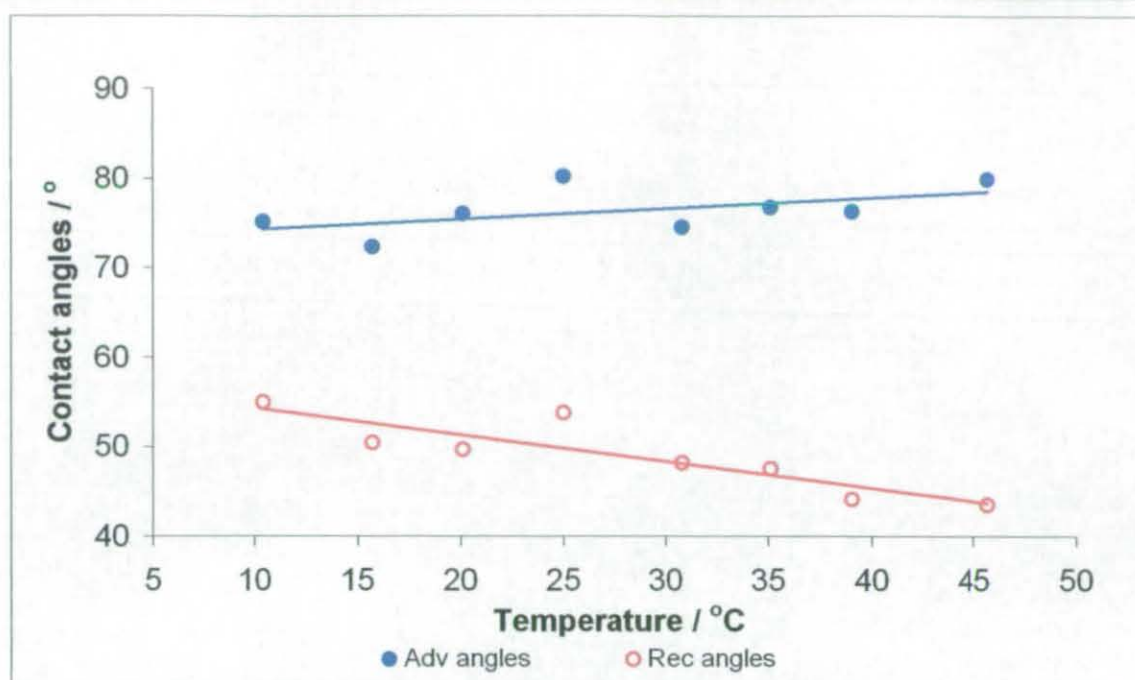


**Figure 4.52** Effect of temperature on contact angles of reactively compounded PS-PVME 1% loading.

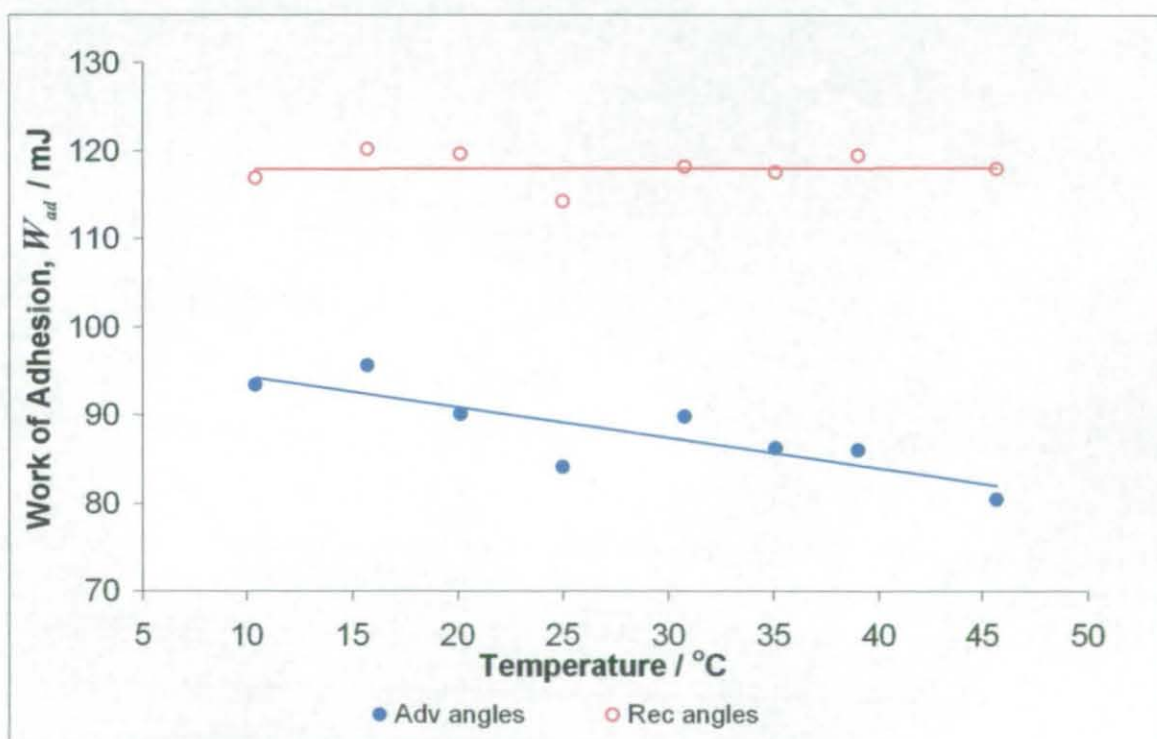


**Figure 4.53** Effect of temperature on work of adhesion of reactively compounded PS-PVME 1% loading.



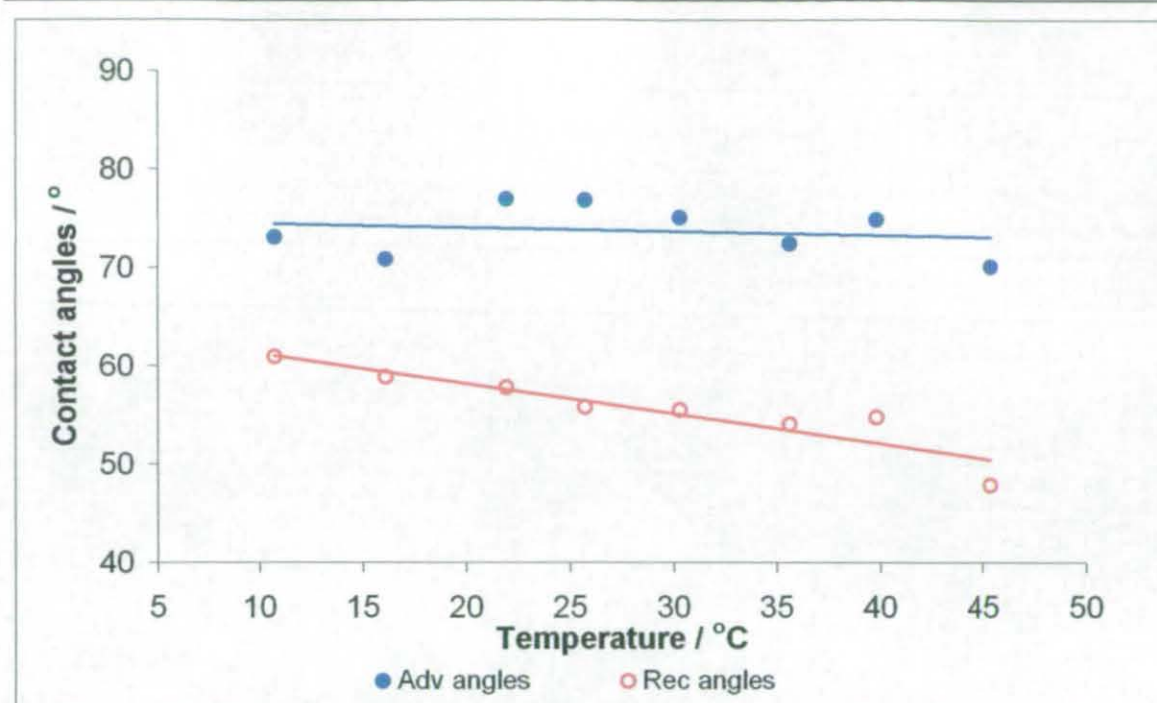


**Figure 4.54** Effect of temperature on contact angles of reactively compounded PS-PVME 10% loading.

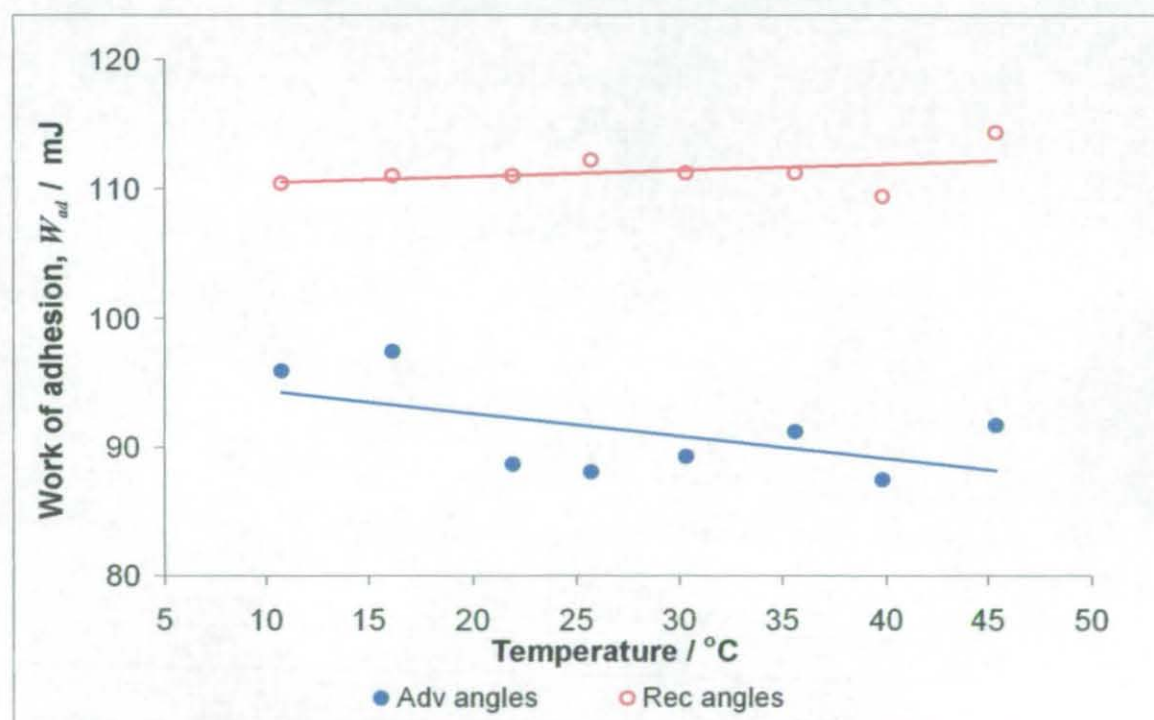


**Figure 4.55** Effect of temperature on work of adhesion of reactively compounded PS-PVME 10% loading.

---

**f) Grafted Polystyrene**

The temperature dependence of contact angle on grafted PS has been evaluated and the results are presented in Figure 4.56. As can be seen, there were increases in both advancing and receding angles with temperature.

The work of adhesion decreased with temperature for both advancing and receding conditions, see Figure 4.57, which meant less work was needed to separate the water from the surface. The contact angle hysteresis was much smaller than that obtained for surface treated samples and was constant throughout the temperature range. The strong dependence of work of adhesion on temperature meant that this sample more closely resembled the surface treated samples, than the compounded ones.

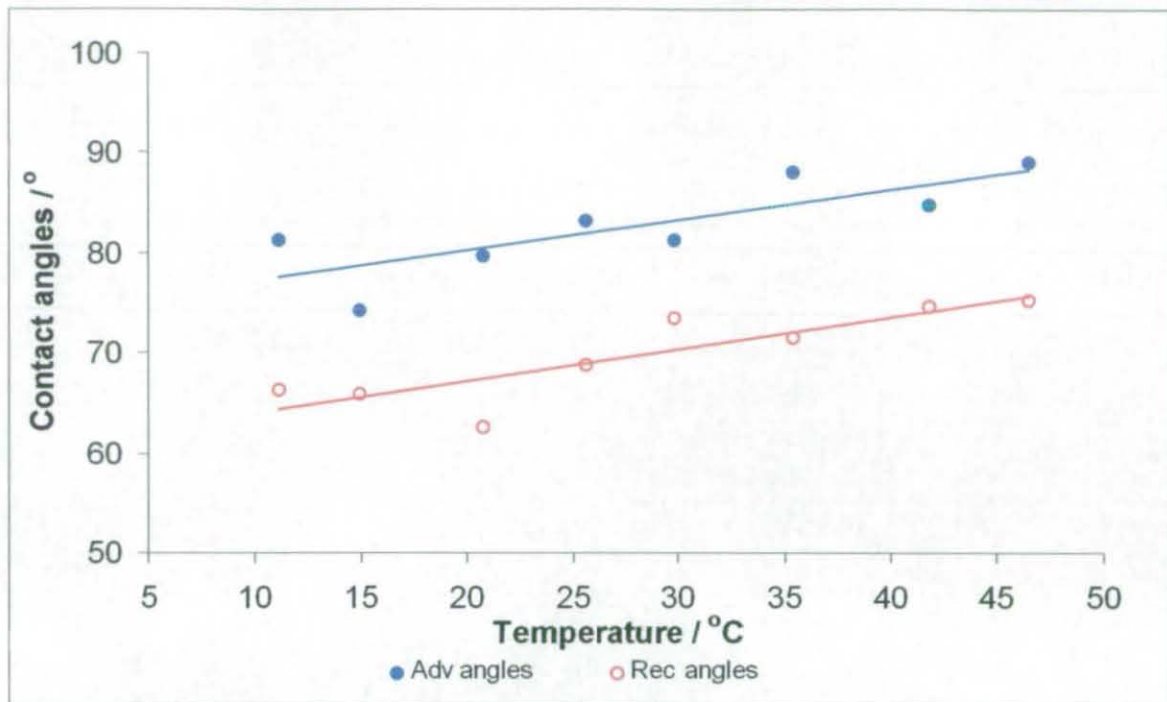


Figure 4.56 Effect of temperature on contact angles of grafted PS.

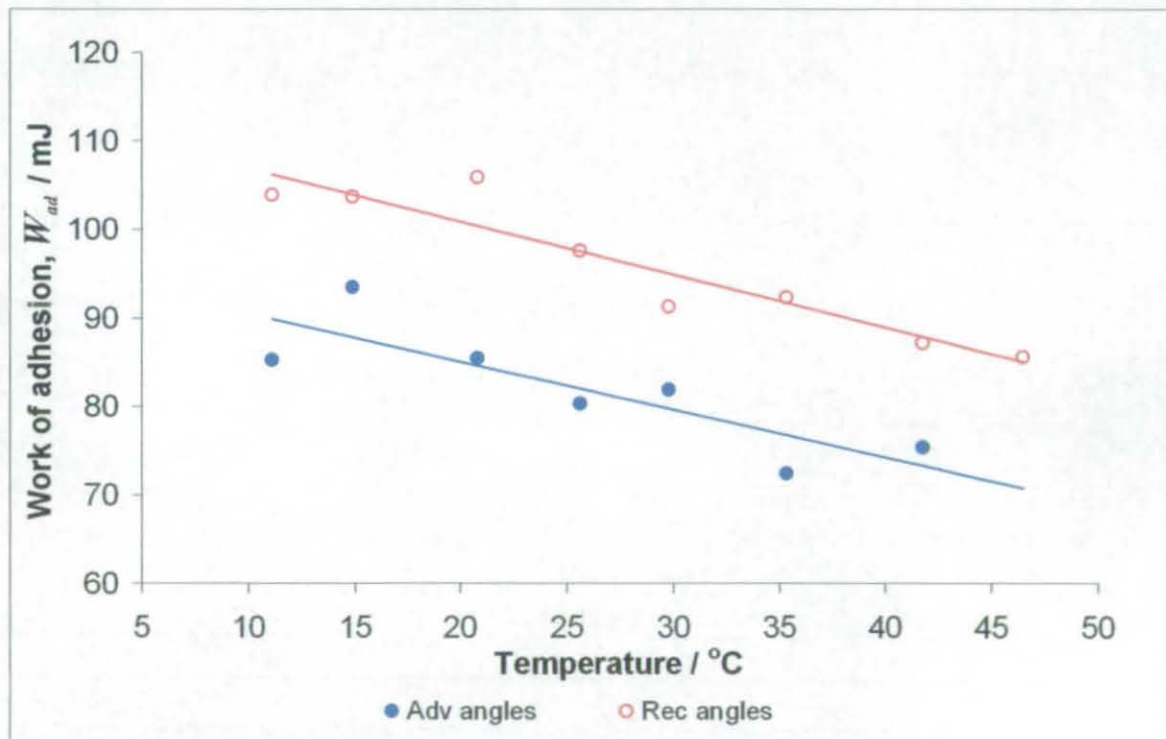


Figure 4.57 Effect of temperature on work of adhesion of grafted PS.



#### 4.8.4 Enthalpy and Entropy of Adhesion

As discussed in the literature survey (Section 2.3.9) the work of adhesion has enthalpic and entropic components. In this study, the enthalpic and entropic contributions for various PS systems were calculated from the slopes of the graphs presented earlier and are tabulated in Table 4.39. Following Padday [79], work of adhesion associated with both advancing and receding angles were used.

From the results in Table 4.39, two general comments can be made. Firstly, it was observed that for some of the samples studied, the work of adhesion varies substantially with temperature and these, therefore, have a large entropy of adhesion. The temperature dependence observed here is not easily accounted for by other theories used to describe work of adhesion. For example, when using the acid-base theory, it is assumed that the work for adhesion is proportional to the enthalpy of acid-base interaction at the interface. It is not clear how this approach can account for the results presented here.

Secondly, the three samples that gave the best adhesion, namely flame treated, chromic acid treated and grafted samples, had high values for the enthalpy and entropy of adhesion, calculated using both advancing and receding angles. High values for the enthalpy of adhesion may be readily interpreted in terms of the number and availability of functional groups on the surface of these samples which can interact with the water. However, the interpretation of the entropy of adhesion ( $S_{ad}$ ) is less clear. The entropy of adhesion is defined by Equation {2.22},

$$S_{ad} = S_s + S_L - S_{SL}$$

where  $S_s$  and  $S_L$  are specific surface excess entropies of the polymer and liquid, respectively.  $S_{SL}$  is the specific surface excess entropy of the interface. For the untreated PS, there is a literature value of  $S_s = 0.072 \text{ mJ m}^{-2} \text{ K}^{-1}$  [197, 213].

Knowing  $S_L = 0.1676 \text{ mJ m}^{-2} \text{ K}^{-1}$  (Appendix C),  $S_{SL}$  can be estimated to be  $0.29 \text{ mJ m}^{-2} \text{ K}^{-1}$ .

When a polymer is surface treated, both  $S_S$  and  $S_{SL}$  will change. The positive values of  $S_L$  observed for all liquids [214] can be attributed to the increased mobility of the surface molecules [72 - 75]. If it is assumed that mobility is also an important contribution to  $S_{SL}$ , then a surface treatment which introduced polar functional groups would probably reduce the mobility of water at the interface. This would then lower  $S_{SL}$  and thus leads to a higher value for  $S_{ad}$ . This simple argument is in agreement with the results in Table 4.39 and other results presented in this thesis. However, it must be said that it is probably a huge over-simplification. The cell model proposed by Van Ness [81, 82] indicates some of the complexities involved in estimating surface and therefore interfacial entropies. There are other factors that may contribute to  $S_{SL}$  and the effect of surface treatment on  $S_S$  has been ignored.

All the contact angle results derived from the contact angle measurements have to be treated with caution. This is because there is always the assumption that an equilibrium property of the surface is being measured. The assumption is implicit in this approach and also in those of Owens and Wendt [60] and the acid-base theory [67, 68]. However, the results presented here do show the value of measuring the temperature dependence of the work of adhesion. It would be probably worth pursuing the temperature dependence of the work of adhesion using some well characterised homopolymers where the  $S_S$  may be estimated. In this way, the factors affecting interfacial entropy could perhaps be better identified and the simple molecular level hypothesis proposed in this thesis could be tested.

**Table 4.39** Work of adhesion ( $W_{ad}$ ), enthalpy ( $H_{ad}$ ) and entropy ( $S_{ad}$ ) of various PS systems at temperature 30°C.

Sample systems	$\theta / ^\circ$	$W_{ad}$ / $\text{mJ m}^{-2}$	$H_{ad}$ / $\text{mJ m}^{-2}$	$S_{ad}$ / $\text{mJ m}^{-2} \text{K}^{-1}$
<b>Untreated</b>	$\theta_{adv}$	75	59	-0.05
	$\theta_{rec}$	83	110	0.09
<b>PS control</b>	$\theta_{adv}$	77	28	-0.07
	$\theta_{rec}$	79	119	0.13
<b>SMA 64:34</b>	$\theta_{adv}$	78	110	0.11
	$\theta_{rec}$	107	166	0.19
<b>Flame treated</b>	$\theta_{adv}$	90	317	0.75
	$\theta_{rec}$	123	481	1.18
<b>Chromic acid treated</b>	$\theta_{adv}$	104	209	0.35
	$\theta_{rec}$	136	254	0.39
<b>PS-SMA 66:34 1% non-reactively compounded</b>	$\theta_{adv}$	76	64	-0.04
	$\theta_{rec}$	97	27	-0.23
<b>PS-SMA 66:34 10% non-reactively compounded</b>	$\theta_{adv}$	77	181	0.34
	$\theta_{rec}$	118	161	0.14
<b>PS-PVME 1% non-reactively compounded</b>	$\theta_{adv}$	79	175	0.32
	$\theta_{rec}$	112	132	0.07
<b>PS-PVME 10% non-reactively compounded</b>	$\theta_{adv}$	78	60	-0.06
	$\theta_{rec}$	102	44	-0.19

PS-SMA 66:34 1% reactively compounded	$\theta_{adv}$	75	180	0.34
	$\theta_{rec}$	89	111	0.07
PS-SMA 66:34 10% reactively compounded	$\theta_{adv}$	77	184	0.36
	$\theta_{rec}$	118	134	0.05
PS-PVME 1% reactively compounded	$\theta_{adv}$	87	193	0.35
	$\theta_{rec}$	118	118	$-2 \times 10^{-3}$
PS-PVME 10% reactively compounded	$\theta_{adv}$	91	153	0.17
	$\theta_{rec}$	111	97	-0.05
Grafted	$\theta_{adv}$	80	240	0.54
	$\theta_{rec}$	95	276	0.60

4.8.5 Summary

It can be concluded that contact angle measurement is not affected by spreading pressure. The temperature dependence contact angle results demonstrated either increasing or decreasing of contact angle values with raising temperature and these varied among the different PS systems. The variation of contact angle hysteresis with temperature gives greater insight into the processes occurring at the surface. Work of adhesion varies with temperature substantially, which results in large entropy adhesion for some samples. This is not taken into account by the acid-base theory.  $S_{ad}$  increased as a result of surface treatment. It is suggested that the increase in  $S_{ad}$  is due to a decrease in the mobility of water molecules at the interface.

## CHAPTER 5 CONCLUSIONS

As stated before, the intention of this work was to physically and chemically examine the surface effects of the various functional groups generated by the surface treatments and other incorporation methods, to compare the effectiveness of these methods in promoting adhesion. Enthalpy and entropy of adhesion of the samples were measured and compared to adhesion bond strength data. The following conclusions were drawn.

### 5.1 SURFACE TREATMENT

Large contact angle hysteresis was seen on both flame and chromic acid treated samples and has been attributed to the surface reorganisation and/or incorporation of water. Heating surface treated samples to temperatures in excess of 50°C did cause a reduction in water contact angles. This was attributed to the reorientation of functional groups in the surface region. These surface changes occur at temperatures well below the  $T_g$  of the polymer, suggesting increased thermal mobility in the surface region.

The chromic acid treated samples have fewer organic functional groups on the surface than the flame treated samples but a higher proportion of them are carboxylic acid groups. This situation is similar to that described in previous studies on polyolefins [6] where it was inferred that the carboxylic acid groups reacted with the epoxy resin. Derivatisation has shown that carboxylic acid groups on the surface of PS contribute significantly to the joint strength with the epoxy adhesive. Derivatisation used in conjunction with adhesion testing is a method that should be used more widely in adhesion research. It is generally applicable and not limited to carboxylic acid groups at any specific type of surface treatment.



---

## 5.2 NON-REACTIVE COMPOUNDING

An increase in surface roughness was observed after extraction and was attributed to the removal of SMA copolymers from the surface or some reorganisation of the groups in the surface. Compounding with SMA copolymers and PVME have been shown to improve the adhesion and was further enhanced after extraction, which was believed to be due to the removal of weak boundary layer and, perhaps, a small effect from the surface roughness. A low loading level has been proven to be effective in achieving the same adhesion as a higher loading level. In addition, derivatisation has shown that the presence of small number of functional groups could contribute the majority of the joint strength for the PS-SMA samples. The amounts of anhydride functional groups needed to achieve the improvement in adhesion were below the detection limit of the XPS spectrometer. The ability of low levels of copolymer to enhance adhesion is important since this means that there is a minimum effect on the bulk properties of the polystyrene.

## 5.3 REACTIVE COMPOUNDING

Extraction did not seem to affect the surface roughness but seems to affect more the receding angles, hence causing large contact angle hysteresis. This may be due to the surface reorganisation of functional groups. Likewise, compounding with initiator and the copolymers promoted adhesion which was further improved by extraction. Low loadings have again been shown to be sufficient to achieve adhesion. Derivatisation has again proven that the presence of the small number of functional groups can have a significant effect on adhesion.

---

## 5.4 GRAFTING

The improvement in the adhesive joint on extraction was again attributed to the removal of weak boundary layer. In this case, the weak boundary layer probably consists of SMA copolymer chains that were not grafted to the substrate. Derivatisation has shown that the presence of the grafted copolymer chains on the PS surfaces do contribute to adhesion. XPS detected low oxygen concentrations at the surface of these samples but the adhesion joint strength was high. This is probably due to the availability of the functional groups in the grafted surface and the fact that they are chemically attached to the polystyrene substrate.

## 5.5 CROSS COMPARISON OF SYSTEMS

In comparison, surface treatment seems to be more effective in promoting adhesion than non-reactive and reactive compounding. Non-reactive compounding appeared to be superior in enhancing adhesion than reactive compounding. This may be due in part to difference in surface roughness and the slightly higher oxygen concentrations at the surface of the non-reactively compounded samples. The grafting of SMA copolymer chains in situ also proved to be useful in improving adhesion. Similar levels of adhesion to the surface treated surfaces were observed. Contact angle hysteresis was lower on the grafted samples suggesting less incorporation of water. This probably reflects the low oxygen concentration on the surface of these samples.

## 5.6 ENTHALPY AND ENTROPY OF ADHESION

For some PS systems, the work of adhesion changes considerably with temperature and resulted in large entropy of adhesion. This is not accounted for by

the acid-base theory. The entropy of adhesion has increased as a result of treatment for some PS systems and the decreased mobility of water molecules at the interface as a result of surface treatment is suggested as one of the factors responsible. The potential for measurement of the entropy of adhesion to give insight into the molecular properties of the interface is an important finding of this work. It has been shown that contact angles can now be measured with sufficient accuracy to allow the determination of enthalpy and entropy of adhesion. This approach could usefully be extended to other systems.

## CHAPTER 6 REFERENCES

1. A. Augsburg, K. Grundke, K. Pöschel, H. J. Jacobasch, A. W. Neumann, **Acta. Polym.**, 49, p417, (1998)
2. J. Höpken, M. Möller, **Macromol.**, 25, p1461, (1992)
3. R. Mason, C. A. Jalbert, P. A. V. O'Rourke Muisener, J. T. Koberstein, J. F. Elman, T. E. Long, B. Z. Gunesin, **Adv. Colloid and Interface Sci.**, 94, p1, (2001)
4. N. G. Gaylord, R. Mehta, V. Kumar, M. Taki, **J. Appl. Polym. Sci.**, 38, p359, (1989)
5. N. G. Gaylord, R. Mehta, D. R. Mohan, V. Kumar, **J. Appl. Polym. Sci.**, 44, p1971, (1992)
6. E. Sheng, **Ph. D. Thesis**, Loughborough University of Technology, (1992)
7. K. W. Allen, **Int. J. Adhesion and Adhesives**, 23, p87, (2003)
8. G. Gierenz, W. Karmann, '**Adhesives and Adhesion Tapes**', Wiley-VCH, (1999)
9. L. H. Lee, '**Fundamentals of Adhesion**', Plenum Press, (1991)
10. B. V. Deryaguin, V. P. Smilga, **J. Appl. Phys.**, 38, p4609, (1967)
11. B. V. Deryaguin, **Research**, 8, p70, (1955)

- 
12. B. V. Deryaguin, **Research**, 8, p363, (1955)
  13. A. D. Roberts, '**Adhesion 1**', ed. K. W. Allen, Applied Science Pub London, p207, (1977)
  14. J. P. Bell, W. T. McCarvill, **J. Appl. Polym. Sci.**, 18, p2243, (1974)
  15. S. S. Voyutskii, '**Autohesion and Adhesion of High Polymers**', Wiley-Interscience, New York, p138, (1963)
  16. H. Schonhorn, '**Adhesion: Fundamentals and Practice**', McLaren and Sons London, p12, (1969)
  17. W. C. Wake, '**Adhesion and the Formulation of Adhesives**', Applied Science Pub London, p89, (1982)
  18. C. W. Jennings, **J. Adhesion**, 4, p25, (1972)
  19. J. N. Israelachvili, D. Tabor, **Proc. Roy. Soc.**, A331, p19, (1972)
  20. D. Tabor, R. H. Winterto, **Proc. Roy. Soc.**, A312, p435, (1969)
  21. S. S. Voyutskii, **Adhesives Age**, 5, p30, (1962)
  22. S. S. Voyutskii, Z. M. Ustinova, **J. Adhesion**, 9, p39, (1977)
  23. R. M. Vasenin, **Adhesives Age**, 8, p21, (1965)
  24. R. M. Vasenin, **Adhesives Age**, 8, p30, (1965)
  25. R. M. Vasenin, '**Adhesion: Fundamentals and Practice**', McLaren and
-

- 
- Sons London, p29, (1969)
26. R. J. Good, **'Treatise on Adhesion and Adhesives'**, 1, ed. R. L. Patrick, Marcel Dekker, New York, p15, (1987)
  27. A. Rattana, M. L. Abel, J. F. Watts, **Int. J. Adhesion and Adhesives**, 26, p28, (2006)
  28. D. E. Packham, **'Handbook of Adhesion'**, John Wiley & Sons Ltd, p5, (2005)
  29. J. J. Bikerman, **Ind. Eng. Chem.**, 59, p40, (1967)
  30. D. M. Brewis, **Int. J. Adhesion and Adhesives**, 13, p251, (1993)
  31. K. W. Allen, **'Aspects of Adhesion 5'**, ed. D. J. Alner, University of London Press, p11, (1969)
  32. B. W. Malpass, D. E. Packham, K. Bright, **J. Appl. Polym. Sci.**, 18, p3249, (1974)
  33. D. E. Packham, **Int. J. Adhesion and Adhesives**, 16, p121, (1996)
  34. D. E. Packham, **'First International Congress on Adhesion Science and Technology'**, Ridderprint bv, p81, (1998)
  35. J. Comyn, **'Adhesion Science'**, Cambridge/Royal Society of Chemistry, (1997)
  36. D. M. Brewis, Chapter 5, **'Industrial Adhesion Problems'**, ed. D. M. Brewis and D. Briggs, Orbital Press, (1985)
-

- 
37. D. G. Rance, Chapter 6, '**Surface Analysis and Pretreatment**', ed. D. M. Brewis, Applied Science Publishers, (1982)
  38. A. Zangwill, '**Physics at Surfaces**', Cambridge University Press, (1988)
  39. S. J. Gregg, '**The Surface Chemistry of Solids**', Chapman and Hall, (1961)
  40. I. Sutherland, R. J. Heath, '**Progress in Rubber and Plastics Tech.**, 14, p151, (1998)
  41. C. M. Chan, Chapter 2, '**Polymer Surface Modification and Characterisation**'. Hanser Publications, (1993)
  42. J. Comyn, '**Int. J. Adhesion and Adhesives**, 12, p145, (1992)
  43. R. Aveyard, D. A. Hayon, '**Principles of Surface Chemistry**', Cambridge University Press, (1973)
  44. J. Kloubek, '**Adv Colloid and Int. Sci.**, 38, p99, (1992)
  45. D. G. Rance, Chapter 3, '**Industrial Adhesion Problems**', ed. D. M. Brewis and D. Briggs, Orbital Press, (1985)
  46. T. Young, '**Trans. Roy. Soc.**, 95, p65, (1805)
  47. D. H. Bangham, R. J. Razouk, '**Trans Faraday Soc.**, 33, p1459, (1937), **Proc. Roy. Soc. London, Ser. A**166, p572, (1938)
  48. R. J. Good, '**J. Colloid and Interface Sci.**, 52, p308, (1975)
  49. R. J. Good, '**J. Adhesion Sci. Tech.**, 6, p1269, (1992)
-

- 
50. L. A. Girifalco, R. J. Good, **J. Phys. Chem.**, 61, p904, (1957)
  51. R. J. Good, **ACS Advances Chem. Ser.**, 43, p74, (1964)
  52. R. J. Good, **Treatise on Adhesion**, 1, ed. R. L. Patrick, Dekker, (1967)
  53. L. A. Girifalco, R. J. Good, **J. Phys. Chem.**, 64, p561, (1960)
  54. R. J. Good, **J. Phys. Chem.**, 60, p810, (1957)
  55. F. M. Fowkes, **J. Phys. Chem.**, 64, p561, (1960)
  56. F. M. Fowkes, **J. Phys. Chem.**, 66, p1863, (1962)
  57. F. M. Fowkes, **J. Phys. Chem.**, 67, p2538, (1963)
  58. F. M. Fowkes, **J. Adhesion**, 4, p155, (1972)
  59. F. M. Fowkes, **Ind. Eng. Chem.**, 56, p40, (1964)
  60. D. K. Owens, R. C. Wendt, **J. Appl. Polym. Sci.**, 13, p1741, (1969)
  61. D. K. Owens, **J. Appl. Polym. Sci.**, 14, p1725, (1970)
  62. S. Wu, **J. Polym. Sci. Part C**, 34, p19, (1971)
  63. S. Wu, **J. Adhesion**, 5, p39, (1973)
  64. S. Wu, **J. Macromol. Sci. Part C**, 10, p1, (1974)
  65. C. A. Ward, A. W. Neumann, **J. Colloid Interface Sci.**, 49, p286, (1974)
-



- 
66. J. K. Spelt, D. R. Absolom, A. W. Neumann, **Langmuir**, 2, p620, (1986)
67. F. M. Fowkes, **J. Adhesion Sci. Tech.**, 1, p7, (1987)
68. C. J. Van Oss, R. J. Good, M. K. Chaudhury, **Langmuir**, 4, p884, (1988)
69. R. S. Drago, G. C. Vogel, T. E. Needham, **J. Amer. Chem. Soc.**, 93, p6014, (1971)
70. R. S. Drago, L. B. Parr, C. S. Chamberlain, **J. Amer. Chem. Soc.**, 99, p3203, (1977)
71. K. J. Huttinger, S. Höhmann-wien, G. Krekel, **J. Adhesion Sci. Tech.**, 6, p317, (1992)
72. M. J. Jaycock, G. D. Parfitt, 'Chemistry of Interfaces', Ellis Horwood Ltd, (1981)
73. P. R. Couchman, W. A. Jesser, **Surf. Sci.**, 34, p212, (1973)
74. R. C. Tolman, **J. Chem. Phys.**, 16, p758, (1948)
75. R. C. Tolman, **J. Chem. Phys.**, 17, p333, (1949)
76. J. M. D. Rio, M. N. Jones, **J. Phys. Chem.**, 105, p1200, (B2001)
77. K. A. T. Silverstein, A. D. J. Haymet, K. A. Oill, **J. Amer. Chem. Soc.**, 120, p3166, (1998)
78. D. M. Huang, D. Chandler, **J. Phys. Chem.**, 106, p2047, (B2002)
-

- 
79. J. Israelachvili, Chapter 8, '**Intermolecular and Surface Forces**', 2<sup>nd</sup> edition, Academic Press, (1992)
80. '**CRC Handbook of Chemistry and Physics**', 73<sup>rd</sup> edition
81. K. E. Van Ness, **Polym. Eng. Sci.**, 32, p122, (1992)
82. K. E. Van Ness, P. R. Couchman, **J. Colloid Interface Sci.**, 182, p110, (1996)
83. C. J. Budziak, E. I. Vargha-Butler, A. W. Neumann, **J. Appl. Polym. Sci.**, 42, p1959, (1991)
84. J. F. Padday, **J. Colloid Interface Sci.**, 28, p557, (1968)
85. R. E. Johnson, R. H. Dettre, **J. Colloid Sci.**, 20, p173, (1965)
86. M. C. Phillips, A. C. Riddiford, **Nature**, 205, p1005, (1965)
87. N. T. Correia, J. J. M. Ramos, M. H. C. V. Adao, E. J. V. Saramago, **Mol. Cryst. Liq. Cryst.**, 300, p45, (1997)
88. W. A. Zisman, **J. Paint Tech.**, 44, p42, (1972)
89. R. N. Wenzel, **Ind. Eng. Chem.**, 28, p988, (1936)
90. R. E. Johnson, R. H. Dettre, **J. Phys. Chem.**, 68, p1744, (1964)
91. A. B. D. Cassie, S. Baxter, **Trans. Faraday Soc.**, 40, p546, (1944)
92. R. E. Johnson, R. H. Dettre, **Surf. Colloid Sci.**, 2, p85, (1969)
-

- 
93. N. Dharmarajan, S. Datta, **Polym.**, 33, p3848, (1992)
  94. C. A. Brighton, G. Pritchard, G. A. Skinner, '**Styrene Polymers: Technology and Environmental Aspects**', Applied Science Publishers, (1979)
  95. W. C. Teach, G. C. Kiessling, '**Polystyrene**', Reinhold Publishing Corporation, (1960)
  96. '**Polystyrene Materials: A Code of Practice**' (pamphlet), The British Plastics Federation, (1963)
  97. J. R. Wünsch, '**Polystyrene: Synthesis, Production and Application**', Rapra Technology Limited, (2000)
  98. F. Chang, Y. Hwu, **Polym. Eng. Sci.**, 31, p1509, (1991)
  99. Y. Gallot, C. Nippler, **Macromol. Symp.**, 16, p41, (1988)
  100. D. J. Walsh, S. Rostami, **Advances in Polym. Sci.**, 70, p121, (1985)
  101. O. Olabisi, '**Polymer-Polymer Miscibility**', Academic Press, (1979)
  102. A. R. Kumar, Y. S. Hu, P. Ansens, S. P. Chum, A. Hiltner, E. Baer, **Macromolecules**, 39, p1496, (2006)
  103. G. N. Kumaraswamy, C. Ranganathaiah, M. V. D. Urs, H. B. Ravikumar, **European Polym. J.**, 42, p2655, (2006)
  104. K. Cho, K. H. Seo, T. O. Ann, **Polym. Journal**, 29, p987, (1997)
-

- 
105. Y. Lee, K. Char, **Macromol.**, 27, p2603, (1994)
106. M. Bank, J. Leffingwell, C. Thies, **J. Polym. Sci.: Polym. Phys. Ed.**, 10, p1097, (1972)
107. T. K. Kwei, T. Nishi, R. F. Roberts, **Macromol.**, 7, p667, (1974)
108. J. M. Ubrich, F. Ben Cheikh Larbi, J. L. Halary, L. Monnerie, **Macromol.**, 19, p810, (1986)
109. S. Pavawongsak, J. S. Higgins, N. Clarke, T.C.B. McLeish, D. G. Peiffer, **Polym.**, 41, p757, (2000)
110. S. Mani, M. F. Malone, H. H. Winter, **Macromol.**, 24, p5451, (1991)
111. H. Gerard, J. S. Higgins, **Macromol.**, 32, p5411, (1999)
112. D. Shi, J. Yang, Z. Yao, Y. Wang, H. Huang, W. Jing, J. Yin, **Polym.**, 42, p5549, (2001)
113. S. G. Flores-gallardo, S. Sánchez-valdes, L. F. Ramos De Valle, **J. Appl. Polym. Sci.**, 79, p1497, (2001)
114. D. C. Clark, W. E. Baker, K. E. Russell, R. A. Whitney, **J. Polym. Sci.: Part A: Polym. Chem.**, 38, p2456, (2000)
115. W. O. Kenyon, G. P. Wough, **J. Polym. Sci.**, 32, p83, (1958)
116. R. T. Swiger, **J. Polym. Sci.**, 13, p1554, (1975)
-

- 
117. R. A. Kurbanova, R. Mirzaoglu, S. Kurbanov, I. Karatas, V. Pamuk, E. Ozcan, A. Okudan, E. Güler, **J. Adhesion Sci. Tech.**, 11, p105, (1997)
118. M. Hajian, C. Sadrmohaghegh, G. Scott, **Eur. Polym. J.**, 20, p135, (1984)
119. R. A. Kurbanova, R. Mirzaoglu, S. Kurbanov, I. Karatas, V. Pamuk, E. Ozcan, A. Okudan, E. Güler, **J. Adhesion Sci. Tech.**, 12, p947, (1998)
120. S. L. Kaplan, P. W. Rose, **Int. J. Adhesion and Adhesives**, 11, p109, (1991)
121. S. Guruvanket, G. M. Rao, M. Komath, A. M. Raichur, **Appl. Surf. Sci.**, 236, p278, (2004)
122. E. Occiello, M. Morra, G. Morini, F. Garbassi, P. Humphrey, **J. Appl. Polym. Sci.**, 42, p551, (1991)
123. R. E. Marchant, C. J. Chou, C. Khoo, **J. Appl. Polym. Sci. : Appl. Polym. Symp.**, 42, p125, (1988)
124. Y. Nakayama, T. Takahagi, F. Soeda, K. Hatada, S. Nagoaka, J. Suzuki, A. Ishitani, **J. Polym. Sci. : Polym. Chem. Ed.**, 26, p559, (1988)
125. M. Strobel, S. Corn, C. S. Lyons, G. A. Korba, **J. Polym. Sci. : Polym. Chem. Ed.**, 23, p1125, (1985)
126. C. P. Ho, H. Yasuda, **J. Appl. Polym. Sci.**, 39, p1541, (1990)
127. J. B. Lhoest, E. Detrait, J. L. Dewez, P. V. deAguilar, P. Bertrand, J. **Biomater. Sci.: Polym. Ed.**, 7, p1039, (1996)
128. A. Nihlstrand, T. Hjertberg, K. Johansson, **Polym.**, 38, p3581, (1997)
-

- 
129. S. Yuen, R. E. Marchant, **J. Appl. Polym. Sci.: Appl. Polym. Symp.**, 54, p77, (1994)
130. R. Foerch, N. S. McIntyre, R. N. S. Sodhi, D. H. Hunter, **J. Appl. Polym. Sci.**, 40, p1903, (1990)
131. Ch. C. Dupont-Gillain, Y. Adrianensen, S. Derclaye, P. G. Rouxhet, **Langmuir**, 16, p8194, (2000)
132. M. Stradal, D. A. I. Goring, **J. Adhesion**, 8, p57, (1976)
133. D. M. Brewis, I. Mathieson, **Adhesion and Bonding to Polyolefins**, Rapra Review Reports, 143, 12, 11, (2002)
134. J. Golebiewski, Z. Zenkiewicz, **Polimery**, 48, p134, (2003)
135. M. Bousmina, P. Bataille, S. Sapieha, H. P. Schreiber, **J. Rheology**, 39, p499, (1995)
136. I. Sutherland, D. M. Brewis, R. J. Heath, E. Sheng, **Surf. Interface Anal.**, 17, p507, (1991)
137. F. Garbassi, F. Occhiello, F. Polato, **J. Mater. Sci.**, 22, p207, (1987)
138. R. P. Popat, **Ph. D. Thesis**, Loughborough University of Technology, (1995)
139. P. Blais, D. J. Carlsson, G. W. Csullog, D. M. Wiles, **J. Colloid and Interface Sci.**, 47, p636, (1974)
140. D. Briggs, V. J. I. Zichy, D. M. Brewis, J. Comyn, R. H. Dahm, M. A. Green, M. B. Konieczko, **Surf. Interface Anal.**, 2, p107, (1980)
-

- 
141. K. Kato, **Polym.**, 9, p419, (1968)
142. V. J. Armond, J. R. Atkinson, **J. Mater. Sci.**, 3, p332, (1968)
143. D. Briggs, D. M. Brewis, M. B. Konieczo, **J. Mater. Sci.**, 11, p1270, (1976)
144. J. L. Garnett, S. V. Jankiesicz, M. A. Long, D. F. Sangster, **Radiation. Phys. Chem.**, 27, p301, (1986)
145. R. D. Goldblatt, J. M. Park, R. C. White, L. J. Matienzo, S. J. Huang, J. P. Johnson, **J. Appl. Polym. Sci.**, 37, p335, (1989)
146. Y. Uyama, Y. Ikada, **J. Appl. Polym. Sci.**, 41, p619, (1990)
147. E. T. Kang, K. G. Neoh, X. Zhang, K. L. Tan, D. J. Liaw, **Surf. Interface Anal.**, 24, p51, (1996)
148. B. Ranby, **Int. J. Adhesion and Adhesives**, 19, p337, (1999)
149. B. Ranby, W. T. Yang, O. Tretinnikov, **Nucl. Instr. And Meth. In Phys. Res. B**, 151, (1-4), May, p301, (1999)
150. F. Severini, M. Pegoraro, L. Yuan, G. Ricca, W. Fanti, **Polym.**, 40, p7059, (1999)
151. Y. Li, X. M. Xie, B. H. Guo, **Polym.**, 42, p3419, (2001)
152. K. Allmer, A. Hult, B. Ranby, **J. Polym. Sci.: Polym. Chem.**, 26, p2099, (1988)
-

- 
153. J. Lopez-Gejo, H. Gliemann, T. Schimmel, A. M. Braun, **Photochemistry and Photobiology**, 81, p777, (2005)
154. G. V. Lubarsky, M. R. Davidson, R.H. Bradley, **Surf. Sci.**, 558, p135, (2004)
155. R. Mason, C. A. Jalbert, P. A. V. O'Rourke Muisener, J. T. Koberstein, J. F. Elman, T. E. Long, B. Z. Gunesin, **Adv. Colloid and Interface Sci.**, 94, p1, (2001)
156. J. Höpken, M. Möller, **Macromol.**, 25, p1461, (1992)
157. S. H. Lee, E. Ruckenstein, **J. Colloid Interface Sci.**, 120, p529, (1987)
158. H. Yasuda, A. K. Sharma, **J. Polym. Sci.**, 19, p1285, (1981)
159. I. Sutherland, E. Sheng, D. M. Brewis, R. J. Heath, **J. Adhesion**, 44, p17, (1994)
160. D. R. Gagnon, T. J. McCarthy, **J. Appl. Polym. Sci.**, 29, p4335, (1984)
161. L. H. Wang, R. S. Porter, **J. Appl. Sci.**, 28, p1439, (1983)
162. A. H. Ellison, W. A. Zisman, **J. Phys. Chem.**, 58, p503, (1954)
163. G. Gillberg, **J. Adhesion**, 21, p129, (1987)
164. D. Briggs, 'Surface Analysis of Polymers by XPS and static SIMS', Cambridge University Press, (1998)
165. H. R. Thomas, J. J. O'Malley, **Macromol.**, 12, p323, (1979)
-



- 
166. R. P. Papat, I. Sutherland, E. Sheng, **J. Mater. Chem.**, 5, p713, (1995)
167. D. S. Everhart, C. N. Reilley, **Anal. Chem.**, 53, p665, (1981)
168. R. A. Dickie, J. S. Hammond, J. E. Devries, J. W. Holubka, **Anal. Chem.**, 54, p2045, (1982)
169. L. J. Gerenser, J. F. Elman, M. G. Mason, J. M. Pochan, **Polym.**, 26, p1162, (1985)
170. D. Briggs, 'Encyclopaedia of Polymer Science and Engineering', 2<sup>nd</sup> edition, ed. J. I. Kroschwitz, 16, p406, (1989)
171. J. M. Pochan, L. J. Gerener, J. F. Elman, **Polym.**, 27, p1058, (1986)
172. A. Chilkoti, B. D. Ratner, **Surf. Interface. Anal.**, 17, p567, (1991)
173. I. Sutherland, E. Sheng, D. M. Brewis, R. J. Heath, **J. Mater. Chem.**, 4, p683, (1998)
174. G. H. Frederickson, A. Ajdari, L. Leibler, J. P. Carton, **Macromol.**, 25, p2882, (1992)
175. H. Hansma, F. Motamedi, P. Smith, P. Hansma, J. C. Wittman, **Polym.**, 33, p647, (1992)
176. C. M. Mate, V. J. Novotny, **J. Chem. Phys.**, 94, p8420, (1991)
177. A. C. M. Yang, B. D. Terris, M. Kunz, **Macromol.**, 24, p6800, (1991)
-

- 
178. B. Collin, D. Chatenay, G. Coulon, D. Ausserre, Y. Gallot, **Macromol.**, 25, p1621, (1992)
179. C. A. Goss, J. C. Brumfield, E. A. Irene, R. W. Murray, **Langmuir**, 8, p1459, (1992)
180. Z. S. Xu, Z. W. Deng, X. X. Hu, L. Li, C. F. Yi, **J. Polym. Sci.: Polym. Chem.**, 43, p2368, (2005)
181. A. Noy, C. D. Frisbie, L. F. Rozsnyai, M. S. Wrighton, C. M. Lieber, **J. Amer. Chem. Soc.**, 117, p7943, (1995)
182. G. J. Vancso, T. D. Allston, I. Chun, L. S. Johansson, G. B. Lin, P. F. Smith, **International Journal of Polymer Analysis and Characterisation**, 3, p89, (1996)
183. D. Whitehouse, **'Surface and their Measurement'**, Hermes Penton Science, p48, (2002)
184. G. Andrew, **'Infrared Spectroscopy of Polymer Blends, Composites and Surfaces'**, C. Hanser, (1992)
185. H. W. Siesler, **'Infrared and Raman Spectroscopy of Polymers'**, M. Dekker, New York, (1980)
186. H. Ishida, **Rubber Chem. Tech.**, 60, p497, (1987)
187. E. G. Koulouri, J. K. Kallitsis, G. Hadziioannou, **Macromol.**, 32, p6242, (1999)
188. E. J. C. Kellar, C. Galiotis, E. H. Andrews, **Macromol.**, 29, p3515, (1996)
-

- 
189. Y. S. Sun, E. M. Woo, **Macromol.**, 32, p7836, (1999)
190. P. Musto, S. Tavone, G. Guerra, C. De Rosa, **J. Polym. Sci. Part B: Polym. Phys.**, 35, p1055, (1997)
191. E. M. Woo, F. S. Wu, **J. Polym. Sci. Part B: Polym. Phys.**, 36, p2725, (1998)
192. S. C. Wu, F. C. Chang, **Polym.**, 45, p733, (2004)
193. S. Whelan, **Final Year B. Sc. Project**, Loughborough University, (2005)
194. A. Chilkoti, B. D. Ratner, D. Briggs, **Chem. Mater.**, 3, p51, (1991)
195. W. D. Harkins, H. F. Jordan, **J. Amer. Chem. Soc.**, 52, p1751, (1930)
196. B. B. Freud, H. Z. Freud, **J. Amer. Chem. Soc.**, 52, p1772, (1930)
197. S. Wu, Chapter 4, '**Polymer Interface and Adhesion**', Marcel Dekker Inc., (1982)
198. J. F. Padday, **Surf. Colloid Sci.**, 1, p101, (1969)
199. P. A. Gorry, **Anal. Chem.**, 62, p570, (1990)
200. G. Stephenson, P. M. Radmore, '**Advanced Mathematical Methods for Engineering and Science Students**', Cambridge University Press, (1990)
201. G. Socrates, '**Infrared Characteristic Group Frequencies: Tables and Charts**', Chichester: Wiley, p52 and p63, (1994)
-

- 
202. D. H. Williams, I. Fleming, '**Spectroscopic Methods in Organic Chemistry**', The McGraw-Hill Companies, p28, (1995)
203. F. Scholl, '**Atlas of Polymer and Plastics Analysis Aids: Spectra and Methods of Identification**', Munich: Carl Hanser Verlag, (1981)
204. D. Y. Kwok, A. W. Neumann, **Colloids and Surf. A: Physicochemical and Eng. Aspects**, 161, p49, (2000)
205. R. N. Shimizu, N. R. Demarquette, **J. Appl. Polym. Sci.**, 76, p1831, (2000)
206. R. Sedev, M. Fabretto, J. Ralston, **J. Adhesion**, 80, p497, (2004)
207. R. E. Johnson, R. H. Dettre, D. A. Brandreth, **J. Colloid and Interface Sci.**, 62, p205, (1977)
208. R. J. Good, **J. Colloid Interface Sci.**, 66, p360, (1978)
209. E. Sheng, I. Sutherland, D. M. Brewis, R. J. Heath, **J. Mater. Chem.**, 4, p487, (1994)
210. H. Yasuda, H. C. Marsh, **J. Polym. Sci.**, 15, p991, (1977)
211. J. D. Andrade, L. M. Smith, D. E. Gregonis, **Surf. Interfacial Aspects of Biomedical Polym.**, 1, p249, (1985)
212. M. R. Alexander, J. D. Whittle, D. Barton, R. D. Short, **J. Mater. Chem.**, 14, p408, (2004)
213. D. Y. Kwok, L. K. Cheung, C. B. Park, A. W. Neumann, **Polym. Eng. Sci.**, 38, p757, (1998)
-

214. J. Lyklema, **Colloids and Surf. A: Physicochemical and Eng. Aspects**, 186, p11, (2001)

## APPENDICES

### APPENDIX A CALCULATION OF CORRECTION FACTOR

The total surface free energy of the water test liquid was determined by the Du Noüy ring method in detachment mode using a torsion balance, which had been calibrated with weights, see Figure A.1. From the calibration graph, the force value corresponding to the surface tension of water test liquid,  $72.8 \text{ mN m}^{-1}$  measured at  $19.9^\circ\text{C}$  by the tensiometer is placed in Equation {A.1} to calculate the measured value of surface tension,  $\sigma^*$ , which has to be corrected using the method of Harkins and Jordan [195]:

$$\sigma^* = F/4\pi R = 9.274 \times 10^{-3} / 4\pi (9.545 \times 10^{-3}) = 77.4 \text{ mN m}^{-1} \quad \{\text{A.1}\}$$

where  $R$  is the radius of the ring from its centre to the centre of the wire.

The correction factor,  $C$ , is a function of  $R^3/V$ .  $V$  is the volume of liquid raised above the free surface at the time when the surface breaks and is expressed as:

$$\begin{aligned} V &= (\sigma^* 4\pi R) / (D-d)g & \{\text{A.2}\} \\ &= [77.4 \times 10^{-3} \times 4 \times \pi \times 9.545 \times 10^{-3}] / [(998.21-1.198) \times 9.8134] \\ &= 9.49 \times 10^{-7} \text{ m}^3 \end{aligned}$$

where  $D$  is the density of the liquid at  $19.9^\circ\text{C}$  [80],  $d$  is the density of air ( $PV=nRT$ ) under experimental conditions at  $19.9^\circ\text{C}$ . The acceleration due to gravity,  $g$ , has been calculated for the latitude and altitude of Loughborough.

$R^3/V$  is calculated as 0.917 and the correction factor, from Harkins and Jordan method [195], is 0.939. Therefore, the actual surface tension (corrected) is:

$$\sigma = \sigma^* \times C = 77.4 \times 0.939 = 72.68 \text{ mN m}^{-1} \tag{A.3}$$

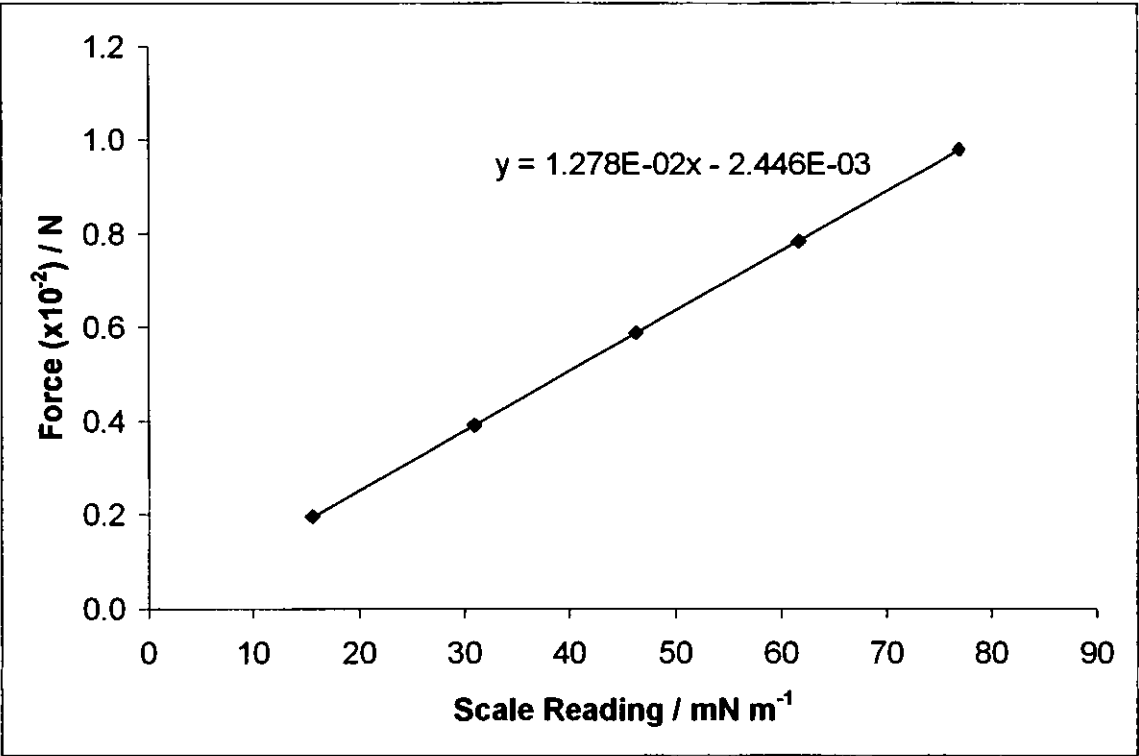


**Figure A.1** Calibration graph of surface tension (scale reading) as a function of force.

---

**APPENDIX B    CALCULATION OF PEAK RATIO  
AND MOLAR RATIO**

**(A)    Peak ratio of SMA copolymers**

Peak ratio of SMA copolymers are calculated from the infrared measurement,

$$\text{Peak ratio} = \frac{A_{(ah)}}{A_{(ring)}}$$

where  $A_{(ah)}$  = area of anhydride peak measured at  $1779 \text{ cm}^{-1}$

where  $A_{(ring)}$  = area of aromatic ring peak measured at  $1449 \text{ cm}^{-1}$

**(B)    Molar absorption coefficients**

Beer Law states that,

$$\text{Absorbance } (A) = \epsilon c \ell$$

therefore,

$$\text{Molar ratio} = \frac{C_{(ah)}}{C_{(ring)}} = \frac{A_{(ah)} \epsilon_{(ring)}}{A_{(ring)} \epsilon_{(ah)}} \quad \text{\{B.1\}}$$

where  $\epsilon$  = molar absorption coefficient,  $c$  = concentration and  $\ell$  = length path.

Using Equation {B.1}, it is possible to estimate the relative magnitudes of the molar absorption coefficients,  $\epsilon_{(ah)}$  and  $\epsilon_{(ring)}$ , see Table B.1.



**Table B.1** Dependence of molar absorption coefficients on copolymer compositions.

<b>S:MA copolymers</b>	<b><math>\epsilon_{(ak)} / \epsilon_{(ring)}</math></b>
50:50	11.46
66:34	15.29
75:25	16.16

The reason why the 50:50 polymer gives such low values for the ratio in Table B.1 is unclear. The values in Table B.1 were then used to determine the surface composition of PS/SMA blends. It is assumed that the molar absorption coefficients were not affected by compounding.

## APPENDIX C CALCULATION OF WORK OF ADHESION

Presented below is a plot of the temperature dependence of the surface free energy of liquid water. The surface entropy of water is calculated from the slope of this graph, Figure C.1 and is therefore  $0.1676 \text{ mJ m}^{-2} \text{ K}^{-1}$ ,

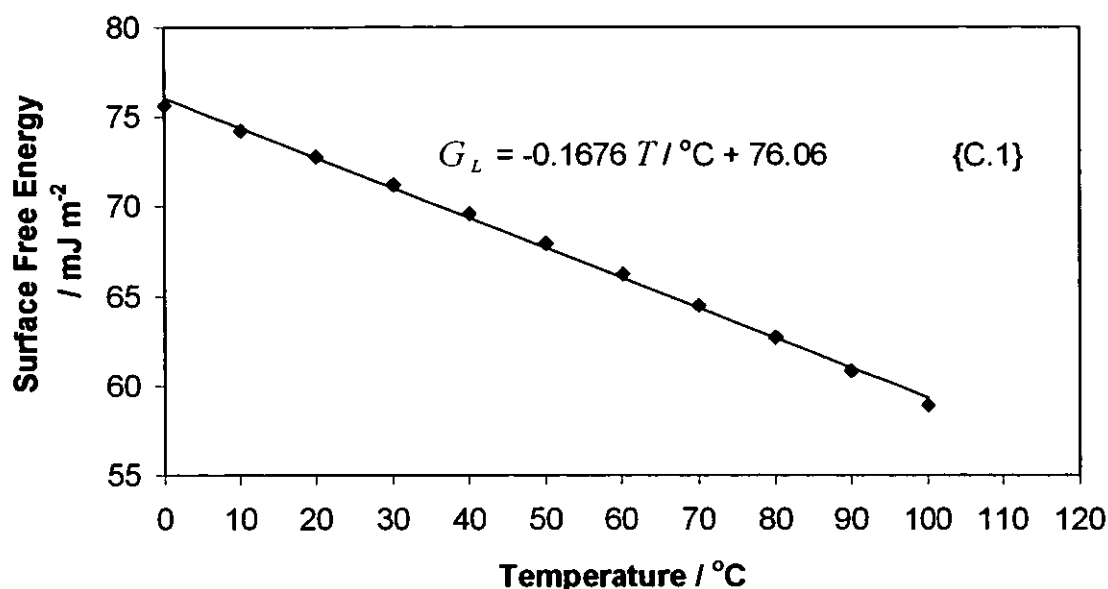


**Figure C.1** Surface free energy of liquid water as a function of temperature [80].

The work of adhesion is given by,

$$W_{ad} = G_L (1 + \cos \theta) \quad \{C.2\}$$

where  $G_L$  is obtained from Equation {C.1},  $T$  is the test temperature and  $\theta$  is the value of contact angle.

---

Using contact angle values of untreated PS for sample calculation,

Test temperature = 15.1°C

$$\theta_{adv} = 90.3^\circ$$

$$\theta_{rec} = 81.3^\circ$$

Substituting test temperature into Equation {C.1},

$$G_L = -0.1676 (15.1) + 76.06 = 73.5 \text{ mJ m}^{-2}$$

(i) For the advancing angle,

Substituting  $G_L$  and  $\theta_{adv}$  into Equation {C.2},

$$\begin{aligned} W_{ad} &= G_L (1 + \cos \theta) \\ &= 73.5 (1 + \cos 90.3) \\ &= 73.1 \text{ mJ m}^{-2} \end{aligned}$$

(ii) For the receding angle,

Substituting  $G_L$  and  $\theta_{rec}$  into Equation {C.2},

$$\begin{aligned} W_{ad} &= G_L (1 + \cos \theta) \\ &= 73.5 (1 + \cos 81.3) \\ &= 84.6 \text{ mJ m}^{-2} \end{aligned}$$

